RISK-VALUE OPTIMIZATION OF PERFORMANCE AND COST FOR PROPELLANT PRODUCTION ON MARS

A Thesis
Presented to
The Academic Faculty

by

Christopher A. Jones

In Partial Fulfillment
of the Requirements for the Degree
Doctor of Philosophy in the
School of Aerospace Engineering

Georgia Institute of Technology
August 2016

RISK-VALUE OPTIMIZATION OF PERFORMANCE AND COST FOR PROPELLANT PRODUCTION ON MARS

Approved by:

Alan W. Wilhite, Advisor
School of Aerospace Engineering
Georgia Institute of Technology

Mitchell Walker
School of Aerospace Engineering
Georgia Institute of Technology

Robert Moses
NASA Langley Research Center
Georgia Institute of Technology

Brian German
School of Aerospace Engineering
Georgia Institute of Technology

Daniel P. Schrage
School of Aerospace Engineering
Georgia Institute of Technology

Date Approved: 1 August 2016

To Mom, Dad, Tim, and Nazia

ever enduring (even enjoying) my ramblings.

ACKNOWLEDGEMENTS

First, I must thank my thesis advisor and mentor throughout my graduate career, Alan Wilhite, for all of his ideas, suggestions, and occasional ultimatums that led to the creation of this thesis. In addition, my NASA mentors, D.R. Komar and Bob Moses, have provided their expertise and talents, for which I am indebted. Dominic DePasquale, whose research served as the launching point for both my Master's project and this research, has been an invaluable guide. I also thank the rest of my committee: Mitchell Walker, Daniel Schrage, Brian German, Jeff Jagoda, and Vitali Volovoi, for their support.

My fellow students, colleagues, and friends of these past few years have also played an indispensable role in the completion of this work. Michael Grimes, Erik Axdahl, Rafael Lugo, Patrick Chai, Timothy Lewis, Jesse Quinlan, and Dale Arney have provided all the cheers, compliments, criticisms, and counsel a graduate student could hope for. Shannon Verstynen, Michael Wagner, Rebecca Jaramillo, Stacy Dees, Shelley Spears, Sharon Bowers, Gay Reilly, Scott Bednar, Kelsey Glomb, and Kate Newmeyer, all members of my adopted Education and Outreach family, were both warm friends and patient sounding boards throughout the latter part of my work. I also thank my colleagues in NASA's Space Mission Analysis Branch for their support, especially Bill Cirillo, Kevin Earle, Jordan Klovstad, and Marie Ivanco.

Of course, none of this would have been possible without the love and encouragement of my friends from before graduate school, and my family. Jesse Sky, Maggie Brock Meekins, A.J. Alon, Jeremy Vanderknyff, Kathryn Johnson Olson, and Jordan Lander have been dear friends and constant supporters ever since we began at Carolina. Finally, my parents, Jack and Beth Jones, and my brother, Timothy Jones,

have been the foundation that has supported me through everything, and I can never hope to find the words to thank them enough.

TABLE OF CONTENTS

LIST OF TABLES

LIST OF FIGURES

NOMENCLATURE

Symbols

α	Specific Mass of Power Supply	[kg/kWe]
ΔV	Delta-V	[m/s]
δ	Declination Angle	[deg]
δ_0	Axial Tilt Angle of Mars	[deg]
$\dot{m}_I$	Rate of Oxygen Electrolyzed per Ampere of Current	[kg/(hr*A)]
$\dot{m}_{O_{2required}}$	Required Oxygen Production Rate	[kg/hr]
η_{cell}	Solar Panel Efficiency	
η_{EOL}	Solar Panel EOL Degradation Efficiency	
$\eta_{H_2conversion}$	Sabatier Hydrogen Conversion Efficiency	
$\eta_{storage}$	Coulombic Efficiency	
λ	Latitude	[deg]
ω	Hour Angle	[deg]
ω_{day}	Daytime Duration	hr
ω_{night}	Nighttime Duration	hr
τ	Optical Clarity	
A_{max}	Maximum Required Solar Area	m^2
A_{solar}	Solar Panel Area	m^2

C_2H_4	Ethylene	
CH_3OH	Methanol	
CH_4	Methane	
CO	Carbon Monoxide	
CO_2	Carbon Dioxide	
e	Eccentricity of Mars Orbit	
$E_{collect}$	Daily Solar Energy Collected	$\frac{We-hr}{day}$
E_{day}	Daytime Energy Requirement	We-hr
E_{night}	Nighttime Energy Requirement	We-hr
$E_{require}$	Total Daily Energy Requirement	We-hr
E_{store}	Energy Storage Requirement	We-hr
$f(z,\tau)$	Optical Clarity Factor	
FV	Future Value	[$M]
G	Solar Flux at Top of Martian Atmosphere	$\frac{W}{m^2}$
G_0	Mean Solar Flux at Mars	$\frac{W}{m^2}$
G_s	Irradiance of Flat Panel at Surface of Mars	$\frac{W}{m^2}$
H	Insolation	$\frac{We-hr}{m^2-day}$
H_2	Hydrogen	
H_2O	Water	
$H_{E,D}$	Engine Development Work-Year Equivalent	

$H_{E,U}$	Engine Unit Work-Year Equivalent	
H_{min}	Minimum Daily Insolation	$\frac{We-hr}{m^2-day}$
$H_{V,D}$	Vehicle less Engine Development Work-Year Equivalent	
$H_{V,U}$	Vehicle less Engine Unit Work-Year Equivalent	
I_{sp}	Specific Impulse	[s]
L_i	Length	[m]
L_s	Areocentric Longitude	[deg]
L_{MAV}	MAV Length	[m]
L_{s0}	Reference Areocentric Longitude	[deg]
L_{total}	MDV Sizing Length	[m]
LO_2	Liquid Oxygen	
M_{solar}	Mass of Solar Power System	kg
M_{store}	Energy Storage System Mass	kg
mf_p	MDV Propellant Mass Fraction	
mf_s	MDV System Mass Fraction	
O/F	Oxidizer-to-Fuel Mass Ratio	
P_{night}	Nighttime Power Requirement	W
P_{peak}	Peak Power Requirement	hr
PV	Present Value	[$M]
R_i	Hypothetical Spherical Radius	[m]

R_*	MDV Sizing Radius	[m]
R_{MAV}	MAV Radius	[m]
R_{max}	Maximum Allowable Radius	[m]
S	MDV Projected Area	[m^2]
T/W_{engine}	Engine Thrust-to-Weight Ratio	
V	Volume	[m^3]
$V_{electrolyzer}$	Electrolyzer Operating Voltage	[V]
W/S	Wing Loading	[m^2/kg]
z	Solar Zenith Angle	[deg]
$T_{Sabatier}$	Sabatier Reaction Temperature	[K]
$P_{theoretical}$	Theoretical Power Requirement for Electrolyzer	[W]

Acronyms

CEA	Chemical Equilibrium with Applications
CER	Cost Estimating Relationship
DDT&E	Design, Development, Testing, and Evaluation
DDT&E	Design, Development, Testing, and Evaluation
EDL	Entry, Descent, and Landing
ERV	Earth Return Vehicle
IMLEO	Initial Mass in Low Earth Orbit
ISPP	In-Situ Propellant Production

ISPP	In-situ Propellant Production
ISRU	In-situ Resource Utilization
LVSSS	Launch Vehicle Sizing and Synthesis Tool
MAV	Mars Ascent Vehicle
MDI	Minimum Daily Insolation
MDV	Mars Descent Vehicle
MTV	Mars Transfer Vehicle
NAFCOM	NASA/Air Force Cost Model
NPV	Net Present Value
NTR	Nuclear Thermal Rocket
PDF	Probability Density Function
RRI	Relative Robustness Integral
RTG	Radioisotope Thermal Generator
RWGS	Reverse Water Gas Shift
SNAP	Systems for Nuclear Auxiliary Power

SUMMARY

The nominal two-and-a-half year round-trip Mars mission requires extensive infrastructure to transport and safeguard its human crew, thus requiring large amounts of Initial Mass in Low Earth Orbit (IMLEO). Any technologies that can reduce this load may have the potential to realize dramatic savings in overall architecture cost. One such technology is the in-situ production of propellant for the Mars ascent vehicle utilizing Martian resources, such as the atmosphere, rather than transporting the propellant from the Earth's surface to the Martian surface. This topic has previously been studied on the basis of the reduction of the IMLEO, because of the assumption that the reduction in IMLEO would lower Earth-to-orbit launch and space transportation costs more than the increase in in-situ propellant production system production and operations cost. However, with low-cost commercial launch now being considered by NASA, the costs of propellant production on Mars may not be a positive trade for these lower launch costs.

Previous in-situ propellant production (ISPP) system models have typically been single-point designs, using simplistic scaling models to estimate the mass of the system as a function of the propellant required. When considered, optimization of the ISPP system has been decoupled from that of the overall architecture; rather, ISPP systems are treated as depending solely on propellant demand and having no bearing on other system design beyond a certain mass requirement. Past studies have used IMLEO as the sole figure of merit in selecting ISPP over a non-ISPP approach, neglecting the effects of ISPP development cost relative to savings from launch vehicle and in-space transportation costs of propellant from Earth. Finally, the large modeling uncertainty

for this relatively unknown system has generally been neglected.

The objective of this research is to evaluate, under uncertainty, an optimal ISPP system for a human-to-Mars mission. To do this, the necessary ISPP approaches and corresponding Mars transportation system architecture (consisting of the Earth-to-orbit, in-space, Mars descent, and ascent transportation systems) must be modeled in such a way that the effects of uncertainty in their performance and mass can be evaluated. With this framework, the sensitivity of the mass, power, volume, and cost of each ISPP approach and transportation architecture includes the uncertainty of its modeling, and the most relevant system architecture dependent parameters for each technology are identified for future research. Additionally, technologies will be compared using this framework to determine which has the greatest chance of success at having the least cost; this design approach will yield a ranked list of preferred ISPP approaches as compared to a non-ISPP baseline approach.

The net present value of the life cycle cost of the architecture will be used as the figure of merit, and a robustness integral, defined herein, will be used to evaluate the uncertainties in the modeling parameters and technologies on the basis of that figure of merit. Several technologies previously proposed in the literature for ISPP will be compared; namely methane production by the Sabatier process, ethylene or methanol derived from the reverse water gas shift, hydrogen or carbon monoxide from Martian resources, and oxygen production from the Martian atmosphere.

The final product of this research is an evaluation of each technology, including the uncertainty in its modeling parameters, as well as a ranked comparison of multiple ISPP approaches. From this, recommendations for an overall approach to Mars ISPP, as well as the most important technologies to be further researched, will be presented. This research serves as a guide to future mission planners, decision makers, and technology investors in planning the best path for the eventual human exploration of Mars.

CHAPTER I

INTRODUCTION

The purpose of this research is to evaluate, with modeling uncertainty, an in-situ propellant production system for a crewed Mars mission architecture. The research provides a method to model several potential systems, permitting identification of both a preferred configuration as well as those system architecture dependent parameters having the greatest impact on that selection.

1.1 Motivation

Previously proposed crewed Mars mission architectures require large initial mass in low Earth orbit (IMLEO), on the order of 1000 tons predicted in the Mars Design Reference Architecture 5.0 [1]; see Figure 1. This mass consists of the vehicles required for in-space transfer from Earth to Mars and back, as well as Mars entry, descent, and landing (EDL) and surface systems for human survival and planetary exploration. These systems require significant investments in technology development, systems development, procurement, launch, and operations costs. Such investments have heretofore proven prohibitive, suggesting that reductions in these costs are required before such a mission becomes feasible.

Multiple Mars exploration architectures have identified in-situ resource utilization (ISRU) as a key enabling technology [1–9]. On Mars, ISRU refers to the use of resources available at the Martian surface, such as the atmosphere or surface resources, to support exploration missions and to supplement resources brought from Earth. Various processes have been proposed to provide water, oxygen, buffer gases, and propellant from combinations of Earth and Martian raw materials [5,9–11]. The goal of these past ISRU systems is to reduce the total mass required from Earth; this

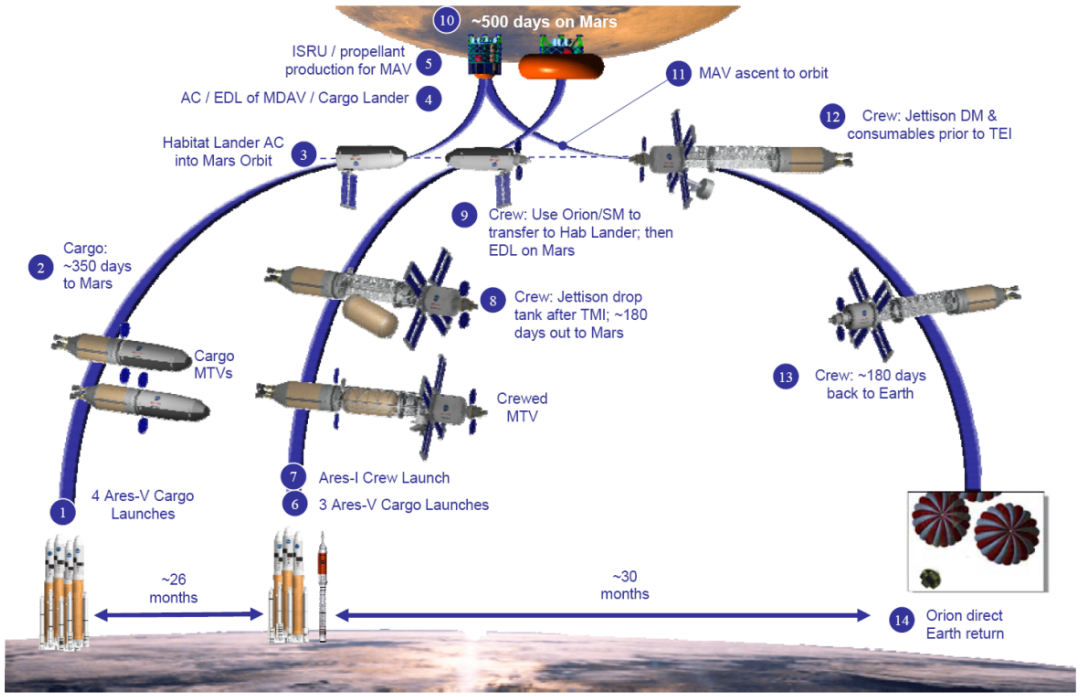

Figure 1: DRA 5 Concept of Operations

reduction in IMLEO reduces the mass to be delivered by the transportation system architecture (Earth-to-orbit, in-space, and Mars descent vehicles), thus reducing the number of vehicles and/or their size.

One area of ISRU identified as possessing the potential to reduce the mass and cost required for a Mars mission is the replacement of propellant brought from Earth for a Mars ascent vehicle (MAV) with a system for producing that propellant from Martian resources; this concept is known as in-situ propellant production (ISPP) [4, 9]. In previous concepts, a chemical plant, production feedstock, power source, and MAV are launched prior to the flight of the human crew to Mars. Upon landing and automated setup, the chemical plant utilizes the feedstock to produce fuel, oxidizer, or both for the MAV [12]. Once the crew arrives, their return propellant will have already been produced. The Mars Design Reference Architecture 5.0 considered two alternative configurations of (two-stage) ascent vehicle and descent vehicle: one with no ISPP, and one with ISPP of the cryogenic oxidizer, with methane fuel delivered

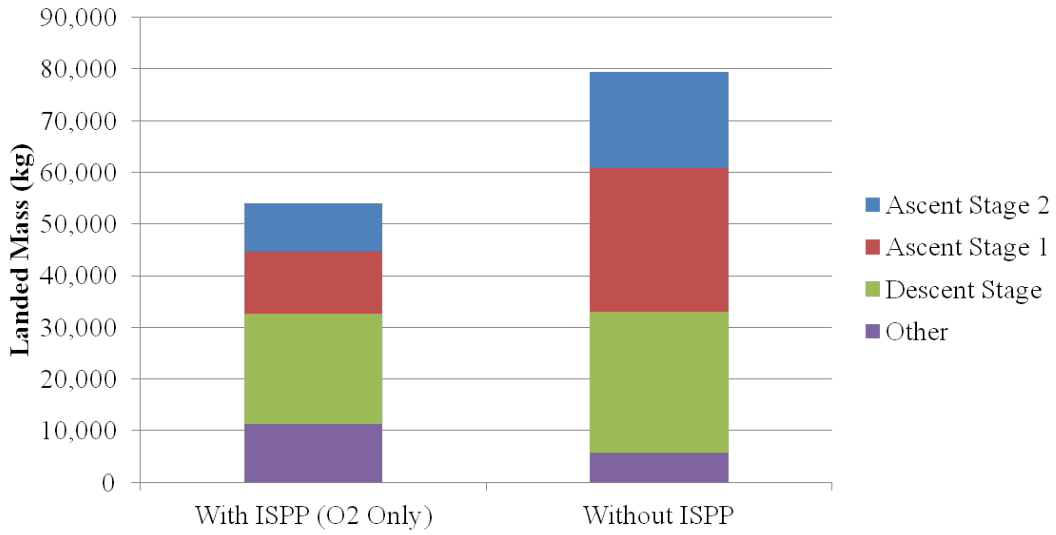

Figure 2: DRA 5 ISPP Mass Comparison

from Earth. The ISPP approach chose to only have oxygen produced due to the simpler technology requirements associated with in-situ oxygen production. With ISPP, the required mass to be landed was over 30 percent less, as shown in Figure 2.

Studies have shown that the total mass of the ISPP system (chemical plant, production feedstock, and power source) has a percentage IMLEO reduction from 20% to 60% [5]; thus the use of ISPP represents a net reduction in transported mass required over transporting the Mars ascent propellant [1, 5, 9, 12]. Previous attempts at determining the degree of savings provided by ISPP have concentrated on the savings in either mass landed on the Martian surface, or IMLEO. The facile assumption is that such mass savings translate to corresponding cost savings; however, the cost to develop and implement these ISPP systems is not trivial and may even surpass the savings realized by their deployment. Some studies in the literature [13, 14] have acknowledged this fact; however, none have made an effort to quantitatively compare the costs of ISPP and non-ISPP approaches. Thus, the consideration of ISPP for Mars as a cost-centric value proposition, rather than a mass-centric one, is an underexplored area of research.

In their consideration of various ISPP processes, several previous studies have presented estimates of the mass, power, and volume requirements of those systems as derived from the requirements of the vehicle being fueled [9, 11, 15]. However, these results have typically been presented as "black box" values with little information about how they were derived; the most detailed reports are mass statements of small scale breadboard systems, with basic extrapolations for larger systems [11, 16]. While a positively correlated, monotonic scaling of these values with propellant demand is a reasonable starting assumption, the variations in system mass, power, and volume may depend on more complex factors than only the system's required propellant output.

Where models have been provided [9, 11, 15, 16], the uncertainty inherent in those models has generally been neglected. Due to the low levels of technical maturity for both the ISPP systems themselves, as well as the Mars Ascent Vehicle to be fueled, the model parameters and design variables cannot be accurately described using single values to understand the risks. Further, changes in those values may have a significant impact on the mass and cost of the system, even to the point of affecting a trade study's choice of preferred process. Therefore, determining the parameters that have the greatest impact on the mass and cost of the systems is critical both for establishing the sensitivity of trade studies to changes in those parameters, as well as for identifying key areas of future research.

1.2 Research Goals and Questions

This research has several goals that will address the above concerns. The first is to develop and integrate systems models for various candidate ISPP systems and MAV designs such that they permit comparison of a range of architectures. The second is to identify the most important parameters governing the performance and cost of those architectures. The third is to identify the best performing architecture (under

uncertainty) for the fueling of a MAV in a crewed Mars architecture.

These goals have been addressed by developing research questions and hypotheses that answer them:

1. How should Mars ISPP technologies be modeled to permit evaluation for crewed Mars architectures?

   Hypothesis: Models that incorporate both physics-derived relationships and relevant empirical data will allow for the evaluation of mass, power, volume, and cost of crewed Mars architectures and their relevant systems.

2. What figure(s) of merit should be used to evaluate ISPP technologies?

   Hypothesis: Selecting configurations with the lowest net present value of the life cycle cost of the crewed Mars architecture, while incorporating uncertainty, will account for relevant performance and economic risk characteristics.

3. How can epistemic uncertainty in modeling ISPP technologies be addressed to determine an optimal architecture?

   Hypothesis: The application of Monte Carlo methods will serve to identify the key parameters driving the uncertainty in modeling ISPP technologies, and performance integrals will be used to select the preferred crewed Mars architecture.

The background of these research questions and the proposed hypotheses, will be discussed in the next chapter.

1.3 Problem Statement

In-situ propellant production shows promise for reducing the required mass, and thus cost, of a crewed Mars architecture. However, previous studies have been confined to small trade spaces, evaluating concepts primarily on the basis of mass savings and with little consideration of model mass uncertainty, cost, and other relevant metrics.

From a review of the literature (see Chapter 2), several candidate ISPP processes were identified. In brief, the possible processes involve the production of a fuel (either a hydrocarbon or hydrogen), oxidizer (oxygen), or both. Based on the combinations of technologies used with each process, architectures that manufacture some or all of the required propellant can be modeled, allowing for consideration of different approaches to utilizing ISPP. Details on each process and the various configurations are given in subsequent chapters.

The requirements that drive the sizing of an ISPP system derive from the requirements of the Mars Ascent Vehicle. Thus, for each propellant combination, a MAV was sized that met the mission needs derived from previous Mars missions; see Section 3.3.2. The fuel and oxidizer masses of the MAV serve as input for the sizing of the ISPP system. Ancillary systems, such as the surface power system required to energize the ISPP process (see Section 3.3.1), are then modeled based on the outputs of the ISPP system modeling. Finally, other transportation elements impacted by the sizing of the MAV and surface systems, such as the descent vehicle (see Section 3.3.3) and in-space transportation vehicle (see Section 3.3.4), are sized, thus providing mass, power, and volume estimates for all of the systems influenced by the choice of ISPP process. Finally, the total IMLEO of all of the above systems is determined to compare the costs of government and commercial launch vehicles.

Understanding the impact on mass of different ISPP technologies only provides partial knowledge. The use of such systems may reduce total mass required, impacting the costs of launching and delivering the mission hardware, but the ISPP systems must themselves be developed, produced, and operated. As these technologies have not reached full maturation, the costs of implementing them must be balanced against the cost savings resulting from their use. Thus, the development, production, operations, and launch costs of *all* impacted elements must be considered to fully understand the value of ISPP to a crewed Mars architecture.

Because the total system architecture has not reached full technological maturation, uncertainty exists in the final values of the mass and cost of these systems. This uncertainty extends to the modeling of the systems themselves; the relevant parameters that guide sizing the systems (e.g. operating temperatures and pressures) are not precisely known. A fuller understanding of the ISPP trade space requires the consideration of this uncertainty. An approach to addressing these trades is discussed in subsequent chapters that serves to identify which parameters are most significant. This approach also permits the identification of optimal mass and cost configurations under uncertainty.

In addressing these challenges, several significant advances in the field of Mars ISPP research have been made. Transparent, detailed models of multiple candidate propellant production processes have been developed, utilizing physics, chemistry, and empirical data. These processes and their corresponding architectures, more intricately coupled than in previous studies, have been traded on the basis on not just IMLEO, but life cycle cost of the architecture, adjusted for time. The uncertainty in the ISPP process modeling has been quantitatively examined and used both to identify the most important parameters affecting the sensitivity of cost, as well as to recommend which technologies hold the most promise for enabling a crewed Mars mission.

1.4 Dissertation Overview

Chapter 1 introduces the purpose of this research: to evaluate multiple ISPP technologies under uncertainty and make recommendations for future crewed Mars architecture planning efforts. This chapter presents the motivation for improving upon the modeling and evaluation of ISPP technologies and their associated architectures. Several research questions are posed, and hypotheses proposed, to address the gaps in this area of space systems analysis.

Chapter 2 presents a review of the literature that will be used to consider the posed research questions. This review includes background on multiple ISPP techniques and their modeling, as well as previous trade studies that have considered the use of ISPP in crewed Mars architectures. Candidate technologies and figures of merit are presented. Finally, the techniques used to evaluate the ISPP technologies and their associated architectures are described.

Chapter 3 describes the proposed method that addresses the goals expressed in Chapter 1. The modeling of ISPP technologies and related architectural elements are explained. The stochastic analysis techniques used to identify key parameters that drive the uncertainty in ISPP modeling are presented. The tools used to select the preferred crewed Mars architecture are shown.

Chapter 4 details the results of this research. Based on the technologies and approaches detailed in Chapter 3, nineteen different crewed Mars architectures are analyzed on the basis of the net present value of the life cycle cost. From these data, the most important parameters of each architecture are identified, as well as the crewed Mars architecture (and corresponding ISPP configuration) that are recommended for future mission planning. A comparison to the results in DRA 5.0 and other architectures is shown.

Chapter 5 provides conclusions about both the results of this research as well as the methods used. This chapter describes future work efforts that can expand upon the performed research, and summarizes the implications for decision makers in the realm of ISPP research and Mars architecture development.

CHAPTER II

BACKGROUND

2.1 Mars Exploration and DRA 5

The previous two statements of United States space policy (2010's National Space Policy of the United States [17] and 2004's Vision for Space Exploration [18]) identify Mars as "the ultimate destination for human exploration of the solar system [19]." "[U]niquely among the extraterrestrial bodies of our solar system, Mars is endowed with all the resources needed to support not only life but the development of a technological civilization [20]." While Mars possesses a challenging environment for human activity, it is more accessible than any body besides the Moon, with atmospheric carbon dioxide and potential surface water that can be used to supplement supplies from Earth.

The most recent reference mission developed by NASA for crewed travel to Mars is the Design Reference Architecture 5.0, or DRA 5 [1]. The concept of operations for the mission, previously shown in Figure 1, is repeated below in Figure 3. The mission consists of two phases: a pre-deployment phase during which two nuclear-powered cargo Mars Transfer Vehicles (MTVs) deliver payload from low Earth orbit to Mars, and a crewed phase during which another MTV delivers the crew to Mars and returns them to Earth after the crew's surface mission. These MTVs are constructed and fueled with hydrogen via multiple heavy-lift launches. This concept of operations called for eleven launches of the Ares V (each with 126 t payload to low Earth orbit), and one launch of the Ares I for the crew, to deliver all the IMLEO.

The masses of the transportation elements in DRA 5 are shown in Figure 4. A nuclear thermal rocket (NTR) propulsion system, which uses the heat of a fission

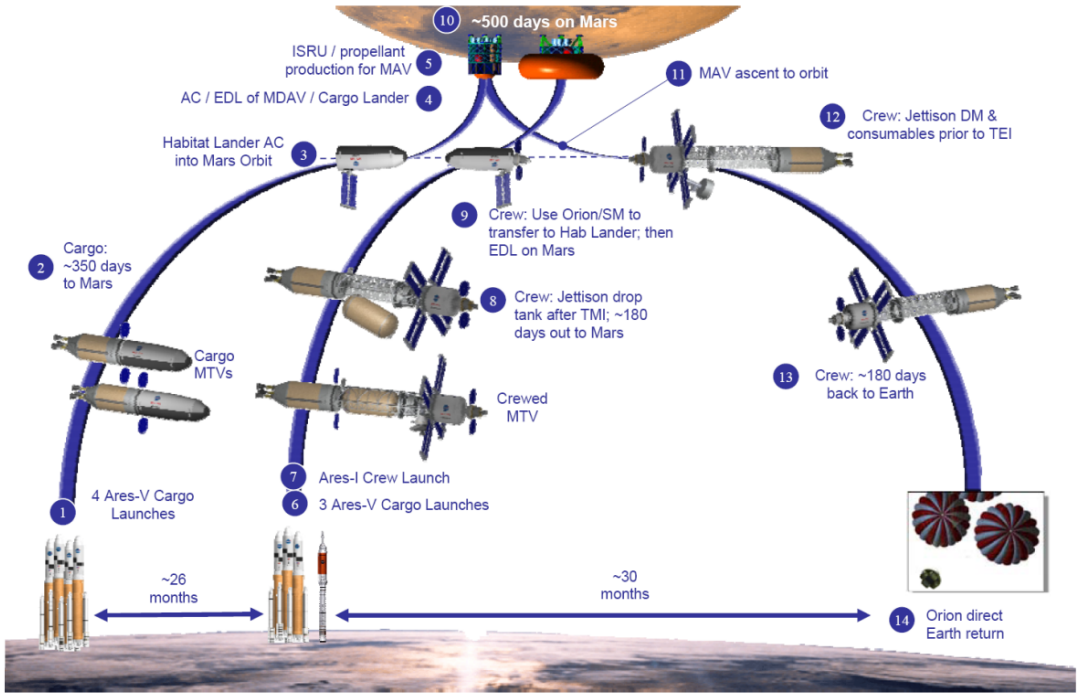

Figure 3: DRA 5 Concept of Operations

reactor to accelerate hydrogen for thrust, is used for the Mars transfer vehicle. The masses of these stages (the bolded stage, in-line, and assembly masses from the figure) are dominated by the hydrogen required for the in-space maneuvers required to transit from Earth to Mars. Of the 849 t of IMLEO required for the three vehicles and their payloads, 408 t is hydrogen propellant that must be thermally maintained while the spacecraft is assembled in low Earth orbit. The payloads of the cargo vehicle consist of a surface habitat, surface mobility systems, ISPP plant, and MAV to return the crew to Mars orbit at the end of the 500 day mission. The crew MTV transports a transit habitat for the in-space journeys to and from Mars, while also providing a descent vehicle to land the crew on Mars at the site of the surface elements. The masses of these payloads (two 103 t cargo landers with aeroshells, and the 62.8 t of crew payload elements listed in the Payload Elements section of the figure) drive the sizing of the propellant requirement, and thus the number of launches needed to implement the architecture.

Reference NTR Transfer Vehicle Summary

Cargo Mission (Single Vehicle, 1 of 2)			**Crewed Mission**		
Vehicle Elements		Mass (t)	Vehicle Elements		Mass (t)
NTR "Core" Stage	Core Stage Dry Mass	33.7	NTR "Core" Stage w/Ext. Rad. Shield	Core Stage Dry Mass	41.7
	LH2 Propellant Load	59.4		LH2 Propellant Load	59.7
	RCS Propellant Load	3.6		RCS Propellant Load	4.9
	Total Core Stage Mass	96.6		Total Core Stage Mass	106.2
	Number of Core Stage	1.0		Number of Core Stage	1.0
	Total Stage Mass	**96.6**		**Total Stage Mass**	**106.2**
In-Line LH2 Tank	In-Line Tank Dry Mass	10.8	In-Line LH2 Tank	In-Line Tank Dry Mass	21.5
	LH2 Propellant Load	34.1		LH2 Propellant Load	69.9
	RCS Propellant Load	1.7		RCS Propellant Load	
	Total In-Line Mass	46.6		Total In-Line Mass	91.4
	Number of Tanks	1.0		Number of Tanks	1.0
	Total In-Line Mass	**46.6**		**Total In-Line Mass**	**91.4**
			Long Saddle Truss & LH2 Drop Tank	Saddle Truss Mass	8.9
				Drop Tank Dry Mass	14.0
				LH2 Propellant Load	73.1
				Total Assembly Mas	**96.0**
			Payload Elements	Short Saddle Truss	4.7
				Conting. Food Caniste	9.8
				2nd Docking Module	1.8
				Fwd RCS Prop Load	3.2
				Transit Habitat	32.8
				CEV/SM + Crew	10.6
Payload	**Total Cargo Lander**	**103.0**		**Total Payload Mass**	**62.8**
	(Aeroshell, PL & Lander)				
Total Cargo Vehicle Mass		**246.2**	**Total Crewed Vehicle Mass**		**356.4**

Figure 4: DRA 5 masses for the cargo flights and crew flights, reproduced from Table 4-1 of DRA 5 [1]. One cargo flight is dedicated to delivery of the Mars ascent vehicle and in-situ propellant production systems.

This architecture is dependent upon the development of a number of new systems. Each requires substantial investment to develop the technologies, components, and integrated subsystems that constitute the vehicles and surface elements. NASA's budget has been stagnant in the past two decades, ranging between 15 and 20 billion FY2011 dollars [21]. Little evidence exists that there will be a significant increase in funding for exploration missions, while the costs of those missions remains higher than project allocations [21]. Thus, the costs of new systems for a Mars exploration mission will play a significant role in determining its feasibility.

In general, space system cost is a function of mass; for example, NASA's Advanced Missions Cost Model has cost increasing in proportion to mass raised to the two-thirds power [22]. The Transcost model is a regression of historical space system cost as a function of mass corrected for technological maturity [23]. The NASA/Air Force Cost Model (NAFCOM) is similar to the Transcost model except that it uses additional programmatic parameters to model its cost estimates, but the ultimate driving variable is still mass [24]. Thus, reducing the mass required in a Mars architecture will likely reduce the cost of that architecture, contingent upon the systems permitting said reduction not costing more to develop and implement than the savings realized by that reduction.

One technology proposed for reducing the mass of a Mars exploration mission is in-situ propellant production [1–6, 9]. Studies have shown that replacing the MAV propellant with a system to produce that propellant locally results in a net mass savings, with as much as a 60% reduction in mass to be transported from Earth to Mars surface [9]. From calculations of the "gear ratios" for landing mass on Mars, each kilogram saved on the Mars surface results in a reduction of between 10.5 and 17 kilograms in low Earth orbit by reducing the mass of the in-space transportation and the entry, descent, and landing (EDL) systems [5, 6]. Thus, replacing a hypothetical 20 t (t is a metric ton, or 1000 kilograms) of ascent propellant with 10 t of ISPP

system results in a landed mass savings of 10 t, or an IMLEO reduction from 105 to 170 t; these savings would be the equivalent of one to two launches of the Space Launch System currently (2016) under development by NASA.

2.1.1 Notable Recent Human Mars Architectures

The most influential non-NASA-authored crewed Mars architecture study is Robert Zubrin's Mars Direct (1991). Portree, in his history of crewed Mars mission planning, says that "[s]ince 1992, NASA has based most of its Mars plans on the Mars Direct concept developed in 1990 by Martin Marietta" [25]. This architecture, released in the aftermath of the NASA 90-Day Study [26], proposed doing a minimalist crewed mission with just two heavy lift launches from Earth: one pre-deploying an ascent stage with ISPP and power systems, and one bringing the crew in an in-space and surface habitat. The proposed mission sequence for Mars Direct is shown in Figure 5. Unlike the subsequent NASA architectures, which split the Mars ascent and Earth return capabilities across distinct vehicles, Mars Direct combined both functions in a single vehicle. This Earth Return Vehicle (ERV) would use 96 t of oxygen and methane propellant derived from 6 t of hydrogen brought from Earth to perform the 6.8 km/s of delta-V required to return to Earth from the surface of Mars. Zubrin assumes that the ISRU system to produce this propellant is 1.1 t, along with a 3.5 t nuclear reactor. Although the architecture shows reduction in mass as compared to the non-ISPP approach used in the NASA 90-Day Study, it is not a direct comparison with common assumptions. Although the NASA architectures that followed did not use ISRU to the same degree as Mars Direct, nor did they make vehicle and production system sizing assumptions as optimistic as Zubrin's, they did incorporate (sometimes partial) propellant production in most of the architectures studied from the 1990s onward [4, 12].

The mission study referred to as "DRM-1" (*Human Exploration of Mars: The*

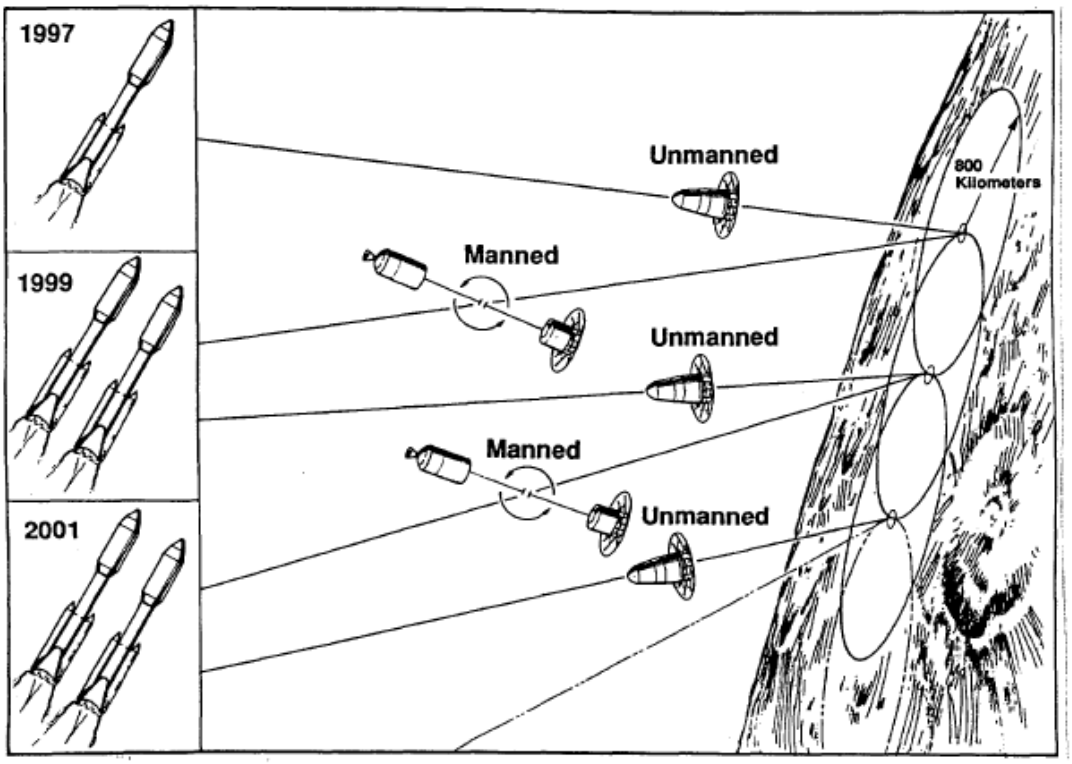

Fig. 1 The Mars Direct mission sequence. Every two years two boosters are launched. One sends an unmanned ERV to fuel itself with methane and oxygen manufactured on Mars at a new site, the other sends a manned hab to rendezvous with an ERV at a previously prepared site.

Figure 5: The mission sequence of the Mars Direct architecture, reproduced from Zubrin et. al. [4].

Reference Mission of the NASA Mars Exploration Study Team, 1997), incorporated ISRU for both propellant production (methane and oxygen for the ascent vehicle) and crew consumable production (water, oxygen, and a nitrogen/argon buffer gas mix). The sequence of events in DRM-1 is shown in Figures 6 and 7. The ISPP was required for the architecture, while the consumables were a reserve cache supplementing those brought from Earth. Propellant production relied on acquiring atmospheric carbon dioxide and reacting it with hydrogen brought from Earth; carbon dioxide electrolysis was used to provide the additional oxygen needed for an ideal ascent rocket mixture ratio. The system was sized to produce 20 t of oxygen and 6 t of methane for the ascent vehicle, along with 23 t of water, 4.5 t of breathable oxygen, and 3.9 t of buffer gas, from 4.5 t of hydrogen over a year; this sizing did not include the systems for storing the hydrogen [3]. The ISRU systems use a 14 t nuclear power system to provide 160 kWe. There is no direct comparison of ISPP and non-ISPP architectures.

In the follow-on study referred to as "DRM-3" (*Reference Mission Version 3.0: Addendum to the Human Exploration of Mars: The Reference Mission of the NASA Mars Exploration Study Team*, 1998), the same ISRU systems as proposed in DRM-1 were used, with two changes. First, the crew consumable production moved from a supplemental role to a critical role; this facilitated the elimination of other payloads that served as motivation for several changes in the architecture. Second, the propellant requirement increased from 26 t to 39 t, with a corresponding increase in required hydrogen from 4.5 t to 5.5 t. The authors claim that the ISRU plant mass decreases from 4.8 t to 3.9 t; this does not appear to include systems for storing the hydrogen [2]. The ISRU systems use a 10.7 t nuclear power system to provide 45 kWe. The sequence of flights from Earth to Mars that enabled DRM-3 is shown in Figure 8. There is not a direct comparison of ISPP and non-ISPP approaches in DRM-3.

Although the later NASA Exploration Systems Architecture Study (ESAS, 2005) focused on plans for a lunar mission, it did briefly consider a crewed Mars mission

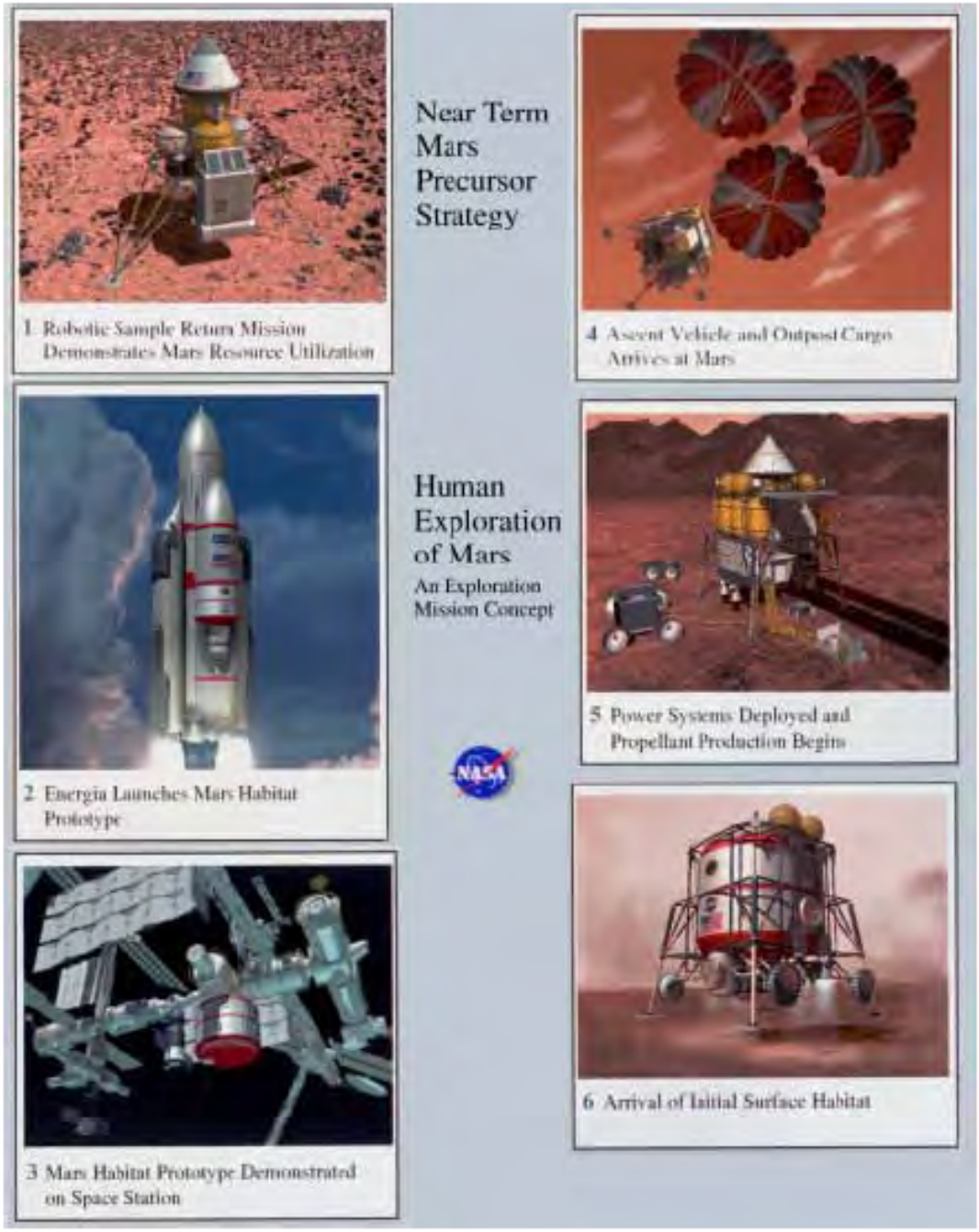

Figure 1-3 General sequence of events associated with first mission to Mars.

Figure 6: The sequence of events in DRM-1, reproduced from Hoffman and Kaplan [3].

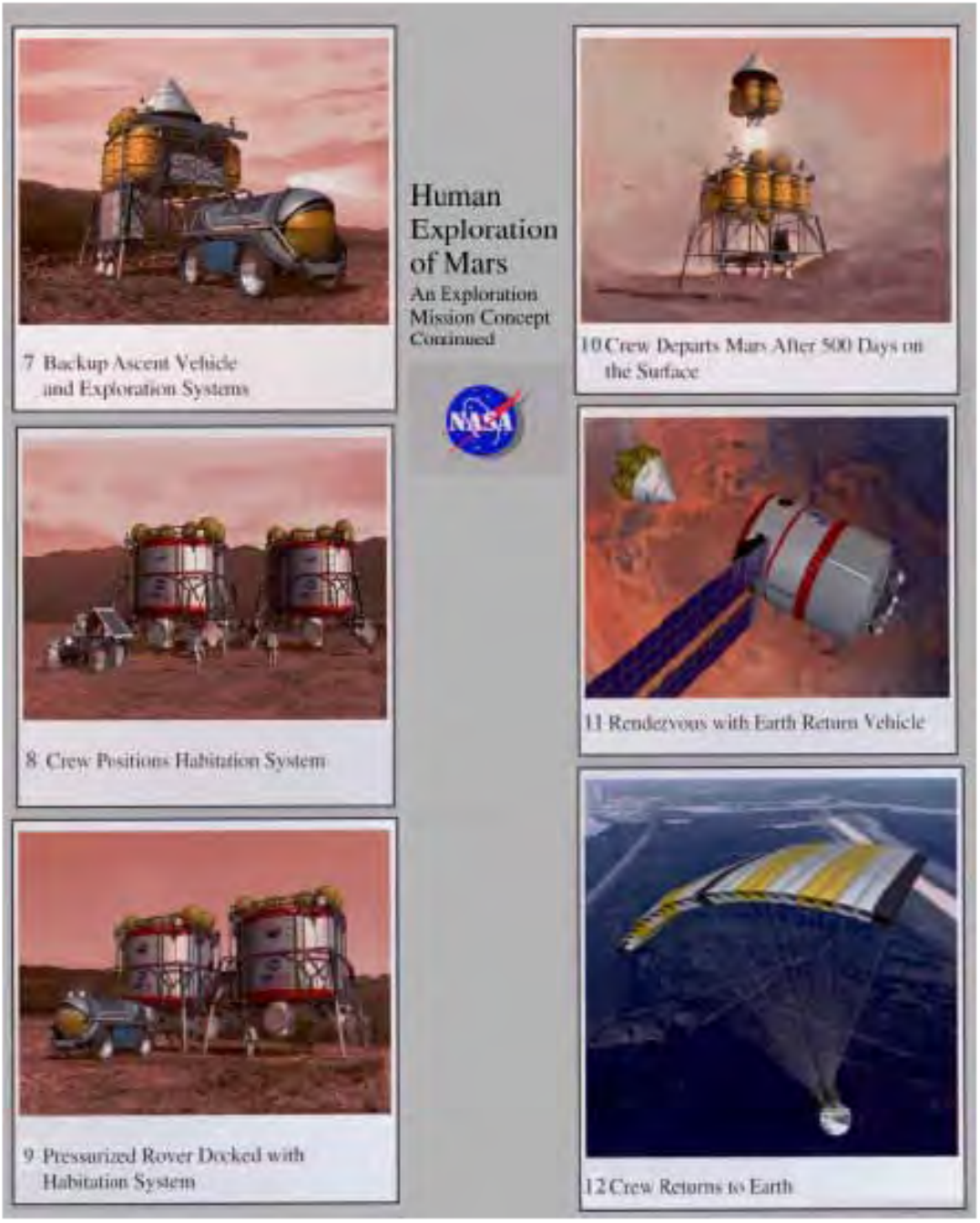

Figure 1-3 General sequence of events continued.

Figure 7: The sequence of events in DRM-1, continued from previous figure, reproduced from Hoffman and Kaplan [3].

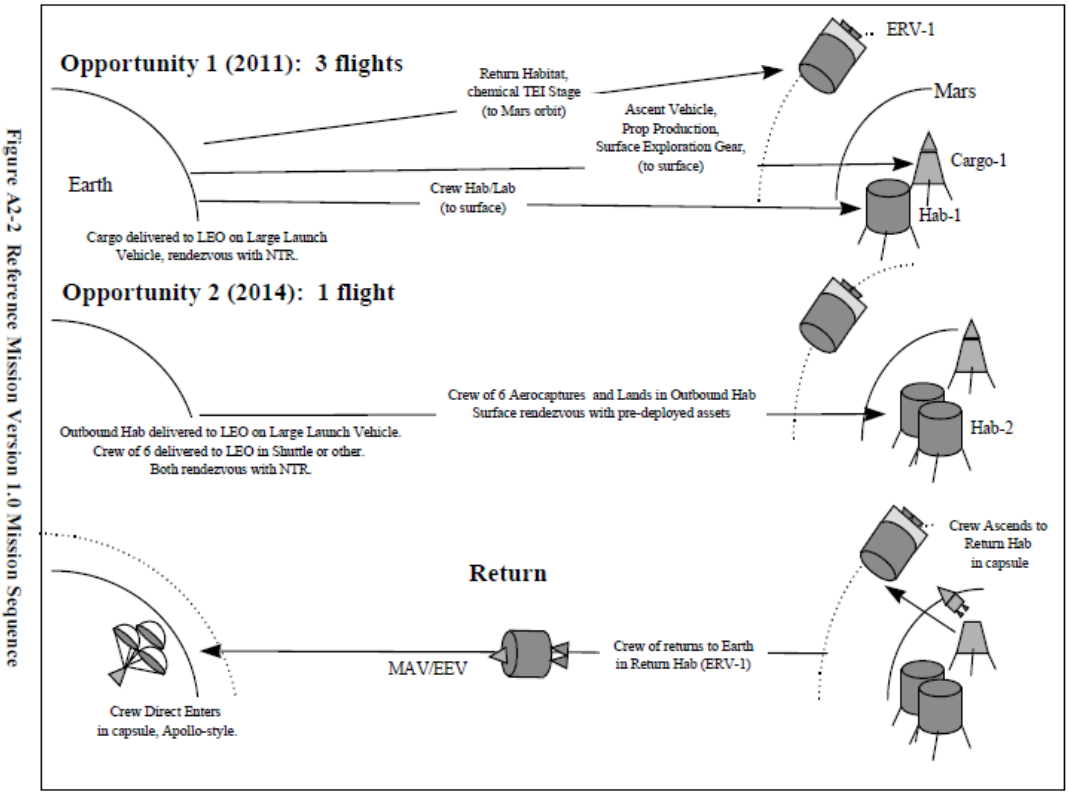

Figure A2-2 Reference Mission Version 1.0 Mission Sequence

Figure 8: The sequence of flights in DRM-3, reproduced from Drake et. al. [2].

(without stating masses). To reduce development risk, there was no Mars ISRU in the proposed architecture; instead, all of the mass needed to sustain the crew at the surface, as well as the ascent vehicle propellant, is delivered from Earth [27]. Follow-on work to revise the architecture during the Constellation program also did not use ISRU [5].

After surveying the previous Mars architectures, Rapp (in Reference [5], 2007) aggregates several common assumptions and develops a representative architecture. This architecture utilizes Martian water to produce methane and oxygen. He calculates that for launching a 5 t payload from the surface of Mars to an undefined elliptical orbit for Earth return, 47 t of propellant would be needed. His assumption for the ISRU system to produce that propellant (not including power, which he accounts for in a separate 30 t cargo landing) is 3.4 t, with a 40.2 kWe power need [5].

In DRA 5 (2009), ISRU was used to supply the oxygen for the ascent vehicle as well as water, oxygen, and buffer gases to make up for losses during extravehicular activity operations, while the ascent vehicle's methane, along with most of the crew consumables, were sent from Earth. This system, with an estimated mass of 1 t and 400 kg of hydrogen, would produce 25 t of oxygen for the ascent vehicle, 2 t of oxygen for the crew, and 133 kg of nitrogen/argon buffer gas, along with an unspecified amount of water (estimated as 3.6 t of water based on the atomic weights of hydrogen and water) [1]. The system was estimated to use between 24 kWe [1] and 30 kWe [10], requiring a 7.4 t nuclear fission power system. Additional trades of other ISRU options were evaluated; those are described in the next section of this chapter.

Figure 9 shows a comparison of the mass of the ISPP system with feedstock in each of the above studies to the mass of the ISPP products. Each of these studies makes different assumptions about the requirements on the ISPP system, as well as the capabilities available and the transportation options for delivering the ISPP system.

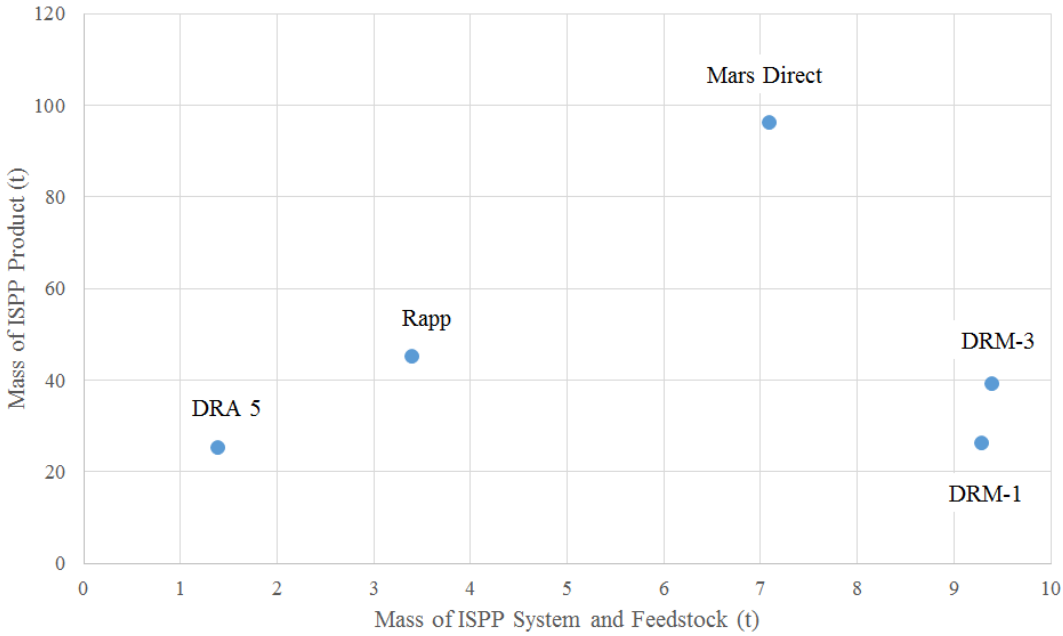

Figure 9: Plot of ISPP system and feedstock mass against ISPP product for key historical studies.

Ignoring DRM-1 and DRM-3, there seems to be a weak linear trend indicating that a larger system provides more product.

Throughout these studies, oxygen production for the ascent vehicle is the most commonly used ISRU approach. Mars Direct, DRM-1, DRM-3, and Rapp all included methane production, while DRA 5 traded methane production, but did not include it in the baseline architecture, because of the additional technologies required and the challenges of either transporting or acquiring hydrogen for fuel production. Mars Direct designed the most aggressive system both in quantity of product, and size of ISRU system; subsequent estimates of ISRU mass for smaller propellant quantities have been several factors higher (DRA 5 used a system twice as massive to produce a quarter of the product). From the DRM-1, DRM-3, and Rapp estimates, all of which produce fuel and oxidizer for the ascent vehicle, the ISRU system for propellant demands between 26 t and 47 t varied between 3.9 t and 6 t, not counting power systems.

The third section of this chapter examines the power requirements for ISRU and the systems needed to provide that power in several proposed missions.

The limited trades performed in these studies considered few options within the domain of ISRU. In DRA 5, a trade was performed between bringing hydrogen from Earth or electrolyzing water on Mars to acquire hydrogen to make methane, or bringing the methane and only producing oxygen. A second trade examined the use of solar and nuclear power for operating the selected ISRU system (bringing methane and producing oxygen). These trades occurred only in the context of the ISRU system and power system; there was no consideration of the impact on the architecture of using different ISRU options. As discussed below, while mass on the Martian surface and in low Earth orbit are useful metrics for understanding the impact of ISRU on Mars missions, they neglect other architectural and campaign figures of merit, especially cost. The fourth section of this chapter discusses this in greater detail.

None of the estimates described above includes an analysis of the uncertainty in modeling these ISRU systems, which are not yet sufficiently technologically matured to allow for precise estimates of system mass, power, and volume. For these systems, the uncertainty surrounding the sizing parameters used can have a significant impact on the preference of different technologies. Thus, there is a need for incorporating uncertainty analysis into the modeling of ISRU systems. The final section of this chapter discusses the approach taken to incorporate the epistemic uncertainty in the formulation of ISRU models.

2.2 In-situ Propellant Production

After the Mars *Viking* spacecraft landings in 1976 returned the first pictures and regolith analysis (the loose matter, dust, soil, and broken rock that makes up the uppermost layer of the surface of Mars) from the surface, interest rose in returning

a sample from Mars to Earth; early proposed approaches would utilize a Mars ascent vehicle rendezvousing with an orbiting Earth return vehicle in an attempt to reduce landed mass [28]. To further reduce the landed mass requirements, Ash et al. in a seminal ISRU paper in 1978 proposed using in-situ propellant production on Mars for the ascent vehicle [28]. Their analysis, which showed it was possible to produce sufficient propellant to permit a direct sample return mission, considered several potential fuels for manufacture from carbon dioxide and water, including carbon monoxide (rejected due to its low specific impulse) and hydrogen. Their study ultimately settled on methane and oxygen, due to the ease of manufacture (relative to other hydrocarbons) and storage (relative to hydrogen).

Subsequent studies further explored the manufacture of these propellants, as well as focusing solely on the production of oxygen [29–32]. After the initial optimism regarding the accessibility of water on Mars in Ash et al.'s 1978 paper, Ramohalli et al. took a more conservative no-water approach in 1985, 1987, and 1989 [29–31]. In these papers, the focus shifted to the consideration of oxygen production at Mars supporting fuel brought from Earth. Methane was selected as the imported fuel in the 1987 study, due to several factors: "the oxidizer-to-fuel mass ratio is high (about 4:1), thus maximizing effectiveness of ISPP; [rocket] performance is good; [methane] liquid temperature is compatible with O_2; and it is a good refrigerant [30]." The preferred technology in those studies is the use of a zirconia membrane to capture oxygen that has been pyrolized from carbon dioxide, as previously described by Lawton and Frisbee [16, 33].

In the aftermath of the NASA 90-Day Study on Human Exploration of the Moon and Mars [26], which showed a campaign that would cost 450 billion dollars and take between 20 and 30 years to perform a brief excursion to the surface [12], Zubrin et al. proposed an ISPP-based Mars mission to reduce costs by an order of magnitude by eliminating many of the systems proposed in the NASA 90-Day Study and focusing

solely on Mars with no systems for or missions to the Moon [4, 12]. This architecture relied on a predeployed ISPP plant, power supply, and Earth return vehicle (ERV) one launch opportunity before the crew would travel to Mars. The ISPP plant manufactured both oxygen and methane using atmospheric carbon dioxide (as the above approaches proposed) and hydrogen brought from Earth (eliminating the question of water acquisition at Mars). The plant was designed such that all propellant was manufactured prior to crew launch, and as a backup, a second ISPP plant, power supply, and ERV would be launched to Mars in parallel (ostensibly to service the subsequent second crew launch, but also serving as a backup to the first crew).

The proposed ISPP system in Mars Direct was based around the Sabatier reaction (Equation 1). This process, combined with the electrolysis of water (Equation 2), allows for the conversion of hydrogen feedstock and collected carbon dioxide into methane and oxygen, at an oxidizer-to-fuel (O/F ratio), assuming perfect conversion, of 2.0. However, the performance (specific impulse) of methane/oxygen engines peaks at higher O/F ratios; Zubrin et al. found 3.5 to be the best O/F ratio [4], while Jones et al. found 3.75 [9]. Thus, an additional source of oxygen is required to operate the engine at peak specific impulses. Zubrin proposes several supplemental oxygen production techniques [4]:

1. Electrolylsis of carbon dioxide (see Equation 3), as previously proposed by Ash [28], Lawton, and Frisbee [16,33]. Such a system, with a sufficient power supply, could theoretically generate any amount of oxygen, as the only input resource is atmospheric carbon dioxide.

2. The reverse water gas shift (RWGS, see Equation 4), which would use heat generated by the Sabatier reaction to react carbon dioxide and hydrogen in the presence of an iron-chrome catalyst to yield additional water, which would be electrolyzed [11,34]; this process could also be used independent of the Sabatier

reaction as an "infinite leverage oxygen machine" [11] to generate arbitrarily large amounts of oxygen using a small, recycled hydrogen feedstock.

3. Pyrolysis of methane (see Equation 5) would undo the production of some of the initially manufactured methane to liberate additional hydrogen to return to the Sabatier reactor; the amount recycled this way could be tuned to yield the desired O/F ratio of oxygen and methane.

$$\mathrm{CO_2} + 4\,\mathrm{H_2} \longrightarrow \mathrm{CH_4} + 2\,\mathrm{H_2O} \tag{1}$$

$$2\,\mathrm{H_2O} \longrightarrow 2\,\mathrm{H_2} + \mathrm{O_2} \tag{2}$$

$$2\,\mathrm{CO_2} \longrightarrow 2\,\mathrm{CO} + \mathrm{O_2} \tag{3}$$

$$\mathrm{CO_2} + \mathrm{H_2} \longrightarrow \mathrm{CO} + \mathrm{H_2O} \tag{4}$$

$$\mathrm{CH_4} \longrightarrow \mathrm{C} + 2\,\mathrm{H_2} \tag{5}$$

The Mars Direct study carried forward the methane pyrolysis option for study due to its simple operational complexity. Jones et al. found that methane pyrolysis is a much more power intensive technique for a given oxygen requirement than other supplemental oxygen production techniques and that the increase in power system size as a result of that added power requirement results in a mass penalty on the order of several tons for the landed mass on Mars [9]. Later work by Zubrin et al. on the development of a reverse water gas shift ISPP system led their research efforts away from methane pyrolysis [11, 34, 35], while the later work of Sridhar et al. at the University of Arizona focused on improving the techniques of carbon dioxide

electrolysis [36–41]. Thus, methane pyrolysis as an option for supplemental oxygen was not carried forward in this research.

Later research by Zubrin et al. considered two alternative fuels for production on Mars based on work on the reverse water gas shift. By operating the RWGS with excess hydrogen, the output of the reactor would be a mixture of carbon monoxide and hydrogen. This mixture, in the presence of an iron Fischer-Tropsch catalyst, would yield ethylene and water, in accordance with Equation 6. Ethylene's benefits as a fuel, relative to methane, include its reduced hydrogen requirement (due to having two carbon atoms per four hydrogen atoms) and its higher boiling point, allowing for liquefaction and storage at ambient temperatures on Mars; however, less work has been done developing the relevant ISPP systems and rocket engines. The other alternative proposed by Zubrin et al. is methanol, leveraging existing syngas reactors with copper-zinc catalysts to produce the fuel from the carbon dioxide and hydrogen mix (see Equation 7). Methanol has a much lower ideal O/F ratio than methane or ethylene, thus reducing requirements on the water electrolysis system that produces oxygen and consumes significant quantities of power. Methanol also does not require cryogenic storage on Mars. However, methanol and oxygen have a lower specific impulse than the other proposed fuels (a theoretical Isp of 340 seconds compared to 365 for methane, 370 for ethylene, and 450 for hydrogen); thus, there exists a tradeoff between the lower power requirement per unit propellant produced, and the greater quantity of propellant required [11].

$$2\,CO + 4\,H_2 \longrightarrow C_2H_4 + 2\,H_2O \tag{6}$$

$$3\,CO + 2\,H_2 \longrightarrow CH_3OH + 2\,CO \tag{7}$$

An additional option for supplemental oxygen considered by the author in Jones

et al. was the transport of supplemental oxygen from Earth. In this concept, no additional ISPP hardware beyond the Sabatier system, producing propellant at an O/F ratio of 2.0, is required; the excess oxygen is stored aboard the MAV. Such a system reduces the power load required relative to carbon dioxide electrolysis, methane pyrolysis, or the RWGS. However, the added landed mass is greater than 15 t; from the gear ratio discussion in Section 2.1, this represents a change in IMLEO requirements of as much as 250 t. Thus, transport of supplemental oxygen from Earth was also not carried forward in this research.

It is also possible to operate the Sabatier system at the O/F ratio of 2.0, but to produce sufficient oxygen by making excess methane. While this approach avoids the need for any secondary oxygen production system, it increases the amount of hydrogen required by 150%. Acquisition, transport, cryogenic storage, and volume of hydrogen have previously been identified as challenges for ISPP [1, 9, 10]; thus, this approach (the production of excess methane from excess hydrogen) is not carried forward in this research.

For an ISPP system producing methane, carbon dioxide electrolysis is preferred [1,9,10], while for ethylene production, the reverse water gas shift is preferred due to its common elements shared with the ethylene reactor [11,34,35]; methanol does not require secondary oxygen production, while hydrogen brought from Earth as fuel is paired with carbon dioxide electrolysis based on the preference found for methane.

In the development of DRA 5, NASA performed several ISPP trades. The manufacture of methane and oxygen was traded against the production of only oxygen, to study the impact of requiring the acquisition of hydrogen (either from Earth or Mars). Both solar and nuclear power were considered for the ISPP systems and other surface elements. The use of only the atmosphere was compared to the use of Martian regolith to provide water, and thus hydrogen. These trades led to several findings reported in the Addendum to DRA 5 [10]:

1. Non-ISPP options may require a prohibitively large (and thus, unfeasible with 2016 technology) entry, descent, and landing (EDL) system; thus, some level of ISPP may be mission-enabling.

2. Mass savings from incorporation of ISPP can permit landing of additional payloads or added payload margins.

3. Hydrogen transport from Earth was ruled out due to the large added volume requirement for EDL (given in the DRA 5 Addendum as on the order of 30 m^3).

4. Nuclear power is more mass and volume efficient than solar power to meet ISPP demands.

5. The use of ISPP results in fewer launches being required.

In his book on ISRU, Rapp surveys several potential ISPP techniques for Mars, including regolith processing for water, carbon dioxide electrolysis, methane production via the Sabatier process, and the reverse water gas shift [6]. Rapp also summarizes and critiques the findings of DRA 5, noting that of the three principle options considered, he evaluates only the production of methane and oxygen from Mars water as feasible. The oxygen-only approach recommended by DRA 5 is rejected due to Rapp's analysis of the requirements of a carbon dioxide electrolysis system, which show substantially higher power levels required than given in DRA 5. The Earth-based hydrogen approach is rejected for the same reason as is given in DRA 5; i.e., the large volume requirement of the required liquid hydrogen. Rapp concludes his analysis by remarking on the lack of NASA research on ISRU concepts in lieu of lunar ISRU, despite the higher payoff expected from Mars ISRU [6].

DRA 5 and Rapp both consider several ISPP technologies, and DRA 5 evaluates three potential ISSP concepts. However, the widest survey of ISPP concepts was given in a Mars Society paper by Kristian Pauly [15]. In this study, thirteen

ISPP approaches were considered, including four propellant combinations (methane, ethylene, methanol, and hydrogen, each with oxygen) and four supplemental oxygen production techniques (water electrolysis, carbon dioxide electrolysis, the reverse water gas shift, and methane pyrolysis); note that not all possible combinations were analyzed. Pauly's analysis compared each ISPP approach's total landed mass (empty MAV, ISPP equipment and feedstock, and nuclear power supply) to a non-ISPP baseline mass; ten of the thirteen concepts required less than 40% of the landed mass of the non-ISPP option, and all were less than 60%. While this is one of the most comprehensive studies of multiple ISPP options, the ultimate figure of merit remains mass landed on the Mars surface; the limitations of this as the sole figure of merit are discussed in Section 2.4. Additionally, the impact of the different ISPP concepts on the transportation architecture was not considered.

Seeking to expand their capability to study the effects of advanced technologies on mission architectures, the Systems Analysis and Concepts Directorate at NASA's Langley Research Center contracted Spaceworks Engineering Incorporated. to develop a detailed model of several of the previously mentioned ISPP concepts. The resulting model permitted trades of system level choices (such as supplementary oxygen production system) to evaluate their impact on the total mass, power, and volume required for the ISPP system [42]. The model includes sizing parameters derived from experimental and theoretical results of previous ISPP studies. However, the model is not designed to analyze alternative propellant concepts (such as those proposed by Zubrin et al. [11, 34]), nor does it include analysis of the systems that drive and are affected by the choice of ISPP concept (the MAV and transportation elements that deliver the MAV and ISPP plant to the surface).

Other than Pauly's study, there has not been an examination of different propellant types for crewed mission scale production. Discussions of alternate propellants have been limited to remarks about methane's high specific impulse relative to other

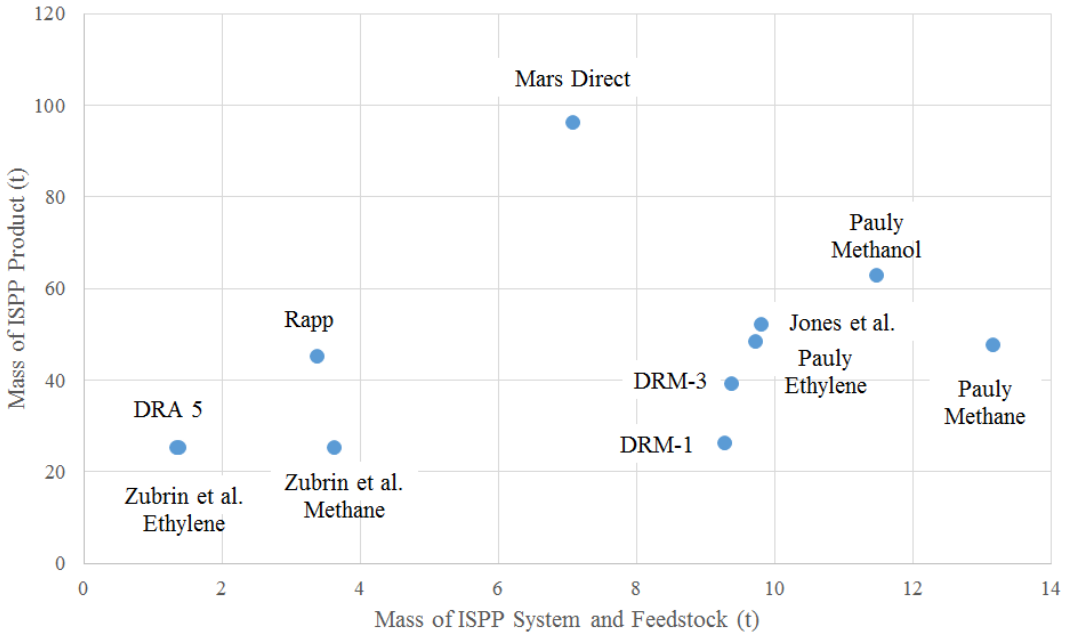

Figure 10: Plot of ISPP system and feedstock mass against ISPP product for key historical studies. Many of these studies do not consider the transportation architecture to deliver the ISPP system.

hydrocarbons and ease of storage relative to hydrogen. However, there has not been a quantitative analysis of the architectural impacts of different propellant types and processing techniques for ISPP. In these studies, the impact of the power system on the total ISPP system is only minimally discussed (a power system trade is presented in the addendum to DRA 5), despite power system mass ranging from 34% to 87% of the combined ISPP system and power system mass.

Figure 10 shows a comparison of the mass of the ISPP system with feedstock in each of the above studies to the mass of the ISPP products. Note that the studies that appear here that did not appear in Figure 9 did not include modeling of the in-space transportation architecture to deliver the ISPP system. As before, there seems to be a weak linear trend indicating that a larger system provides more product, with Mars Direct a distinct outlier as a highly efficient system.

Figure 11 shows the morphological matrix of ISPP options described above. Four

Trade	Option 1	Option 2	Option 3	Option 4	Option 5
Fuel	Methane	Ethylene	Methanol	Hydrogen	
Type	Hydrogen from Earth	Earth water	Mars water	Only oxygen production	No ISPP
Oxygen Production Method	Carbon dioxide electrolysis	Water electrolysis	Methane pyrolysis	Bring from Earth	Excess fuel production

Figure 11: The morphological matrix of ISPP options. The three oxygen production methods highlighted in red are not modeled in this study for reasons discussed in Section 2.2.

different fuels, five different methods of producing oxygen to meet O/F ratio requirements, and five types of ISPP use are shown. Within the trade space defined by these options, three of the five oxygen production methods are removed for reasons described above. Each of the four fuels and five ISPP types maps to a possible ISPP approach, with one redundant combination: using hydrogen as the fuel while bringing it from Earth is equivalent to using hydrogen as fuel while only including oxygen production from ISPP. Thus, there are nineteen possible approaches delineated by the combination of those two trades. For each of those approaches, one or both of the remaining oxygen production methods is used for meeting the O/F ratio requirements; these are described in Section 3.1.

2.3 Surface Power

Any ISPP system capable of supplying propellant to the ascent vehicle, and preventing excessive boiloff of that propellant, requires a surface power system. Additionally, the non-ISPP systems, operating both before the crew arrives and during their stay, also require power. The long durations (hundreds of days) of Mars missions, combined with limits in miniaturization of batteries and fuel cells, require that a dedicated power supply be capable of producing that power at Mars. Power is 87% of the ISPP mass in DRA 5 [1]; thus, it is critical to define the ISPP power required and

corresponding power source. Unlike missions with lower power requirements (of a few hundred Watts) such as previous Mars rovers [43], which utilized radioisotope thermal generators (RTG), a Mars surface mission will require power levels at least two orders of magnitude higher [1,2]. The trade studies in DRA 5 and its addendum suggest power requirements of 23 kWe for the crew and 32 kWe for the ISPP system (in DRA 5, the power supply was sized to the ISPP load; the crew did not arrive until after propellant production was complete); other ISPP studies have identified necessary power levels up to 150 kWe [9, 15, 44, 45].

2.3.1 Solar Power for Mars

The two primary power technologies proposed in DRA 5 and previous crewed Mars architectures are solar power and nuclear fission. Space solar power technologies such as those aboard the International Space Station are more mature than in-space high power nuclear fission concepts, but have several drawbacks. To match the continuous operation capability of a nuclear power source, a solar power source must be sized to a higher power requirement to charge a secondary power source for nighttime operation (80 kWe for eight hours of operation and charging as compared to 26 kWe for continuous operation in DRA 5) assuming an equatorial or low-latitude system [10]; polar systems present challenges due to the additional requirements on the Mars EDL system, and are not considered in this research. Additionally, such a system is vulnerable to drops in efficiency due to variations in solar energy received during the Martian year and dust storms abrading the panels. In general, the solar flux at Mars's distance from the sun is approximately 590 W/m^2, nearly half that of the 1060 W/m^2 found at Earth's surface [46]; that flux falls off further due to variations in time of year, atmospheric opacity, and zenith angle [47].

The Martian dust also impacts the performance of solar power [48]. Landis and Jenkins reviewed the data on dust accumulation and solar cell degradation on the

Mars Pathfinder rover and calculated a degradation of 0.28% per day [49]; they based this analysis on the Mars Adherence Experiment result and found the dust rate to match the measured solar cell degradation [50]. Crisp et al.'s model of gallium arsenide/germanium solar cell degradation, which combined the Pathfinder data with theory, showed a rate of 0.4% to 0.5% per day for the first 20 days, followed by a 0.1% degradation per subsequent day [51]. The experimental results obtained by Gaier and Perez-Davis showed that the abrasion of Mars dust reduced solar panel coverglass transmittance by between 2% and 40%, depending upon particle size and velocity, as well as accumulation [52]; this is in line with previous work showing that iron oxide dust was highly abrasive for radiator surfaces [53]. Landis, looking at potential impacts over the course of a two-year mission, calculated that degradations in performance due to accumulation of dust would range from 22% to 89% (on the order of the timeline in DRA 5 for ISPP operation) [54].

While dust mitigation strategies may be able to ameliorate the impact of dust on the solar panels themselves, the Martian dust storms also impact the amount of light that is available even to undamaged panels. Both James et al. [55] and Landis and Appelbaum [56] note that due to the light scattering effects of the dust, vertically oriented sun tracking arrays do not outperform horizontal fixed arrays that can collect both direct and indirect insolation. Haberle et al. showed that horizontal systems are superior to sun-tracking systems when optical depth (the measurement of how opaque the atmosphere is due to dust) exceeded unity, as commonly occurs during dust storms [57].

Several studies have considered the mass and solar array area required to enable a crewed Mars mission. Haberle et al. proposed a human outpost that would operate at 25 kWe during the day and 12.5 kWe during the night, requiring approximately 700 kg of solar arrays and either 150 kg for a regenerative fuel cell system or 1800 kg for a Li-SO2 battery; their analysis included the impact of the efficiencies of power

management and distribution systems, but not the masses of those systems). They also considered an approach similar to Mars Direct [4] that would supply 370 MWe-hr of energy over the daytimes of the Martian spring and summer to fuel an ascent vehicle (with no nighttime operation); that system required 1850 m^2 solar arrays and was 1700 kg [57].

Littman compared a solar power system integrating regenerative fuel cells for nighttime power and a nuclear system for a Martian outpost. The solar arrays were sized to produce 370 kWe, while the nuclear system was sized to generate 210 kWe (the higher power requirement of the solar system is to charge the fuel cells for nighttime power). The integrated solar system was 14000 kg, while the nuclear system was 8000 kg [58].

James et al. estimated power requirements between 60 kWe and 200 kWe for a Mars base. Using data from Haberle et al., they estimated that a 100 kWe solar power system at the Viking 1 site would require 4000 m^2 of solar panels and would be 3500 kg, for a specifc power (the ratio of system mass to output power) of 35 kg/kWe. This estimate was for only the solar power system itself, and did not include energy storage hardware to survive the night [44].

Kerslake and Kohout sized a thin film solar cell based power system for a human Mars mission that provided 107 kWe during the day and 7 kWe during the night for both ISRU and crew operations over an 1130 day mission (the ISRU system produced propellant over the span of one Mars opportunity, while the crew performed their mission during the subsequent opportunity). The resulting integrated system included 7200 kg for the photovoltaic arrays, 1300 kg for a regenerative fuel cell, and 2100 of power management hardware, yielding a total system mass of 10600 kg. The array area was 6200 m^2. Mass sizing parameters were given for several components of the system; they are shown in Table 1 [59].

Wead sized an integrated solar power system (including arrays, fuel cells, and

Table 1: Solar Power System Component Sizing Parameters [59]

Component	Value	Description
Membrane	0.2 $\frac{kg}{m^2}$	Solar cell membrane
Structure	0.8 $\frac{kg}{m^2}$	Structure supporting solar cell membrane
PMAD	17.4 $\frac{kg}{kWe}$	Power Management and Distribution
Fuel Cell	4.3 $\frac{kg}{kWe-hr}$	Regenerative fuel cell with radiator

power management and distribution) and a nuclear power system for supplying 160 kWe to a potential Mars outpost. The solar power system masses were distributed between 5400 kg and 23000 kg, while the nuclear power masses varied from 10700 kg to 14000 kg. Wead observed that political challenges associated with nuclear systems were a reason to prefer solar systems, but discussed neither the wide range of masses nor the relative importance of political risk as compared to system mass [45].

Balint's calculations showed that for power levels greater than 5.5 kWe for Mars surface systems, solar power required more mass than nuclear fission systems. These calculations included the reactor, radiation shielding, and power conversion hardware for the nuclear systems, while omitting the supporting components and structures for solar arrays. Thus, this crossover point is conservative for determining the power requirement at which nuclear systems become more efficient than solar systems at the surface of Mars [60].

Petri et al. designed two solar power systems as part of the Space Exploration Initiative's 90 Day Study. The first generation system supplied 25 kWe during both day and night using a combination of arrays and regenerative fuel cells, with a mass of 3000 kg. The second generation system supplied 75 kWe during the day and night, with a mass of 9000 kg [61].

Cooper et al. compared two solar power technologies (silicon rollout blanket arrays and inflexible tracking arrays) with two nuclear power technologies (nuclear fission

with power conversion provided by either a Brayton cycle or Stirling cycle), along with regenerative fuel cell and battery technologies. The mission for comparison was a 100 kWe requirement at the equator of Mars. The solar arrays were approximately 25000 m^2, and the integrated solar power systems required between 4000 kg (for rollout arrays with regenerative fuel cells) and 20000 kg (for tracking arrays with Li-ion batteries). The nuclear systems required between 5500 kg (for a Stirling power cycle) and 10000 kg (for a Brayton power cycle) [62].

DRA 5 traded solar and nuclear power to operate both the ISPP systems and the habitat. The solar power system was sized for operating the ISPP system only during an eight hour daytime period, rather than continuing operations during the nighttime off fuel cell energy storage. For sizing, DRA 5 assumed opacities varying from 0.9 on clear days to 5.0 during dust storms. These dust storms were assumed to impact 50 sols (Mars days) of the 550 sol mission. The study also assumed a daily solar panel degradation of 0.2% per day, more optimistic than the constant rate of Landis and Jenkins, but more conservative than Crisp et al's long duration rates. This system, capable of providing 96 kWe during the day to surface systems and fuel cells, had a mass of 22000 kg, and an area of 4300 m^2 [10].

The International Space Station's solar arrays, at station completion, have a mass of 63 t and an area of 3300 m^2. These arrays can produce 262 kWe [63].

Comparing the results of these studies on the basis of specific power (α), as a function of daytime power requirement, shows that the solar systems range from approximately 34 kg/kWe (for the high power systems of Wead) to 242 kg/kWe (for the International Space Station system); see Figure 12 and Table 2. The systems that are not integrated masses (from Haberle et al. and James et al.) are highlighted in red. At the low α levels, these systems are comparable to nuclear systems discussed below, while the higher α systems are several times more massive (and present additional challenges in deploying and cleaning thousands of square meters of solar panels).

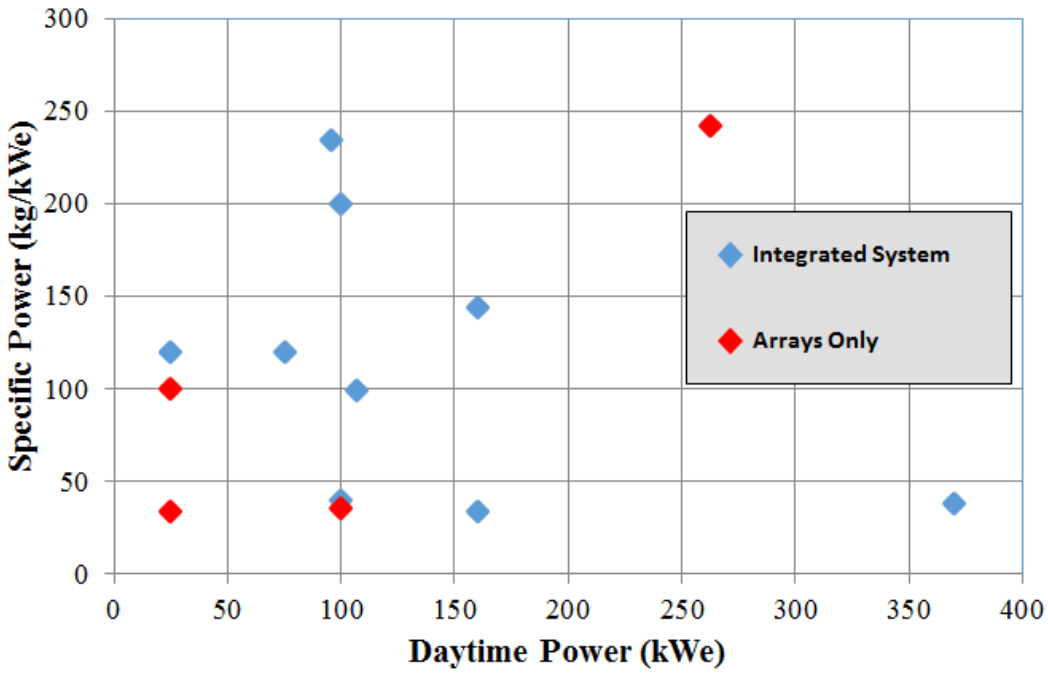

Figure 12: Specific mass as a function of daytime power for Mars surface solar power systems. The points in red are not integrated system masses.

A model based on the solar flux model described in Appelbaum et al. [47], using subsystem sizing data from Kerslake and Kohout [59], and parametric data from Bailey and Raffaelle [64], is used in this research in conjunction with ISPP power requirement models to compare solar and nuclear power options for ISPP.

Three potential classes of solar power technology have been considered for Mars missions. Traditional cells that use crystalline silicon are based on the oldest solar technology in use on Earth, and for in-space applications, have conversion efficiencies on the order of 20%. Thin film solar panels, which can deliver more power per unit area due to the reduced amount of material required, have lower efficiencies between 11% and 14%. Multi-junction cells, which use layers of films of different materials, each with varying band gap energies and thus different spectra that are absorbed, are the most efficient cells (although more complex to manufacture), with efficiencies

Table 2: Solar Power System Performance

Source	**Corrected Value ($\frac{kg}{kWe}$)**	**Note**
Haberle et al. (Fuel Cell)	34	No Power Management and Distribution
Wead (Low Bound)	34	
James et al. (Fuel Cell)	35	No Energy Storage
Littman	38	
Cooper et al. (Low Bound)	40	
Kerslake and Kohout	99	
Haberle et al. (Battery)	100	No Power Management and Distribution
Petri et al.	120	
Wead (High Bound)	144	
Cooper et al. (High Bound)	200	
DRA 5.0	235	
ISS	242	Only arrays and structure

ranging from 27% to 38%. Current in-space mission designs commonly call for triple-junction cells, as the high efficiencies favorably trade with the higher costs; DRA 5 uses triple junction gallium arsenide/Germanium panels with an efficiency of 29% [10,64]. This range of cell efficiencies is incorporated in the present solar power model.

2.3.2 Nuclear Power for Mars

Even for nuclear systems, with their compact design and capability for long-term continuous operation, the mass requirement for the levels of power needed by ISPP and habitats is not trivial. In DRA 5, the ISPP system mass was 945 kg, while the fission surface power system to operate it and other systems was estimated at 7800 kg; thus, the power system's mass is 87% of the combined ISPP and power mass [10]. Rapp et al.'s sizing of multiple ISPP production options (including using Earth water, Martian water, and Earth hydrogen) have more optimistic fractions ranging from 38% to 60% [13]. Pauly's methane-based ISPP options range between 34% and 44% [15]. With the exception of Rapp's estimates for an ISPP system using Martian water processing, all of these options require at least 1000 kg of power plant mass. Thus, an understanding of the sizing of surface power plants is necessary to understanding the total masses that must be landed and transported.

Aftergood's history of space nuclear power identifies the Systems for Nuclear Auxiliary Power (SNAP) program of 1955 as the beginning of American research efforts into deploying nuclear power in space [65]. Many of the subsequently deployed systems were RTGs; although one spacecraft, the 1965 Snapshot mission, did demonstrate 43 days of operation at 500 We. The Soviet space program deployed a number of reactors, although they also suffered several failed launches [65].

At the time of Aftergood's survey, the SP-100 reactor program, a "cornerstone" of American space nuclear efforts, was targeting the development of a 100 kWe reactor weighing between 3000 and 4600 kg [65]. The program was a joint effort of the

Department of Defense, Department of Energy, and NASA [66]. An update given in 1986 cited then-existing capabilities of 2600 kg for a 20 kWe reactor system and presented a value for a to-be-matured SP-100 technology of 2000 kg for a 30 kWe reactor system [67]. By 1992, however, cost overruns and changing requirements led to the Department of Defense canceling its funding for the SP-100 [68].

Multiple options have been proposed for implementing nuclear power on Mars (or in other space applications). Sandia National Laboratories surveyed different nuclear power concepts for power production in the range of 5 to 1000 kWe [69]. A brief description of each concept follows.

Out-of-Core Thermionic Reactors

A thermionic power system directly converts the heat radiated from a high-temperature source into electricity. An assembly of fuel plates and moderating graphite trays, further controlled by boron carbide and beryllium rods, serves as the heat source. According to the Sandia report, a 10 kWe assembly would be "approximately 26 cm in diameter and 48 cm long," and the "maximum core and surface temperatures are expected [during operation] to be approximately 2300 K and 2000 K, respectively." [69] The termionics would operate at about 1860 K, and would be cooled by a heat pipe radiator system operating at 1000 K. The overall efficiency of electrical production is estimated at approximately 12%. Figure 13, reproduced from the Sandia report, shows an example of the reactor system.

In-Core Thermionic Reactors

In-core systems utilize enclosed thermionic fuel elements, consisting of several stacked fuel/converter cells, as shown in Figure 14. Each cell consists of fuel and a thermionic conversion system, which is then cooled at the element level by a NaK coolant loop. The Sandia report describes several variations on the concept depending on the particular fuel used and the power level required. The efficiency of electrical production is estimated at 8.5% [69].

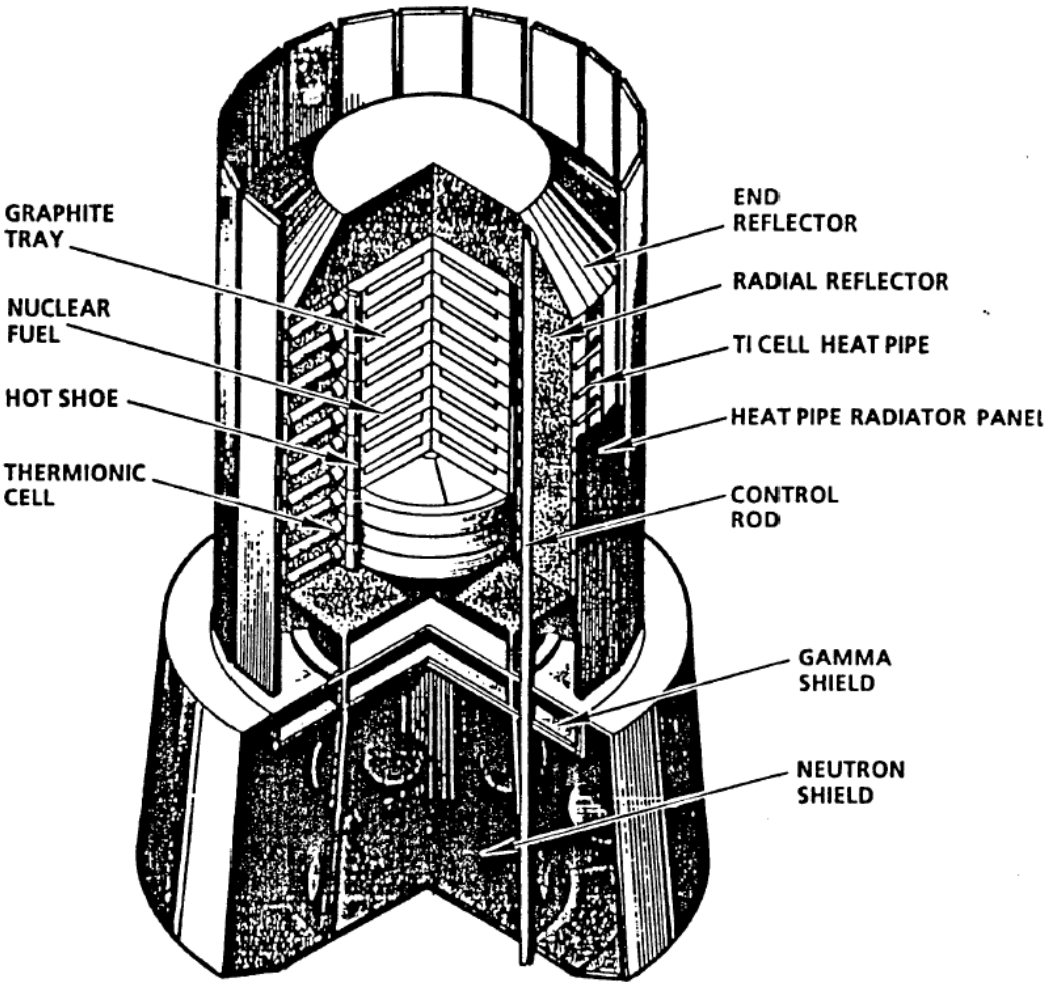

Figure 13: Out-of-Core Thermionic Reactor diagram [69].

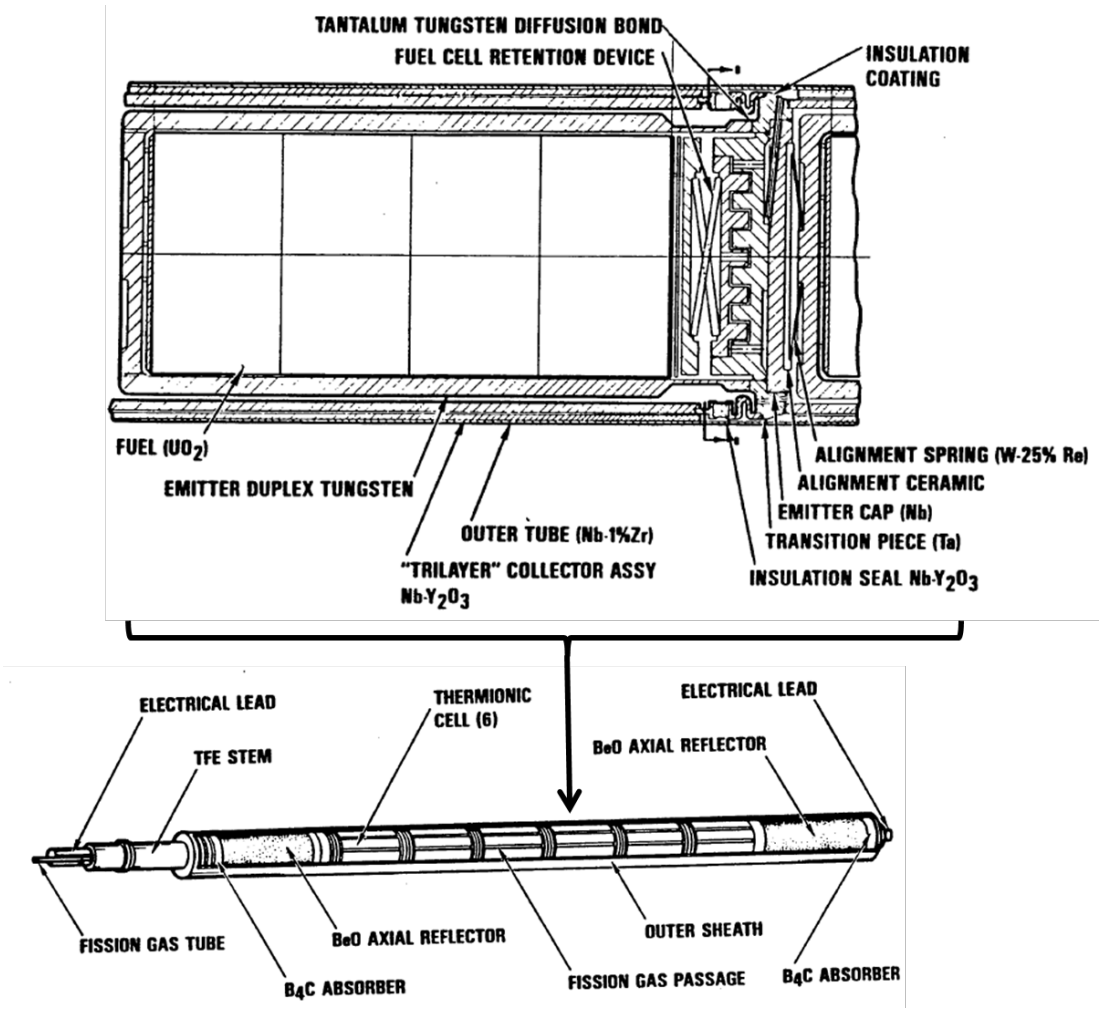

Figure 14: Thermionic fuel cell and fuel element [69].

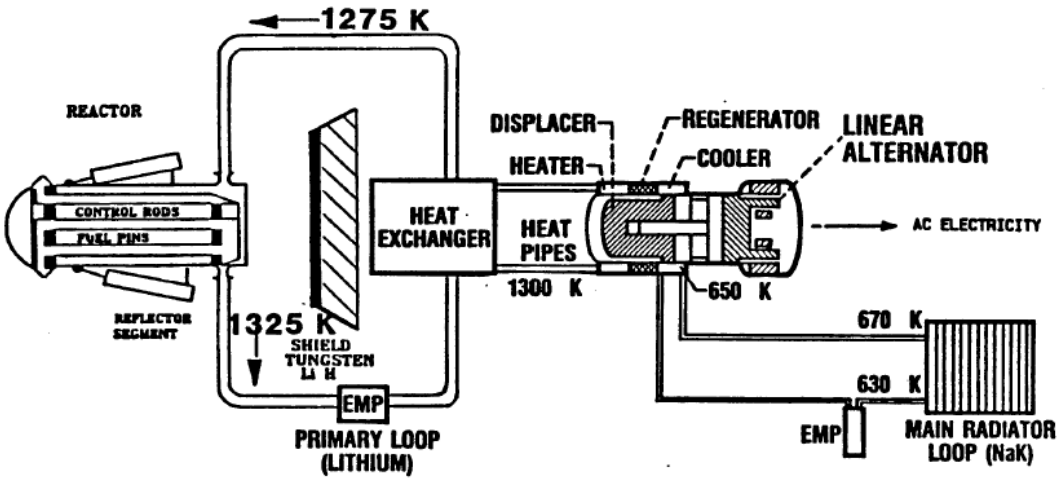

Figure 15: Stirling cycle power system linked with the SP-100 reactor [69].

SP-100 Derived Reactors

Several power systems are possible using the SP-100's fuel configuration as a heat source. The reference approach used in the SP-100 project uses multiple lithium coolant loops to transport heat from uranium nitride fuel pellets. The lithium coolant then passes through silicon germanium thermoelectric cells; these cells generate electricity from the heat carried in the flow using the Peltier-Seebeck effect. This effect, also referred to as the thermoelectric effect, is the creation of a voltage when two different metals are joined together are at different temperatures [70]. The waste heat is then rejected by radiators. The Sandia report estimates the efficiency at approximately 4%, but notes that "the system mass in the 100 kWe range is moderate, and no moving components are required for power conversion or fluid flow." [69]

Three additional approaches utilize the heat carried by the lithium coolant as the hot side of a power cycle. A Stirling engine system, using helium as the working fluid, could achieve 30% cycle efficiency but would require relatively cold (520 K to 620 K) output temperatures, thus requiring large radiators. A diagram of the Stirling power cycle is shown in Figure 15 [69].

A Rankine system would use an intermediate heat exchanger (heated by the

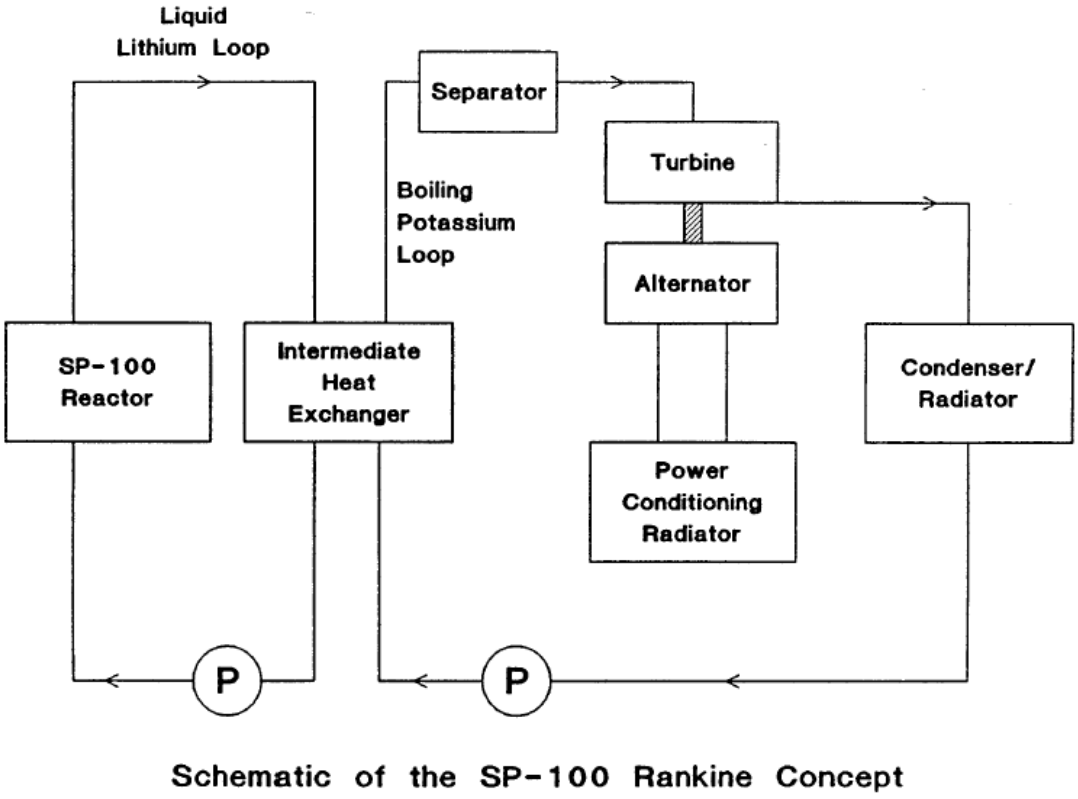

Figure 16: Rankine power cycle linked with the SP-100 reactor. For the corresponding Brayton cycle, the condenser would be replaced by a compressor on the same shaft as the turbine [69].

lithium coolant) to vaporize a potassium working fluid. The potassium vapor would be expanded through a turbine connected to a generator before being condensed. The condenser would then serve as the hot side of a radiator, while the fluid would be pumped to the lithium heat exchanger. Such a system, shown in Figure 16, might achieve an efficiency of about 22% [69].

A Brayton cycle would use the energy from the lithium coolant to heat a compressed helium-xenon gas. The high-temperature, high-pressure gas would be expanded through a turbine, which would drive both an alternator (to generate electricity) and a downstream compressor (to repressurize the working fluid before it returned to the lithium heat exchanger). The overall system would achieve an efficiency of about 22% [69]. The Brayton cycle is similar to the Rankine system in

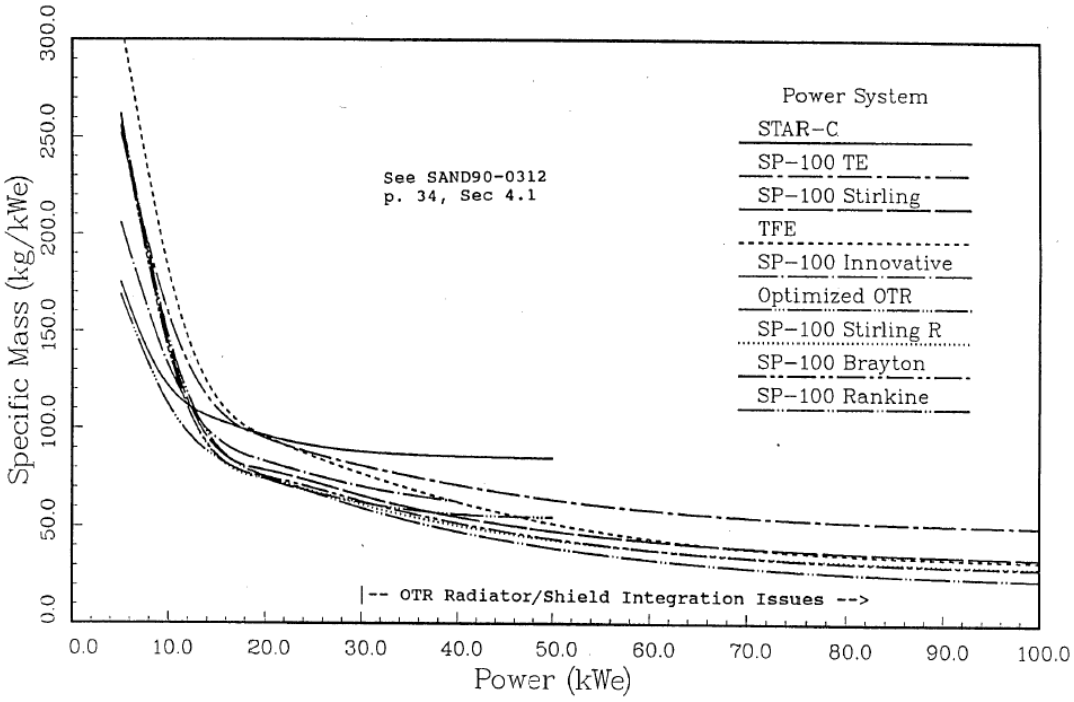

Figure 17: Specific mass estimates for nuclear power systems up to 100 kWe [69].

Figure 16, but with the condenser replaced by a compressor attached to the turbine shaft.

Together, these concepts can be grouped according to the power conversion systems that generate electricity from the heat generated by the nuclear fuel. The five types described in the Sandia report align with the five classes described in Mason's surveys of space nuclear power options: thermionics, thermoelectrics, Stirling, Rankine, and Brayton systems [71–73]. Both the Sandia report and Mason's papers present estimates of masses of the power system (typically consisting of the reactor itself and power conversion system, sometimes also including the power management and distribution and cabling hardware required for a complete system) at different power levels. These results are commonly reported in one of two ways: the mass itself, or the specific mass α, in kg/kWe. Figure 17 shows the Sandia estimates of specific mass for power levels up to 100 kWe [69]. Figure 18 shows Mason's assessment of specific mass for power levels between 10 kWe and 1000 kWe [73].

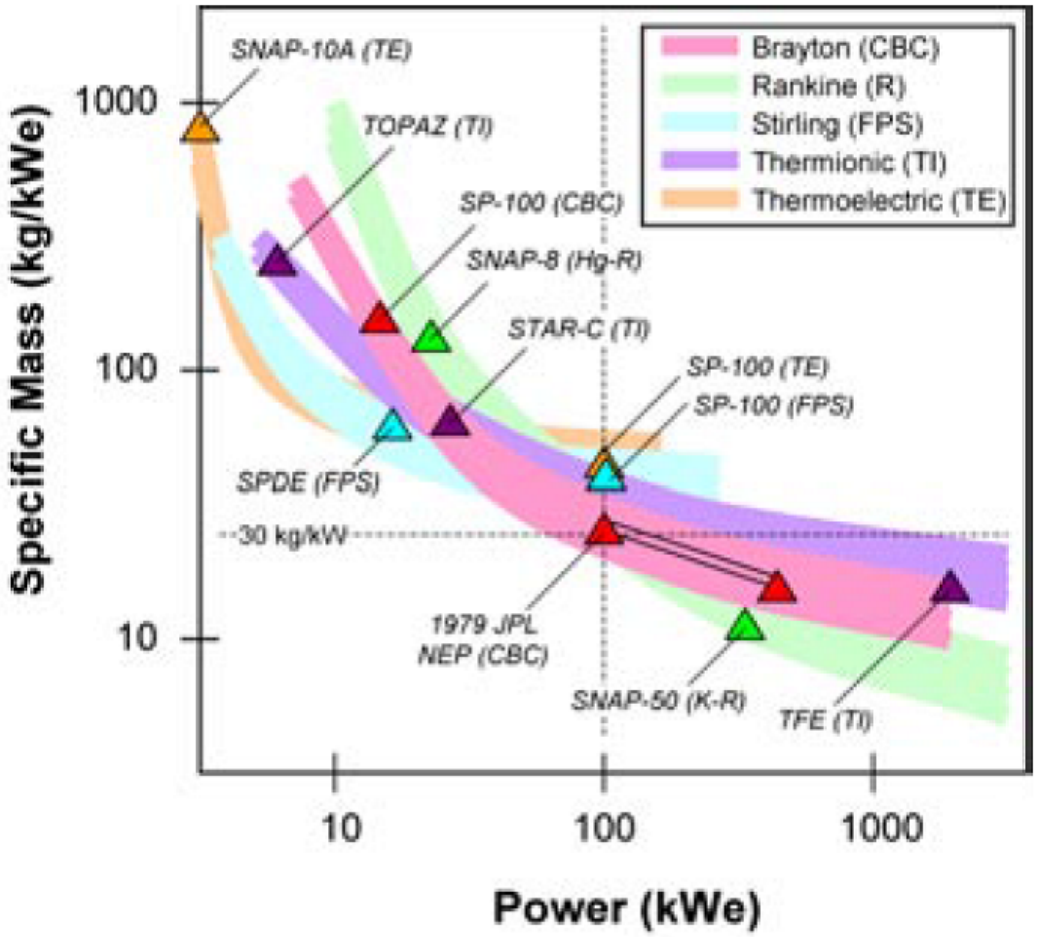

Figure 18: Specific mass estimates for nuclear power systems between 10 kWe and 1000 kWe [73].

In Figure 17, STAR-C and Optimized OTR correspond to the Out-of-Core Thermionic reactor concept. TFE is an In-Core Thermionic reactor. SP-100 TE and SP-100 Innovative refer to two thermoelectric concepts with the SP-100 system. SP-100 Stirling and SP-100 Stirling R refer to two metals used for the Stirling engine: a superalloy and a refractory metal, respectively. SP-100 Brayton and SP-100 Rankine refer to their corresponding power cycles, wrapped around the SP-100 reactor.

At power levels greater than 30 kWe, the SP-100 Rankine approach has the lowest system mass. Assuming a demand of 30 kWe (as estimated in DRA 5), the power system total mass would come to approximately 1800 kg, while a power system supplying 100 kWe would require approximately 2300 kg. At these power levels, the Brayton and Stirling R systems have almost identical masses (1900 kg and 2900 kg for 30 kWe and 100 kWe, respectively). The thermoelectric concept at 30 kWe and 100 kWe correspond to masses of 2400 kg and 5000 kg, while the preferred of the high power thermionic concepts (TFE) has masses of 2300 kg and 3200 kg, respectively. As specific masses, these values range from 23 kg/kWe (for a 100 kWe Rankine system) to 81 kg/kWe (for a 30 kWe thermoelectric system).

Figure 18 shows the results of Mason's survey of the five nuclear power types. In this report [73], the focus is on nuclear power systems for energizing a nuclear electric propulsion concept, yielding lower mass estimates than Mason's estimates for surface systems [72]. In Mason's survey, the Stirling concept performs best from 10 kWe to 70 kWe, after which the Brayton and Rankine cycles possess the lowest specific masses. Mason identifies 30 kg/kWe at 100 kWe as a key point for performance for the nuclear electric propulsion concept. This aligns with an estimate of 3000 kg for the power system, similar to the Sandia estimate for the Brayton cycle.

Mason's comparison of nuclear power systems for surface and in-space applications shows the surface systems having specific masses approximately three times greater

than in-space systems. Mason states that this results from the in-space power system's "reduced shielding, shorter cabling, and the shared radiator configuration" as compared to similar surface systems [72]. Thus, Mason gives a specific mass for a 100 kWe Brayton system as 74 kg/kWe (relative to the corresponding in-space system at 26 kg/kWe), with an advanced concept (utilizing higher radiator areal density, hotter temperatures, and higher voltages) having a specific mass of 42 kg/kWe. Another comparison of gas cooled and liquid metal cooled Brayton reactors by Mason gives specific masses for a 160 kWe reactor of 75 kg/kWe and 67 kg/kWe, respectively [71].

The most recent design effort of a space nuclear power system occured during the Jet Propulsion Lab an NASA's Prometheus Project, which set out to design a nuclear electric propulsion system capable of visiting Jupiter's moons. As a follow-on to that study to feed the 2005 Exploration Systems Architecture Study, part of the team analyzed developing a surface power system based on the technologies identified in the Prometheus Project. Their estimate for a 50 kWe power system, using Brayton conversion, for deployment to the moon was 6500 kg, for a specific mass of 130 kg/kWe [74].

By the time of the studies that fed DRA 5's surface nuclear power system design both lower power levels and higher specific masses were reported relative to earlier studies. The Mars architecture required a 30 kWe reactor, with specific masses ranging as high as 266 kg/kWe [1]; these values resulted from a decision in the space nuclear reactor sizing community to emphasize conservatism, simplicity, and robustness [75, 76]. Of note, the ISPP system corresponding to that power demand was based solely on producing oxidizer for the ascent vehicle, with methane brought from Earth and stored aboard the MAV.

As evidenced by the wide range of α for integrated nuclear power systems, shown in Figure 19 and Table 3, a significant uncertainty exists in the mass of the power source used for ISPP. Further, because of the high fraction of total ISPP mass represented

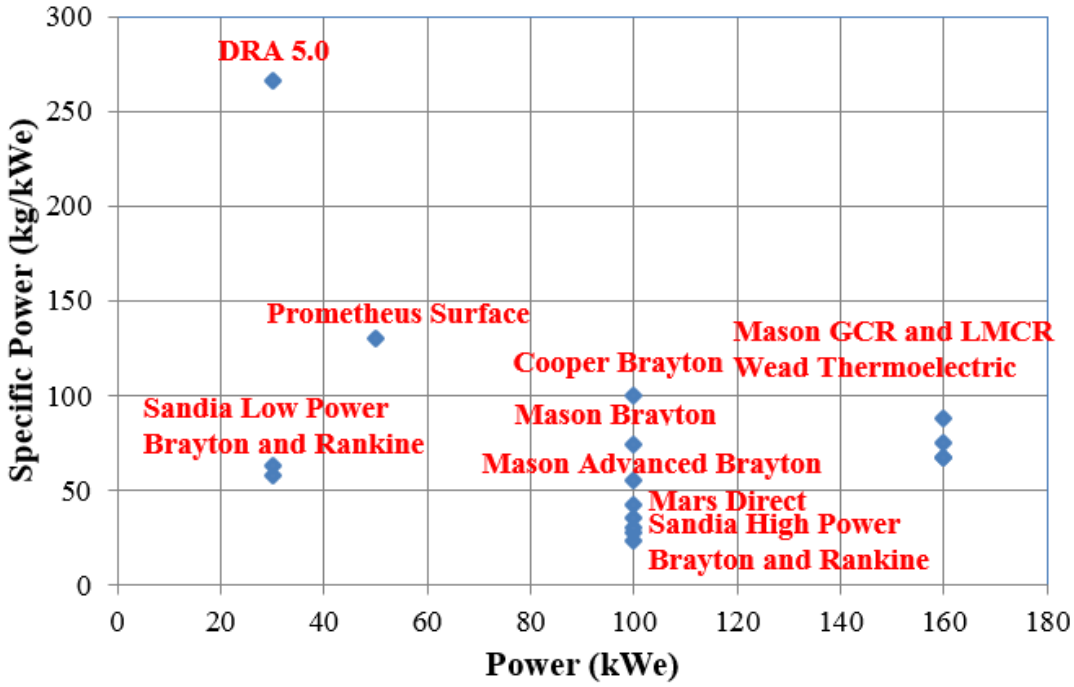

Figure 19: Specific mass and power levels for space nuclear power systems.

by the power system, this uncertainty can have a large impact on the trade between ISPP options. To understand the impact of power system mass on the ISPP system and associated architecture, each ISPP architecture was compared using different estimates of specific mass derived from above. Bounding values based on the high power Sandia estimates (23 kg/kWe) and the sizing in DRA 5 (266 kg/kWe) will bracket the best and worst case scenarios. This approach yields an understanding into the impact of the uncertainty in power system modeling and reveals the relative impact of power requirements on ISPP architectures as compared to the sizing of the ISPP systems and other transportation elements.

2.3.3 Evaluation of Solar Power for Mars

From the data shown in Tables 2 and 3, the domain of specific mass for solar (from 34 to 235 $\frac{kg}{kWe}$) and nuclear (from 23 to 266 $\frac{kg}{kWe}$) power systems are similar. However, the power requirement that is multiplied by α for solar power systems is impacted

Table 3: Nuclear Power System Performance

Source	**Power (kWe)**	α ($\frac{kg}{kWe}$)
Sandia High Power Rankine	100	23
Sandia High Power Brayton	100	28
Mason In-space Brayton	100	30
Mars Direct	100	35
Mason Advanced Brayton (Surface Power)	100	42
Cooper et al. Stirling	100	55
Sandia Low Power Rankine	30	58
Sandia Low Power Brayton	30	63
Mason Liquid Metal Cooled Reactor	160	75
Wead Thermoelectric (Low Bound)	160	67
Mason Brayton (Surface Power)	100	74
Mason Gas Cooled Reactor	160	75
Wead Thermoelectric (High Bound)	160	88
Cooper et al. Brayton	100	100
Prometheus (Surface Power)	50	130
DRA 5.0	30	266

by several non-ideal effects. Because solar power is only available during part of the day, either the ISPP system must be oversized (relative to a similar system powered by a nuclear system) to meet the demand while operating only during daylight, or the solar power system must be oversized to charge batteries and/or fuel cells for nighttime operation. Additionally, Martian dust has two compounding effects: it impacts the insolation that reaches the solar panels (thus requiring more area per unit power collected), and it can degrade the panels, further reducing their efficiency. Thus, the solar power system design power (which is multiplied by α for the system sizing) is greater than the required power (calculated from the ISPP analysis).

The following analysis evaluates the profile of available solar power at Mars throughout the year as a function of the factors described above. It includes a comparison of two approaches to providing sufficient power for a reference ISPP power requirement, a sensitivity analysis of key parameters of those approaches, and an evaluation of the impact of technological improvements. The nomenclature of the model of available solar power, as well as the data on the effects of atmospheric opacity based on zenith angle and time of year, are drawn from Appelbaum and Floods review of solar power for the Viking landers [47].

At any time, the solar flux incident on a flat panel depends on four variables: latitude λ, areocentric longitude (a measure of Mars's position in its orbit of the sun) L_s, hour angle (a measure of the time of day on Mars) ω, and optical clarity (a measure of the impact of dust in blocking or scattering light) τ. In Appelbaum and Flood, τ has a dependency on L_s based on the effects seen at Viking 1's location; for simplicity, that data is used here [47]. The latitude used in this analysis is 30 degrees, based on proposed landing sites in DRA 5.0 [1].

The solar flux at the top of the Martian atmosphere G varies about the mean value G_0 throughout the year according to Equation 8. The eccentricity e of Mars is 0.093377, and the reference longitude L_{s0} is 248 degrees [47]. The solar zenith angle

z is computed via Equation 9, with the declination angle δ computed in Equation 10. The axial tilt of Mars δ_0 is 24.936 degrees [47]. Combining these equations yields the irradiance on a flat panel at the Martian surface G_s, given in Equation 11. An empirical factor that captures the impact of optical clarity and zenith angle, given in Appelbaum and Flood, is $f(z, \tau)$ [47].

$$G = G_0 * \frac{(1 + e * cos(L_s - L_{s0}))^2}{(1 - e^2)^2} \tag{8}$$

$$cos(z) = sin(\lambda) * sin(\delta) + cos(\lambda) * cos(\delta) * cos(\omega) \tag{9}$$

$$sin(\delta) = sin(L_s) + sin(\delta_0) \tag{10}$$

$$G_s = G * cos(z) * f(z, \tau) \tag{11}$$

The energy collected over the course of a particular Martian day is based on the integration of the surface flux G_s, modified by the efficiency of the solar panel in converting incident flux to usable power (η_{cell}) and the cell's degradation from its beginning of life to end of life (η_{EOL}), and is referred to as the insolation H (in units of $\frac{We-hr}{m^2-day}$); see Equation 12. The daily energy collected $E_{collect}$ is then the product of the insolation and the solar panel area A_{solar}, as in Equation 13. Nominal values for the cell efficiency (0.29) and end of life efficiency (0.9) are taken from DRA 5.0; sensitivities of mass to these parameters are evaluated below. The choice of the solar panel area thus determine whether the energy collected meets the energy required.

$$H = \int_{\omega=0}^{\omega=360} G_s * \eta_{cell} * \eta_{EOL} d\omega \tag{12}$$

$$E_{collect} = H * A_{solar} \tag{13}$$

Two approaches were considered for calculating the energy requirements. In the first, the nighttime power requirement P_{night} and duration ω_{night} are used to estimate the energy that will need to be used during nighttime E_{night}, modified by the efficiency of storing energy in a battery or fuel cell system (known as the coulombic or Faraday

efficiency $\eta_{storage}$); see Equation 14. The nominal value for the storage efficiency was 0.5, taken from DRA 5.0; a sensitivity of system mass to that parameter is evaluated below. That energy, added to the energy needed during the day E_{day} (see Equation 15), determine the total energy that must be collected during the daytime $E_{require}$ (see Equation 16). By dividing that requirement by the minimum daily insolation (MDI) during the year H_{min}, the maximum required area A_{max} is computed in Equation 17. That area is then used for sizing as described below.

$$E_{night} = P_{night} * \omega_{night} * \eta_{storage} \tag{14}$$

$$E_{day} = P_{day} * \omega_{day} \tag{15}$$

$$E_{require} = E_{day} + E_{night} \tag{16}$$

$$A_{max} = \frac{E_{require}}{H_{min}} \tag{17}$$

The other approach includes the sizing in the determination of the area of the solar panel. Rather than size the area to provide power to match the minimum insolation (with excess capability on days with better insolation), the energy storage system can instead be sized to make up power requirements on days with lower insolation, leading to smaller arrays but larger power storage. To determine the minimal area required to facilitate using energy storage to supplement daytime power needs, the mass of the combined array and storage system is used as an objective function to be minimized by choice of area. For each day in the Martian year, the energy to be collected depends on the available insolation on the next day and the energy storage system's capacity. Thus, an iterative calculation is used to converge on the minimum area that supplies sufficient energy on all days of the year. In this research, a numerical integration of the insolation throughout both the day and the year (Equation 12) was used along with the sizing model below to compute the combined system mass; the minimum area was then iteratively computed for a given latitude, power requirement, and system technology.

The mass model used is based on the data in Kerslake and Kohout's system sizing for a Mars surface solar power system (see Table 1). In that model, the mass of the membrane containing the cells themselves, "encapsulant, adhesive, cell contacts and interconnects, and substrate" was given as 0.2 $\frac{kg}{m^2}$ of array area [59]. The "launch containment structures, deployment structures, and/or inflation/rigidization equipment", collectively the array structure mass, was given as 0.8 $\frac{kg}{m^2}$ of array area [59]. Associated system masses were sized based on the peak power requirement: the array regulator unit (2.5 $\frac{kg}{kWe}$), direct current switcing unit (8 $\frac{kg}{kWe}$), remote power control (0.6 $\frac{kg}{kWe}$), and output panels (0.6 $\frac{kg}{kWe}$ [59]. Equation 18 gives the mass M_{solar} for the solar power system as a function of the peak power P_{peak} (in kWe) and area A_{solar} (in m^2). The energy storage system, a fuel cell, was sized using a linear regression fit through fuel cell system masses sized for deployment on top of the lunar lander during the Lunar Surface Systems study [77]. The regression is given in Equation 19; E_{store} is the amount of energy to be stored (in We-hr) and M_{store} is the mass of the storage system (in kg). The objective function in the iterative approach described above is the sum of the masses M_{solar} and M_{store}.

$$M_{solar} = (0.2 + 0.8) * A_{solar} + (2.5 + 8 + 0.6 + 0.6) * P_{peak} \tag{18}$$

$$M_{store} = 1838 + 0.001429 * E_{store} \tag{19}$$

The two approaches described were evaluated using two test ISPP power requirements. In one case, the ISPP system operated during an 8 hour daytime at a power requirement of 89.3 kWe, while non-operational power requirements derived from DRA 5.0 provided the 16 hour nightime power requirement of 19.0 kWe. In the second case, the ISPP system was operated continuously, with the energy storage system sized to accommodate the constant power requirement of 32.4 kWe [10]. The lower power requirement for continuous operation derives from the smaller, less power intensive ISPP system needed to produce the required propellant load over the longer

Table 4: Solar Power System and Energy Storage Masses

Power Requirement	**Approach**	M_{solar}	M_{store}	**Total Mass**
Day 89.3, Night 19.0	MDI	7616	2707	10323
Day 89.3, Night 19.0	Iterative	7805	3007	10812
Day 32.4, Night 32.4	MDI	6816	3319	10135
Day 32.4, Night 32.4	Iterative	6338	3369	9707

time.

The masses M_{solar} and M_{store} for the two power requirements, using the two approaches, are given in Table 4. The power requirements are given in kWe, while the masses are in kg. For the 8 hour daytime operation requirement, the iterative approach implementation of an oversized energy storage system to provide make up power leads to increases in both masses relative to the MDI approach, yielding the highest mass approach of the four options. At the lower power requirement of the continuous operation requirement, the iterative approach energy storage system requirements grow the storage system only slightly, and the savings from the smaller arrays relative to the MDI leads to the lowest total mass of the four options. For all options, the daily insolation H, flux at the top of the atmosphere G, and optical clarity τ are plotted as a function of areocentric longitude L_s in Figure 20. The changes in daily insolation track the variation in optical clarity much more closely than the gradual oscillation of flux.

The values of η_{cell} and $\eta_{storage}$ depend on the technology deployed at Mars, while η_{EOL} depends on both technical capabilities as well as environmental effects. To understand the impact of these efficiencies, the two iterative cases above were run with alternate values of each parameter, and the resulting total mass was plotted against that parameter. For the cell efficiency, the high value of 0.379 was taken from a record set by Sharp in their design of triple-junction, non-concentrator solar cell efficiency [78], while a low value of 0.19 was taken from Bailey and Raffaelle's

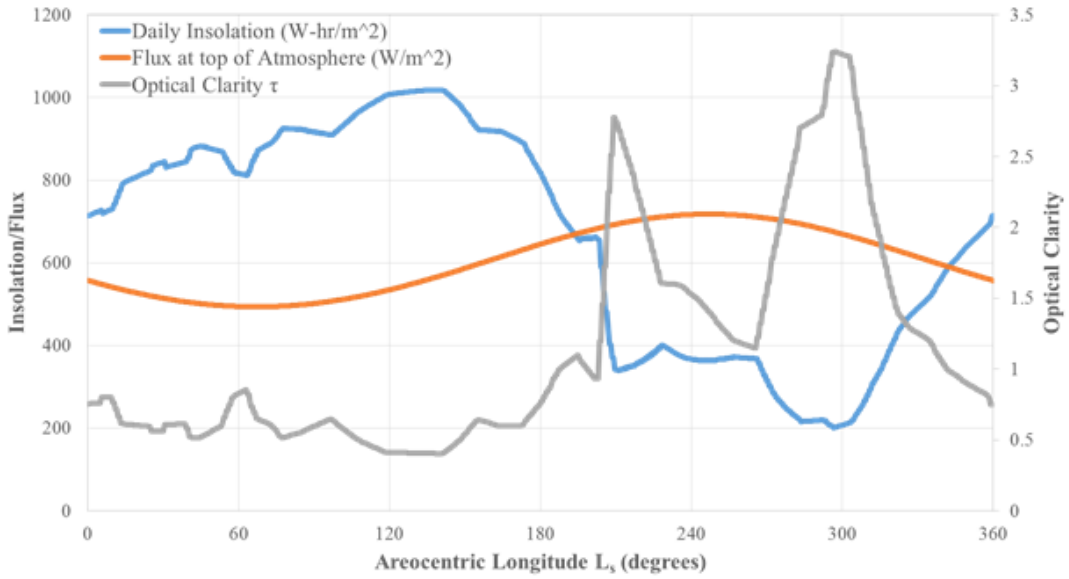

Figure 20: Daily Insolation, Flux at Top of the Martian Atmosphere, and Optical Clarity throughout the Martian Year.

survey of conventional solar panels [64]. For the coulombic efficiency, a high value of 0.9 was taken from Larson and Wertz's discussion of energy storage technology [79] and a low value of 0.4 was taken from the Department of Energy's summary of fuel cell technologies [80]. For the degradation effect, the 0.9 assumed in DRA 5.0 is used as a high value [10], while lower values of 0.78 and 0.11 were taken from Landis's analysis [54].

Figures 21, 22, and 23 show the results of these sensitivities. The 8 hour operation and 24 hour operation cases are shown. The energy storage efficiency has a smaller variation in mass (and thus α) than the other two parameters, as the energy storage system is less than 40% of the total mass across all the points shown in the figure. At the worst case degradation, the mass grows to as much as 6 times that at lower values of degradation; thus there is a need for a technology that mitigates the degradation caused by environmental factors. Among all 18 plotted points, the minimum total system mass is 7987 kg, with a corresponding α of 247 $\frac{kg}{kWe}$, and a required area of 4952 m^2.

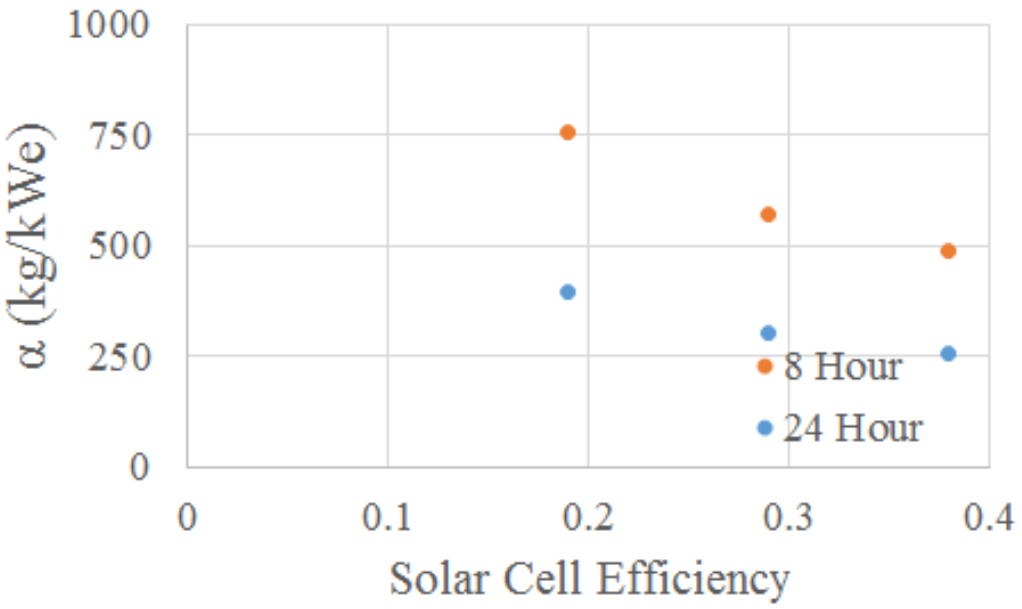

Figure 21: Sensitivities of α for 8 hour and 24 hour operation to η_{cell}.

Table 5: Solar and Nuclear Power Comparison

Power Requirement	**Approach**	**Total Mass**
Day 89.3, Night 19.0	Solar	9230
Day 32.4, Night 32.4	Solar	7987
Day 32.4, Night 32.4	Nuclear (α = 23 kg/kWe)	745
Day 32.4, Night 32.4	Nuclear (α = 266 kg/kWe)	8618

This α, calculated using the real, non-ideal effects that would exist on Mars, is greater than that of the solar power systems discussed in Table 2 and most of those for nuclear power systems (Table 3); thus, a solar power system requires more mass than all but the most conservative estimates of a nuclear system, in addition to the requirement to deploy and clean thousands of square meters of array. For comparison, Table 5 shows the masses of the minimal mass solar power systems from the above sensitivity, as well as the masses of nuclear power systems using the best and worst values of α from Table 3. Therefore, for the power systems considered in the rest of this research, only nuclear power systems are considered.

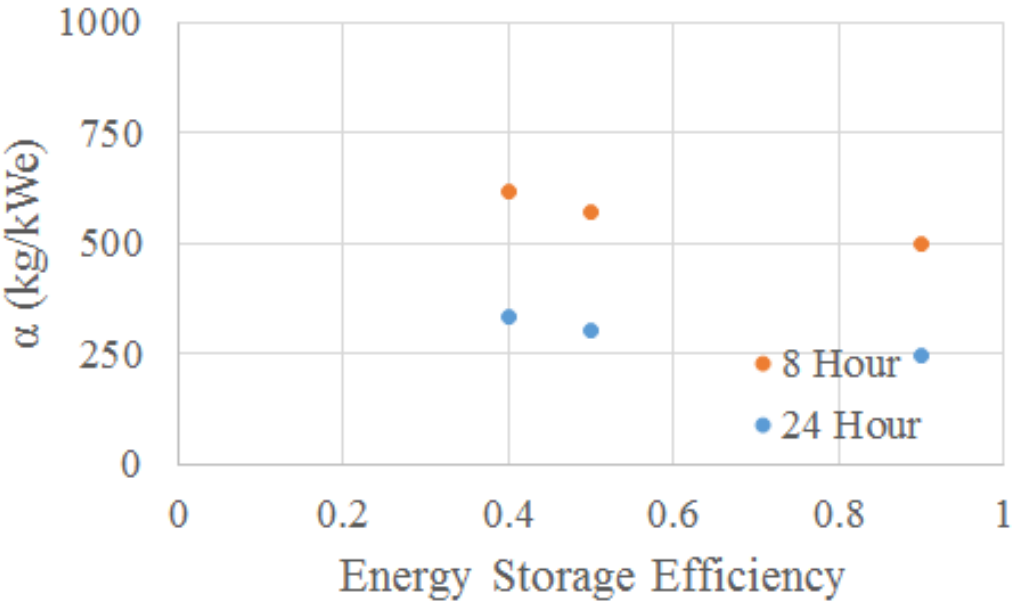

Figure 22: Sensitivities of α for 8 hour and 24 hour operation to $\eta_{storage}$.

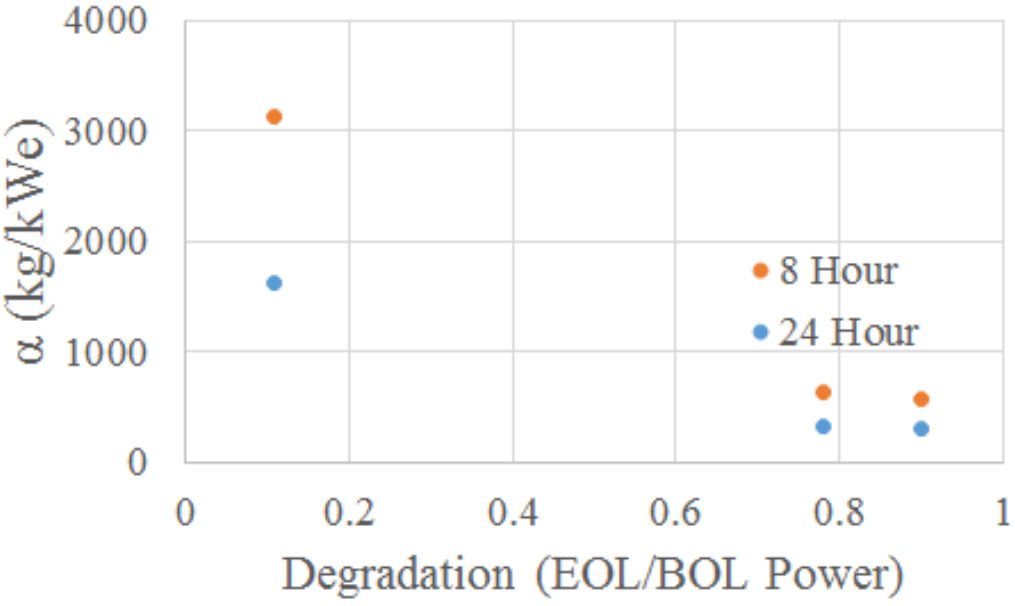

Figure 23: Sensitivities of α for 8 hour and 24 hour operation to η_{EOL}.

Human Exploration Of Mars

ISRU Propellants (Oxidizer)	Figure of Merit	No ISRU Propellants
Lower Mass: 54 mT	DAV Landed Mass	Higher Mass: ~79 mT
~ 820 mT (Nuclear); ~1250 mT (Chem.)	IMLEO Mass for 1 mission	~910 mT (Nuclear); 1420 mT (Chem.)
9 (Nuclear); 12 (Chemical)	Number of Ares V Launches Per Mission (125 MT Launch System)	10 (Nuclear); 14 (Chemical)
More	Power Required	Less
More complex operations and infrastructure; surface rendezvous required for abort to orbit	Complexity of Surface Operations	Less Complex operations; no surface rendezvous required for abort to orbit
Greater Flexibility do to the ability to produce more fuel for roving/hopping/EVA	Mission Flexibility (contingency re-planning)	Less Flexibility
Advantage	PLOM	Slightly higher risk attributed to more launches and higher IMLEO
No discriminator	Cost Through First Mission	No discriminator
Advantage	Cost Through Third Mission	Disadvantage

Figure 24: Figures of Merit for ISPP use in DRA 5.0

2.4 Cost

Previous studies of ISPP use have primarily focused on either landed mass on Mars or IMLEO as the figure of merit in choosing whether a particular ISPP approach is worthwhile [9, 12–14]. In the latest Mars reference architecture [1], several figures of merit were considered; however, the level of fidelity for those other than mass was limited, as shown in Figure 24. While mass and number of launches were quantified, other concerns such as flexibility, complexity, and cost were presented only on a qualitative basis. Such an approach allows for an initial understanding of the benefits of ISPP, but does not fully capture the trade; the increased operational complexity and development costs required to implement such a system are neglected.

One method to determine whether or not a particular technology is worth including in an architecture is to determine if the benefits of developing and implementing that technology exceed the costs (economic and other) of so doing [81]. The benefits may include better performance, lower mass, and increased reliability, while the costs could include greater complexity and increased development or production costs. As

each of these aspects is quantified differently, the selection among technologies requires either a way to balance the competing tensions of all of these metrics, or a way to compare them by a single figure of merit.

In this research, the latter approach is taken, with cost as the basic figure of merit used to evaluate both benefits and drawbacks. Improvements in performance and reductions in mass translate into cost savings, while the effects of new technologies and more complex systems translate into cost increases. Each mission approach considered in this study aims to satisfy the same mission requirements [1, 82], so such a comparison will make it possible to select the technologies that lead to the lowest cost.

To fully evaluate the impact of developing and implementing different ISRU approaches for propellant production, the considered costs must include those required to mature and build the relevant systems that replace the propellant brought along in a non-ISRU approach, as well as any operations and production costs. Further, the changes in design of the MAV will impact the cost of that system, and must be incorporated. Finally, the other architectural elements that are impacted by the use of an ISRU system (such as the transfer vehicles delivering the mass to Mars) must be modeled and costed. All of these costs together comprise the life cycle cost of an architecture, from initial design, development, testing, and evaluation (DDT&E) to production, launch, and operation [83].

Depending on the technological maturity of different ISRU systems, and particularly as compared to a non-ISRU approach, such systems might become ready for deployment at different times. To address this temporal element, the costs being compared should be resolved into their present worth. Net present value (NPV) is an approach that allows for an equitable comparison of options [84]. NPV is defined as the difference in the present value of benefits and the present value of costs. In this research, the benefits will have been previously translated into cost savings; hence,

the selected technology will be that which has the minimal present value of its life cycle cost.

The present value PV is calculated from the future value FV (that is, the value that a given item will have at a particular time in the future), the difference in years between the present and that future date n, and the nominal discount rate i (equal to the sum of the inflation rate and the real discount rate) [85], as shown in Equation 20. For this analysis, the future values include the DDT&E costs, the hardware production costs, launch costs, and operations cost during the mission. Each of these costs is incurred at different times; hence, the individual present values are computed and then summed for the net present value of the life cycle cost of an architecture.

$$PV = FV * (1 + i)^{-n} \tag{20}$$

Although many variables impact system performance and cost, not all variables have equal impact [86]. It is thus important to identify the variables that have the greatest impact on cost, as those are the ones that must be considered in sensitivity analyses and technology forecasting [86]. In particular, the uncertainty inherent in modeling new technologies and their impact on an architecture requires additional analysis beyond the straightforward modeling described above. Monte Carlo methods have been used to examine the impact of cost uncertainty in space system design [87].

2.5 Epistemic Uncertainty in Modeling

Consider a system sizing model, such as that shown in Figure 25. This model takes as input two vectors $\mathbf{x}$ and $\mathbf{k}$, and returns an output vector $\mathbf{y}$. The vector $\mathbf{x}$ contains the design variables that are independent of the model, while the vector $\mathbf{k}$ represents the model parameters that map a particular input vector $\mathbf{x}$ to a particular vector of outputs values $\mathbf{y}$. Thus,

$$\mathbf{y} = f(\mathbf{x}, \mathbf{k}) \tag{21}$$

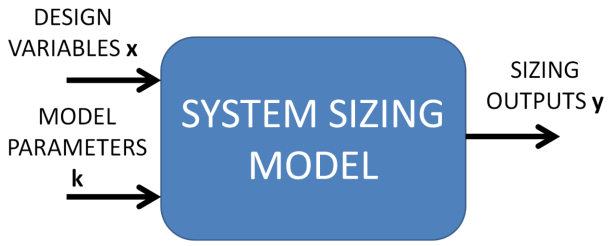

Figure 25: General system sizing model.

and the system sizing model is the set of relations contained in f that map **x** and **k** to **y**.

As an example, consider a simple sizing model for a power plant. In this model, the mass of the power plant system is a linear function of the power requirement, while the volume is a quadratic function of the power requirement. The equations modeling such a system would be of the form:

$$Mass = a * Power + b \tag{22}$$

$$Volume = c * Power^2 + d * Power + e \tag{23}$$

where the constants a, b, c, d, and e would depend on the technology of the particular power plant in question. Then the design variable vector **x** is a one element vector consisting solely of the power requirement; the model parameter vector **k** is a five element vector consisting of a through e; and the output vector **y** is a two element vector consisting of the *mass* and the *volume*.

Let a *deterministic* sizing model be one for which the values of each element in **k** are known and fixed. Thus, **y** maps to a single vector of values given a particular **x**. For such a model, two kinds of optimization problem can be defined: single-objective and multi-objective. In a single-objective optimization problem, the goal is to minimize or maximize one member y_i of the output vector **y**. To do this, the particular instance x_j of the design variable vector **x** must be found that achieves the required minimization or maximization. Numerous techniques are available to solve this problem [88].

In a multi-objective optimization problem, the goal is to minimize or maximize each of multiple members of $\mathbf{y}$. In the non-trivial case, the design vector x_j that does this for one y_i will not do so for all of the other y_m (m $\neq$ i). Thus, it becomes necessary to apply a method that addresses the competing design tensions of each member of $\mathbf{y}$. Several methods have been proposed for doing so [89].

An additional layer of complexity is added when constraints on the elements of $\mathbf{x}$ are added. These traditionally take the form of equality constraints and inequality constraints, shown in Equations 24 and 25. When the values of the design variables are constrained, modifications must be made to unconstrained methods in both the single and multi-objective optimization problems [88, 89].

$$g(\mathbf{x}) < \mathbf{0} \tag{24}$$

$$h(\mathbf{x}) = \mathbf{0} \tag{25}$$

Throughout all the variations of optimization problems described above, the model has been assumed to be a constant; that is, $\mathbf{k}$ has not varied. For well understood systems, this may be a reasonable assumption; however, less technologically mature concepts have inherent uncertainty in their modeling. Thus, $\mathbf{k}$ can no longer be considered a fixed vector; rather, there exists a distribution of possible values for each k_i.

A *stochastic* model, then, is one where the elements of $\mathbf{k}$ are not fixed. Thus, it is insufficient to state that a single output $\mathbf{y}$ results from a particular input $\mathbf{x}$. In their discussion of decision making under uncertainty, and the application of stochastic models, Bertsimas and Thiele remark that "[p]oint foreccasts are meaningless (because they are always wrong) and should be replaced by range forecasts." Cox and Siebert observe that "A statement of the result of a measurement is only complete if it provides an estimate of the quantity concerned (often known as the measurand) and a quantitative measure of the reliability of that estimate, namely, the uncertainty

associated with it [90]". In the absence of certainty in all of the inputs and parameters of a model, the model's outputs cannot be given as a single value.

The Monte Carlo method offers a technique for evaluating the impact of the unfixed elements of **k**. Durga Rao et al. note that sampling methods such as the Monte Carlo method are one approach to addressing epistemic uncertainty, remarking on its use as "current practice [...] to propagate epistemic uncertainties [91]". Evaluation of the model involves sampling values of each k_i from probability distributions. By repeating this process and evaluating the model many times, a range of values of **y** can be generated. Through Cox and Siebert's analysis of Monte Carlo methods, they show that the combination of a model and distributions on the inputs will yield a distribution of outputs; this can be used to characterize the uncertainty of those outputs [90].

Wübbeler et al. show that "if a quantity is known to lie within an interval (and no further information is given), a uniform PDF [probability density function] would be assigned [92];" for the selection of distributions for model parameters with sparsely known information (as occurs in modeling advanced technologies), a uniform distribution can be used. The Monte Carlo approach also addresses issues related to non-linear models, while permitting the numerical combination of multiple sources of uncertainty [93]. Ferson and Ginzburg state that for addressing epistemic uncertainty (that is, about the parameters of the model), interval analysis is appropriate [94].

Roy and Oberkampf observe that a combinatorial approach to interval analysis for evaluating epistemic uncertainty can require "extraordinarily large" numbers of samples when the number of parameters to be evaluated becomes more than "a handful" [95]. In their sample problem, they use uniform distributions of their epistemically uncertain parameter in the course of evaluating the combined effects of epistemic and aleatory uncertainty. This research adopts that same method (the use of uniform distributions for modeling epistemic uncertainty), although it omits

the modeling of aleatory uncertainty. Hofer et al. also uses Monte Carlo sampling for studying the epistemic uncertainty in model parameters, via a two-stage nested Monte Carlo simulation to capture the epistemic and aleatory effects [96]. Hofer et al. conclude "that an epistemic uncertainty analysis [...] can easily be performed on the basis of a Monte Carlo simulation with a moderate sample size independent of the number of epistemic uncertainties involved." A related approach is described in Tammineni et al., wherein Monte Carlo simulation of a cost model, and evaluation of cumulative distribution function (CDF) of the resulting outputs, is used in the conceptual decision making process [97]; this research also operates in the conceptual decision making domain.

Chen et al. propose a method that combines response surface modeling and a multiobjective optimization referred to as the compromise decision support problem to identify solutions that minimize variations in both epistemic and alleatory parameters [98]. This approach is shown to be useful for problems where the objective is to minimize deviation from targeted means of a process. The approach uses a quadratic response surface model of a process as the operating function for the decision support problem; this response surface model mitigates the computational expense of the original problem. Chen et al. observe that their method is applicable when a second order model is sufficiently accurate over the variable range of interest, and when the statistical distribution of the variation is normal. The approach used in this research is not so computationally expensive that a response surface model is necessary to permit many evaluations. The uncertainty around the parameters examined in this research and their statistical distribution (uniform distributions between lower and upper bounds are used due to the lack of knowledge necessary to formulate normal distributions) preclude the application of Chen et al.'s method.

The compromise decision support problem, as proposed by Mistree et al., reformulates multiple objective functions into goals: deviations from target values of each

objective, with a new single objective function (called the achievement function) being the minimization of the combination of the deviations [99]. This approach allows for single objective function optimization techniques to be applied. This approach is particularly suited to problems where target values exist for each objective, or where Simon's satisficing (a solution that sufficiently satisfies all figures of merit, even if it is not optimal [100]) is sufficient [101]. In this research, a single objective is used for evaluation (the net present value of the life cycle cost of each architecture), and is being minimized; there is not a target value from which to deviate. Mistree et al.'s method would facilitate evaluation of deviation from a nominal design of an architecture (especially with multiple goals being considered), and could be applied to a subsequent analysis wherein the objective function was a minimization of those deviations, rather than the minimization of a figure of merit.

Du and Chen propose two alternatives to Monte Carlo simulation to reduce computational expense: system uncertainty analysis and concurrent sub-system uncertainty analysis [102]. Both techniques allow evaluation of means and variances of performance distributions, with fewer model evaluations that all-in-one system level analysis. The models in this research are not computationally expensive; thus, Du and Chen's techniques do not provide significant savings in the time required to generate results in this research. However, for more detailed analysis of ISPP systems (e.g. analysis of coupled thermal and electric behavior, as discussed in Du and Chen), their techniques may facilitate more rapid calculation.

Schultz et al. use CDFs to characterize the risk profiles of alternatives in a decision making process under uncertainty [103]. They observe that in comparing CDFs, the choice of risk posture impacts the calculation of utility for each alternative. They propose the calculation of utility scores to evaluate each alternative; the normalized relative robustness integral used in Section 4.4 is isomorphic to their approach. A risk-neutral posture gives equal weighting to all probabilities between 0 and 1 on the

CDF, and allows for the application of the method described in Section 3.6.

The approach used in this research models the epistemically uncertain parameters with uniform distributions, as in Roy and Oberkampf's work, and samples from those distributions to evaluate models of each ISPP architecture. This results in a set of values of each figure of merit, which can then be collected into CDFs. These CDFs describe the fraction of samples that are less than or equal to particular values of each figure of merit. Because the approach taken in this research only samples from the distribution, rather than exploring the combinatorial range of lower and upper bounds of each parameter (a similar limitation to that described by Roy and Oberkampf), the lowest and highest values of the figure of merit do not necessarily correspond to the minimum and maximum possible values that can be attained by the model.

Thus, this approach may understate the range of each ISPP architectures figures of merit; this is a limitation of the proposed technique. However, this research is concerned with the relative, rather than absolute, values of the figures of merit across ISPP architectures. As this approach is applied uniformly across each ISPP architectures, it is assumed that the impact of not capturing the extremes of a figure of merit does not contribute to the relative comparison of each architecture. The application of this approach is described in Section 3.6, while potential avenues to explore the impact of these limitations and assumptions are described in Section 5.2.1.

The CDFs of figures of merit resulting from distributions on each epistemically uncertain parameter are used in this research to evaluate the relative sensitivity of those figures of merit. This approach is related to one-at-a-time sensitivity analysis methods as described by Hamby, where the effect on model outputs is examined for each variable at lower and upper bounds while holding all other variables at nominal values [104]. Hamby shows that one-at-a-time methods generally result in similar rankings of parameter sensitivity as more computationally expensive methods. Chen et al. present a method for an analysis of variance (ANOVA) approach applied to

global sensitivity analysis that uses metamodels to facilitate analytic estimates of uncertainty [105]. The approach in this research is more computationally expensive than Hamby's technique, as Monte Carlo simulations are applied while executing the one-at-a-time sensitivity analysis, rather than only examining evaluations at the lower and upper bounds. However, it is still tractable via Monte Carlo analysis. Further, as the analysis in Section 4.4 uses distributions for all model parameters, the formulation of the computational models is conducive to allowing for Monte Carlo simulation for either individual or multiple parameter variations. Thus, a hybrid technique that uses simulation to perform one-at-a-time analysis similar to that described by Hamby is used to estimate the lower and upper bounds of the figure of merit as each parameter is varied. The resulting "tornado" diagrams in Section 4.2 are a typical form of presenting the results of sensitivity analysis (Parnell et al. describe their use in decision analysis [106]), albeit with a plotting of the absolute value of the difference between high and low values rather than showing the actual high and low values.

CHAPTER III

MODELING

3.1 ISPP Process Models

The ISPP processes considered in this research follow the form shown in Figure 26. Local resources, acquired via a system brought from Earth, may be combined with imported resources in a reaction that produces fuel and byproducts. The fuel is separated and stored aboard the MAV, while the byproducts are further processed to yield oxidizer, that is stored aboard the MAV, and other products. Some of these products can be recycled back into the system, while waste products are typically vented or otherwise discarded.

3.1.1 Methane

Each of the four fuel types, and each of the approaches to acquiring the requisite hydrogen, maps to an instantiation of the above process. Figure 27 shows the process for combining hydrogen imported from Earth with local atmospheric carbon dioxide to yield methane and oxygen for the MAV. The Sabatier reaction yields methane and water as products; the methane is liquified and stored, while the water is electrolyzed to yield hydrogen and oxygen. The oxygen is liquified and stored, while the hydrogen is recycled back into the Sabatier reaction. In this process, each kilogram of hydrogen yields approximately 4 kilograms of methane and 8 kilograms of oxygen, which results in an O/F ratio of 2.

Because the methane and oxygen propellant combination performs best at O/F ratios greater than 2, a secondary process is needed to produce the additional required oxygen. For options based on using water from either Earth or Mars, the electrolysis of water that produces the requisite hydrogen also produces enough oxygen to reach

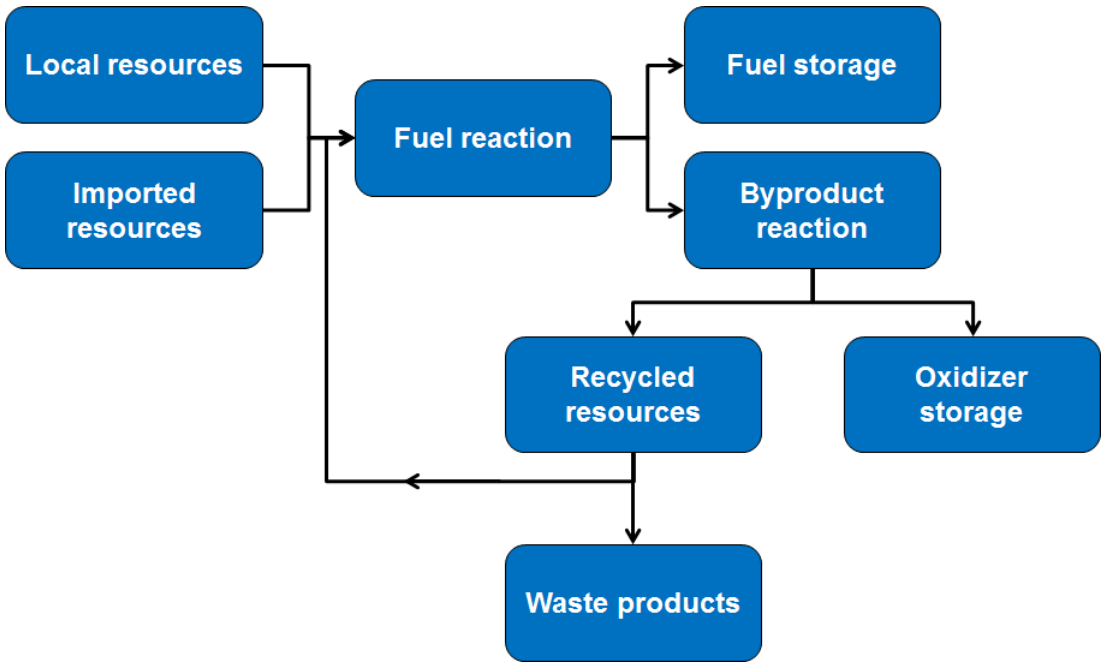

Figure 26: A generalized formulation of an ISPP process.

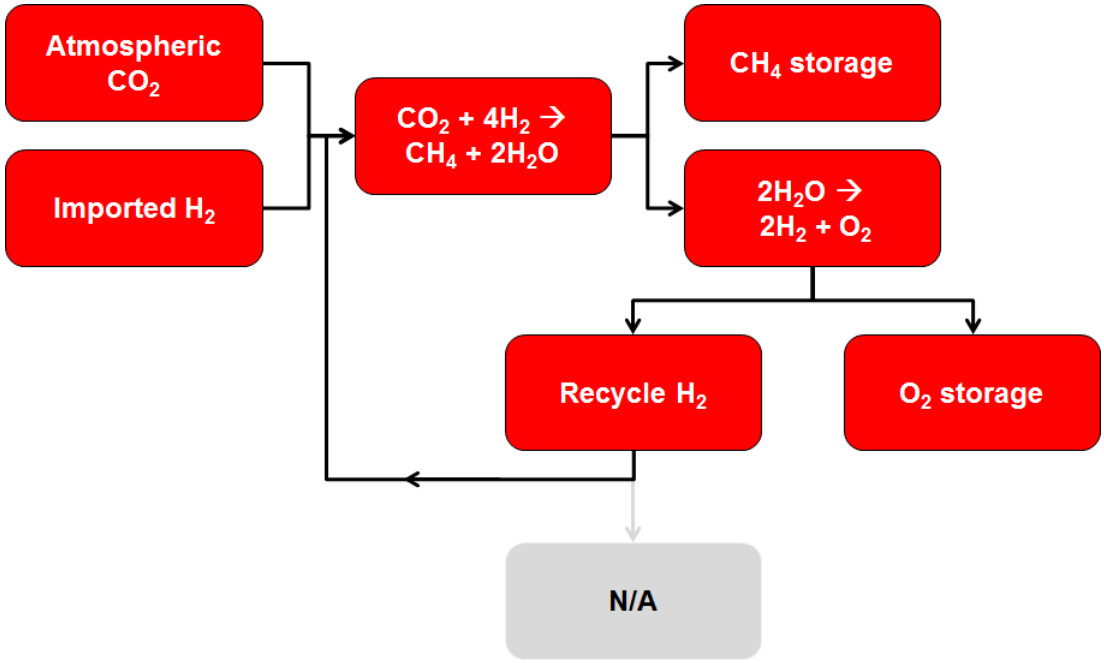

Figure 27: The ISPP Process that uses hydrogen imported from Earth to manufacture methane and oxygen.

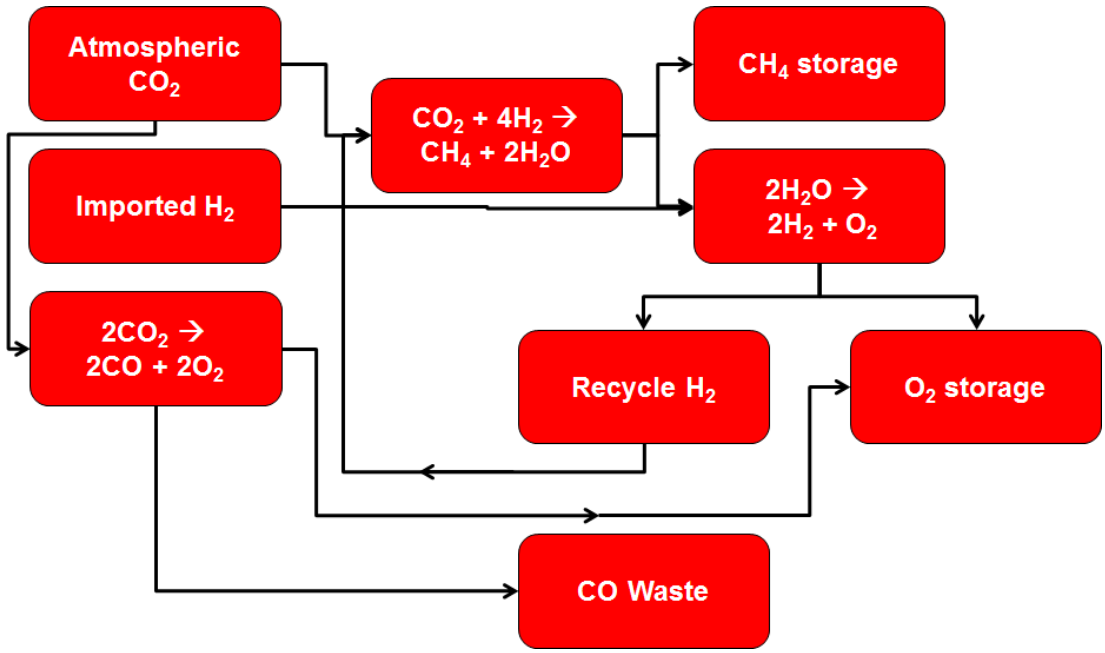

Figure 28: The ISPP Process that uses hydrogen imported from Earth to manufacture methane and oxygen, including carbon dioxide electrolysis to produce oxygen.

the ideal O/F ratio. When bringing hydrogen from Earth, the additional oxygen is manufactured using carbon dioxide electrolysis. This process utilizes the same carbon dioxide acquisition system as the methane production process, scaled up to accommodate the total carbon dioxide requirement, and separates the gas into carbon monoxide (which is vented) and oxygen (which is liquified via the same cryocooler as the oxygen emerging from the water electrolysis system). Figure 28 shows the integrated approach that produces methane and oxygen at the ideal O/F ratio.

If water is used to provide the source hydrogen, it is provided in one of two ways: in a water tank from Earth (see Figure 29), or via a water acquisition system on Mars. The Mars water acquisition system consists of two components: a vehicle that collects regolith for processing and a plant that extracts water from the regolith and disposes of the processed regolith. The water is electrolyzed to produce hydrogen, for the Sabatier reaction, and oxygen, to provide the supplementary oxygen needed to raise the O/F from 2.0 to 3.5. Figure 30 shows the process for methane production

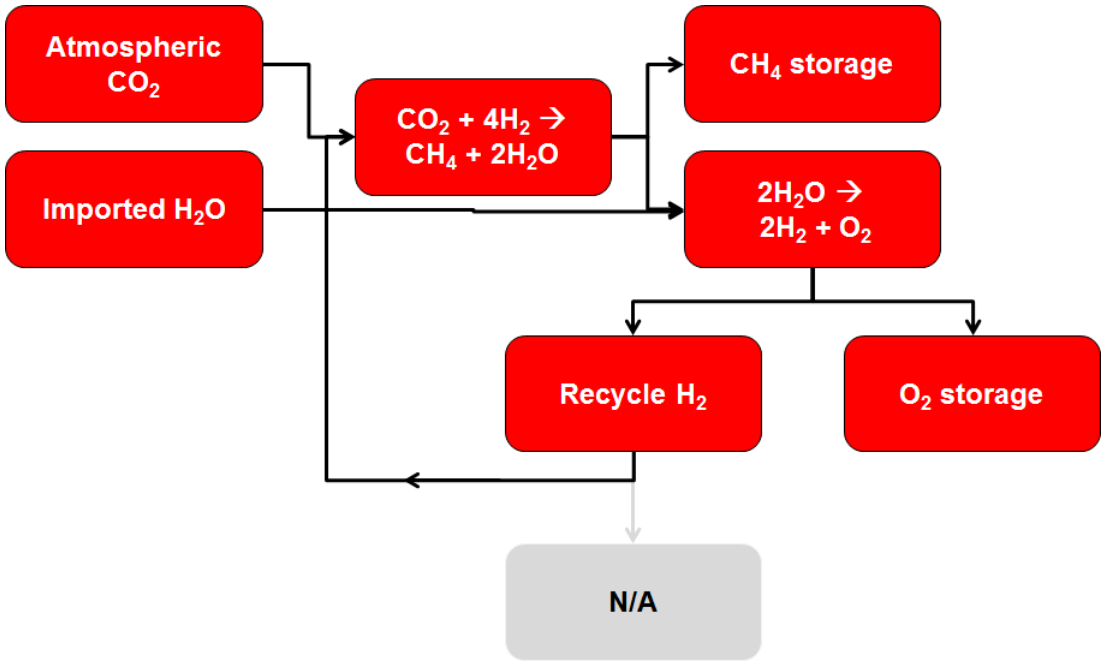

Figure 29: The ISPP Process that uses water imported from Earth to manufacture methane and oxygen.

using Mars water.

The partial ISPP approach associated with methane sees the MAV deployed with its methane already produced, while the oxygen is produced via carbon dioxide electrolysis. This approach is shown in Figure 31.

3.1.2 Ethylene

Ethylene production is similar to methane production, but with an additional reaction required in the formation of the fuel. The reverse water gas shift reactor combines carbon dioxide and a stoichiometric excess of hydrogen to produce carbon monoxide, hydrogen, and water. The water is sent to the electrolyzer as in methane production, while the carbon monoxide and hydrogen are combined in a Fischer-Tropsch reactor to produce ethylene and water. The ethylene is stored, while the water is electrolyzed. Figure 32 shows the process. Similarly to the methane cases, the source of hydrogen can come from Earth water (see Figure 33) or water acquired on Mars (see Figure 34). Also under consideration is the use of carbon dioxide electrolysis to produce oxygen

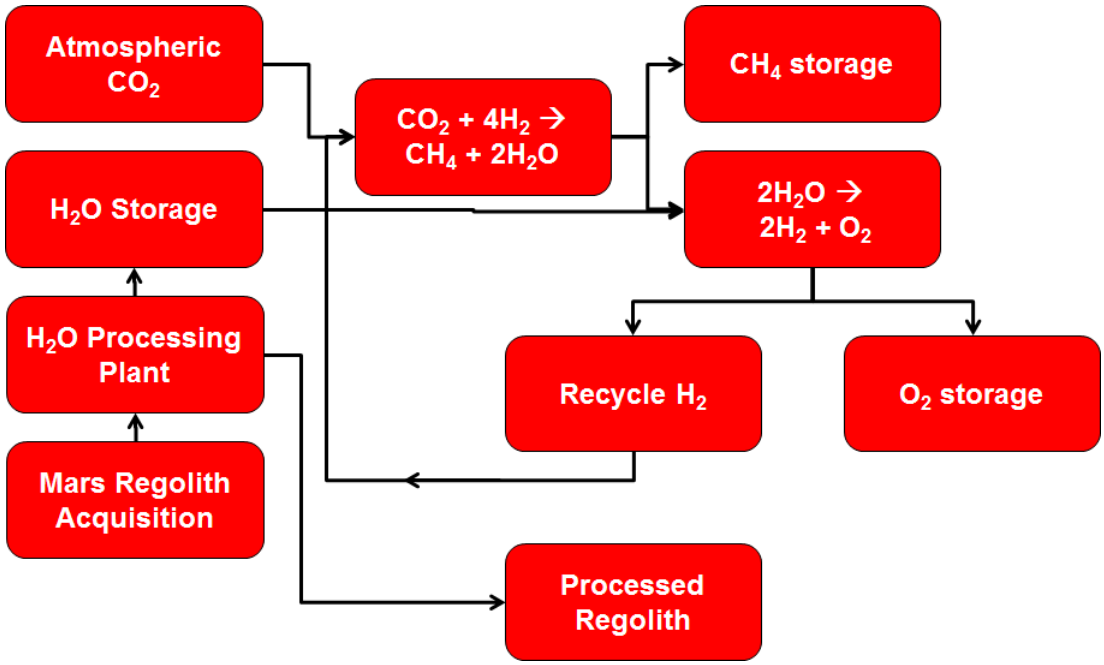

Figure 30: The ISPP Process that uses water acquired on Mars to manufacture methane and oxygen.

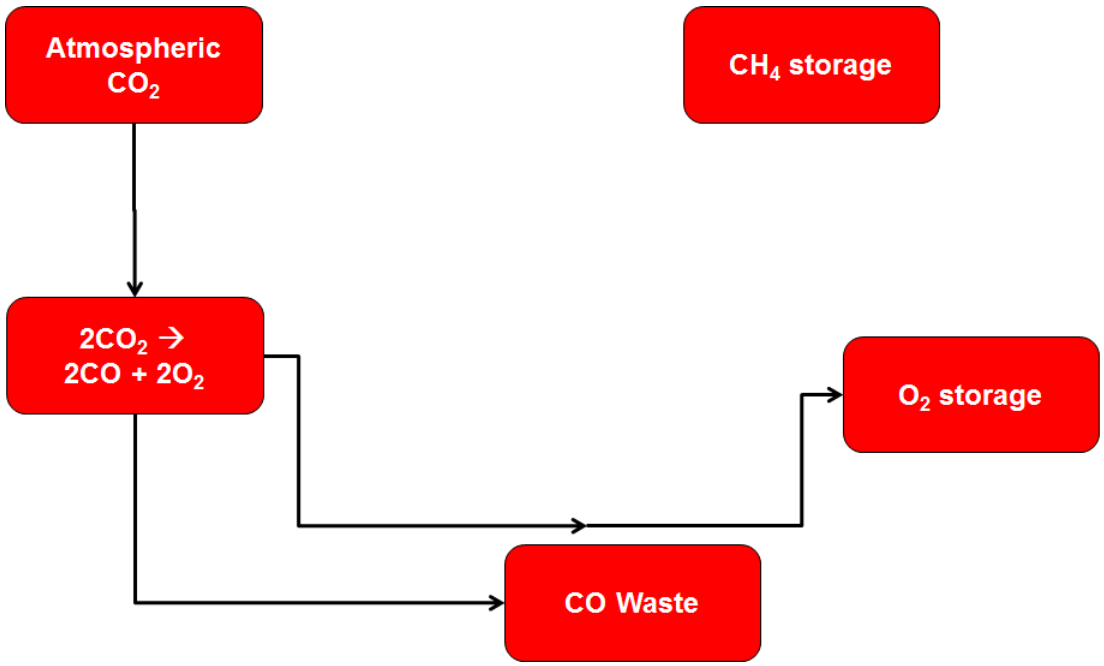

Figure 31: The ISPP Process that uses imported methane and acquires carbon dioxide on Mars to produce oxygen.

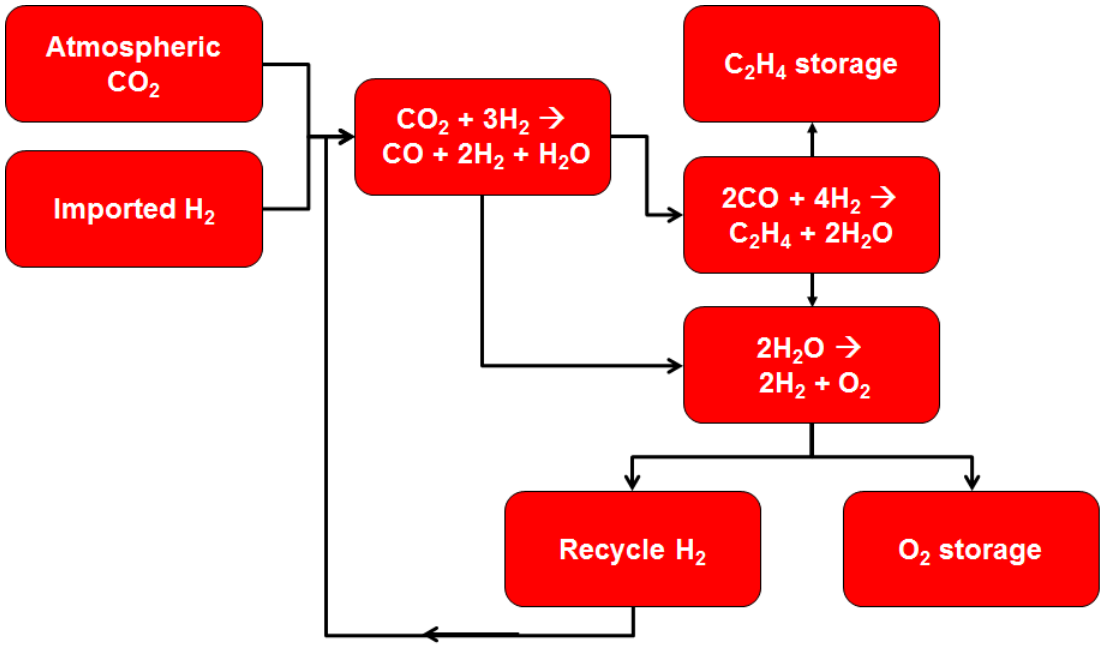

Figure 32: The ISPP Process that uses hydrogen imported from Earth to manufacture ethylene and oxygen via the reverse water gas shift.

with ethylene brought from Earth, as shown in Figure 35.

3.1.3 Methanol

Methanol production follows a similar process to ethylene production in each case. The reactor for methanol production from the carbon monoxide and hydrogen mix utilizes a copper-zinc catalyst, but the other process steps are functionally identical. The processes for production of methanol from imported hydrogen (Figure 36), imported water (Figure 37), and water acquired on Mars (Figure 38) are shown, as is the process for importing methanol and only producing the oxygen required via carbon dioxide electrolysis (Figure 39).

3.1.4 Hydrogen

Hydrogen can be used as the fuel for the MAV without converting it into a hydrocarbon. Water, either from Earth (Figure 40) or Mars (Figure 41), can be electrolyzed,

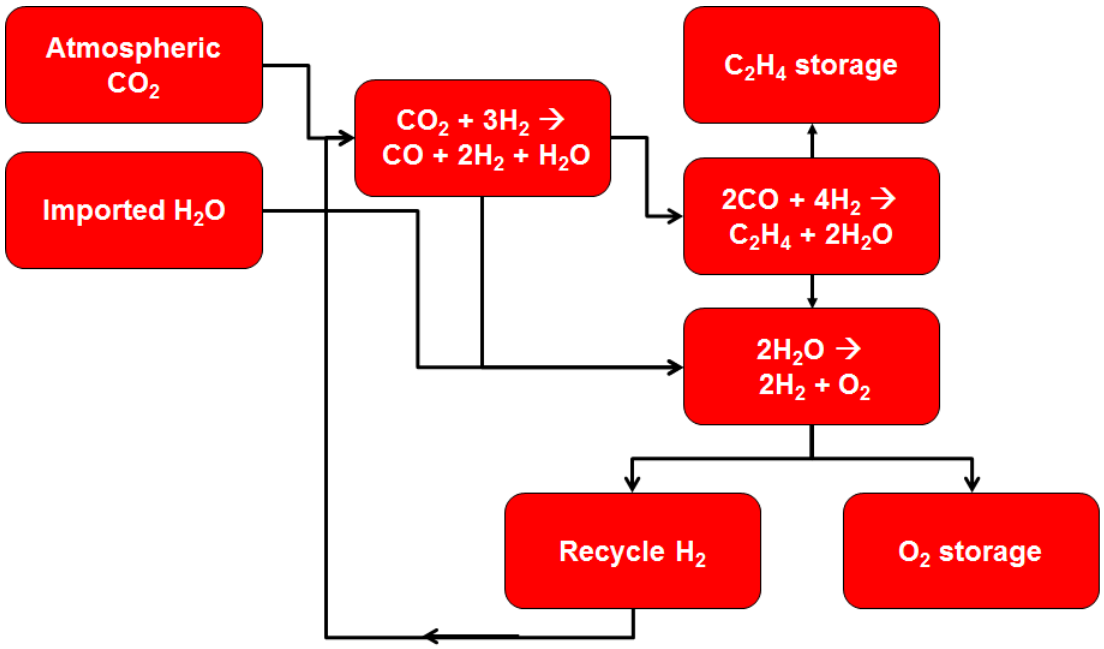

Figure 33: The ISPP Process that uses water imported from Earth to manufacture ethylene and oxygen via the reverse water gas shift.

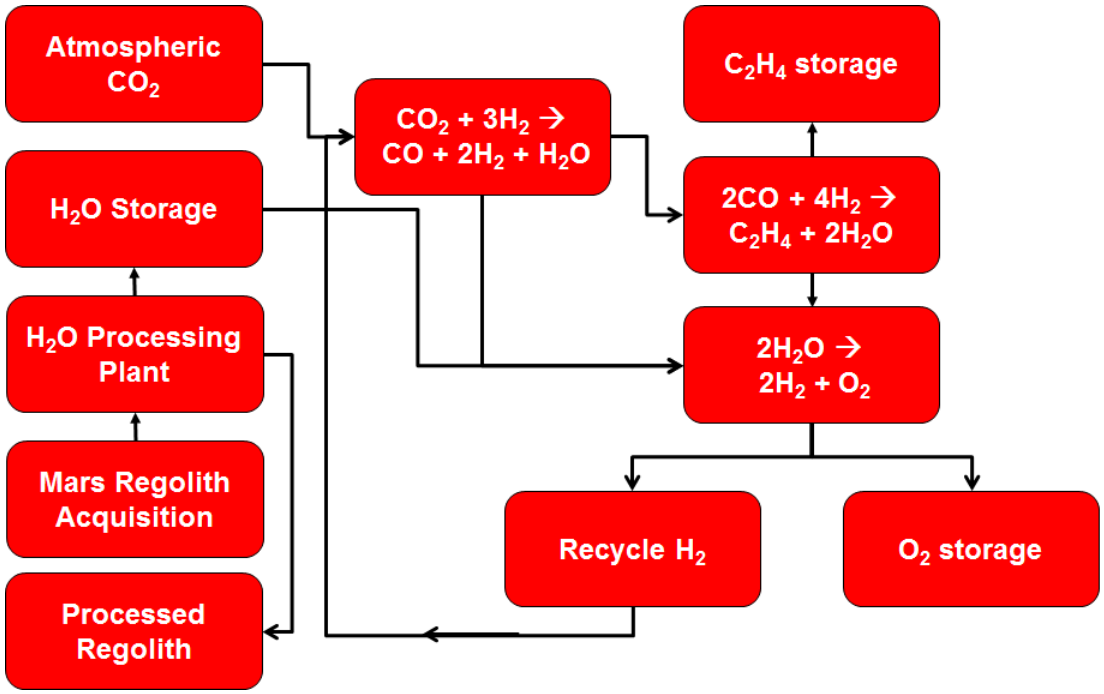

Figure 34: The ISPP Process that uses water acquired on Mars to manufacture ethylene and oxygen via the reverse water gas shift.

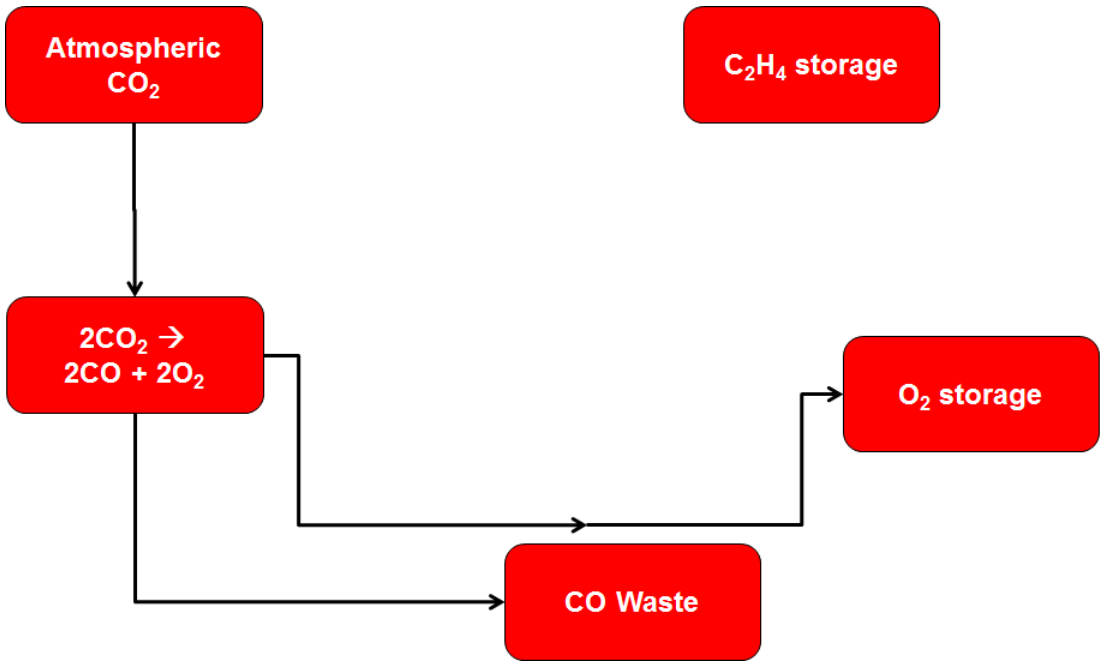

Figure 35: The ISPP Process that uses imported ethylene and acquires carbon dioxide on Mars to produce oxygen.

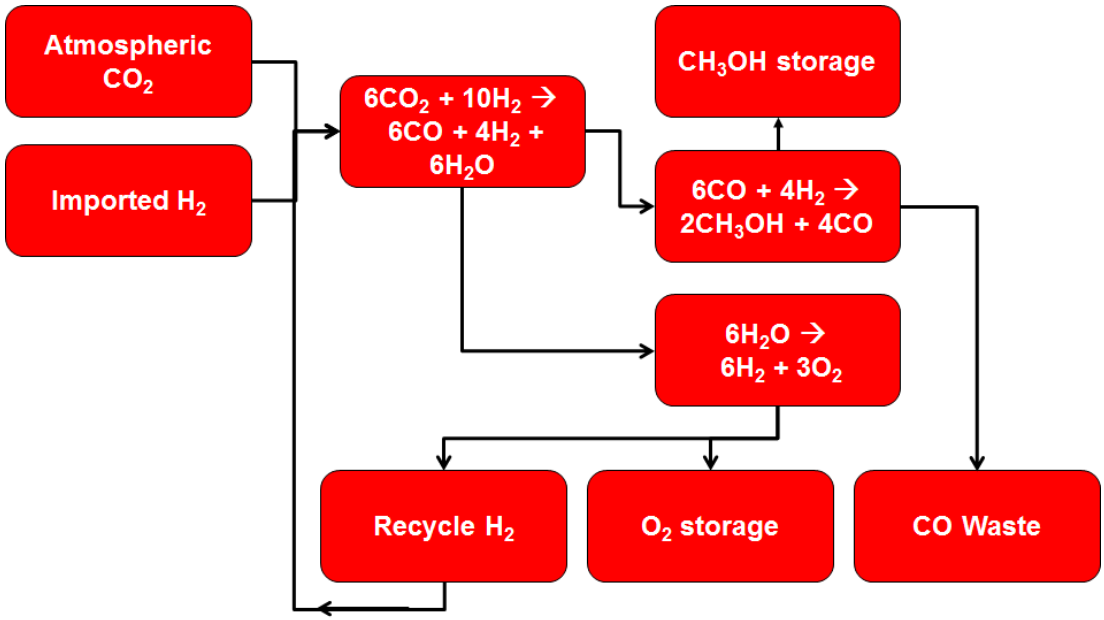

Figure 36: The ISPP Process that uses hydrogen imported from Earth to manufacture methanol and oxygen via the reverse water gas shift.

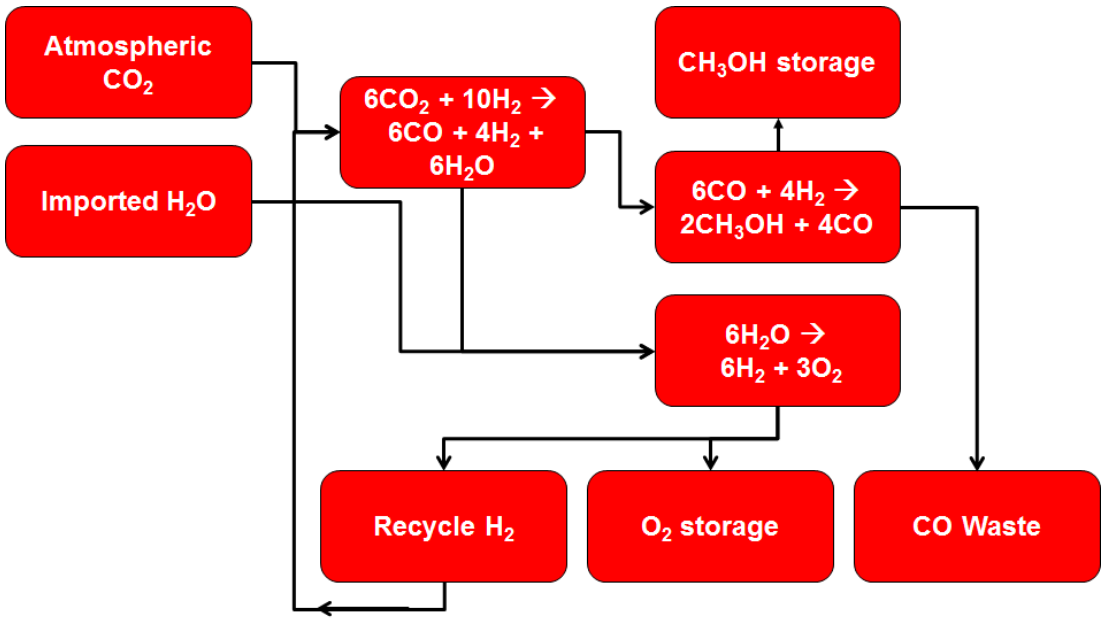

Figure 37: The ISPP Process that uses water imported from Earth to manufacture methanol and oxygen via the reverse water gas shift.

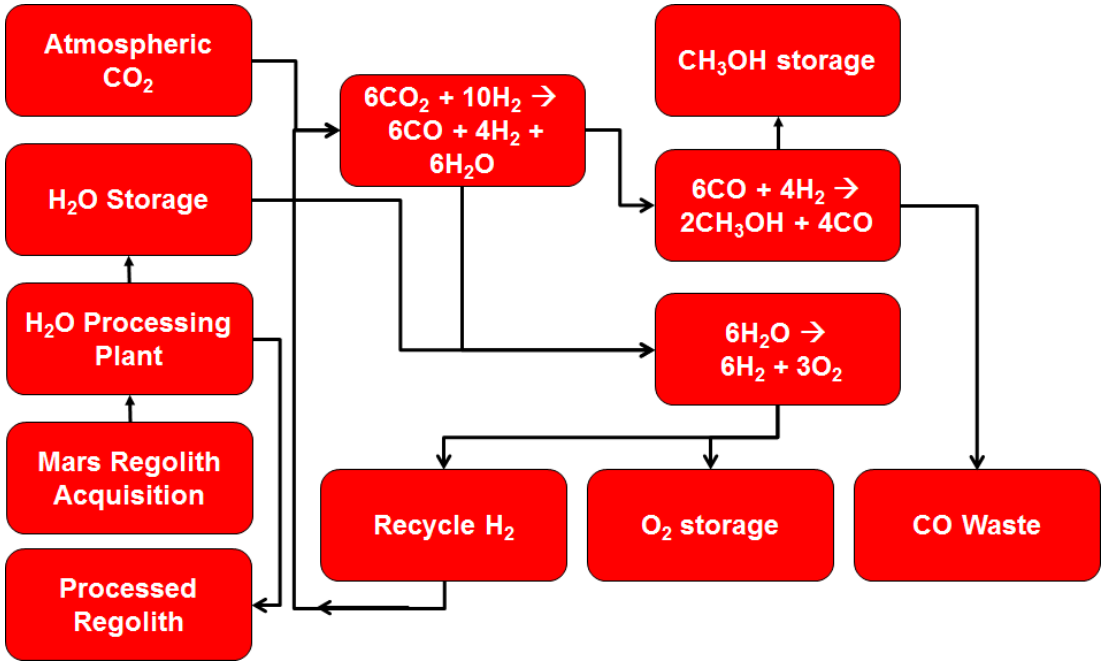

Figure 38: The ISPP Process that uses water acquired on Mars to manufacture methanol and oxygen via the reverse water gas shift.

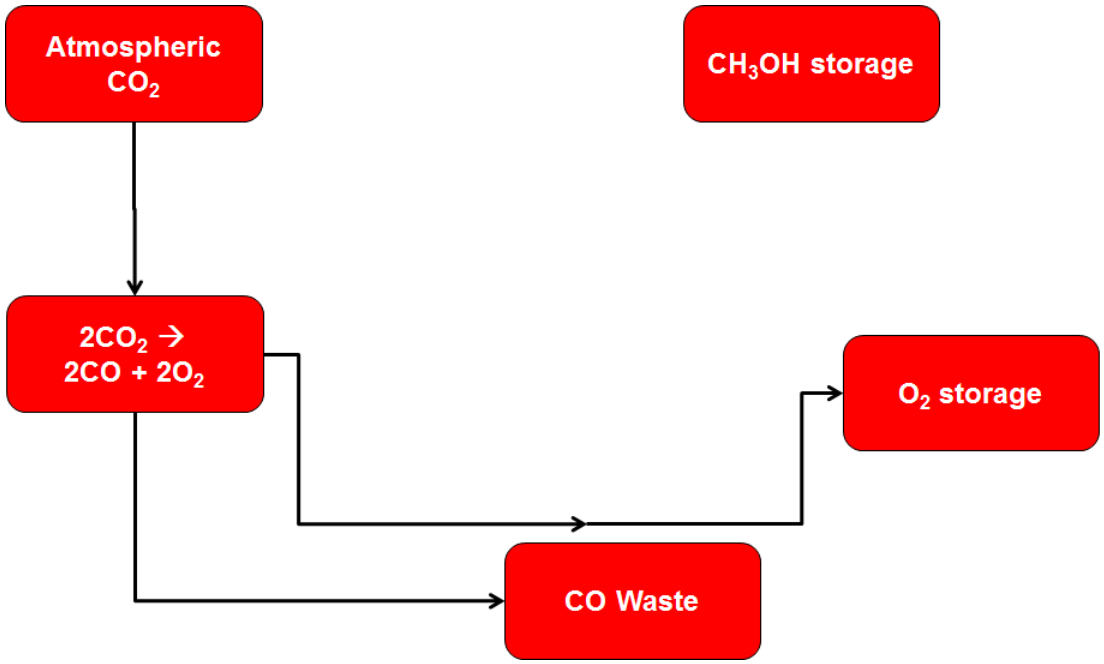

Figure 39: The ISPP Process that uses imported methanol and acquires carbon dioxide on Mars to produce oxygen.

with both products liquified and stored aboard the MAV for later use. The other option is to transport hydrogen from Earth and manufacture oxygen via carbon dioxide electrolysis (Figure 42); this is equivalent to the import hydrogen and oxygen only options described above for the hydrocarbon fuels.

The above describes fifteen architectures to be modeled: four each using methane, ethylene, and methanol as the fuel, and three using hydrogen. As an additional basis of comparison, four other architectures are considered in this research: for each fuel type, both the fuel and oxidizer are brought from Earth, and no ISPP is performed. In comparing the architectures, this will allow for an understanding of whether ISPP is beneficial relative to a non-ISPP option. The total number of architectures being considered is thus nineteen.

Several simplifying assumptions are made in the formulation of these architectures. For the architectures that bring both fuel and oxidizer from Earth, it is assumed that all of the cryogenic capabilities for the imported propellant is aboard the MAV, as

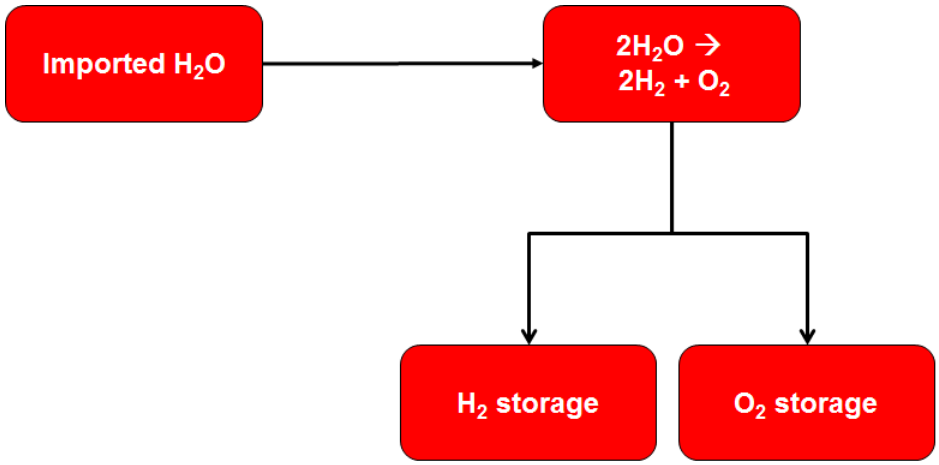

Figure 40: The ISPP Process that uses water imported from Earth to manufacture hydrogen and oxygen.

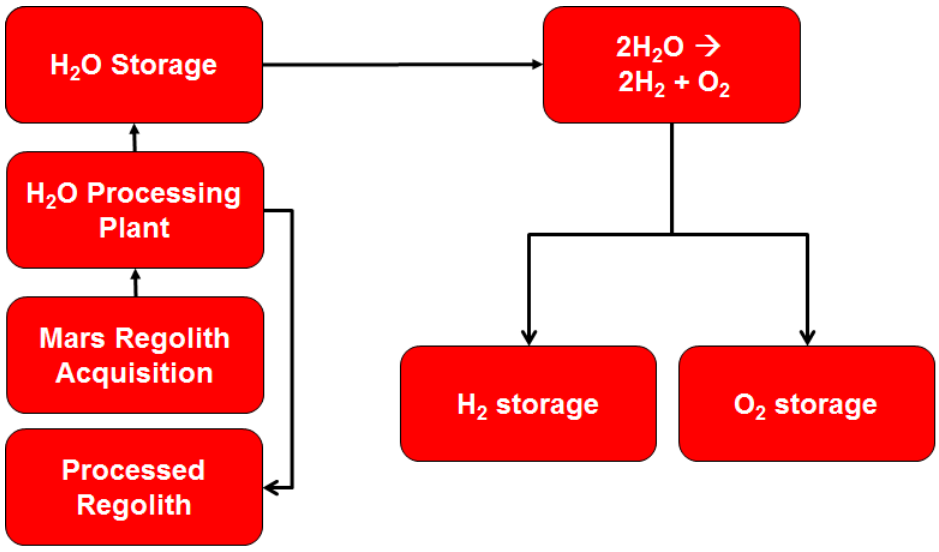

Figure 41: The ISPP Process that uses water acquired on Mars to manufacture hydrogen and oxygen.

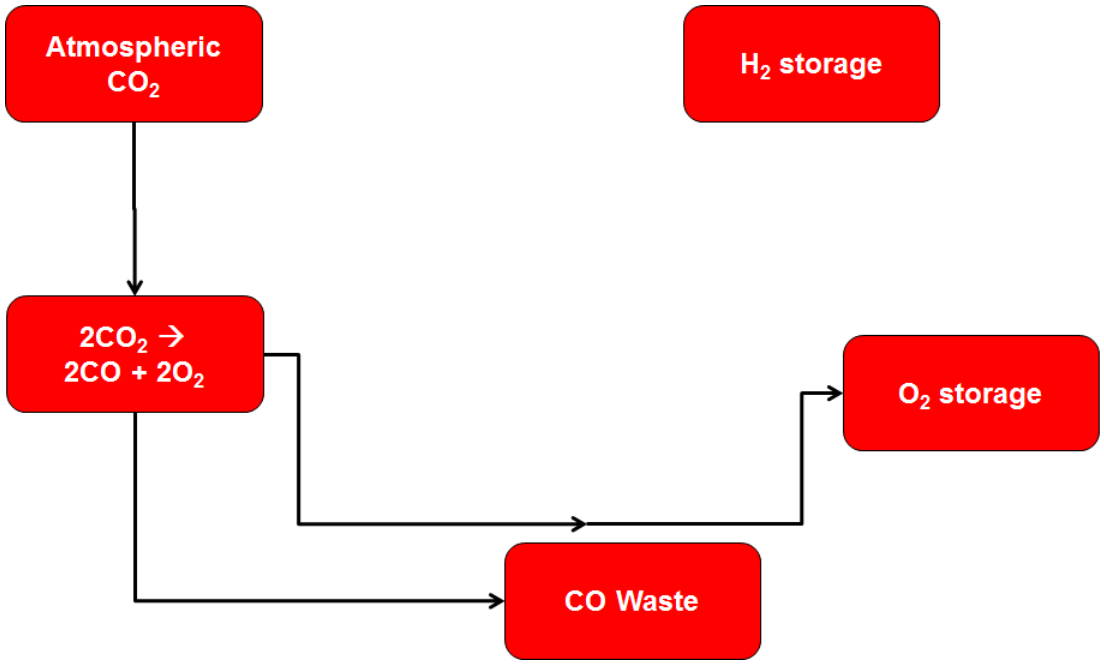

Figure 42: The ISPP Process that uses imported hydrogen and acquires carbon dioxide on Mars to produce oxygen.

well as the power for those cryogenic capabilities; in reality, a separate power source from the MAV would likely be used to maintain the cryogenic state of the propellant. Although the volumetric impacts of tanks and other hardware do impact the sizing of the transportation elements bringing those systems to Mars, it is assumed that there is no upper limit on volume; in reality, launch vehicle shroud constraints would lead to geometric constraints on vehicle size. Similarly, for purposes of accounting for launch costs, all IMLEO is aggregated; in reality, payloads such as vehicles and ISPP systems would have to be manifested on individual launch vehicles, especially for smaller commercial vehicles.

3.2 ISPP Element Models

The models of each of the functional elements for the ISPP systems are described below. The code used to model each system is included in Appendix A. Note that in the equations in this section, some unit conversion terms have been omitted; these are included in the code in Appendix A. Parameters denoted with a footnote are

treated as fixed during the Monte Carlo runs.

3.2.1 Carbon Dioxide Acquisition

The carbon dioxide acquisition system uses an adsorption bed to collect carbon dioxide. The bed is exposed to the Martian environment during the night, and is then heated during the day to outgas the carbon dioxide from the sorbent bed. The canister also compresses the carbon dioxide before it is passed through a valve to the Sabatier reactor, reverse water gas shift reactor, and/or carbon dioxide electrolyzer. Zeolite 5A, a synthetic micro-porous mineral, is the sorbent bed material. Heat fins and a radiator are used to manage the temperatures for nighttime adsorption and daytime outgassing.

The carbon dioxide demand (from all systems requiring carbon dioxide) and days of ISPP operation drive the carbon dioxide rate required for sizing the sorbent bed, along with the temperature and pressure properties of the Zeolite. From the sizing of the sorbent bed, the canister is sized using the packing efficiency of the sorbent and a fixed length-to-diameter ratio for the cylinder. The heat fins and radiator are sized based on the temperature difference between the canister and the Martian night to promote adsorption, while the heater power and insulation mass are sized based on the Zeolite heat of desorption and the temperature difference between the canister and the Martian day.

The model is derived from the Spaceworks model of a Zeolite adsorber, canister, and heater [42], which in turn is based on the properties described in Chang's Mars carbon dioxide sorbent patent [107], Rapp et al.'s modeling of carbon dioxide adsorbents [108], and the properties described for Mulloth and Finn's zeolite carbon dioxide adsorber for spacecraft use [109].

The functional requirements, associated physical components, and relevant equations are given in Table 6. The parameters used in modeling the carbon dioxide

Table 6: Carbon Dioxide Adsorber Functional Requirements

Function	Physical Components	Relevant Equations
Acquisition of carbon dioxide from ambient atmosphere	Sorbent bed	30
Collection and pressurization	Tank	33, 37
Thermal management	Insulation, heater, radiator	35, 38-40

acquisition system are given in Table 7.

Table 7: Carbon Dioxide Adsorber Parameters

Parameter Name	Nominal Value	Source	Description
CO2 fraction atm[1]	95%	[79, 108, 110]	Concentration of carbon dioxide in the Martian atmosphere
Outgas temp high	523 [K]	[107]	Temperature of carbon dioxide during outgassing
Outgas press high	600 [torr]	[108]	Pressure of carbon dioxide during outgassing
Outgas press low	6 [torr]	[108]	Pressure of carbon dioxide after valve release
Catalyst density	643 [kg-m$^-$3]	[108]	Density of zeolite adorbent material
Tank L to D ratio	3.6	[108]	Ratio of tank cylindrical barrel length to diameter
Tank safety factor	2	[22, 42]	Multiplier on the tank burst pressure used in the estimation of tank mass from volume and pressure
Tank mass factor	5000 [m]	[22, 42]	Parameter used in the estimation of tank mass from volume and pressure

[1]This variable is treated as fixed during Monte Carlo runs.

Tank insulation density	1.27 [kg-m^{-}2]	[42]	Density of thermal insulation material
Tank insulation thickness	6.3 [cm]	[111]	Thickness of thermal insulation material on interior tank
Heat fin density	2700 [kg-m^{-}3]	[70]	Density of aluminum
Heat fin thickness	0.3 [mm]	[112]	Thickness of heat fins
Heat fin area per length	7.65 [m^{-}1]	[108]	Scaling parameter used in calculating heater mass
Fan piping Htbar to-Catalyst ratio	10%	[79]	Ratio of fan, piping, and heat transfer bar mass to catalyst mass
Radiator area parameter	1.27 E-07 [m^{2}-K^{-}1-s^{-}1]	[108]	Parameter to estimate radiator area based on temperature difference and operation time
CO2 adsorber op-Time	12 [hr]	[108]	Time for CO2 adsorber to collect carbon dioxide per cycle
Night temp[1]	200 [K]	[108]	Nighttime temperature on surface of Mars; used to size radiator
Radiator density	3.3 [kg-m^{-}2]	[79]	Areal density of radiator
Cp catalyst	1.01 [kJ-kg^{-}1-K^{-}1]	[108]	Specific heat capacity of zeolite adsorbent material
Valve open temp	273 [K]	[108]	Temperature of system after valve opening; used to compute heating power requirements

The total carbon dioxide need, days of operation, and time for the adsorber to operate were used to estimate the required collection rate in Equation 26. The pressure of outgassing was used to compute the difference in the carbon dioxide loading of the adsorbent when saturated and when empty [107] in Equations 27 through 29. The adsorbent catalyst mass was then computed from the required rate and loading

difference in Equation 30; the catalyst volume is then computed from the density. The carbon dioxide inner and outer tank volumes and masses (along with the insulation mass between the two tanks) are computed from the catalyst volume via Equations 31 through 37. The masses of the heat fins, radiator, and other heat transfer equipment are shown in Equations 38 to 40. The heating power depends on the thermal properties of the catalyst, the amount of carbon dioxide collected each night, and correlations of heat of adsorption as a function of carbon dioxide loading on the zeolite catalyst [109], shown in Equations 41 to 48.

$$CO2_{rate\_required} = \frac{CO2_{demand}}{(days\_of\_operation) * (CO2\_adsorber\_opTime)} \tag{26}$$

$$CO2_{loading\_high} = 0.0201 * ln(Outgas\_press\_low) + 0.1337 \tag{27}$$

$$CO2_{loading\_low} = 0.001 * e^{0.0046*(Outgas\_press\_high)} \tag{28}$$

$$Loading\_difference = CO2_{loading\_high} - CO2_{loading\_low} \tag{29}$$

$$Catalyst\_mass = \frac{CO2_{rate\_required} * daily\_operation\_time}{Loading\_difference} \tag{30}$$

$$Tank\_internal\_radius = (Catalyst\_volume/(\pi * (\frac{4}{3} + Tank\_L\_to\_D\_ratio * 2)))^(1/3) \tag{31}$$

$$Tank\_internal\_length = Tank\_internal\_radius * 2 * Tank\_L\_to\_D\_ratio \tag{32}$$

$$Tank\_internal\_mass = (Tank\_internal\_pressure) * Tank\_safety\_factor * Catalyst\_volume/g_0/Tank\_mass\_factor \tag{33}$$

$$Tank\_internal\_surface\_area = (4 * \pi * \frac{\sqrt{2}}{2} * Tank\_internal\_radius^2) + (2 * \pi * Tank\_internal\_radius * (Tank\_internal\_length - 2 * Tank\_internal\_radius)) \tag{34}$$

$$Insulation\_mass = Tank\_internal\_surface\_area * Tank\_insulation\_density \tag{35}$$

$$Tank\_external\_volume = \frac{4}{3} * \pi * (Tank\_internal\_radius + Tank\_insulation\_thickness)^3 + \pi * (Tank\_internal\_radius + Tank\_insulation\_thickness)^2 * (Tank\_internal\_length + 2 * Tank\_insulation\_thickness) \tag{36}$$

$$Tank\_external\_mass = Tank\_internal\_pressure * Tank\_safety\_factor * Tank\_external\_volume / g_0 * Tank\_mass\_factor \tag{37}$$

$$Heat\_fin\_mass = Tank\_internal\_length * Heat\_fin\_area\_per\_length * pi * Tank\_internal\_radius^2 * Heat\_fin\_t * Heat\_fin\_density \tag{38}$$

$$Radiator\_mass = Radiator\_density * Radiator\_area\_parameter * CO2\_adsorber\_opTime * (Outgas_temp_high - Night_temp) \tag{39}$$

$$Fan\_piping\_andHTbar\_mass = Fan\_piping\_HTbar\_toCatalyst\_ratio * Catalyst\_mass \tag{40}$$

$$Heat\_to\_warm\_V = Catalyst\_mass * Cp\_catalyst * (Outgas\_temp\_high - Valve\_open\_temp) \tag{41}$$

$$CO2\_mass\_per\_night = CO2\_rate\_required * daily\_operation\_time \tag{42}$$

$$Heat\_of\_adsorption\_high = -1334 * CO2\_loading\_low^2 - 14.793 * CO2\_loading\_low + 44.823 \tag{43}$$

$$Heat\_of\_adsorption\_low = -1334 * CO2\_loading\_high^2 - 14.793 * CO2\_loading\_high + 44.823 \tag{44}$$

$$Delta\_heat\_of\_adsorption = Heat\_of\_adsorption\_high - Heat\_of\_adsorption\_low \tag{45}$$

$$CO2\_per\_night = 0.044 * CO2\_mass\_per\_night \tag{46}$$

$$Heat\_of\_adsorption = Delta\_heat\_of\_adsorption * CO2\_per\_night \quad (47)$$

$$Heating\_power = (Heat\_to\_warm\_V + Heat\_of\_adsorption)/daily\_operation\_time \quad (48)$$

The code used for modeling the carbon dioxide acquisition system is given in Appendix A.1.1.

3.2.2 Mars Water Acquisition

The Mars water acquisition system uses two regolith excavators to collect regolith and transport it to a processing plant. The excavators, which alternate between an operation time and a charging time (i.e. one is collecting and delivering regolith while the other is recharging), collect regolith from the top surface of Mars. The plant heats the regolith to approximately 600 K to desorb the water, which is then passed through a gas clean-up process before being condensed for use by the water electrolyzer.

The hydrogen demand drives the water demand, which in conjunction with the total production time based on the days of ISPP operation, drives the water collection rate. In combination with the concentration of water in the regolith (a parameter in the stochastic analysis), this in turn drives the regolith collection rate. The excavators and plant mass, power, and volume are sized based on linear relationships to regolith collection rate.

The model is derived from the data published in the addendum to DRA 5.0, with linear fits of mass, power, and volume as functions of regolith rate. The data, derived from Table 3-23 of the Addendum, are shown in Figure 43 [10].

The functional requirements, associated physical components, and relevant equations are given in Table 8. The parameters used in modeling the Mars water acquisition system are given in Table 9.

Table 9: Mars Water Excavator and Plant Parameters

Parameter Name	Nominal Value	Source	Description
Water concentration	3%	[1, 10]	Concentration of water by mass in the Martian regolith
E M multi	10.2 [hr]	[10], Equation 51	Slope of linear regression of excavator mass vs regolith acquisition rate
E M const	398 [kg]	[10], Equation 51	Intercept of linear regression of excavator mass vs regolith acquisition rate
E P multi	0.0155 [hr]	[10], Equation 52	Slope of linear regression of excavator power vs regolith acquisition rate
E P const	0.334 [kWe]	[10], Equation 52	Intercept of linear regression of excavator power vs regolith acquisition rate
E V multi	0.1532 [hr]	[10], Equation 53	Slope of linear regression of excavator volume vs regolith acquisition rate
E V const	-0.3157 [m^3]	[10], Equation 53	Intercept of linear regression of excavator volume vs regolith acquisition rate
P M multi	3 [hr]	[10], Equation 54	Slope of linear regression of regolith plant mass vs regolith acquisition rate
P M const	384 [kg]	[10], Equation 54	Intercept of linear regression of regolith plant mass vs regolith acquisition rate
P P multi	0.3423 [hr]	[10], Equation 55	Slope of linear regression of regolith plant power vs regolith acquisition rate
P P const	5.54 [kWe]	[10], Equation 55	Intercept of linear regression of regolith plant power vs regolith acquisition rate
P V multi	0.0626 [hr]	[10], Equation 56	Slope of linear regression of regolith plant volume vs regolith acquisition rate

P V const	2.334 [m^3]	[10], Equation 56	Intercept of linear regression of regolith plant volume vs regolith acquisition rate

The required water rate depends on the hydrogen demand, production time, and proportion of hydrogen in water in Equation 49. The regolith rate is then the water rate divided by the water concentration in Equation 50. As in DRA 5.0, two excavators are assumed; the combined mass, power, and volume of the two are calculated using the linear regressions of regolith rate in Figure 43 in Equations 51 to 53. Similarly, the water plant is scaled linearly based on required regolith rate in Equations 54 to 56.

$$Water\_rate\_actual = H2_{demand}/total\_production\_time/0.112 \tag{49}$$

$$Regolith\_rate\_actual = Water\_rate\_actual/Water\_concentration \tag{50}$$

$$Excavator\_mass = E\_M\_multi * Regolith\_rate\_actual + E\_M\_const \tag{51}$$

$$Excavator\_power = E\_P\_multi * Regolith\_rate\_actual + E\_P\_const \tag{52}$$

$$Excavator\_volume = E\_V\_multi * Regolith\_rate\_actual + E\_V\_const \tag{53}$$

$$Plant\_mass = P\_M\_multi * Regolith\_rate\_actual + P\_M\_const \tag{54}$$

$$Plant\_power = P\_P\_multi * Regolith\_rate\_actual + P\_P\_const \tag{55}$$

$$Plant\_volume = P\_V\_multi * Regolith\_rate\_actual + P\_V\_const \tag{56}$$

The code used for modeling the Mars water acquisition system is given in Appendix A.1.2.

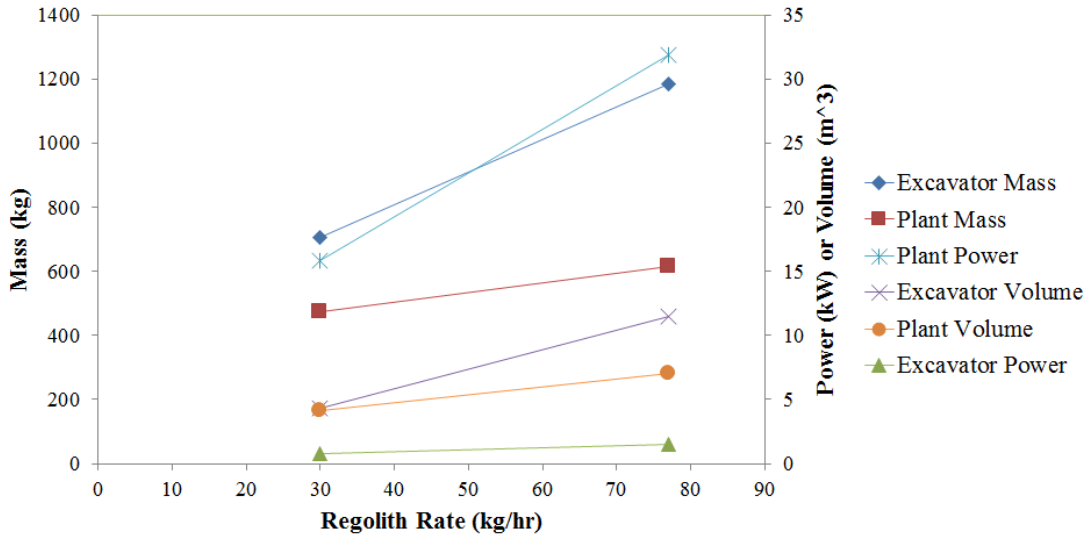

Figure 43: Mass, power, and volume of the Mars water excavators and plant as a function of the required regolith processing rate [10].

Table 8: Mars Water Excavator and Plant Functional Requirements

Function	**Physical Components**	**Relevant Equations**
Acquisition of regolith	Excavator	51
Transport of regolith	Excavator	51
Regolith processing	Plant	54
Water production	Plant	54

3.2.3 Sabatier Reactor

The Sabatier reactor combines carbon dioxide and hydrogen to form methane and water; the methane is stored for use on the ascent vehicle, while the water is sent to the water electrolysis system to be separated into hydrogen and oxygen. The system consists of a ruthenium-alumina catalyst bed contained in a reaction chamber, as well as a condenser/separator for isolating the methane and water products. Although the process is exothermic, start-up power is required to run a heating coil to initialize the process.

The required methane production rate, a function of total methane needed and time available to produce it, is used in conjunction with the reaction temperature to size the reactor volume. DePasquale notes that "the reaction proceeds at a faster rate at higher temperatures, but there is a lower conversion of reactants to products" [42]. The reactor mass is sized from the reactor volume and cylindrical sizing parameters: length-to-diameter ratio, wall thickness, and chamber wall density. The condenser/separator is sized from the heat rejection requirements for isolating the methane and water vapor. The start-up heater mass is sized based on the heat requirements to initially raise the input hydrogen and carbon dioxide to the reaction temperature.

The geometric parameters for estimating reactor cylinder sizing come from Zubrin et al.'s work at Pioneer Astronautics in the 1990s [34]. The chemical properties of the reaction are derived from Lunde and Kester's work on methane formation in the presence of a ruthenium catalyst [113]. The material properties of the nichrome heating wire come from the WireTronic Inc. data sheet [114].

The functional requirements, associated physical components, and relevant equations are given in Table 10.The parameters used in modeling the Sabatier reactor are given in Table 11.

Table 10: Sabatier Reactor Functional Requirements

Function	**Physical Components**	**Relevant Equations**
Methane and water production	Reaction chamber, catalyst	72, 73
Water collection	Condenser	97
Thermal management	Insulation, wire, heater	75, 76, 87, 88

Table 11: Sabatier Reactor Parameters

Parameter Name	**Nominal Value**	**Source**	**Description**
H2 conversion eff	Equation 225	[115]	Efficiency of converting hydrogen via Sabatier process
Reaction temp	523 [K]	[115]	Sabatier process reaction temperature
Chamber V to Gas V ratio	8	[113, 115]	Ratio of chamber volume to volume of gas during reaction for sizing
Chamber residence time multiplier	3	[41, 115]	Increases size of chamber volume to accommodate reaction rate
Chamber L to D ratio	3.5	[113, 115]	Defines ratio between length and diameter of reaction chamber
Reaction chamber t	2 [cm]	[42]	Thickness of reaction chamber wall
Chamber wall density	7850 [kg-m$^-$3]	[70]	Density of steel
Catalyst density	1 [g-cc$^-$1]	[113]	Density of ruthenium-aluminum catalyst
Insulation density	50 [kg-m$^-$3]	[116]	Density of thermal insulation material
Heatup temp	473 [K]	[41]	Temperature to preheat Sabatier reaction chamber; used to size heater

Daytime temp[1]	240 [K]	[108, 110]	Daytime temperature on surface of Mars; used to size heater
Heatup time	2 [hr]	[42]	Time to operate heater to raise reaction chamber temperature
Heat transfer eff	90%	[42]	Efficiency of heat input into reaction chamber vs heat generated by heater
Specific heat of catalyst	238 [J-kg$^-$1-K$^-$1]	[117]	Specific heat capacity of ruthenium
Specific heat of wall	900 [J-kg$^-$1-K$^-$1]	[117]	Specific heat capacity of aluminum
Heating wire diameter	0.25 [cm]	[114]	Diameter of nichrome heating wire
Wire resistivity	1.08 E-06 [Ohm-m]	[114]	Resistivity of nichrome heating wire
Wire density	8400 [kg-m$^-$3]	[114]	Density of nichrome heating wire
Heater packing factor	3	[42]	Scaling factor from wire mass to heater mass
Specific heat of water[1]	4181 [J-kg$^-$1-K$^-$1]	[118]	Specific heat capacity of liquid water
Specific heat of methane[1]	2200 [J-kg$^-$1-K$^-$1]	[118]	Specific heat capacity of methane
Heat transfer coefficient	700 [W-m$^-$2-K$^-$1]	[42]	Heat transfer coefficient for water and methane condenser
Water boil temp[1]	373 [K]	[118]	Boiling point of water at 1 atmosphere of pressure
Condenser t	2 [cm]	[42]	Thickness of condenser wall
Condenser density	7850 [kg-m$^-$3]	[70]	Density of steel
Condenser massFactor	2	[42]	Multiplier on condenser mass to account for plumbing

The reactant flow rate into the Sabatier reactor is calculated using Equation 57.

The catalytic reaction rate on a molar basis (in micromol-cc^{-}1-s^{-}1), which drives the sizing of the reaction temperature, is based on the correlation developed by DePasquale and shown in Equations 58 (for temperatures less than 523 K) and 59 (for temperatures greater than or equal to 523 K) [42]. The enthalpy of the reaction is based on the data developed by Globus shown in Equation 60 [119]. The reactant flow rate, and catalytic reaction rate are used to calculate the catalyst volume in Equations 61 to 64. The cylindrical Sabatier reaction chamber is sized using this volume, and the masses of the chamber wall, catalyst, insulation, and other parts are calculated in Equations 65 to 76. The nichrome wire heater is sized by first calculating the power required to heat the catalyst and wall in Equations 77 to 80, then by computing the geometry and mass of the wire and heater in Equations 81 to 88. The condenser used to separate the water and methane is sized based on the flow rate and thermal parameters of the two products in Equations 89 to 97. The heat to sustain the reaction is given by Equation 80, while the heat produced by the reaction is given by Equation 98; since the reaction is exothermic, the heat produced exceeds the heat required and the input power required for the Sabatier reactor is 0. The masses of the components (Equations 72, 73, 75, 76, 87, 88, and 97) are summed for the total system mass.

$$Reactant\_flow\_rate = CH4_{demand}/production\_time * 3.25/H2\_conversion\_eff \tag{57}$$

$$Catalytic\_reaction\_rate = 4.192595E-09 * e^{0.04521818*Reaction\_temp} \tag{58}$$

$$Catalytic\_reaction\_rate = 6.5084E-04 * e^{0.02220601*Reaction\_temp} \tag{59}$$

$$\begin{aligned} Reaction\_enthalpy = (-0.000029 * (Reaction\_temp - 273)^2 + 0.057211 \\ *(Reaction\_temp - 273) + 163.590212) \end{aligned} \tag{60}$$

$$Gas\_volume\_atReaction = Reactant\_flow\_rate/Catalytic\_reaction\_rate \tag{61}$$

$$Required\_chamber\_volume = Gas\_volume\_atReaction * ChamberV\_to\_GasV\_ratio \tag{62}$$

$$Chamber\_volume_RTM = Required\_chamber\_volume * Chamber\_residence\_time\_multiplier \tag{63}$$

$$Catalyst\_volume = Chamber\_volume\_RTM - Gas\_volume\_atReaction \tag{64}$$

$$Reaction\_chamber\_diameter = (4 * Chamber\_volume\_RTM / (\pi * Chamber\_LtoD\_ratio))^{\frac{1}{3}} \tag{65}$$

$$Reaction\_chamber\_radius = Reaction\_chamber\_diameter/2 \tag{66}$$

$$Reaction\_chamber\_length = Reaction\_chamber\_diameter * Chamber\_LtoD\_ratio \tag{67}$$

$$Reaction\_chamber\_circumference = Reaction\_chamber\_diameter * \pi \tag{68}$$

$$Reaction\_chamber\_outerV = \pi * Reaction\_chamber\_length * (Reaction\_chamber\_radius + Reaction\_chamber\_t)^2 \tag{69}$$

$$Reaction\_chamber\_innerV = \pi * Reaction\_chamber\_length * (Reaction\_chamber\_radius)^2 \tag{70}$$

$$Wall\_volume = (Reaction\_chamber\_outerV - Reaction\_chamber\_innerV) \tag{71}$$

$$Wall\_mass = Wall\_volume * Chamber\_wall\_density \tag{72}$$

$$Catalyst\_mass = Catalyst\_volume * Catalyst\_density \tag{73}$$

$$Reaction\_chamber\_area = Reaction\_chamber\_circumference * Reaction\_chamber\_length \tag{74}$$

$$Insulation\_mass = Reaction\_chamber\_area * Insulation\_density \tag{75}$$

$$Other\_parts\_mass = Wall\_mass * Other\_parts\_fraction \tag{76}$$

$$Required\_deltaT = Heatup\_temp - Daytime\_temp \tag{77}$$

$$Catalyst_heating_power = Catalyst\_mass * Cp\_of\_catalyst * (Required\_deltaT/(Heatup\_time))/Heat\_transfer\_eff \tag{78}$$

$$Wall\_heating\_power = Wall\_mass/2 * Cp\_of\_wall * (Required\_deltaT/(Heatup\_time))/Heat\_transfer\_eff \tag{79}$$

$$Total\_heating\_power = Catalyst\_heating\_power + Wall\_heating\_power \tag{80}$$

$$Heating\_wire\_crosssecA = \pi * (Heating\_wire\_diameter/2)^2 \tag{81}$$

$$Wire\_loop\_count = Reaction\_chamber\_length/Heating\_wire\_diameter \tag{82}$$

$$Wire\_length = Wire\_loop\_count * Reaction\_chamber\_circumference \tag{83}$$

$$Wire\_resistance = Wire\_resistivity * Wire\_length/Heating\_wire\_crosssecA \tag{84}$$

$$Wire\_current = sqrt(Total\_heating\_power/Wire\_resistance) \tag{85}$$

$$Wire\_volume = Wire\_length * Heating\_wire\_crosssecA \tag{86}$$

$$Wire\_mass = Wire\_volume * Wire\_density \tag{87}$$

$$Heater\_mass = Wire\_mass * Heater\_packing\_factor \tag{88}$$

$$Condenser\_diam = Reaction\_chamber\_diameter/2 \tag{89}$$

$$Cp\_average = (2.25 * Cp\_of\_water + Cp\_of\_CH4)/3.25 \tag{90}$$

$$Sabatier\_exit\_temp = Reaction\_temp \tag{91}$$

$$Heat\_to\_reject = Reactant\_flow\_rate * Cp\_average * (Sabatier\_exit\_temp - Water\_boil\_temp) \tag{92}$$

$$Condenser\_length = Heat\_to\_reject/(Heat\_transfer\_coefficient * Condenser\_diam * \pi * (Sabatier\_exit\_temp - Water\_boil\_temp)) \tag{93}$$

$$Condenser\_outerV = \pi * (Condenser\_diam/2 + Condenser\_t)^2 * Condenser\_length \quad (94)$$

$$Condenser\_innerV = \pi * (Condenser\_diam/2)^2 * Condenser\_length \quad (95)$$

$$Condenser\_volume = (Condenser\_outerV - Condenser\_innerV) \quad (96)$$

$$Condenser\_mass = Condenser\_volume * Condenser\_density * Condenser\_massFactor \quad (97)$$

$$Power\_of\_reaction = Reactant\_flow\_rate * Reaction\_enthalpy \quad (98)$$

The code used for modeling the Sabatier reactor system is given in Appendix A.1.3.

3.2.4 Reverse Water Gas Shift and Ethylene/Methanol Reactor

The system for production of either ethylene or methanol combines the reverse water gas shift with either a Fischer-Tropsch or syngas reaction to produce the corresponding fuel and oxygen. In the RWGS reactor, input carbon dioxide and hydrogen are reacted in the presence of a copper catalyst at temperatures above 500 K [42] to produce water and carbon monoxide. The output stream is routed to a condenser/separator and membrane to isolate the two products. The water is sent to the water electrolyzer, while the carbon monoxide, in conjunction with additional hydrogen, is sent to the fuel reactor.

The reaction equilibrium constant of the RWGS depends on temperature. Thus, the temperature, along with the fuel and oxygen requirements from the MAV, determine the sizing of the reaction chamber volume. This volume also depends upon the chamber residence time required to achieve equilibrium. The reactor mass is sized from the reactor volume and cylindrical sizing parameters: length-to-diameter ratio, wall thickness, and chamber wall density. The mass of the catalyst also depends upon the reaction flow rate. Achieving the required temperature for the reaction requires a

Table 12: Reverse Water Gas Shift and Ethylene Reactor Functional Requirements

Function	Physical Components	Relevant Equations
Production of carbon monoxide and water	Reactor, shell	127, 128
Water collection	Condenser, pump	149, 147
Capture hydrogen	Membrane	150
Thermal management	Insulation, wire, heater	129, 145-146
Production of ethylene	Ethylene reactor	151

heater, as well as insulation to maintain the target temperature against the Martian environment. The heater is sized as a function of the thermal power required for reaction enthalpy, heat for input reactants, and preventing heat loss to the environment. The condenser/separator and membrane are sized based on a percentage of reactor mass from historical data sources. The fuel reactor volume and mass are sized as a percentage of the RWGS reactor volume and mass based on estimates made by Zubrin et al.

The geometric parameters for the reactor sizing come from Zubrin et al.'s work at Pioneer Astronautics in the 1990s [11]. Reaction data come from a later paper by Zubrin et al. [35]. The material properties of the nichrome heating wire come from the WireTronic Inc. data sheet [114]. The condenser/separator and membrane mass fractions come from Zubrin et al.'s work on RWGS system experiments [35]. The fuel reactor volume and mass fractions come from sizing estimates made during trade studies performed by Zubrin et al. [11].

The functional requirements, associated physical components, and relevant equations are given in Table 12 and Table 13.The parameters used in modeling the ethylene reactor are given in Table 14. The parameters used in modeling the methanol reactor are given in Table 15.

Table 13: Reverse Water Gas Shift and Methanol Reactor Functional Requirements

Function	Physical Components	Relevant Equations
Production of carbon monoxide and water	Reactor, shell	127, 128
Water collection	Condenser, pump	149, 147
Capture hydrogen	Membrane	150
Thermal management	Insulation, wire, heater	129, 145-146
Production of methanol	Methanol reactor	152

Table 14: Reverse Water Gas Shift and Ethylene Reactor Parameters

Parameter Name	Nominal Value	Source	Description
Reaction temp	873 [K]	[11, 35]	Temperature for reverse water gas shift reaction
Chamber inlet press	1 [atm]	[11, 35]	Pressure of RWGS reaction chamber
Chamber res time	0.025 [s]	[120, 121]	Time for reactants to remain in chamber
Chamber L to D ratio	2	[120, 121]	Ratio of chamber cylindrical barrel length to diameter
Chamber wall t	2 [cm]	[42]	Thickness of chamber wall
Chamber wall density	7850 [kg-m$^-$3]	[70]	Density of steel
Unit to chamber size multi	1.5	[42]	Ratio of volume of RWGS chamber to full reactor system
Ratio quartz to catalyst	3	[11, 120]	Ratio of quartz mass to catalyst and support mass
Reactant feedRate STP to catalyst ratio	80 [cc-min$^-$1-g$^-$1]	[11, 120]	Flow rate of reactants at standard temperature and pressure per mass of catalyst
Catalyst loading	10 %	[11, 122]	Parameter for estimating support mass as a function of catalyst mass

Cp hydrogen[1]	14.57 [J-g^{-}1-K^{-}1]	[42]	Specific heat capacity of hydrogen at 650 K; used as a mean value during reaction
Cp CO2[1]	1.102 [J-g^{-}1-K^{-}1]	[42]	Specific heat capacity of carbon dioxide at 650 K; used as a mean value during reaction
Insulation t	2 [cm]	[42]	Thickness of thermal insulation material
Insulation density	50 [kg-m^{-}2]	[42, 116]	Areal density of thermal insulation
Reactor shell conductivity	14 [W-m^{-}1-K^{-}1]	[70]	Thermal conductivity of steel
Insulation conductivity	0.033 [W-m^{-}1-K^{-}1]	[116]	Thermal conductivity of thermal insulation
Other parts mass ratio	20%	[42]	Mass of sensors, inlet, outlet, and other parts as a fraction of reactor mass
HT eff	80%	[42]	Efficiency of heat transfer from heater to reactor
Wire D	0.25 [cm]	[114]	Diameter of nichrome heating wire
Wire resistivity	1.08 E-06 [Ohm-m]	[114]	Resistivity of nichrome heating wire
Wire density	8400 [kg-m^{-}3]	[114]	Density of nichrome heating wire
Heater packing factor	3	[42]	Scaling factor from wire mass to heater mass
Separation CO2 recovery	92%	[123]	Fraction of carbon dioxide that is recovered from downstream flow
Separation H2 recovery	95%	[123]	Fraction of hydrogen that is recovered from downstream flow
Condenser separator mass ratio to reactor	70%	[35]	Mass of condenser and separator as a fraction of reactor mass
Membrane mass ratio to reactor	40%	[35]	Mass of membrane as a fraction of reactor mass

Pump mass multi	1	[42]	Growth factor on pump mass from empirical fits
Pump power multi	1	[42]	Growth factor on pump power from empirical fits
Volume RWGS multi reactor V	2.5	[42]	Parameter to estimate volume of integrated system as a function of reactor volumes
C2H4 reactor mass multi	1	[35]	Estimation of ethylene reactor mass as a function of RWGS reactor mass
C2H4 reactor V multi	1	[35]	Estimation of ethylene reactor volume as a function of RWGS reactor volume
C2H4 H2 eff	90%	[123]	Estimate of conversion efficiency of hydrogen into ethylene
C2H4 CO2 eff	90%	[123]	Estimate of conversion efficiency of carbon dioxide into ethylene

Table 15: Reverse Water Gas Shift and Methanol Reactor Parameters

Parameter Name	**Nominal Value**	**Source**	**Description**
Reaction temp	873 [K]	[11, 35]	Temperature for reverse water gas shift reaction
Chamber inlet press	1 [atm]	[11, 35]	Pressure of RWGS reaction chamber
Chamber res time	0.025 [s]	[120, 121]	Time for reactants to remain in chamber
Chamber L to D ratio	2	[120, 121]	Ratio of chamber cylindrical barrel length to diameter
Chamber wall t	2 [cm]	[42]	Thickness of chamber wall

Chamber wall density	7850 [kg-m$^-$3]	[70]	Density of steel
Unit to chamber size multi	1.5	[42]	Ratio of volume of RWGS chamber to full reactor system
Ratio quartz to catalyst	3	[11, 120]	Ratio of quartz mass to catalyst and support mass
Reactant feedRate STP to catalyst ratio	80 [cc-min$^-$1-g$^-$1]	[11, 120]	Flow rate of reactants at standard temperature and pressure per mass of catalyst
Catalyst loading	10 %	[11, 122]	Parameter for estimating support mass as a function of catalyst mass
Cp hydrogen[1]	14.57 [J-g$^-$1-K$^-$1]	[42]	Specific heat capacity of hydrogen at 650 K; used as a mean value during reaction
Cp CO2[1]	1.102 [J-g$^-$1-K$^-$1]	[42]	Specific heat capacity of carbon dioxide at 650 K; used as a mean value during reaction
Insulation t	2 [cm]	[42]	Thickness of thermal insulation material
Insulation density	50 [kg-m$^-$2]	[42, 116]	Areal density of thermal insulation
Reactor shell conductivity	14 [W-m$^-$1-K$^-$1]	[70]	Thermal conductivity of steel
Insulation conductivity	0.033 [W-m$^-$1-K$^-$1]	[116]	Thermal conductivity of thermal insulation
Other parts mass ratio	20%	[42]	Mass of sensors, inlet, outlet, and other parts as a fraction of reactor mass
HT eff	80%	[42]	Efficiency of heat transfer from heater to reactor
Wire D	0.25 [cm]	[114]	Diameter of nichrome heating wire
Wire resistivity	1.08 E-06 [Ohm-m]	[114]	Resistivity of nichrome heating wire
Wire density	8400 [kg-m$^-$3]	[114]	Density of nichrome heating wire

Heater packing factor	3	[42]	Scaling factor from wire mass to heater mass
Separation CO2 recovery	92%	[123]	Fraction of carbon dioxide that is recovered from downstream flow
Separation H2 recovery	95%	[123]	Fraction of hydrogen that is recovered from downstream flow
Condenser separator mass ratio to reactor	70%	[35]	Mass of condenser and separator as a fraction of reactor mass
Membrane mass ratio to reactor	40%	[35]	Mass of membrane as a fraction of reactor mass
Pump mass multi	1	[42]	Growth factor on pump mass from empirical fits
Pump power multi	1	[42]	Growth factor on pump power from empirical fits
Volume RWGS multi reactor V	2.5	[42]	Parameter to estimate volume of integrated system as a function of reactor volumes
CH3OH reactor mass multi	1	[35]	Estimation of methanol reactor mass as a function of RWGS reactor mass
CH3OH reactor V multi	1	[35]	Estimation of methanol reactor volume as a function of RWGS reactor volume
CH3OH H2 eff	90%	[123]	Estimate of conversion efficiency of hydrogen into methanol
CH3OH CO2 eff	90%	[123]	Estimate of conversion efficiency of carbon dioxide into methanol

The theoretical hydrogen and carbon dioxide requirements depend on the total propellant demand for either ethylene or methanol and oxygen (from the ascent vehicle

sizing described below in Figures 49 and 50) , the O/F ratio (see Table 37), and the stoichiometric balance of the reverse water gas shift and fuel production equations (Equations 4, 6, and 7, reproduced below); the resulting calculations for ethylene are given in Equations 102 and 103, and the calculations for methanol are given in Equations 104 and 105. The equilibrium constant of the reverse water gas shift is based on the relationship given in Kolb et al. [124] in Equation 106, which is used to compute the quantities of hydrogen and carbon dioxide converted into carbon monoxide and water in the reverse water gas shift according to the method used by DePasquale [42] in Equations 107 and 108. The actual requirements of hydrogen and carbon dioxide are calculated in Equations 109 and 110, and the losses in the RWGS process are calculated in Equations 111 and 112. The total hydrogen and carbon dioxide to feed into the propellant production system for each fuel type depends on the theoretical hydrogen and carbon dioxide requirements, the losses, and the efficiencies of the fuel production processes; these demands are calculated in Equations 113 and 114 for ethylene and Equations 115 and 116 for methanol. The mass flow rates for hydrogen and carbon dioxide are based on the actual requirements and the production time, calculated in Equations 117 and 118. These mass flow rates are then used to estimate the volumetric flow rates using the ideal gas law (evaluated at both the reaction temperature and chamber inlet pressure given in Tables 14 and 15, and at standard temperature and pressure). The total volumetric flow rate at a particular temperature condition is given in Equation 119.

The reverse water gas shift chamber volume is based on the total volumetric flow rate of both the hydrogen and carbon dioxide at the reaction temperature and the chamber residence time (see Equation 120), and the total reactor volume is based on the chamber volume (see Equation 121). The shell volume of the reactor is based on the calculations in Equations 122 to 126, and the shell mass is calculated in Equation 127. The mass of the catalyst and supporting mass depends on the total volumetric

flow rate at standard temperature and pressure, as shown in Equation 128. The insulation mass depends on the reactor surface area as computed from its diameter and length (Equation 129), while the additional support mass is calculated from the shell mass 130. The masses are summed to the total reverse water gas shift reactor mass in Equation 131.

The reaction enthalpies for the reverse water gas shift (Equation 99), the ethylene formation reaction (Equation 100), and the methanol formation reaction (Equation 101) are given in Table 16, from Zubrin et al. [11]. The thermal power required for the reverse water gas shift is calculated in Equation 132, while the thermal power generated by the ethylene and methanol formation reactions is given in Equations 133 and 134, respectively. The heating requirements to prepare the incoming streams of carbon dioxide and hydrogen are calculated in Equations 135 and 136 from the temperature difference and specific heats, while the power requirement is calculated in Equation 137. The heat loss due to conduction through the reactor walls and insulation is calcuated in Equation 138. The total thermal power requirement is the sum of the reverse water gas shift and fuel reaction powers, the thermal power for heating, and the heat losses, divided by the heat transfer efficiency parameter in Tables 14 and 15, shown in Equations 139 and 140.

The nichrome wire heater is sized by computing the geometry and mass of the wire and heater in Equations 141 to 145, with the final mass of the heater in Equation 146. The rotary vane pump mass and power are estimated from a stepwise linear regression performed by DePasquale [42], with the mass and power each functions of the total volumetric flow rate at standard temperature and pressure, expressed in cubic meters per hour. Table 17 shows the slope and intercept for the mass regressions, while Table 18 shows the power regressions in each range of flow rates. The pump mass and pump power are then multiplied by the parameters *Pump_mass_multi* and *Pump_power_multi*, respectively; these are growth factors DePasquale applied to the

empirical regressions [42]. The masses of the condenser, membrane, and ethylene and methanol reactors are estimated as fractions of the reverse water gas shift reactor total mass, and are calculated in Equations 149 to 152. The ethylene and methanol reactor volumes are based on the reverse water gas shift volume, calculated in Equations 153 and 154. The total system mass is the sum of Equations 131, 147, 146, 149, 150, and either 151 (for ethylene) or 152 (for methanol). The total power is the sum of either Equation 139 (for ethylene) or 140 (for methanol) and Equation 148, while the total volume is the sum of Equations 121 and either Equation 153 (for ethylene) or 154 (for methanol).

$$\mathrm{CO_2 + H_2 \longrightarrow CO + H_2O} \tag{99}$$

$$\mathrm{2\,CO + 4\,H_2 \longrightarrow C_2H_4 + 2\,H_2O} \tag{100}$$

$$\mathrm{3\,CO + 2\,H_2 \longrightarrow CH_3OH + 2\,CO} \tag{101}$$

$$\begin{aligned} H2\_required\_theory = max(&0.144 * prop\_demand/(1 + O/F), \\ &0.063 * O/F * prop\_demand/(1 + O/F)) \end{aligned} \tag{102}$$

$$\begin{aligned} CO2\_required\_theory = max(&3.138 * prop\_demand/(1 + O/F), \\ &1.375 * O/F * prop\_demand/(1 + O/F)) \end{aligned} \tag{103}$$

$$H2\_required\_theory = 0.126 * prop\_demand/(1 + O/F) \tag{104}$$

$$\begin{aligned} CO2\_required\_theory = max(&4.121 * prop\_demand/(1 + O/F), \\ &2.750 * O/F * prop\_demand/(1 + O/F)) \end{aligned} \tag{105}$$

$$K_{eq,RWGS} = e^{4577.8/Reaction\_temp - 4.33} \tag{106}$$

$$Eq_{C}O2_{c}onverted_{p}er_{p}ass = 1 - 1/(1 + 1/\sqrt{K_{eq,RWGS}}) \tag{107}$$

$$Eq_{H}2_{c}onverted_{p}er_{p}ass = 1 - 1/(1 + 1/\sqrt{K_{eq,RWGS}}) \tag{108}$$

$$H2\_required\_actual = H2\_required\_theory / Eq\_H2\_converted\_per\_pass \tag{109}$$

$$CO2\_required\_actual = CO2\_required\_theory / Eq\_CO2\_converted\_per\_pass \tag{110}$$

$$H2\_separation\_losses = H2\_required\_actual * (1 - Eq\_H2\_converted\_per\_pass) * (1 - Separation\_H2\_recovery) \tag{111}$$

$$CO2\_separation\_losses = CO2\_required\_actual * (1 - Eq\_CO2\_converted\_per\_pass) * (1 - Separation\_CO2\_recovery) \tag{112}$$

$$H2\_feed\_after\_recycle = H2\_required\_theory/C2H4\_H2\_eff + H2\_separation\_losses \tag{113}$$

$$CO2\_feed\_after\_recycle = CO2\_required\_theory/C2H4\_CO2\_eff + CO2\_separation\_losses \tag{114}$$

$$H2\_feed\_after\_recycle = H2\_required\_theory/CH3OH\_H2\_eff + H2\_separation\_losses \tag{115}$$

$$CO2\_feed\_after\_recycle = CO2\_required\_theory/CH3OH\_CO2\_eff + CO2\_separation\_losses \tag{116}$$

$$H2\_flow\_rate = H2\_required\_actual/production\_time \tag{117}$$

$$CO2\_flow\_rate = CO2\_required\_actual/production\_time \tag{118}$$

$$Total\_V\_flow\_rate_{Tcondition} = H2\_flow\_rate + CO2\_flow\_rate \tag{119}$$

$$Chamber\_V = Total\_V\_flow\_rate_{reactT} * Chamber\_res\_time \tag{120}$$

$$Reactor\_V = Chamber\_V * Unit\_to\_chamber\_size\_multi \tag{121}$$

$$Reactor\_D = (4 * Reactor\_V/(\pi * Chamber\_L\_to\_D\_ratio))^{\frac{1}{3}} \tag{122}$$

Table 16: Reaction Enthalpies for Ethylene and Methanol [11]

Reaction	**Enthalpy [kJ-kg^{-1}]**
Reverse Water Gas Shift	817
Ethylene Formation	-331
Methanol Formation	-176

$$Reactor\_L = Reactor\_D * Chamber\_L\_to\_D\_ratio \tag{123}$$

$$Outer\_V = \pi * (Reactor\_D/2 + Chamber\_wall\_t)^2 * Reactor\_L \tag{124}$$

$$Inner\_V = \pi * (Reactor\_D/2)^2 * Reactor\_L \tag{125}$$

$$Shell\_V = Outer\_V - Inner\_V \tag{126}$$

$$Shell\_mass = Shell\_V * Chamber\_wall\_density \tag{127}$$

$$\begin{aligned} Catalyst\_mass = Total\_V\_flow\_rate_{STP} \\ /Reactant\_feedRate\_STP\_to\_catalyst\_ratio/Catalyst\_loading \\ *(1 + Ratio\_quartz\_to\_catalyst) \end{aligned} \tag{128}$$

$$Insulation\_mass = \pi * Reactor\_D * Reactor\_L * Insulation\_density \tag{129}$$

$$Other\_parts\_mass = Shell\_mass * Other\_parts\_mass\_ratio \tag{130}$$

$$\begin{aligned} Reactor\_total\_mass = Shell\_mass + Catalyst\_mass \\ +Insulation\_mass + Other\_parts\_mass \end{aligned} \tag{131}$$

$$\begin{aligned} Reaction\_thermal\_power = RWGS\_reaction\_enthalpy \\ *(H2\_flow\_rate + CO2\_flow\_rate) \end{aligned} \tag{132}$$

$$\begin{aligned} C2H4\_thermal\_power = C2H4\_reaction\_enthalpy \\ *(H2\_flow\_rate + CO2\_flow\_rate) \end{aligned} \tag{133}$$

$$CH3OH\_thermal\_power = CH3OH\_reaction\_enthalpy * (H2\_flow\_rate + CO2\_flow\_rate) \tag{134}$$

$$CO2\_heating\_requirement = (Reaction\_temp - Daytime\_temp) * Cp\_CO2 \tag{135}$$

$$H2\_heating\_requirement = (Reaction\_temp - Daytime\_temp) * Cp\_hydrogen \tag{136}$$

$$Thermal\_power\_heating = (CO2\_heating\_requirement * CO2\_flow\_rate + H2\_heating\_requirement * H2\_flow\_rate) \tag{137}$$

$$\begin{aligned} Heat\_loss = (((ln(Reactor\_D/2 + Chamber\_wall\_t)/(Reactor\_D/2) \\ *(1/(2 * \pi * Reactor\_shell\_conductivity * Reactor\_L))) \\ +((ln(Reactor\_D/2 + Chamber\_wall\_t + Insulation\_t) \\ /(Reactor\_D/2 + Chamber\_wall\_t)) \\ *(1/(2 * \pi * Insulation\_conductivity * Reactor\_L)))) \end{aligned} \tag{138}$$

$$Total\_thermal\_power\_required = (Reaction\_thermal\_power + Thermal\_power\_heating + Heat\_loss + C2H4\_thermal\_power)/HT\_eff \tag{139}$$

$$Total\_thermal\_power\_required = (Reaction\_thermal\_power + Thermal\_power\_heating + Heat\_loss + CH3OH\_thermal\_power) /HT\_eff \tag{140}$$

$$Wire\_crosssecA = \pi * (Wire\_D/2)^2 \tag{141}$$

$$Wire\_loops = Reactor\_L/Wire\_D; \tag{142}$$

$$Wire\_length = Wire\_loops * \pi * Reactor\_D \tag{143}$$

$$Nichrome\_V = Wire\_crosssecA * Wire\_length \tag{144}$$

$$Nichrome\_mass = Wire\_density * Nichrome\_V \tag{145}$$

Table 17: Pump Mass Data for Reverse Water Gas Shift Reactor [42]

Lower Bound	Upper Bound	Mass Slope	Mass Intercept
0	6	2.9	5.6
6	26	0.5	21.2
26	80	1.2	4.5
80	178	0.8	46.3
178	1150	1.1	-16.8

Table 18: Pump Power Data for Reverse Water Gas Shift Reactor [42]

Lower Bound	Upper Bound	Power Slope	Power Intercept
0	7.8	56.7	19
7.8	26.8	7.6	406
26.8	80	29.3	-173
80	178	28.0	-73
178	1150	17.7	1769

$$Heater\_mass = Heater\_packing\_factor * Nichrome\_mass \tag{146}$$

$$Pump\_mass = Mass\_Slope * Total\_V\_flow\_rate_{STP} + Mass\_Intercept \tag{147}$$

$$Pump\_power = Power\_Slope * Total\_V\_flow\_rate_{STP} + Power\_Intercept \tag{148}$$

$$\begin{aligned} Condenser\_mass = Reactor\_total\_mass \\ *Condenser\_separator\_mass\_ratio\_to\_reactor \end{aligned} \tag{149}$$

$$Membrane\_mass = Reactor\_total\_mass * Membrane\_mass\_ratio\_to\_reactor \tag{150}$$

$$C2H4\_reactor\_mass = Reactor\_total\_mass * C2H4\_reactor\_mass\_multi \tag{151}$$

$$\begin{aligned} CH3OH\_reactor\_mass = Reactor\_total\_mass \\ *CH3OH\_reactor\_mass\_multi \end{aligned} \tag{152}$$

$$C2H4\_reactor\_V = Reactor\_V * C2H4\_reactor\_V\_multi \tag{153}$$

$$CH3OH\_reactor\_V = Reactor\_V * CH3OH\_reactor\_V\_multi \tag{154}$$

The code used for modeling the RWGS and ethylene system is given in Appendix A.1.4. The code used for modeling the RWGS and methanol system is given in Appendix A.1.5.

3.2.5 Water Electrolysis

The water electrolysis system is used to create hydrogen and oxygen from the various input streams of water. Potential sources of water (depending on the architecture) include a water storage tank, Sabatier reactor, RWGS reactor, and Mars water processing plant. A proton exchange membrane applies a voltage to ionize the hydrogen atoms, leading to dissociation of the oxygen atoms. Multiple passes are required due to the low percentage of oxygen and hydrogen conversion (on the order of two to three percent [42]).

The power required for the electrolyzer is a function of the oxygen or hydrogen production rate and the operating voltage; the production rate determines the current required. The mass of the electrolyzer is calculated from the power and historical power-to-mass ratios for proton exchange membrane electrolyzers.

The operating voltage of the electrolyzer comes from the work of Thunnissen et al. [125] and Iacomini and Sridhar [126]. The relationship between production rate and current requirements comes from Clark's analysis [127] as well as Rapp's investigations [6]. The power-to-mass ratio data comes from DRM 1 [3] and from Sridhar et al. [41].

The functional requirements, associated physical components, and relevant equations are given in Table 19.The parameters used in modeling the water electrolyzer are given in Table 20.

Table 19: Water Electrolyzer Functional Requirements

Function	Physical Components	Relevant Equations
Oxygen and hydrogen production	Electrolyzer	166
Water storage	Tank	33, 165

Table 20: Water Electrolyzer Parameters

Parameter Name	Nominal Value	Source	Description
Percent flow utilization	3%	[126, 128–130]	Fraction of water electrolyzed during each pass of the electrolyzer
Operating voltage	1.5 [V]	[125, 126, 128, 129]	Voltage of the water electrolyzer
O2 mass rate for 1A	0.298 [g-hr$^-$1]	[37, 126]	Amount of oxygen electrolyzed per ampere input; used for power requirement calculation
Water V to flowRate	0.016 [m^3-s-kg$^-$1]	[131]	Parameter that scales the water tank volume of the flow rate of electrolyzed water
Volume struct fraction	10%	[42]	Volume growth multiplier accounting for structure of plumbing
Percent heat loss	15%	[42]	Power lost as heat during electrolysis
Power to mass ratio	23 [We-kg$^-$1]	[3, 41]	Mass of electrolyzer as a function of required power
Tank fill fraction	90%	[42]	Fraction of tank volume filled with water
Tank mass factor	5000 [m]	[22, 42]	Parameter used in the estimation of tank mass from volume and pressure

Tank safety factor	2	[22, 42]	Multiplier on the tank burst pressure used in the estimation of tank mass from volume and pressure
Percent H2 recycle	98%	[34, 115, 123]	Fraction of hydrogen that is captured from electrolysis

The total water into the electrolyzer is based on the total water to be converted, the production time, and the fraction of the total water throughput that is electrolyzed in each pass, and is calculated in Equation 155. The oxygen production rate is based on the water electrolyzed in each pass of the electrolyzer, and is calculated in Equation 156. The power required for the electrolyzer depends on the oxygen production rate and is calculated in Equations 157 to 159. The tank used for electrolysis (which differs from water tanks used elsewhere in the architectures) is based on the total liquid accumulated in the tank and the tank sizing method of Larson and Pranke [22], and is calculated in Equations 160 to 165. The electrolyzer mass itself is based on historical data on power-to-mass ratios, and is calculated in Equation 166. The total mass of the system is the sum of the tank mass (Equation 165) and electrolyzer mass (Equation 166).

$$Liquid\_flow\_rate = H2O\_available/production\_time\ /Percent\_flow\_utilization \tag{155}$$

$$O2\_production\_rate = H2O\_available/production\_time * \frac{8}{9} \tag{156}$$

$$Current\_required = O2\_production\_rate/O2\_mass\_rate\_for\_1A \tag{157}$$

$$Power\_process = Current\_required * Operating\_voltage \tag{158}$$

$$Total\_power = Power\_process * (1 + Percent\_heat\_loss) \tag{159}$$

$$Volume\_water = Liquid\_flow\_rate * Water\_V\_to\_flowRate \tag{160}$$

$$Volume\_storage\_tank = Volume\_water/Tank\_fill\_fraction \tag{161}$$

$$Tank\_radius = (\frac{3}{4} * Volume\_storage\_tank/\pi)^{\frac{1}{3}} \tag{162}$$

$$Tank\_area = 4 * pi * Tank\_radius^2 \tag{163}$$

$$Pressure\_on\_tank\_bottom = H2O\_available * g_0/(Tank\_area/2) \tag{164}$$

$$\begin{aligned} Tank\_mass = (Pressure\_on\_tank\_bottom) * Tank\_safety\_factor \\ /Tank\_mass\_factor/g_0 * Volume\_storage\_tank \end{aligned} \tag{165}$$

$$Electrolyzer\_mass = Total\_power/Power\_to\_mass\_ratio \tag{166}$$

The code used for modeling the water electrolysis system is given in Appendix A.1.6.

3.2.6 Carbon Dioxide Electrolysis

The carbon dioxide electrolysis system is used to create oxygen from the carbon dioxide produced by the acquisition system. This system is used for the oxygen-only architectures, as well as for the methane architecture using hydrogen brought from Earth. A zirconia electrolyte is used to conduct oxygen atoms from ionized carbon dioxide molecules. The power required for the electrolyzer is a function of the oxygen production rate and the operating voltage; the production rate determines the current required. The mass of the electrolyzer is calculated from the power and historical power-to-mass ratios for zirconia solid oxide electrolyzers. The operating voltage of the electrolyzer comes from the work of Minh et al. [132]. DePasquale uses the same relationship between production rate and current requirements as used for water electrolysis [42]; as before, that data come from Clark's analysis [127] as well as Rapp's investigations [6]. The power-to-mass ratio data comes from DRM 1 [3].

Table 21: Carbon Dioxide Electrolyzer Functional Requirements

Function	**Physical Components**	**Relevant Equations**
Oxygen production	Electrolyzer	175

The functional requirements, associated physical components, and relevant equations are given in Table 21.The parameters used in modeling the carbon dioxide electrolyzer are given in Table

The oxygen production rate depends on the total oxygen demand and the available production time in Equation 167. The percent utilization (the amount of oxygen extracted as a function of the total oxygen in the carbon dioxide available) is based on a regression of the data in Minh [132] and shown in Figure 44 and Equation 168. The power required for the electrolyzer depends on the oxygen production rate and is calculated in Equations169 to 171. The current density is based on a regression of the data in Minh [132] shown in Figure 44 and Equation 172; this data is used to estimate the wafer area and thickness in Equations 173 and 174. The mass is based on power to mass ratio data for carbon dioxide electrolyzers in DRM 1 [3] and is calculated in Equation 175, while the volume is calculated in Equation 176.

$$O2\_production\_rate = O2\_demand/production\_time \tag{167}$$

$$Percent\_utilization = 7.12157E-05 * e^{5*Voltage} \tag{168}$$

$$Current\_required = O2\_production\_rate/O2\_mass\_rate\_for\_1A \tag{169}$$

$$Power\_process = Voltage * Current\_required \tag{170}$$

$$Total\_power = Power\_process * (1 + Percent\_heat\_loss) \tag{171}$$

$$Current\_density = 0.0022268 * e^{2.92651*Voltage} \tag{172}$$

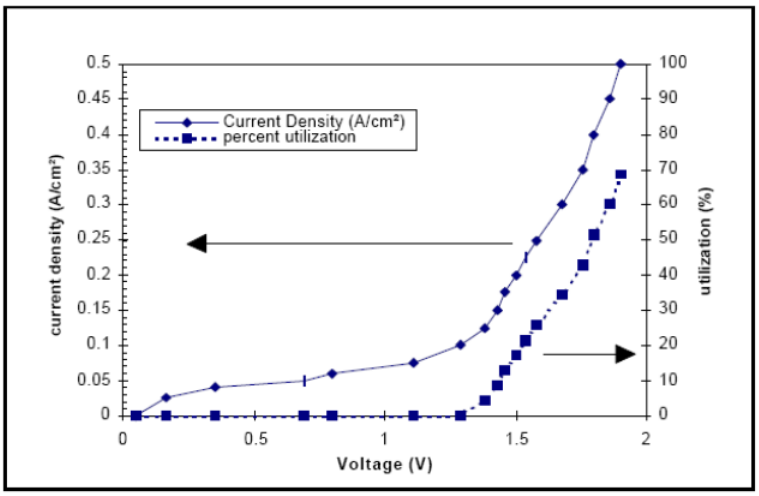

Figure 3. Performance curves of a 5 cm x 5 cm cell at 800°C.

Figure 44: Relationship between current density and carbon dioxide percent utilization to operating voltage of a CO_2 electrolyzer, reproduced from Reference [132].

$$Wafer\_area = Current\_required/Current\_density \tag{173}$$

$$Thickness = \sqrt{Wafer\_area} * t\_to\_L\_ratio \tag{174}$$

$$Electrolyzer\_mass = Total\_power/Power\_to\_mass\_ratio \tag{175}$$

$$Volume = Wafer\_area * Thickness \tag{176}$$

Table 22: Carbon Dioxide Electrolyzer Parameters

Parameter Name	Nominal Value	Source	Description
Operating voltage	1.85 [V]	[126, 132]	Voltage of the carbon dioxide electrolyzer
O2 mass rate for 1A	0.298 [g-hr$^-$1]	[37, 126]	Amount of oxygen electrolyzed per ampere input; used for power requirement calculation
Percent heat loss	25%	[42]	Power lost as heat during electrolysis
Power to mass ratio	29.73 [We-kg$^-$1]	[3]	Mass of electrolyzer as a function of required power

t to L ratio	0.1	[132]	Ratio of zirconia wafer thickness to length; used in volume calculation

The code used for modeling the carbon dioxide electrolysis system is given in Appendix A.1.7.

3.2.7 Cryocoolers

Methane, oxygen, and hydrogen are cryogens at Mars surface temperatures, and thus require cryocoolers both to liquefy the products of ISPP processes, and to maintain the temperature of stored products. Two types of cryocoolers are considered in this study: Brayton cycle cryocoolers and Stirling/Pulse Tube cryocoolers. DePasquale describes the two systems: "Both are closed-loop refrigerators whereby work is performed on a working gas, and this gas removes heat from the target gas via a heat exchanger. The Brayton Cycle cryocooler employs a recuperative heat exchanger with the working gas flowing in a continuous loop around the cycle. Stirling/Pulse Tube cryocoolers employ a regenerative cycle whereby the working gas alternately flows across a bed of heat adsorbing material to recover heat between hot and cold flows" [42].

The thermal power to be removed from the cryogenic fluid is calculated from the liquefaction enthalpy change and the heat leak from the ambient environment. The electrical power required is sized as a multiple of the thermal power based on historical cryocooler efficiency data. Historical mass estimating relationships for the two types of cryocoolers, based on thermal power requirements, are used to calculate the mass of the cryocoolers (including recirculation pumps). For each cryogenic fluid, both pumps are sized, and the less massive of the two is used in the analysis.

Table 23: Methane Cryocooler Functional Requirements

Function	**Physical Components**	**Relevant Equations**
Thermal management	Brayton/Stirling cryocooler	184-185

Table 24: Oxygen Cryocooler Functional Requirements

Function	**Physical Components**	**Relevant Equations**
Thermal management	Brayton/Stirling cryocooler	184-185

Table 25: Hydrogen Cryocooler Functional Requirements

Function	**Physical Components**	**Relevant Equations**
Thermal management	Brayton/Stirling cryocooler	184-185

Table 26: Cryocooler Modeling Data

Cryogen	$T_{initial}$ **[K]**	$T_{storage}$ **[K]**	$h_{liquefaction}$ **[J-g**$^{-}$**1]**
Methane	Sabatier Temperature (Table 11)	111	512
Oxygen	298	90	213
Hydrogen	240	20	454

The enthalpy data for cooling and liquefaction come from Salerno and Kittel [133] and Notardonato's [111] studies of cryogenic storage on the surface of Mars. The ratio of electrical to thermal power comes from a survey of several studies of space cryocoolers [134–138]. The mass estimating relationships come from Salerno and Kittel and Notardonato's studies [111,133], while the volume estimating relationships come from the same studies as the electrical to thermal power data [134–138].

The functional requirements, associated physical components, and relevant equations are given in Tables 23, 24, and 25.The parameters used in modeling the methane cryocooler are given in Table 27. The parameters used in modeling the oxygen cryocooler are given in Table 28. The parameters used in modeling the hydrogen cryocooler are given in Table 29.

For each cryocooler, the thermal cooling required depends on the enthalpy to reduce the fluid to its storage temperature, as well as the latent heat that must be removed to accomplish the phase change to liquid. Each fluid has an assumed initial temperature given in Table 26, while the ambient temperature is conservatively assumed to be the daytime temperature of 240 K [108,110]. Linear fits of the enthalpy as a function of temperature are used to compute the enthalpy to cool the fluid from its initial temperature to its storage temperature based on the data in Figure 45, from Reference [133], are given in Equations 177 to 179. The latent heats of each fluid are also included in Table 26. From this information, the total enthalpy change required by the cryocooler is given in Equation 180. The total heat to be removed is then the product of the total enthalpy change, the production rate of the cryogenic fluid, and the cycle efficiency, shown in Equation 181. The electrical power required for the Stirling and Brayton cryocoolers are calculated in Equations 182 and 183. The masses of the Stirling and Brayton cryocoolers are based on the equations given in Salerno and Kittel [133] and repeated in Equations 184 and 185. The volumes of the Stirling and Brayton cryocoolers are calculated in Equations 186 and 187.

Table 27: Methane Cryocooler Parameters

Parameter Name	**Nominal Value**	**Source**	**Description**
Daytime temp[1]	240 [K]	[108, 110]	Daytime temperature on surface of Mars; used to size cryocooling load
Tank temp[1]	112 [K]	[118]	Storage temperature for methane
CH4 latent heat[1]	512 [J-g$^-$1]	[111, 133]	Energy to be extracted to condense methane
Power eff Stirling	7%	[134–138]	Ratio of thermal cooling to electrical input power required for Stirling cycle cryocooler
Power eff Brayton	7%	[134–138]	Ratio of thermal cooling to electrical input power required for Brayton cycle cryocooler
Volume to cooling-Power Stirling	7.1 E-05 [m^3-We$^-$1]	[134–138]	Parameter to estimate volume of Stirling cycle cryocooler as a function of power
Volume to cooling-Power Brayton	7.1 E-05 [m^3-We$^-$1]	[134–138]	Parameter to estimate volume of Brayton cycle cryocooler as a function of power

Table 28: Oxygen Cryocooler Parameters

Parameter Name	**Nominal Value**	**Source**	**Description**
Daytime temp[1]	240 [K]	[108, 110]	Daytime temperature on surface of Mars; used to size cryocooling load
Tank temp[1]	90 [K]	[118]	Storage temperature for oxygen
O2 latent heat[1]	213 [J-g$^-$1]	[111, 133]	Energy to be extracted to condense oxygen

Power eff Stirling	7%	[134–138]	Ratio of thermal cooling to electrical input power required for Stirling cycle cryocooler
Power eff Brayton	7%	[134–138]	Ratio of thermal cooling to electrical input power required for Brayton cycle cryocooler
Volume to cooling-Power Stirling	7.1 E-05 [m^3-We^-1]	[134–138]	Parameter to estimate volume of Stirling cycle cryocooler as a function of power
Volume to cooling-Power Brayton	7.1 E-05 [m^3-We^-1]	[134–138]	Parameter to estimate volume of Brayton cycle cryocooler as a function of power

Table 29: Hydrogen Cryocooler Parameters

Parameter Name	**Nominal Value**	**Source**	**Description**
Daytime temp[1]	240 [K]	[108, 110]	Daytime temperature on surface of Mars; used to size cryocooling load
Tank temp[1]	20 [K]	[118]	Storage temperature for hydrogen
H2 latent heat[1]	454.3 [J-g^-1]	[111, 133]	Energy to be extracted to condense hydrogen
Power eff Stirling	7%	[134–138]	Ratio of thermal cooling to electrical input power required for Stirling cycle cryocooler
Power eff Brayton	7%	[134–138]	Ratio of thermal cooling to electrical input power required for Brayton cycle cryocooler
Volume to cooling-Power Stirling	7.1 E-05 [m^3-We^-1]	[134–138]	Parameter to estimate volume of Stirling cycle cryocooler as a function of power

Volume to cooling-Power Brayton	7.1 E-05 [m^3-$We^{-}1$]	[134–138]	Parameter to estimate volume of Brayton cycle cryocooler as a function of power

$$h_{CH_4} = 2.08 * T_{CH_4} - 209 \tag{177}$$

$$h_{O_2} = 0.912 * T_{O_2} - 82.6 \tag{178}$$

$$h_{H_2} = 13 * T_{H_2} - 142 \tag{179}$$

$$h_{total} = h_{T_{initial}} - h_{T_{storage}} + h_{liquefaction} \tag{180}$$

$$Q_{thermal} = h_{total} * Cryogen\_production\_rate/Cycle\_eff \tag{181}$$

$$Stirling\_power = Q_{thermal}/Power\_eff\_Stirling \tag{182}$$

$$Brayton\_power = Q_{thermal}/Power\_eff\_Brayton \tag{183}$$

$$Stirling\_mass = (Q_{thermal}^{0.7} * ((Daytime\_temp - T_{storage})/T_{storage})^{1.45}) \tag{184}$$

$$Brayton\_mass = (172 * T_{storage}^{-0.85} * Q_{thermal}^{0.52}) \tag{185}$$

$$Stirling\_volume = Q_{thermal} * Volume\_to\_coolingPower\_Stirling \tag{186}$$

$$Brayton\_volume = Q_{thermal} * Volume\_to\_coolingPower\_Brayton \tag{187}$$

The code used for modeling the methane cryocooler is given in Appendix A.1.8. The code used for modeling the oxygen cryocooler is given in Appendix A.1.9. The code used for modeling the hydrogen cryocooler is given in Appendix A.1.10.

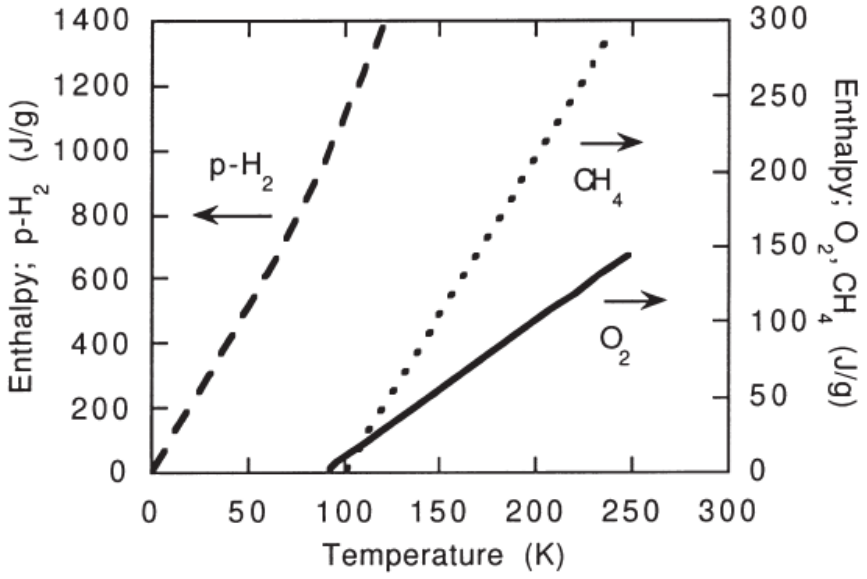

Figure 45: Enthalpy vs temperature for hydrogen, oxygen, and methane, reproduced from Reference [133].

3.2.8 Tanks and Lines

The fuel and oxidizer tanks are part of the ascent vehicle, and thus are included in the MAV mass. However, any water tank or hydrogen tank (except when hydrogen is used as a fuel) is another element of the ISPP system.

The hydrogen volume for storage is based on the mass of hydrogen and its liquid density. The burst pressure of the hydrogen tank is calculated from the vapor pressure of the liquid and a factor of safety. The burst pressure and volume, along with a tank mass factor, are used to estimate the mass of the tank. A parametric estimate of insulation mass is made from the surface area of the tank, and added to the tank mass for the total mass.

The water volume is calculated from the mass of water and its liquid density. DePasquale assumes the burst pressure is the pressure of the water on the lower half of the tank in the presence of gravity (Earth's gravity, for the maximum load case) [42]. A tank mass factor and factor of safety are used to estimate the mass of

Table 30: Water Tank Functional Requirements

Function	Physical Components	Relevant Equations
Storage	Tank	192
Thermal management	Insulation	193

Table 31: Hydrogen Tank Functional Requirements

Function	Physical Components	Relevant Equations
Storage	Tank	199
Thermal management	Insulation	201

the tank.

A tank mass factor of 5000 m and and a factor of safety of 2.0 are taken from the work of Larson and Pranke [22]. For the piping and lines running between systems, Zubrin et al.'s 20% mass fraction is used [35].

The functional requirements, associated physical components, and relevant equations are given in Tables 30 and 31.The parameters used in modeling the water tank are given in Table 32. The parameters used in modeling the hydrogen tank are given in Table 33.

Table 32: Water Tank Parameters

Parameter Name	Nominal Value	Source	Description
H2O density[1]	1000 [kg-m$^-$3]	[118]	Density of liquid water
Tank fill fraction	90%	[42]	Fraction of tank volume filled with water
Tank mass factor	5000 [m]	[22, 42]	Parameter used in the estimation of tank mass from volume and pressure
Tank safety factor	2	[22, 42]	Multiplier on the tank burst pressure used in the estimation of tank mass from volume and pressure

Insulation density	1.27 [kg-m$^-$2]	[42]	Density of thermal insulation material

Table 33: Hydrogen Tank Parameters

Parameter Name	**Nominal Value**	**Source**	**Description**
H2 density[1]	71 [kg-m$^-$3]	[118]	Density of liquid hydrogen
H2 temp[1]	20 [K]	[118]	Storage temperature for hydrogen
H2 pressure[1]	172800 [Pa]	[118]	Vapor pressure of hydrogen at 20 K
Tank mass factor	5000 [m]	[22, 42]	Parameter used in the estimation of tank mass from volume and pressure
Tank safety factor	2	[22, 42]	Multiplier on the tank burst pressure used in the estimation of tank mass from volume and pressure
Tank barrel L to D	1	[42]	Ratio of tank cylindrical barrel length to diameter
Insulation density	1.27 [kg-m$^-$2]	[42]	Density of thermal insulation material
Tank dome factor	0.707	[42]	Ratio of tank dome height to tank cylindrical barrel diameter

The volume of the spherical water tank is based on the total water stored, its density, and the fraction of the tank that is filled in Equation 188. The water tank mass and insulation based are based on the volume of the water tank and the tank

sizing method of Larson and Pranke [22] and is calculated in Equations 189 to 193.

$$Volume\_tank = H2O\_mass/H2O\_density/Tank\_fill\_frac \tag{188}$$

$$Tank\_R = (Volume\_tank * \frac{3}{4}/\pi)^{\frac{1}{3}} \tag{189}$$

$$Tank\_A = 4 * \pi * Tank\_R^2 \tag{190}$$

$$Tank\_pressure\_bot = H2O\_mass * g_0/(Tank\_A/2) \tag{191}$$

$$Tank\_mass = Tank\_pressure\_bot * Tank\_safety\_factor /Tank\_mass\_factor/g_0 * Volume\_tank \tag{192}$$

$$Tank\_insulation\_mass = Tank\_A * Insulation\_density \tag{193}$$

The volume of the cylindrical hydrogen tank is calculated from the volume of hydrogen required (Equation 194) and the geometry of the dome and barrel sections, calculated in Equations 195 to 198. The mass of the tank is calculated via the tank sizing method of Larson and Pranke [22], shown in Equation 199. The tank surface area and insulation mass are calculated in Equations 200 and 201.

$$Tank\_internal\_V = H2\_mass/H2\_density \tag{194}$$

$$Tank\_diameter = (Tank\_internal\_V/(\frac{1}{4} * \pi *Tank\_barrel\_L\_to\_D + \pi/6 * Tank\_dome\_factor))^{\frac{1}{3}} \tag{195}$$

$$Tank\_radius = Tank\_diameter/2 \tag{196}$$

$$Tank\_top\_dome\_V = (\frac{4}{3} * \pi * Tank\_dome\_factor *Tank\_radius^3)/2 \tag{197}$$

$$Tank\_bottom\_dome\_V = Tank\_top\_dome\_V \tag{198}$$

$$Tank\_mass = H2\_Pressure * Tank\_safety\_factor *Tank\_internal\_V/9.81/Tank\_mass\_factor \tag{199}$$

$$Tank\_surface\_area = (4 * \pi * Tank\_dome\_factor * Tank\_radius^2) + (2 * \pi * Tank\_radius * Tank\_diameter * Tank\_barrel\_L\_to\_D) \quad (200)$$

$$Tank\_insulation\_mass = Tank\_surface\_area \; Insulation\_density \quad (201)$$

The code used for modeling the water tank is given in Appendix A.1.11. The code used for modeling the hydrogen tank is given in Appendix A.1.12.

3.3 Other Architectural Elements

3.3.1 Surface Power Supply

Previously in this research, a nuclear power source was shown to have less mass than a solar approach, even under conservative assumptions for the nuclear system's performance. Thus, the larger analysis that follows uses a nuclear system. The surface power supply provides the requisite power for the ISPP system. The nuclear fission power system is defined using ratios of specific mass, volume, and cost. It is assumed that a single system, sized for the ISPP power requirements, will suffice to meet the mission's power needs; the benefits and costs of including a redundant power supply are outside the scope of this research.

The mass of the power supply is estimated from the power requirement of the ISPP system, and a specific mass parameter α. The precise value of α is unknown, as such a system has not yet been built and flown. However, the literature suggests a range of values from 23 to 266 kg/kWe [10, 69, 71–73], with lower values of α as the power requirements increases. Each time an ISPP architecture is modeled, unless a particular value of α is prescribed (as in the first four scenarios examined in Section 4.4), the value is generated from a continuous uniform distribution using those bounds as the minimum and maximum (see the fifth scenario in Section 4.4). This yields a range of masses for the power supply as a function of the power required.

The volume and cost of the power supply are also unknown; similar parameters

Table 34: Lunar Nuclear Plant Cost Estimates [139]

Element	Value
Mass (kg)	5400
DDT&E Cost ($FY2006)	200
Unit Cost ($FY2006)	67
Lower Bound	75%
Upper Bound	175%

to the specific mass can be used to estimate their value. The specific volume (as a function of power system mass) has a nominal value of 0.0043 m^3/kg, with a uniform distribution of between 80% and 120% of this value used for sampling [71]. The specific Design, Development, Testing, and Evaluation (DDT&E cost (as a function of mass) has a nominal value of 0.037 $M/kg, while the specific unit production cost has a nominal value of 0.012 $M/kg [139]. DePasquale et al. give both of these costs an uncertainty range from 75% of nominal to 175% of nominal; thus, a uniform distribution between those bounds is sampled each time a power supply cost is estimated. These values are taken from the cost estimates and masses presented for a nuclear power system for lunar ISRU, summarized in Table 34. With the application of these parameters, the power supply's volume and costs are passed to the architecture for use in sizing the MDV, as well as for compilation in the overall architectural metrics.

3.3.2 Mars Ascent Vehicle

The Mars Ascent Vehicle (MAV) delivers a fixed payload through a fixed ΔV (derived from DRA 5.0 and earlier reference architectures [1, 140], see Table 35) at the conclusion of the surface mission. The functional requirements of the MAV are given in Table 36. The vehicle is a two-stage vehicle, with a ΔV split chosen to minimize gross mass. Sizing of the vehicle is based on the Launch Vehicle Sizing and Synthesis Tool

Table 35: MAV Requirements

Name	Value	Description
$m_{payload}$	5805 kg	Payload lifted to Martian orbit
ΔV	5625 $\frac{m}{s}$	Performance required for transfer from LEO to Mars

Table 36: Mars Ascent Vehicle Functional Requirements

Function	Physical Components	Relevant Equations
Ascent from surface	Inert mass, Propellant mass	Figures 48-51
Propellant storage	Body Structure mass	Figures 48-51, Line 2

(LVSSS) [141, 142] and propulsion characteristics based on the those of the RL10A-4-2 (see Table 37 for modeling data) [143] and NASA's Chemical Equilibrium with Applications (CEA)[2]. The CEA model, using the RL10A-4-2 engine characteristics in Table 37 and an O/F ratio of 5.5, matched the Isp of 451 s of the RL10A-4-2 [143]. Note that the RL10 was fired using methane; thus, although actual engine design for each propellant type would likely yield different engine configurations, a fixed engine design is used in this research for all four fuels. Figure 46 shows the Mars ascent vehicle, based on a design similar to the one considered in DRA 5.0 [144]. A detailed description of this process follows.

1. For each propellant combination, a sweep of oxidizer-to-fuel ratio (O/F) is used along with fixed engine data to estimate the frozen flow vacuum specific impulse (I_{sp}) of the propulsion system. The engine data was derived from an RL10A-4-2 engine (which is an expander cycle engine still in use on Centaur rocket) along with chemical properties of the fuel and oxidizer, given in Table 37. From this, a relationship between O/F ratio and I_{sp} is found.

[2]http://www.grc.nasa.gov/WWW/CEAWeb/

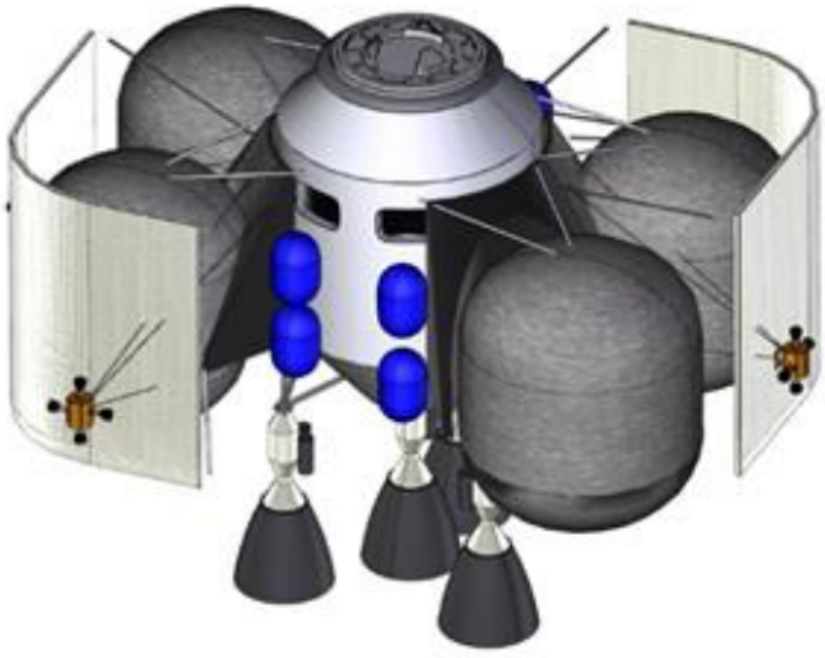

Figure 46: Two-stage Mars ascent vehicle, as considered in Reference [144], similar to the system considered in DRA 5.0.

2. This relationship, along with the MAV requirements from Table 35, are inputs for LVSSS. For these values, LVSSS sizes a two-stage MAV, with the mass of the second stage serving as the payload for the first. A sweep of O/F ratios then yields the propellant, inert, and engine masses of the MAV, and the optimal O/F ratio is found by minimizing gross mass (minimizing dry mass may give lower cost, but an evaluation of the differences between the two objective functions is not considered in this research). Because the model does not consider the impact on propulsion system design of using low O/F ratios (for example, the optimal O/F ratio for the hydrogen MAV was found to be 4.4, lower than the typical 6.0 used in recent hydrogen-burning engines such as the Space Shuttle Main Engine [145]), the optimal gross mass O/F ratio is close to the optimal Isp O/F ratio; future modeling of the MAV that accommodates this effect may change the preferred O/F ratio, as the optimal Isp does not necessarily define

Table 37: Engine Data

Name	CH_4	C_2H_4	CH_3OH	H_2
Chamber Pressure P_C	3.9 MPa	3.9 MPa	3.9 MPa	3.9 MPa
Fuel Temperature T_f	109 K	169 K	176 K	20 K
Oxidizer Temperature T_{ox}	90 K	90 K	90 K	90 K
Area Ratio ϵ	84	84	84	84
Vacuum T/W_{engine}	60.53	60.53	60.53	60.53
Specific Impulse	359 s	357 s	330 s	459 s
Optimal O/F Ratio	3.0	2.1	1.3	4.4

the optimal vehicle.

3. Using the propellant mass, O/F ratio, and fuel and oxidizer densities (Table 38), the volumes of the fuel and oxidizer tanks are found, and used to determine dimensions of the MAV. The tanks are sized as either spheres or cylinders with spherical endcaps, following the method described in Section 3.3.3.

4. The propellant mass, system mass, and engine mass are then used to estimate the DDT&E and unit costs of the MAV via the Transcost model, further described in Section 3.4.1.

5. The mass, geometry, and costs of the MAV are passed to the architecture file for use in sizing the MDV, as well as for compilation in the overall architectural metrics.

The plot of specific impulse for each propellant combination is shown in Figures 47. The mass breakdowns for the two-stage ascent vehicle at the gross mass optimal O/F ratio (as identified in this research, with the caveat that a more detailed propulsion analysis may yield a different optimal O/F ratio) for each propellant combination are shown in Figures 48 (Methane), 49 (Ethylene), 50 (Methanol), and 51 (Hydrogen).

Table 38: Propellant Densities

Name	Density
L_{O2}	1140 $\frac{kg}{m^3}$
CH_4	423 $\frac{kg}{m^3}$
C_2H_4	568 $\frac{kg}{m^3}$
CH_3OH	787 $\frac{kg}{m^3}$
H_2	71 $\frac{kg}{m^3}$

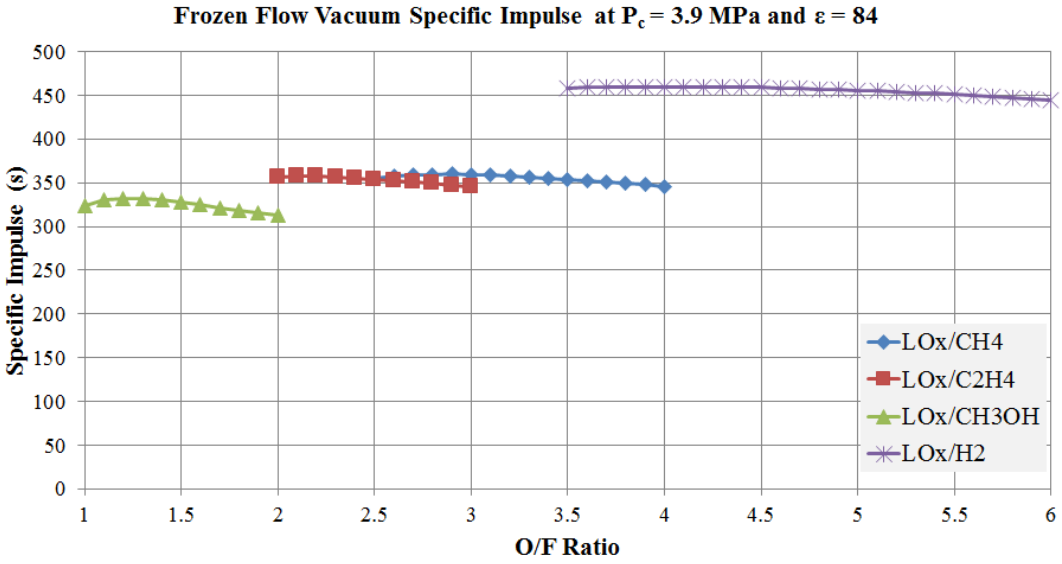

Figure 47: Frozen flow vacuum specific impulse for oxygen and each fuel, generated from CEA using the RL10A-4-2 engine.

LOX/CH4 2-stage Ascent Vehicle, O/F Ratio = 3.0		1st Stage	2nd Stage
1. Aerodynamic Surfaces		0	0
2. Body Structure		2133	843
3. Induced Environmental Protection		0	0
4. Launch Recovery and Docking		0	0
5. Main Propulsion		1052	494
6. Orient Control Separation		0	0
7. Prime Power		165	164
8. Power Conversion and Distribution		137	137
9. Guidance and Navigation		0	549
10. Instrumention		0	229
11. Communication		0	482
12. Environmental Control		485	485
13. Armament		0	0
14. Personnel Provisions		0	0
15. Crew Station Control Panel		0	0
16. Range Safety and Abort		69	70
16a. Mass Growth Allowance		406	295
17. Personnel		0	0
19. Ordanance		20	21
20. Ballast		0	0
	Dry Mass	4467	3770
21. Residual Propellant		440	280
22. Reserves		647	280
23. Inflight Losses		643	278
24. Thrust Decay Propellant		0	0
26. Thrust Propellant Buildup		0	0
27. Pre-Ignition Losses		0	0
	Inert Mass	5558	4331
	Gross Mass	61728	24031
	Propellant Mass	32139	13895
	Propellant Burn 1	32139	13895
	Payload Burn 1	24031	5805
	DeltaV Burn 1	2588	3038

Figure 48: Mass breakdown for the 2-stage oxygen and methane ascent stage, generated from LVSSS.

LOX/C2H4 2-stage Ascent Vehicle, O/F Ratio = 2.1		1st Stage	2nd Stage
1. Aerodynamic Surfaces		0	0
2. Body Structure		2121	834
3. Induced Environmental Protection		0	0
4. Launch Recovery and Docking		0	0
5. Main Propulsion		1096	517
6. Orient Control Separation		0	0
7. Prime Power		165	164
8. Power Conversion and Distribution		137	137
9. Guidance and Navigation		0	549
10. Instrumention		0	229
11. Communication		0	482
12. Environmental Control		485	485
13. Armament		0	0
14. Personnel Provisions		0	0
15. Crew Station Control Panel		0	0
16. Range Safety and Abort		69	70
16a. Mass Growth Allowance		409	296
17. Personnel		0	0
19. Ordanance		20	21
20. Ballast		0	0
	Dry Mass	4502	3785
21. Residual Propellant		443	281
22. Reserves		656	282
23. Inflight Losses		651	280
24. Thrust Decay Propellant		0	0
26. Thrust Propellant Buildup		0	0
27. Pre-Ignition Losses		0	0
	Inert Mass	5605	4350
	Gross Mass	62345	24175
	Propellant Mass	32566	14020
	Propellant Burn 1	32566	14020
	Payload Burn 1	24175	5805
	DeltaV Burn 1	2588	3038

Figure 49: Mass breakdown for the 2-stage oxygen and ethylene ascent stage, generated from LVSSS.

LOX/CH3OH 2-stage Ascent Vehicle, O/F Ratio = 1.3		1st Stage	2nd Stage
1. Aerodynamic Surfaces		0	0
2. Body Structure		2475	905
3. Induced Environmental Protection		0	0
4. Launch Recovery and Docking		0	0
5. Main Propulsion		1331	599
6. Orient Control Separation		0	0
7. Prime Power		165	164
8. Power Conversion and Distribution		137	137
9. Guidance and Navigation		0	549
10. Instrumention		0	229
11. Communication		0	482
12. Environmental Control		485	485
13. Armament		0	0
14. Personnel Provisions		0	0
15. Crew Station Control Panel		0	0
16. Range Safety and Abort		69	70
16a. Mass Growth Allowance		468	309
17. Personnel		0	0
19. Ordanance		20	21
20. Ballast		0	0
	Dry Mass	5150	3950
21. Residual Propellant		498	304
22. Reserves		815	326
23. Inflight Losses		809	324
24. Thrust Decay Propellant		0	0
26. Thrust Propellant Buildup		0	0
27. Pre-Ignition Losses		0	0
	Inert Mass	6468	4582
	Gross Mass	73503	26563
	Propellant Mass	40472	16176
	Propellant Burn 1	40472	16176
	Payload Burn 1	26563	5805
	DeltaV Burn 1	2588	3038

Figure 50: Mass breakdown for the 2-stage oxygen and methanol ascent stage, generated from LVSSS.

LOX/LH2 2-stage Ascent Vehicle, O/F Ratio = 4.4		1st Stage	2nd Stage
1. Aerodynamic Surfaces		0	0
2. Body Structure		1614	764
3. Induced Environmental Protection		0	0
4. Launch Recovery and Docking		0	0
5. Main Propulsion		683	365
6. Orient Control Separation		0	0
7. Prime Power		165	164
8. Power Conversion and Distribution		137	137
9. Guidance and Navigation		0	549
10. Instrumention		0	229
11. Communication		0	482
12. Environmental Control		485	485
13. Armament		0	0
14. Personnel Provisions		0	0
15. Crew Station Control Panel		0	0
16. Range Safety and Abort		69	70
16a. Mass Growth Allowance		317	278
17. Personnel		0	0
19. Ordanance		20	21
20. Ballast		0	0
	Dry Mass	3490	3544
21. Residual Propellant		323	227
22. Reserves		365	189
23. Inflight Losses		363	188
24. Thrust Decay Propellant		0	0
26. Thrust Propellant Buildup		0	0
27. Pre-Ignition Losses		0	0
	Inert Mass	4181	3962
	Gross Mass	41478	19171
	Propellant Mass	18127	9404
	Propellant Burn 1	18127	9404
	Payload Burn 1	19171	5805
	DeltaV Burn 1	2588	3038

Figure 51: Mass breakdown for the 2-stage oxygen and hydrogen ascent stage, generated from LVSSS.

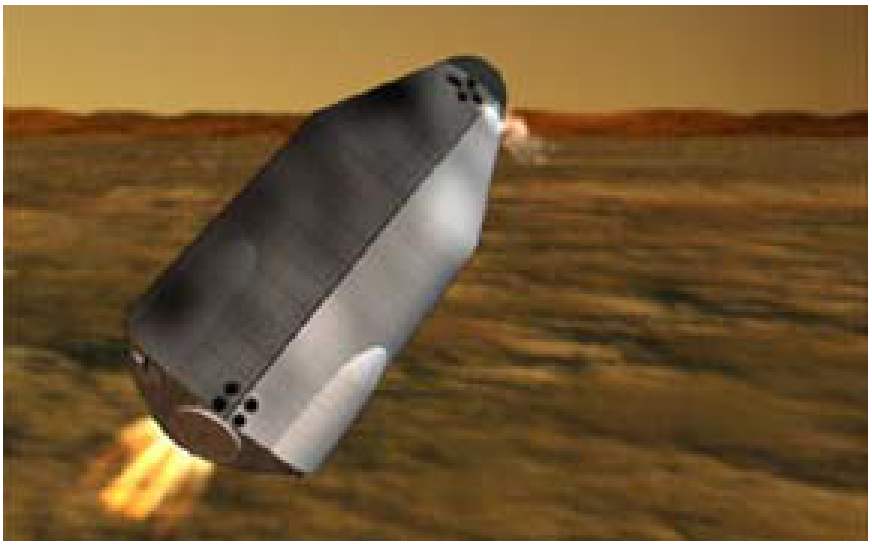

Figure 52: Mars descent vehicle, which performs aerobraking using the Martian atmosphere and a propulsive terminal descent, as considered in DRA 5.0 [10].

The code used for the methane MAV is given in Appendix A.2.1. The code used for the ethylene MAV is given in Appendix A.2.2. The code used for the methanol MAV is given in Appendix A.2.3. The code used for the hydrogen MAV is given in Appendix A.2.4.

3.3.3 Mars Descent Vehicle

The Mars Descent Vehicle (MDV) is defined herein as the vehicle that delivers the Mars Ascent Vehicle, In-Situ Propellant Production (ISPP) system, and power supply to the Martian surface, by performing aerobraking using the Martian atmosphere and a propulsive terminal descent. Figure 52 shows the vehicle concept from DRA 5.0. The MDV, in turn, serves as the payload for the Mars Transfer Vehicle (MTV). This arrangement is analogous to that present for one of the cargo flights in DRA 5.0 [1].

A parametric model of the MDV has been developed for use within the modeling framework of this research. The reason for resizing the MDV (rather than adapting that described in DRA 5.0) is that the various elements of the ISPP system possess different volumes, leading to growth (or, perhaps, reduction) in the size of the MDV

Table 39: Mars Descent Vehicle Functional Requirements

Function	Physical Components	Relevant Equations
Transport MAV and ISPP to surface	Propellant, System, Engine masses	205 - 207

relative to the DRA 5.0 model. Thus, the impact of the MAV, ISPP, and power system volumes on the overall architecture is captured in the sizing and costing of the MDV (and by extension, the Mars Transfer Vehicle that delivers the MDV). The functional requirement of the MDV is given in Table 39.

As the focus of this research is on understanding the system level impacts of these volumes on the MDV, rather than determining precise dimensions, the following method was used to size the MDV:

1. For the ith element of the ISPP system, as well as the power supply, determine the Hypothetical Spherical Radius R_i that would correspond to a sphere with a volume equal to that of the ISPP system element.

2. If R_i does not exceed a prescribed Maximum Allowable Radius R_{max} , treat the element as a sphere and assign it a Length L_i equal to R_i. Otherwise, fix R_i at R_{max}, and size a cylinder with spherical endcaps using R_i. This cylinder will have a total Length (equal to the sum of the barrel length and twice the endcap radius R_i) L_i given by the following formula:

$$L_i = \frac{(V - \frac{4}{3}\pi R_i^3)}{(\pi R_i^2)} + 2R_i \tag{202}$$

   where V is the volume of the element.

3. Let R_* be the maximum of all R_i and R_{MAV} , and let L_{total} be the sum of all L_i and L_{MAV} . Then the Projected Area S of the MDV is twice the product of R_* and L_{total} (see Equation 203

$$S = 2 * R_* * L_{total} \tag{203}$$

4. The total mass of the MDV can be estimated by using the Wing Loading W/S as a similarity parameter, calculated from the mass and area found in DRA 5.0's description of the MDV [1]; see Equation 204. This mass can then be subdivided into propellant mass, system mass, and engine mass using similarity parameters calculated from the masses given in DRA 5.0 and a given engine thrust-to-weight ratio [1]; see Equations 205, 206, and 207. The values of these parameters are given in Table 40. These parameters were computed by dividing the masses of each element (propellant, system less engine, and engine) by the entry system mass (for the three mass parameters), and by dividing the projected area by the entry system mass to calculate the wing loading. The source data from DRA 5.0 is given in Table 41. The engine and propulsion system masses are assumed to be 10% and 90% of the non-aeroshell mass, respectively. The balance of the mass is thermal protection system.

$$M_{MDV,entrysystem} = \frac{S}{W/S} \tag{204}$$

$$M_{MDV,prop} = M_{MDV,entrysystem} * mf_p \tag{205}$$

$$M_{MDV,propulsion} = M_{MDV,entrysystem} * mf_s \tag{206}$$

$$M_{MDV,eng} = \frac{M_{entrysystem} + M_{MDV,payload}}{T/W_{engine} * g_{Mars}} \tag{207}$$

5. The propellant mass, system mass, and engine mass are then used to estimate the DDT&E and unit costs of the MDV via the Transcost model, further described in Section 3.4.1.

6. The mass and costs of the MDV are passed to the architecture file for use in sizing the MTV, as well as for compilation in the overall architectural metrics.

The code used for the MDV is given in Appendix A.2.5.

Table 40: Similarity Parameters for MDV Sizing

Name	Value	Description
W/S	$4.2857 * 10^{-3}$ [m^2/kg]	Wing Loading, used to calculate mass from projected area
mf_p	0.1977	MDV propellant mass fraction, used to calculate propellant mass from total mass
mf_s	0.2115	MDV system mass fraction, used to calculate system mass from total mass
T/W_{engine}	80	MDV engine thrust-to-weight ratio, used to calculate engine mass from total mass
g_{Mars}	3.711 [m/s^2]	Gravity at Mars

Table 41: MDV Source Data [1]

Name	Value
Projected Area (m^2)	300
Entry System Mass (kg)	69800
Propellant Mass (kg)	13800
Propulsion System (Tanks and Engine)	16400

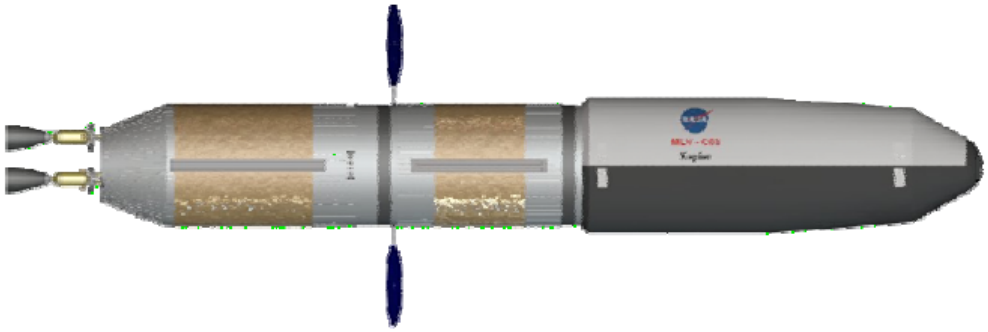

Figure 53: Nuclear thermal rocket Mars transfer vehicle, as considered in DRA 5.0 [1].

3.3.4 Mars Transfer Vehicle

The Mars Transfer Vehicle (MTV) is defined herein as the vehicle that delivers the Mars Descent Vehicle (MDV), and its surface payloads, from Earth orbit to Martian orbit. It is analogous to the Nuclear Thermal Rocket (NTR) MTV described in DRA 5.0 [1]. Figure 53 shows the vehicle concept from DRA 5.0. The MTV, along with its payload, are used to determine the Initial Mass in Low Earth Orbit (IMLEO) of an architecture, which in turn is used to calculate the launch cost.

A parametric model of the MTV has been developed for use within the modeling framework of this research. The reason for resizing the MTV (rather than adapting that described in DRA 5.0) is that the varying sizes of the ISPP system, MAV, power supply, and MDV all impact the performance requirements of the MTV. Thus, the impact of the MAV, ISPP, power system, and MDV masses on the overall architecture is captured in the sizing and costing of the MTV (and by extension, the total launch cost of the architecture). The functional requirement of the MTV is given in Table 42.

As the focus of this research is on understanding the system level impacts of these volumes on the MTV, rather than determining precise dimensions, the following

Table 42: Mars Transfer Vehicle Functional Requirements

Function	Physical Components	Relevant Equations
Transport MDV and payloads to Mars sphere of influence	Propellant mass, Inert mass	209, 210

Table 43: MTV Sizing Parameters from DRA 5.0 [1].

Name	Value	Description
ΔV	4014 $\frac{m}{s}$	Performance required for transfer from LEO to Mars
g_0	9.80665 $\frac{m}{s^2}$	Gravitational acceleration
I_{sp}	900 s	Specific impulse for MTV propulsion (nuclear thermal rocket)
f	0.322	Inert mass fraction

method was used to size the MTV:

1. The payload of the MTV is the MDV and its accompanying payloads (the MAV, ISPP system, and power supply). This mass, along with several parameters extracted from DRA 5.0 (see Table 43 [1]), are used to perform an inert mass fraction sizing of the MTV using the following equations:

$$MR = \exp \frac{\Delta V}{g_0 I_{sp}} \tag{208}$$

$$m_{prop} = m_{payload} \frac{(1-f)(MR-1)}{1-fMR} \tag{209}$$

$$m_{inert} = m_{prop} \frac{f}{1-f} \tag{210}$$

2. As with the MDV, the engine mass is estimated based on the required in-space system thrust-to-weight ratio (0.2) and a nominal engine thrust-to-weight (20).

3. The propellant mass, system mass, and engine mass are then used to estimate the DDT&E and unit costs of the MDV via the Transcost model, further described in Section 3.4.1.

4. The mass and costs of the MTV are passed to the architecture file for compilation in the overall architectural metrics.

The code used for the MTV is given in Appendix A.2.6.

3.4 Cost Modeling

3.4.1 Transcost

Transcost is a cost estimating tool for evaluating the development and production cost of transportation vehicles [23]. It consists of cost estimating relationships relating the engine, vehicle, and propellant masses to work year equivalents via a set of regressions of historical system mass and multiplication of complexity factors; these work year equivalents can then be translated into dollars in a particular year using the Transcost conversion function. These costs are used for the three transportation elements in each architecture: the MAV, the MDV, and the MTV.

The Transcost model input variables are the engine mass, vehicle mass (less engines), propellant mass, propellant type (e.g. hydrogen or hydrocarbon), and number of units, and returns the DDT&E and unit costs of the system dry mass and engine mass in FY2006 millions of dollars. Three additional parameters in the model are used to determine complexity factors that modify these costs: the "newness" of the system (the Transcost measurement of the degree to which new technology is needed), the experience level of the team, and the number of quality engine firings. Across all of the architectures considered in this research, each vehicle was assumed to be at the maximum level of newness, have access to a fully experienced team in development, and go through 1000 quality engine firings before use, similar to the test regime of human-rated engines such as the J-2 and F-1 [146].

The Transcost cost equations used in this research are given in Equations 211 through 218, and the parameters in those equations are given in Table 44.

Table 44: Transcost Vehicle Costing Parameters [23].

Name	Value	Description
f_1	1.4	Degree of new technology required (1.4 is maximum)
f_2	1.24	Cost parameter based on number of equality engine firings before engine use
f_3	0.4	Factor for level of experience of team; smaller means more experienced (0.4 is minimum)

For hydrogen,

$$k_* = 1.9726 * m_{propellant}^{\frac{-0.2705*m_{propellant}}{m_{vehicle}}} \tag{211}$$

For other fuels,

$$k_* = 5.2014 * m_{propellant}^{\frac{-0.4036*m_{propellant}}{m_{vehicle}}} \tag{212}$$

Calculating the work-year equivalent required for the engines and vehicles, where H is the work-year equivalent and the subscripts E, V, D, and U correspond to the engine, the vehicle less engine, development cost, and unit cost,

$$H_{E,D} = 277 * m_{engine}^{(0.48*f_1*f_2*f_3)} \tag{213}$$

$$H_{V,D} = 100 * m_{vehicle}^{(0.555*f_1*f_3*k_*)} \tag{214}$$

$$H_{E,U} = 3.15 * m_{engine}^{(0.535*n_{units})} \tag{215}$$

$$H_{V,U} = 1.4182 * m_{vehicle}^{0.6464} \tag{216}$$

Converting work-year equivalent to FY2006 millions of dollars,

$$Cost_{DDT\&E} = (H_{E,D} + H_{V,D}) * 0.2592 \tag{217}$$

$$Cost_{Unit} = (H_{E,U} + H_{V,U}) * 0.2592 \tag{218}$$

The MATLAB code used to apply the Transcost model is given in Appendix A.2.7.

Table 45: NAFCOM Programmatic Parameters [24, 147].

Parameter	Value	Setting Description
Manufacturing Methods	3	Moderate advances in manufacturing techniques required
Engineering Management	2	Few design changes required
New Design	6	New design, with substyem model or prototype validated in relevant environment
Funding Availability	2	Some infrequent delays possible
Test Approach	2	Moderate testing, with qualification at the prototype/protoflight level
Integration Complexity	2	A moderate number of major interfaces involving multiple contractors or centers
Pre-Development Study	2	One study contract, between nine and eighteen months

3.4.2 NAFCOM

The NASA/Air Force Cost Model uses historical data from many previous aerospace systems, in conjunction with multiple programmatic parameters, to make parametric cost estimates of DDT&E and unit costs [24]. The subsystem costs, using cost estimating relationships (CERs) derived from analogous systems, are computed as a function of the quantities of different types of mass (e.g. structural elements, thermal control systems). Programmatic parameters include Manufacturing Methods, Engineering Management, New Design, Funding Availability, Test Approach, Integration Complexity, and Pre-Development Study. These parameters influence the complexity factors applied to the CERs in NAFCOM. The values used in this analysis are given in Table 45, based on the similar NAFCOM modeling scenario used in Arney [147].

For each ISPP subsystem described above, three representative cases were sized using the ISPP mass estimations. These were used in NAFCOM 2008 to generate power-law CERs to be used during the architecture analysis in a manner similar to

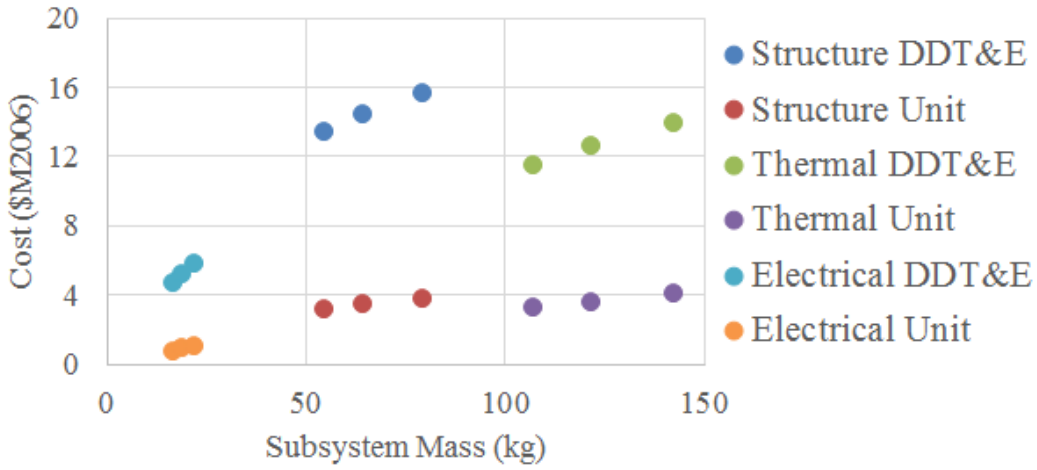

Figure 54: Subsystem structural, thermal, and electrical masses and their DDT&E and unit costs, used to generate cost estimating relationships in NAFCOM 2008.

Table 46: NAFCOM ISPP Subsystem Cost Estimating Parameters

Mass Type	DDT&E A	DDT&E B	Unit A	Unit B
Structure	1.2704	0.6847	0.0925	0.7645
Thermal	2.7497	0.3988	0.5276	0.4526
Electrical	0.5880	0.7420	0.0365	1.1107

that used by Arney [147]. The subsystem is divided into masses in each category available within NAFCOM; those masses are then used with the corresponding CER to estimate the DDT&E and unit costs of the subsystem. The subsystem masses and cost data used to generate the CERs are shown in Figure 54. The cost equations for each kind of mass (structure, thermal, and electrical) are given in Equations 219 and 220, and the coefficients are given in Table 46.

$$Cost_{DDT\&E} = A * Mass^{B} \tag{219}$$

$$Cost_{Unit} = A * Mass^{B} \tag{220}$$

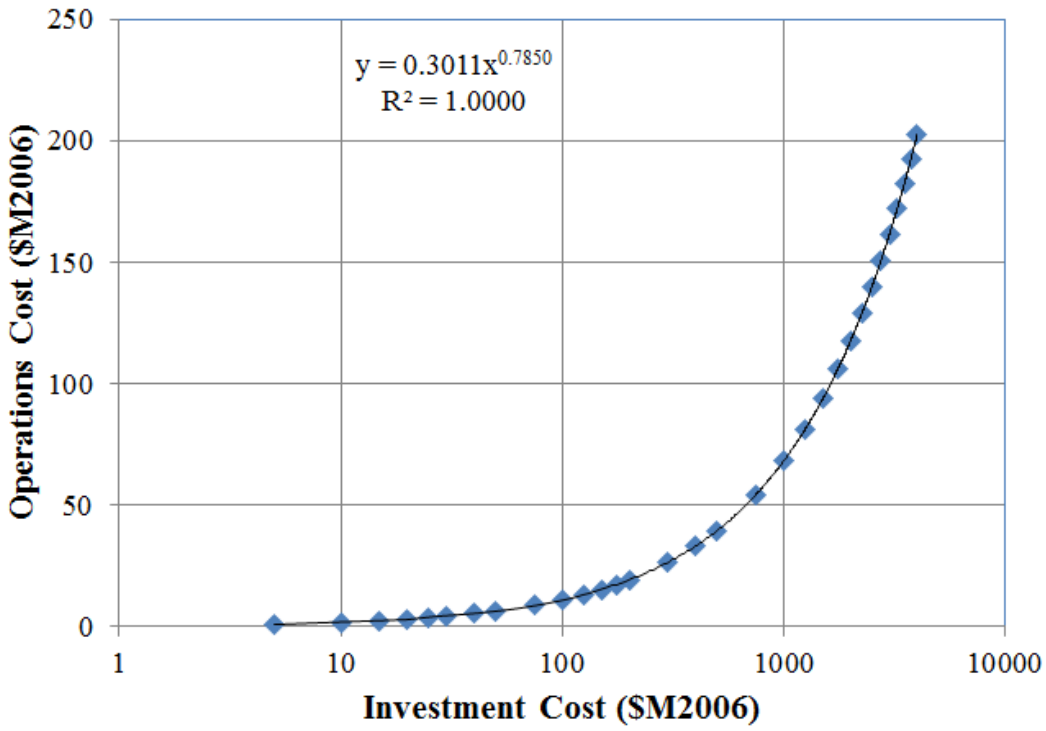

Figure 55: Operations cost as a function of investment (DDT&E plus Unit) cost, from Reference [149].

3.4.3 Architecture Costing

Additional cost elements are modeled at the architecture level in this research. The impact of launch costs is captured using a launch cost parameter, measured in dollars per kilogram of initial mass in low Earth orbit. This parameter can range from \$2500/kg for a Falcon Heavy to \$30000/kg for a large NASA launch vehicle [147,148]. Operations cost is modeled using a power law regression fit to data provided by the NASA Mission Operations Cost Model [149]; see Figure 55 and Equation 221, where investment cost is the sum of DDT&E and Unit costs. These costs are added to the DDT&E and unit costs of each element to determine the life cycle cost.

$$Cost_{Operations} = 0.3011 * (Cost_{DDT\&E} + Cost_{Unit})^{0.785} \tag{221}$$

The net present value is calculated by spreading the costs according to a beta

distribution with parameters 0.32 and 0.68, as described in the NASA Cost Estimating Handbook [83]. In this research, a distinction is made between systems that are considered "manned" and "unmanned" for the purposes of determining the cost spreading durations. Because they would be used for transporting crew, the transportation elements (the MAV, MDV, and MTV) are treated as "manned", and the surface systems are treated as "unmanned." For "manned" systems, the DDT&E and units costs are spread over a 92 month period, based on the mean duration found in Wilhite et al. [150]. For "unmanned" systems, the DDT&E and units costs are spread over a 62 month period, based on the mean duration found in Wilhite et al. [150]. Launch costs are incurred following this period, and the ops costs are spread over the subsequent 16 months (500 days of ISPP operation). These costs are then discounted using a nominal discount rate of 3% [83, 85] from a reference start date of 2020. The final NPV is then deflated into FY2006 dollars (consistent with the costs calculated from Transcost and NAFCOM).

3.5 Integrated Architecture Modeling

With the ISPP system, power system, MAV, MDV, and MTV modeling defined, an architecture can be modeled for evaluation via the robustness integrals described in the next section. Note that an architecture, as defined here, is not equivalent to an architecture in the classic sense: here, it does not encompass all of the systems required to perform a crewed mission to Mars, but instead those directly associated with delivering the MAV and ISPP system (if present). Thus, the MDV is sized only to deliver the requisite surface systems associated with the MAV: the vehicle itself, any ISPP hardware, and any power systems. Likewise, the MTV is sized to deliver the MDV. Other surface elements, such as habitats, and their associated transportation systems, are not included in this analysis; this research assumes that the choice of ISPP system for the MAV does not impact those other systems.

Fuel	Type	α	LC
CH_4 (Methane)	From Earth	23 kg/kWe	$2500/kg
C_2H_4 (Ethylene)	Earth Water	266 kg/kWe	$30000/kg
CH_3OH (Methanol)	Mars Water	U(23,266) kg/kWe	U(2500,30000) $/kg
H_2 (Hydrogen)	O_2 Only		
	No ISPP		

Figure 56: Morphological matrix of the architectures and scenarios considered in this research.

Figure 56 shows the morphological matrix of architectures and scenarios considered in this research. The nineteen architectures considered described in Section 3.1 come from the combinatorial selection of fuels and ISPP type in the first two columns (note that hydrogen from Earth and hydrogen with oxygen only are redundant, hence nineteen rather than twenty architectures). The nineteen architectures are analyzed under five scenarios in Section 4.4; these scenarios result from the combinatorial selection of the first two entries in the α (power system specific mass) and LC (launch cost to low Earth orbit) columns, as well as the uniform distributions of both in the third row of those columns (see the scenario descriptions in Section 4.4 for additional detail).

The flow of an architecture model is shown in Figure 57. Given the fixed payload and delta-V requirements defined in Section 3.3.2 and the optimal O/F ratio based on the gross mass of the vehicle as sized in LVSSS, the MAV's propellant requirements, vehicle mass, and costs are computed. The propellant requirements, and the time available for manufacture (nominally, 500 days as in DRA 5 [1]), are used by the ISPP model as described in Section 3.1 to size the ISPP system's mass, power, volume, and cost. The resulting power requirement is used with the specific power to size the surface power source's mass, volume, and costs, as described in Section 3.3.1. With all the payloads for the MDV now sized, the MDV is sized according to the method in Section 3.3.3. Finally, the MTV is sized to deliver the MDV, as in Section 3.3.4.

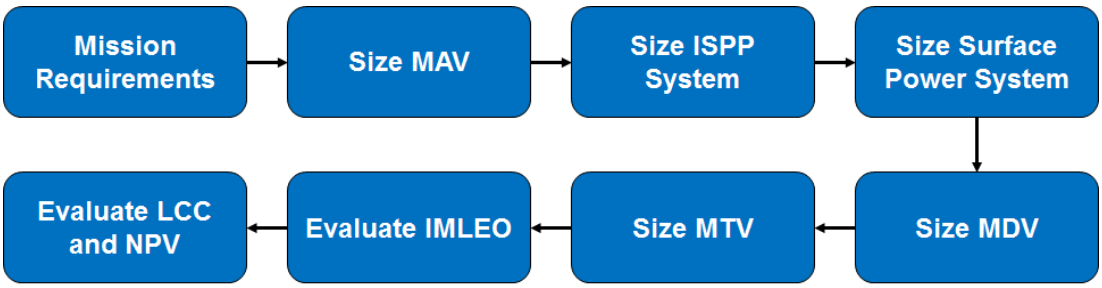

Figure 57: Flowchart of an architecture in this research.

The total masses, powers, and volumes of all systems are collected, as well as the DDT&E and unit costs of all systems. The launch cost is computed by multiplying the initial mass in low Earth orbit by the launch cost parameter, which is either fixed or chosen from a distribution. The ops cost is calculated from the DDT&E and unit costs of all systems. The life cycle cost is transformed to net present value, yielding the figure of merit with which to evaluate the architecture.

An example of the integrated architecture model code is shown in Appendix A.2.8.

3.6 Robustness Integral Analysis

In this research, an approach has been developed to consider the uncertainty in these model parameters. The sampled results (values of $\mathbf{y}$) can then be collected as a cumulative distribution function, as shown in Figure 58. In this plot, the horizontal axis contains the domain of values of y_i (in this example, life cycle cost of a Sabatier ISPP system), while the vertical axis represents the fraction of all runs at or below a particular value of y_i. Thus, the spread of the results obtained from sampling values of k_i can be determined; this width is a measure of the sensitivity of the value of y_i to variations in k_i. If the width is large, the sensitivity is greater, and the system is less robust to variations in the value of the model parameter.

For more advanced system models, such as those used to size the various elements of an ISPP system, the relative impact of each model parameter can be determined in a similar manner. By fixing nominal values for all but one model parameter, and

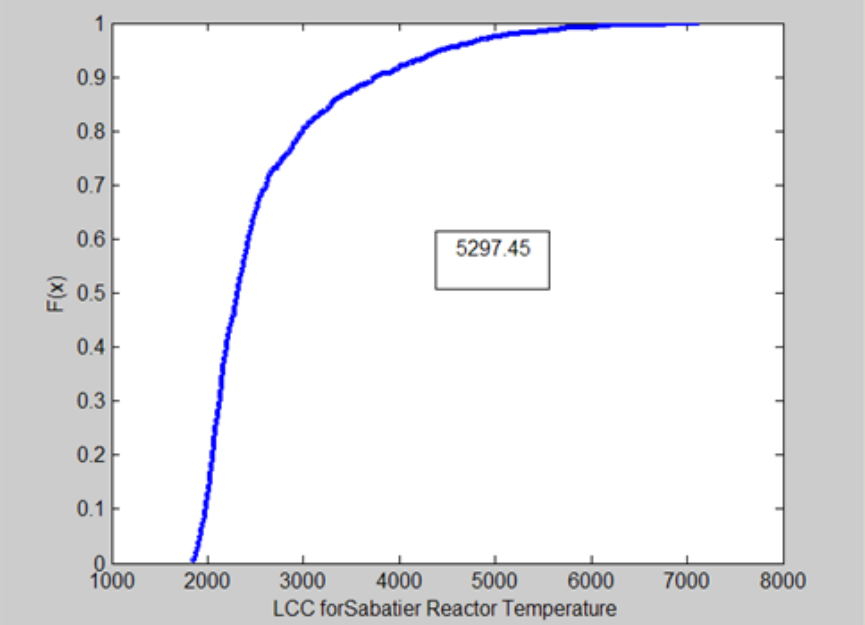

Figure 58: Cumulative distribution function of life cycle cost based on sampling values of the model parameter Sabatier Reactor Temperature. The value in the box is the width of the CDF from $\mathrm{F}(\mathbf{x}) = 0$ to $\mathrm{F}(\mathbf{x}) = 1$.

applying a distribution to the variable model parameter, distributions of each figure of merit can be found, and the width of the CDF (the metric of sensitivity) can be determined. The parameters can then be ranked by the magnitude of their widths, thus identifying the most important parameters. This approach can be applied to each ISPP architecture considered, leading to lists of ranked parameters for each system.

By applying distributions to all model parameters, the full spread of possible values of each y_i can be found. This, in turn, presents a method for comparing different technologies on a robust basis. Consider several competing technologies (such as alternative approaches to propellant production via ISPP), each with a distinct model as in Equation 21. Through the Monte Carlo approach of sampling from distributions on all model parameters, a CDF for each technology and each y_i emerges. As an example, Figure 59 shows a notional view of CDFs for three technologies. The x-axis is the output y_i, and the vertical axis is the value of the CDF, indicating

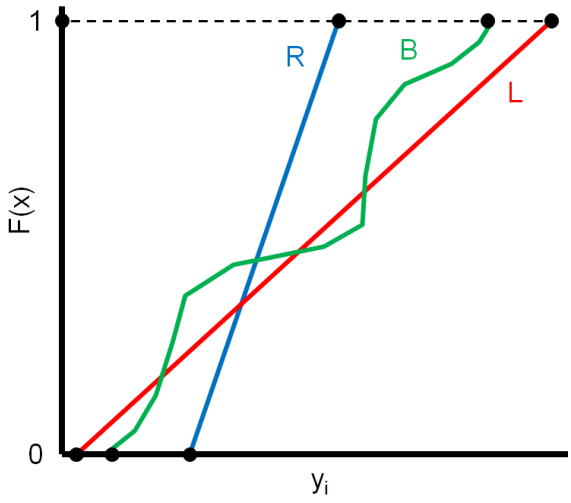

Figure 59: Notional CDFs for three technologies R, B, and L.

the percentage of values that are less than or equal to the corresponding value of y_i. Assuming that minimizing y_i is the objective, technology L takes on the lowest possible values, while technology R is the most robust: it has the narrowest spread between its low and high values.

Picking among the three technologies depends on the particular criteria being used. If there is a particular threshold of interest of y_i (for example, an upper limit on mass), then the percentage of cases for each technology that are less than that threshold can be used as the discriminator among technologies. In Figure 60, depending on if the threshold is at a, b, or c, then the technology chosen varies. At a, technology L has the greatest chance of being successful, with technology B having a lower change and technology R having none. By comparison, at c, technology R now rates the best, then technology B, followed by technology L.

A second method is to define a particular desired chance of success, and then see which technology offers the best performance for that chance. In Figure 61, s represents the desired chance of success, while y_{sR}, y_{sL}, and y_{sB} represent the values corresponding with that probability. Thus, technology R has s percent chance of being at or below threshold y_{sR}, while technologies L and B have lower chances of

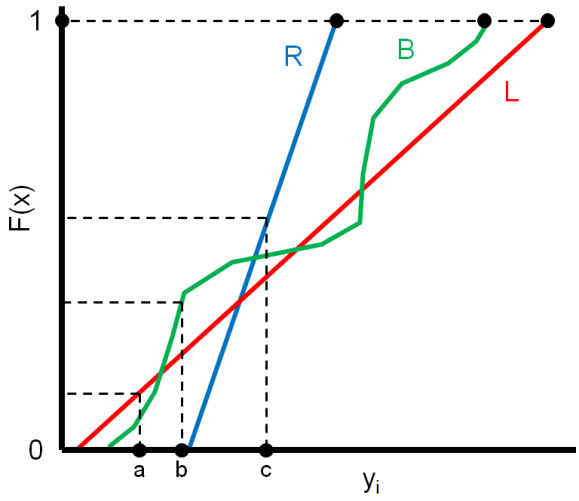

Figure 60: Notional CDFs for three technologies, with thresholds of y_i.

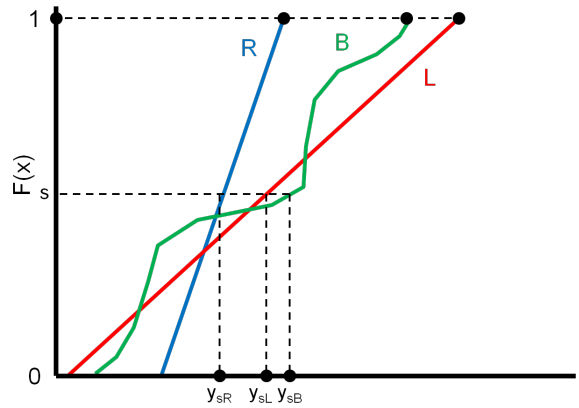

Figure 61: Notional CDFs for three technologies with a fixed chance of success s.

reaching y_{sR}, and have s percent chance of success of being below higher values.

Which of the three technologies is preferred, and by what value, depends on the particular chance of success. In Figure 61, at low chances of success, technology L is preferred, while technology R is preferred at higher chances of success (technology B is omitted for simplicity). The degree to which technology L is better than or worse than technology R at a given chance of success s is the difference of the values at s, defined below as the value v_s.

$$v_s = y_{sL} - y_{sR} \tag{222}$$

For a given chance of success, the value v_s can be evaluated as above. Independent of a given chance of success, and assuming no preference for some chances of success over others (that is, a risk-neutral posture as in [103]), the value can be evaluated over the range from 0 to 1 via integration. That is, the integrated value over the entire range, defined here as the *relative robustness integral* (RRI), is defined below.

$$RRI = \int_0^1 v_s \mathrm{d}s \tag{223}$$

This relative robustness integral provides a metric for evaluating the difference between two CDFs independent of a particular threshold of y_i or of a particular chance of success s. It is equivalent to the difference in areas under the two CDFs, adjusted to be of equal width for an equal basis of comparison, as shown in Figure 62 (omitting technology B). The pink area, in the lower left part of the figure, represents the area over which technology L outperforms technology R, while the teal area, in the upper right part of the figure, represents the area over which technology R outperforms technology L. For this analysis, the teal area includes all the space from d (the point where technology R reaches a CDF value of 1) to e (the point where technology L reaches a CDF value of 1), as over this range of y_i technology R continues to outperform technology L; beyond e, both technologies have equivalent CDF values.

If the value of the relative robustness integral is positive, technology L is preferred over technology R, by an amount equal to the value of the relative robustness integral. If the value of the relative robustness integral is negative, technology R is preferred over technology L. The relative robustness integral changes sign, but not magnitude, depending on which technology is the baseline technology, and which is the compared technology. Thus, the selection of a particular technology as the baseline allows for pairwise evaluation of the CDFs of technologies for a particular figure of merit.

For multiple technologies (as in Figure 59), the same approach can be applied, selecting a single baseline and comparing each technology against that baseline. The

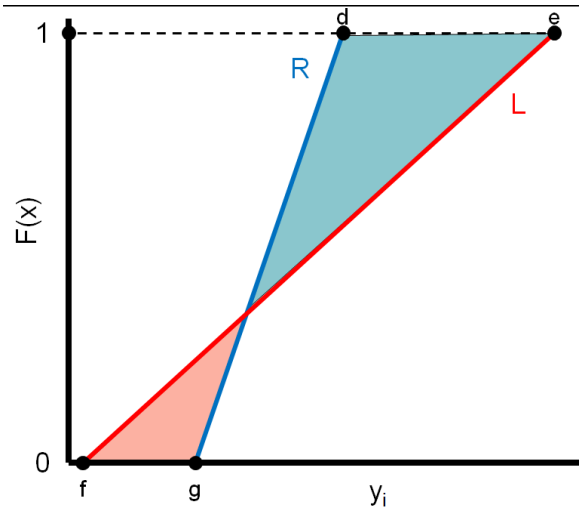

Figure 62: Two notional CDFs and the geometric representation of the relative robustness integral

technologies are then ranked from most positive RRI to most negative RRI, with the baseline falling between the least positive RRI technology and the least negative RRI technology. The selection of which technology is the baseline is irrelevant; the same rankings will be developed regardless of the particular selection of the baseline, and the spacing between each technology will be consistent. These rankings can then be used to select among technologies.

In this research, the technologies being compared are different architectures to propellant production on Mars: different fuels and oxidizers and the corresponding engines, tanks, and other elements of a MAV that depend on the selection of propellant. Additionally, the trade space will consider alternative architectures to producing a given fuel or oxidizer. For each technology, models in the form of Equation 21 are developed, and the above method is applied to determine two items for each architecture: the ranked list of parameters according to each parameters robustness CDF width, and the technology's standing in the overall comparison of relative robustness integrals.

The 152 parameters identified in Tables 7 through 33 are each varied according to one of two distributions: either a uniform distribution between 80% and 120%

of the nominal value, or between minimum and maximum values identified by the results in Section 4.2. The first distribution is the basis of the sensitivity analysis performed in Section 4.2; the goal of which is to identify which parameters have the greatest impact on the net present value of the life cycle cost of the architecture. An implicit assumption of this method is that the parameters do not have both minimal impact on the figure of merit within the prescribed range and significant impact beyond that range (e.g. minimal impact at 80% of nominal, but high impact at 40% of nominal); while it is likely that many variables do have such an impact at more extreme variations, this research identifies those variables that have significant impact even with relatively small variations in their values. The resulting variables that have the greatest impact over this range are the identified values for which more precise minima and maxima are defined, based on the results in Section 4.2.

The Monte Carlo simulations in Sections 4.3 and 4.4 are based on the distributions found from the work in Section 4.2. For the results in Sections 4.3 and 4.4, each of the 152 parameters is varied based on whichever distribution is identified (from 80% to 120% of nominal if the parameter is not identified as having a significant impact, and from its identified minimum to maximum if the parameter does have a significant impact). The multiple runs of each architecture then yield multiple values of element masses, power requirements, volumes, and costs; the means of these for each of the nineteen architectures is given in Section 4.3, while the CDFs and relative robustness integrals of the net present value of the life cycle cost under multiple scenarios is given in Section 4.4.

CHAPTER IV

RESULTS

4.1 Method Validation to Other ISPP Architectures

The system architecture model was validated by comparing its results to the system sizing given in Mars Direct [4], DRM 1 [3], DRM 3 [2], DRA 5 [1], and Rapp's study [5]. All of the architectures provide mass, and power estimates for the ISPP system, while DRA 5 also provides a volume estimate. Additionally, each architecture provides an estimate of the IMLEO required to transport the ISPP systems and ascent vehicle to the surface of Mars; this value is used to validate the transportation architecture modeling. The DRA 5 architecture is analogous to Architecture 4 (CH_4 brought from Earth, only O_2 produced at Mars), and Rapp's architecture is analogous to Architecture 3, while the other architectures are analogous to Architecture 1. The CDFs for ISPP mass, ISPP power, and ISPP volume generated for the corresponding architecture are shown below, with vertical lines corresponding to the literature values for those architecture. Additionally, the means of those CDFs are compared to the corresponding literature values for each validation architecture.

Mars Direct is the most optimistic analysis in estimating ISPP system mass requirements, with its mass coming in lighter than the minimum values in the Monte Carlo simulation despite having higher propellant demands than the MAV in this research (the Mars Direct MAV is designed to return directly to Earth rather than ascend to a rendezvous in Mars orbit, hence the higher propellant demand). Subsequent analyses have commented on the small mass numbers of the Mars Direct system [2, 3]. Mars Direct describes bringing a 100 kWe power system, but does not delineate the amount of power used by the ISPP system as a fraction of the total

Table 47: Mars Direct Validation Inputs

Name	Value	Description
O_2 Required	74,667 [kg]	Oxygen for Mars Ascent Vehicle
CH_4 Required	21,333 [kg]	Methane for Mars Ascent Vehicle
Days	267 [day]	Days for ISPP operations
Hours	24 [hr]	Hours of daily operation

Table 48: Mars Direct Validation

Name	Mars Direct	Model
Mass of ISPP	1.1 [t]	3.1 [t]
Mass of Feedstock	6 [t]	6.4 [t]
Mass of Power Plant	3.5 [t]	4.4 [t]
Power for ISPP	100 [kWe]	44 [kWe]
IMLEO (including ISPP, MAV, MDV, MTV)	40 [t] [1]	N/A

surface power requirement; hence, the total 100 kWe quantity is given here. The inputs into the Mars Direct validation are given in Table 47, while the mean results of modeling the Mars Direct systems are given in Table 48. The stochastic validation of ISPP system mass and power are given in Figures 63 and 64. Due to the significantly different transportation architecture proposed in Mars Direct from that modeled in this research, no stochastic comparison is made for IMLEO.

Although the model is capable of modeling an approach analagous to that in DRA 5 (producing methane with hydrogen brought from Earth), the mass results of the model do not match those in Mars Direct due to the small size of the Mars ISPP system in that study. Further, the model does not match the power results of Mars Direct, as there is no data on the proportion of the 100 kWe used by the ISPP system.

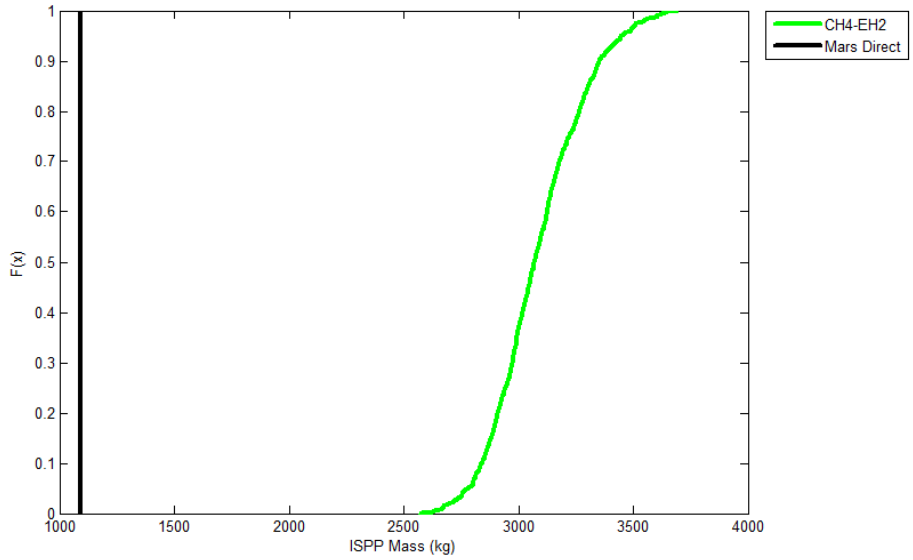

Figure 63: ISPP system mass based on Mars Direct, with value given in Mars Direct on the vertical black line (1091 kg) [4].

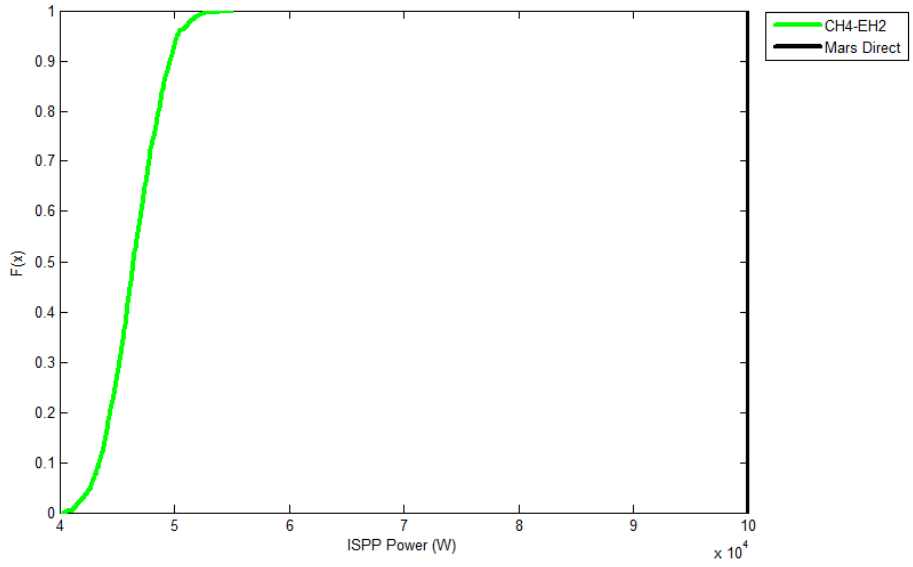

Figure 64: ISPP system power based on Mars Direct, with value given in Mars Direct on the vertical green line (100,000 W) [4].

Table 49: DRM 1 Validation Inputs

Name	Value	Description
O_2 Required	24500 [kg]	Oxygen for Mars Ascent Vehicle
CH_4 Required	6000 [kg]	Methane for Mars Ascent Vehicle
Days	500 [day]	Days for ISPP operations
Hours	24 [hr]	Hours of daily operation

DRM 1 uses propellant production to supply the MAV. In addition to the propellant requirements listed in Table 49, an additional ISRU demand exists for supplemental crew consumables. As a result, additional mass and power are included in the ISPP system mass and power requirement to accommodate those additional demands. The inputs into the DRM 1 validation are given in Table 49, while the mean results of modeling the DRM 1 systems are given in Table 50. The stochastic validation of ISPP system mass, power, and IMLEO are given in Figures 65 through 67.

The model overestimates the mass of the DRM 1 ISPP system. This results from the DRM 1 data not including the hydrogen cryocooler and tank to store the hydrogen brought from Earth. Removing the mass of those systems (1003 kg) from the estimate of the model yields a mean mass of 4.8 t, matching the DRM-1 system mass. Although not calculated in the model, it is expected that the reduction in resulting IMLEO from removing the hydrogen cryocooler and tank would shift the mean IMLEO in Table 50 closer to that in DRM 1.

Similarly to DRM 1, DRM 3 has crew consumable demands beyond the propellant requirements of the MAV. As a result, additional mass and power are included in the ISPP system mass and power requirement to accommodate those additional demands. The inputs into the DRM 3 validation are given in Table 51, while the mean results of modeling the DRM 3 systems are given in Table 52. The stochastic validation of

Table 50: DRM 1 Validation

Name	DRM 1	Model
Mass of ISPP	4.8 [t]	5.8 [t]
Mass of Feedstock	4.5 [t]	5.3 [t]
Mass of Power Plant	14 [t]	6.6 [t]
Power for ISPP	72.27 [kWe]	66 [kWe]
IMLEO (including ISPP, MAV, MDV, MTV)	216.6 [t]	223 [t]

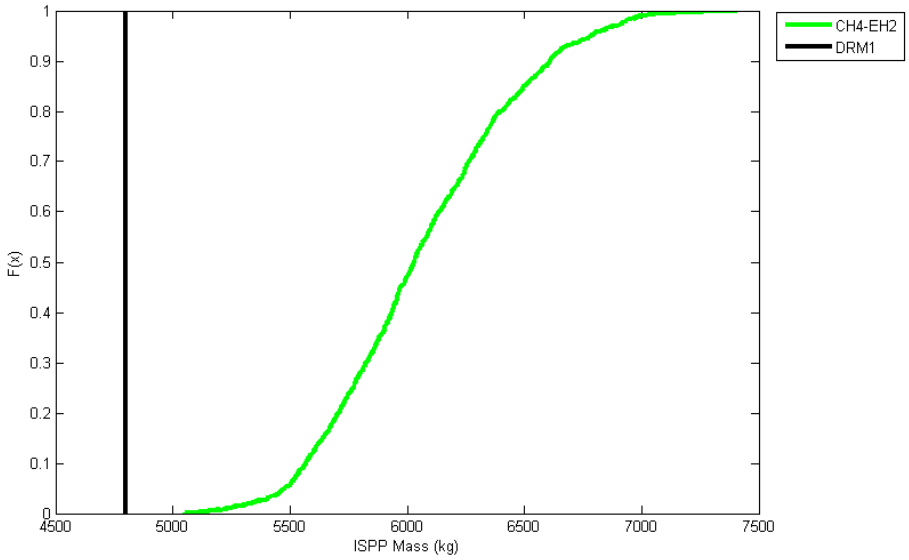

Figure 65: ISPP system mass based on DRM 1, with value given in DRM 1 on the vertical black line (4800 kg) [3].

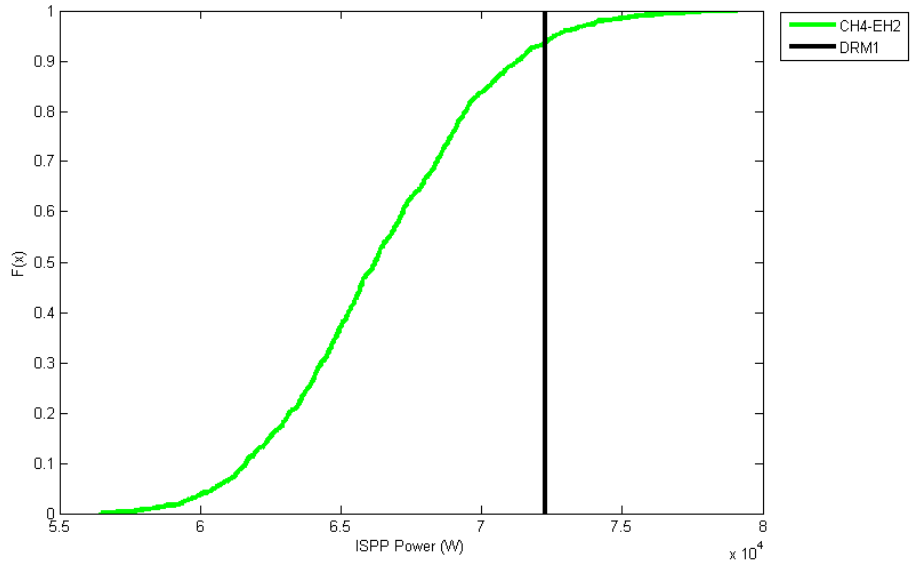

Figure 66: ISPP system power based on DRM 1, with value given in DRM 1 on the vertical green line (72,270 W) [3].

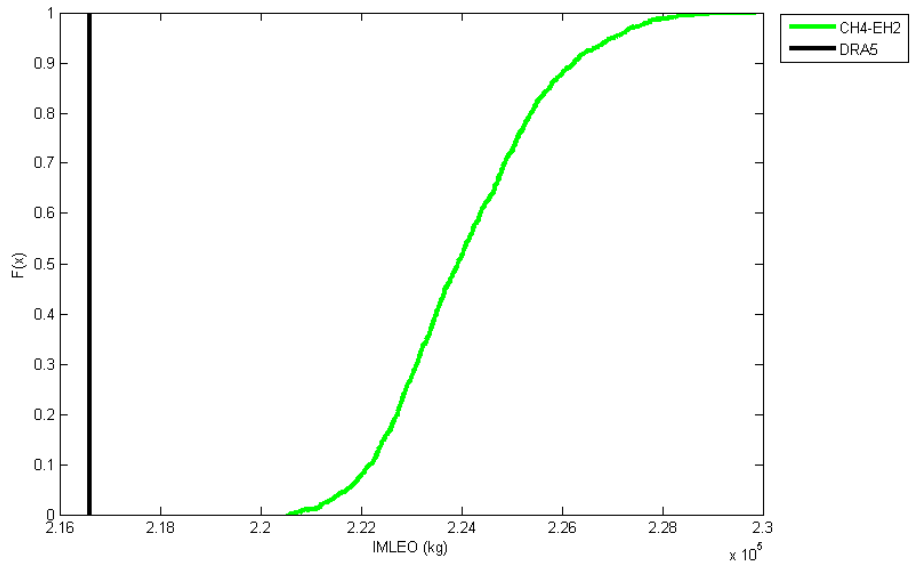

Figure 67: IMLEO for transporting ISPP and MAV based on DRM 1, with value given in DRM 1 on the vertical green line (216,600 kg) [3].

Table 51: DRM 3 Validation Inputs

Name	Value	Description
O_2 Required	30000 [kg]	Oxygen for Mars Ascent Vehicle
CH_4 Required	9000 [kg]	Methane for Mars Ascent Vehicle
Days	500 [day]	Days for ISPP operations
Hours	24 [hr]	Hours of daily operation

Table 52: DRM 3 Validation

Name	DRM 3	Model
Mass of ISPP	3.9 [t]	6.2 [t]
Mass of Feedstock	5.5 [t]	5.8 [t]
Mass of Power Plant	10.7 [t]	7.1 [t]
Power for ISPP	41 [kWe]	71 [kWe]
IMLEO (including ISPP, MAV, MDV, MTV)	205.1 [t]	218 [t]

ISPP system mass, power, and IMLEO are given in Figures 68 through 70.

As with DRM 1, the results of the model overestimate the ISPP system mass in part due to the lack of hydrogen cryocooler and tank masses in DRM 3. Removing those elements (1239 kg) from the estimate of the model in Table 52 yields a mean mass of 5.0 t. The remaining difference is driven by the unclear modeling assumptions in DRM 3; note that the demands on the ISPP system increased from DRM 1, but the total system mass decreased. DRM 3 does not give a reason for this change. Similarly, it is unclear why the power requirement decreased in DRM 3 relative to DRM 1.

Rapp also places a crew consumable production demand on his ISPP system, which increases the system mass and power requirements. However, his mass and power estimates for systems other than the water acquisition are less than those calculated using this research's methods. This is why the total ISPP mass and power

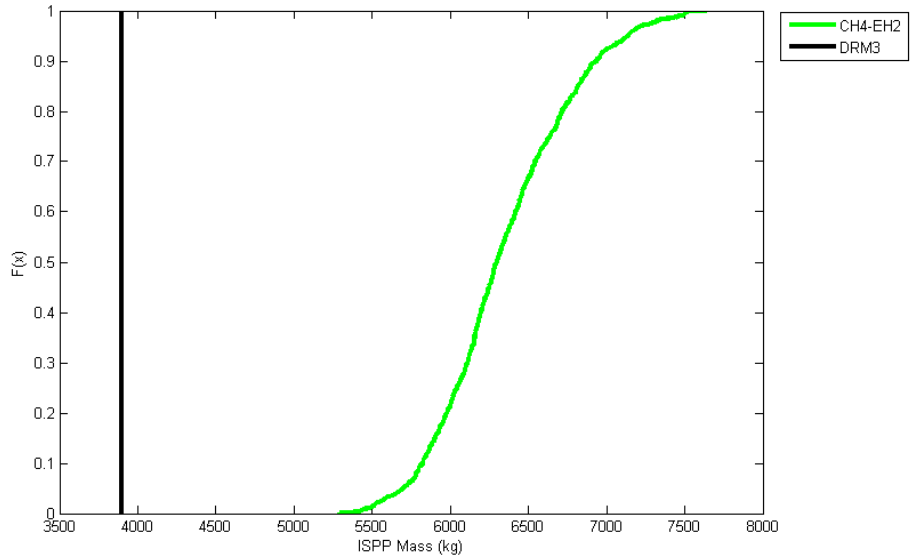

Figure 68: ISPP system mass based on DRM 3, with value given in DRM 3 on the vertical black line (3900 kg) [2].

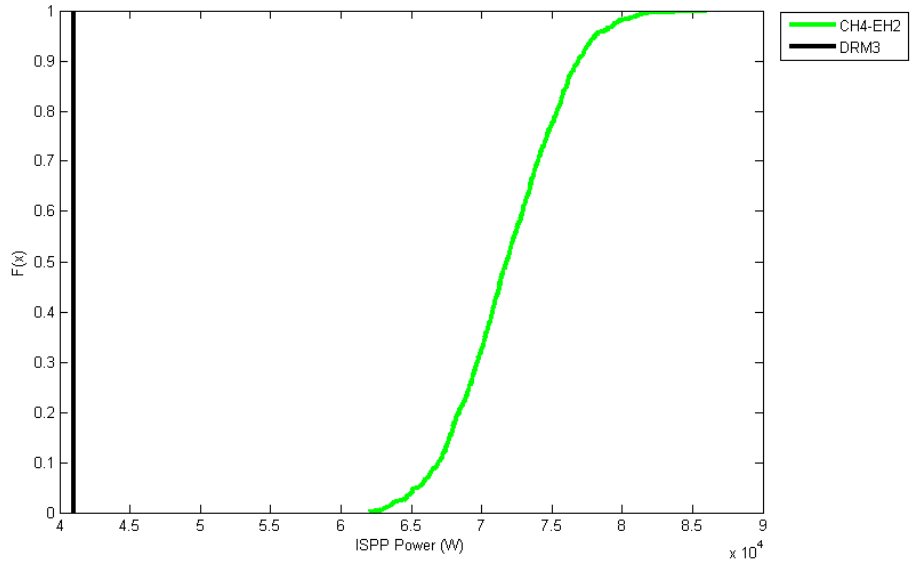

Figure 69: ISPP system power based on DRM 3, with value given in DRM 3 on the vertical green line (41,000 W) [2].

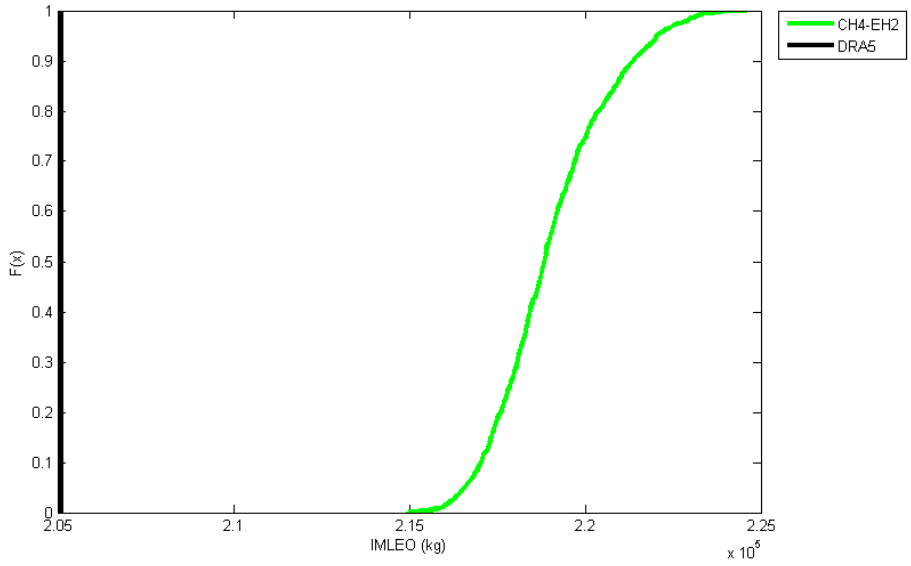

Figure 70: IMLEO for transporting ISPP and MAV based on DRM 3, with value given in DRM 3 on the vertical green line (205,100 kg) [2].

Table 53: Rapp Validation Inputs

Name	Value	Description
O_2 Required	36,156 [kg]	Oxygen for Mars Ascent Vehicle
CH_4 Required	10,846 [kg]	Methane for Mars Ascent Vehicle
Days	500 [day]	Days for ISPP operations
Hours	24 [hr]	Hours of daily operation

requirement are near to and less than the lower bounds of the Monte Carlo results, respectively. The inputs into the Rapp validation are given in Table 53, while the mean results of modeling the Rapp systems are given in Table 54. The stochastic validation of ISPP system mass, power, and IMLEO are given in Figures 71 through 73.

In DRA 5, two copies of the ISPP system are delivered to the surface of Mars, providing a redundant system; these higher values are accounted for in the data shown below. All three DRA 5 figures of merit (mass, Figure 74; power, Figure 75; and volume, Figure 76) lie within the bounds of the corresponding CDFs; the tool

Table 54: Rapp Validation

Name	Rapp	Model
Mass of ISPP	3.4 [t]	3.8 [t]
Mass of Feedstock	0 [t]	0 [t]
Mass of Power Plant	4.2 [t]	4.6 [t]
Power for ISPP	41 [kWe]	46 [kWe]
IMLEO (including ISPP, MAV, MDV, MTV)	134 [t]	118 [t]

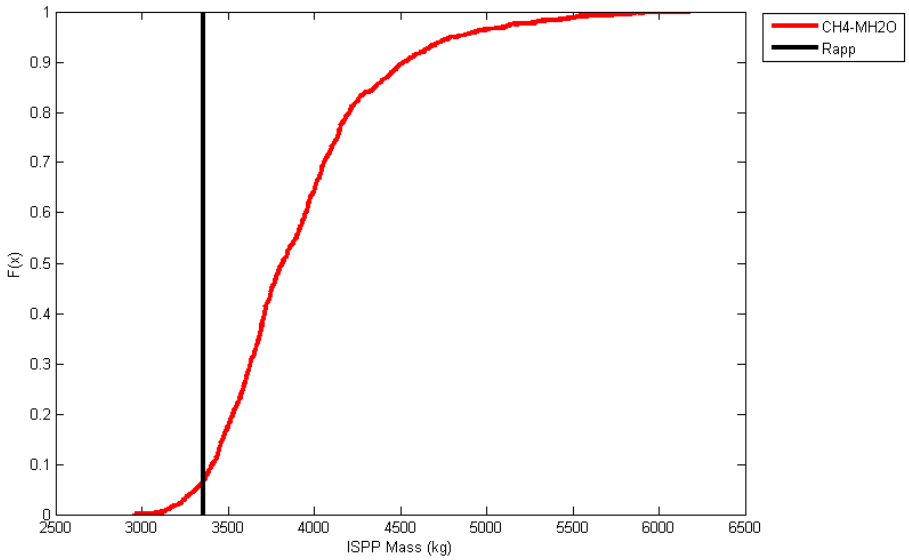

Figure 71: ISPP system mass based on Rapp, with value given in Rapp on the vertical black line (3400 kg) [5].

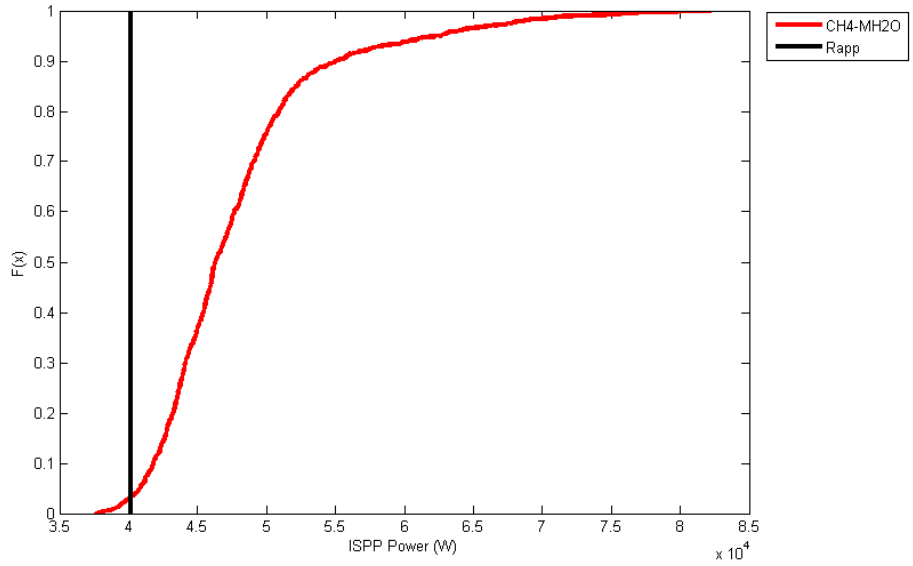

Figure 72: ISPP system power based on Rapp et al., with value given in Rapp et al. on the vertical green line (40,200 W) [5].

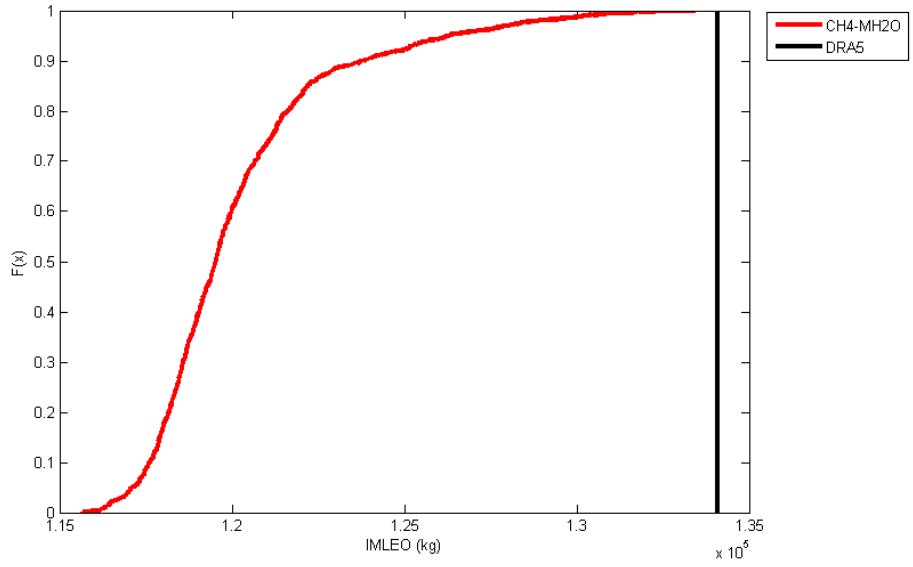

Figure 73: IMLEO for transporting ISPP and MAV based on Rapp, with value given in Rapp on the vertical green line (134,100 kg) [5].

Table 55: DRA 5 Validation Inputs

Name	Value	Description
O_2 Required	23100 [kg]	Oxygen for Mars Ascent Vehicle
CH_4 Required	6600 [kg]	Methane brought from Earth and cryocooled
Days	500 [day]	Days for ISPP operations
Hours	24 [hr]	Hours of daily operation

Table 56: DRA 5 Validation

Name	DRA 5	Model
Mass of ISPP	1.1 [t]	0.9 [t]
Mass of Feedstock	0 [t]	0 [t]
Mass of Power Plant	7.8 [t]	5.3 [t]
Power for ISPP	47.42 [kWe]	53 [kWe]
Volume of ISPP	1.72 [m^3]	1.1 [m^3]
IMLEO (including ISPP, MAV, MDV, MTV)	246.2 [t]	244 [t]

is thus anchored to the most recent NASA ISPP analysis. The inputs into the DRA 5 validation are given in Table 55, while the mean results of modeling the DRA 5 systems are given in Table 56. The stochastic validation of ISPP system mass, power, and IMLEO are given in Figures 74 through 77.

Of the five studies above, the model's stochastic results encompass those of the two most recent (DRA 5 and Rapp). This is expected, as the models used in Rapp and DRA 5 are based on many of the same studies used in the construction of the model. The model does not match the results in Mars Direct, due to the optimistic estimates used in sizing the ISPP system [2, 3]. The model overestimates the mass, power, and IMLEO for DRM 1 and DRM 3. For DRM 1, this is due to the lack of hydrogen tank and cryocooler in the ISPP mass estimate in the NASA study. For DRM 3, the same effect occurs, in addition to an unexplained decrease in ISPP mass and power relative to DRM 1 despite increased production requirements.

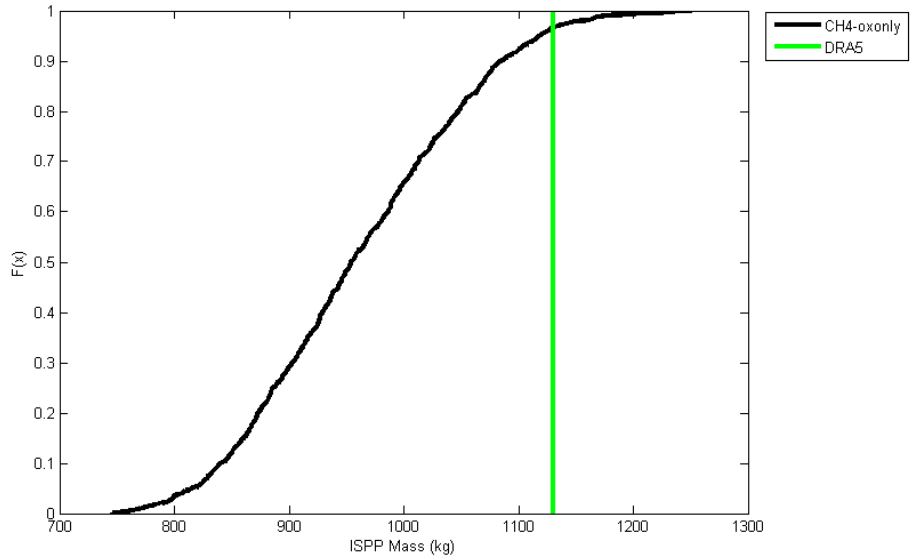

Figure 74: ISPP system mass based on DRA 5, with value given in DRA 5 on the vertical green line (1130 kg) [1].

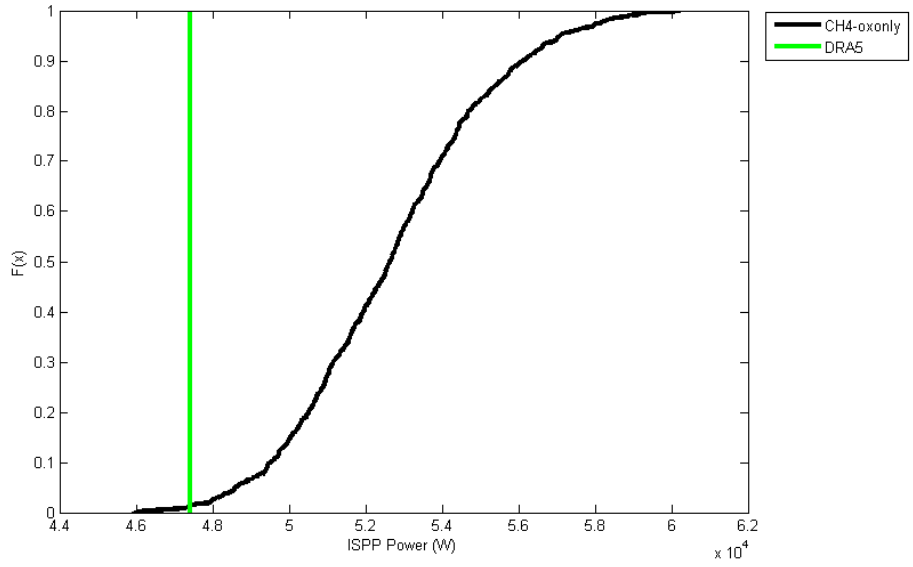

Figure 75: ISPP system power based on DRA 5, with value given in DRA 5 on the vertical green line (47,420 W) [1].

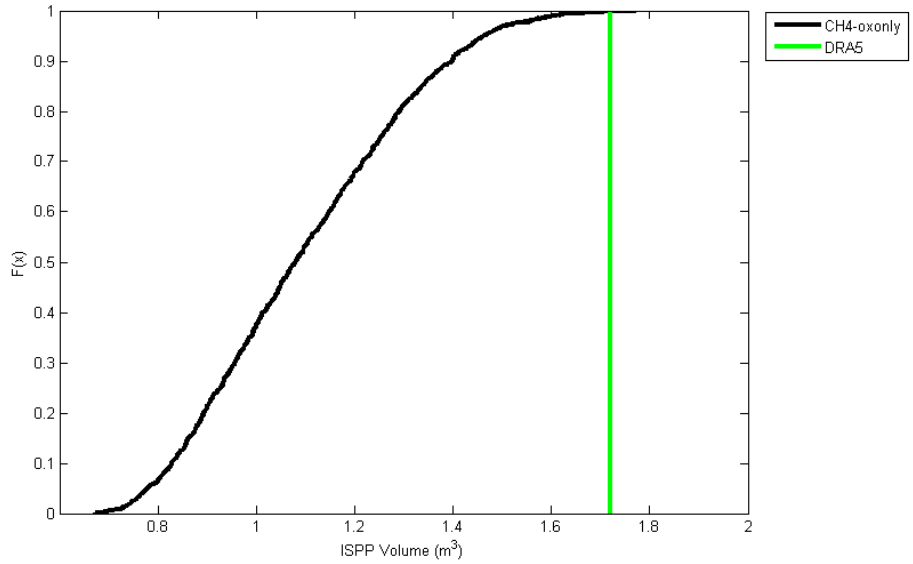

Figure 76: ISPP system volume based on DRA 5, with value given in DRA 5 on the vertical green line (1.72 m^3) [1].

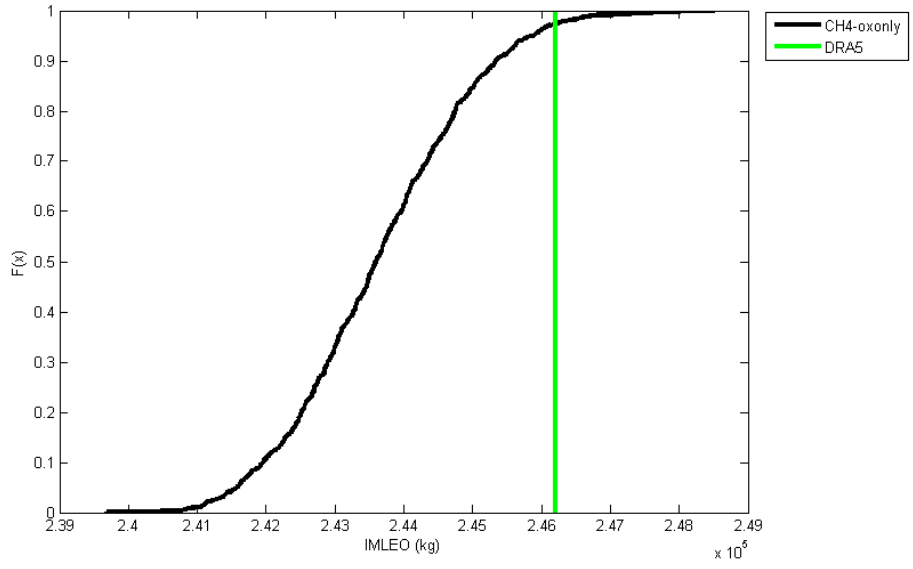

Figure 77: IMLEO for transporting ISPP and MAV based on DRA 5, with value given in DRA 5 on the vertical green line (246,200 kg) [1].

4.2 Parameter Range Identification

4.2.1 Setup

The identification of which parameters are most sensitive in the modeling of each ISPP architecture proceeded as follows.

1. Nominal values for each model parameter were fixed based on those used in the Spaceworks tool, or as calculated from sources (for those not defined in the Spaceworks tool).

2. For each model parameter permitted to vary (that is, those not based on physical fundamentals), a uniform distribution of between 80% and 120% of the nominal value was generated (e.g. if the nominal value of the water electrolyzer power-to-mass ratio is 23 We/kg, then the lower and upper bounds of the uniform distribution are 18.4 We/kg and 27.6 We/kg, respectively). If the lower or upper bound for a parameter that is a percentage (i.e., that must be between 0 and 1.0) would exceed 0 or 1.0, then the bound is fixed at the corresponding integer.

3. Varying only one parameter at a time (with all others fixed at their nominal values), Monte Carlo sampling was performed from the distribution 1000 times; each time, the model value was used to size the ISPP system and corresponding architecture.

4. The resulting values of each output variable (particularly net present value of the life cycle cost) are collected and plotted as a CDF. The width of that CDF (that is, the maximum net present value of the life cycle cost minus the minimum net present value of the life cycle cost) was used as the sensitivity for that model parameter.

5. The sensitivities for all parameters is collected into a list, ranked from greatest

to least. The most significant parameters are thus those that place at the top of that list.

This process is repeated for each ISPP architecture (thus, 15 of the 19 total architectures). The result lists the most significant parameters for each architecture. These results can be plotted on a "tornado plot" to show the magnitude of the sensitivity for each parameter. These results are shown in the next section.

4.2.2 Tornado Plots

The tornado plot for Architecture 1 (CH_4 with H_2 imported from Earth) is shown in Figure 78. By far the most significant parameter (by a greater than two-to-one margin) is the reaction temperature of the Sabatier process for methane formation. The temperature drives the reaction rate, which in turn drives the sizing of the reactor chamber and other components of the architecture. The second most significant factor is the conversion efficiency of hydrogen into methane; as the efficiency goes down, more hydrogen is required, which impacts the systems related to its storage and transfer (including the hydrogen cryocooler, MDV, and MTV). The final parameter that has a distinctive impact is the operating voltage of the carbon dioxide electrolyzer; this drives the efficiency of converting carbon dioxide to oxygen, and thus the amount of carbon dioxide that must be captured.

The tornado plot for Architecture 2 (CH_4 with H_2O imported from Earth) is shown in Figure 79. While the magnitude of the impact of reaction temperature remains similar, the conversion efficiency of hydrogen is now the most significant factor. This is due to the nature of hydrogen acquisition in the architecture: any excess hydrogen increases the amount of water that must be brought from Earth (and electrolyzed at Mars), which has a larger impact on the payload requirements of the MDV and MTV due to the additional oxygen that is carried with the excess hydrogen. The next four parameters on the list are all related to water operations: the rate of

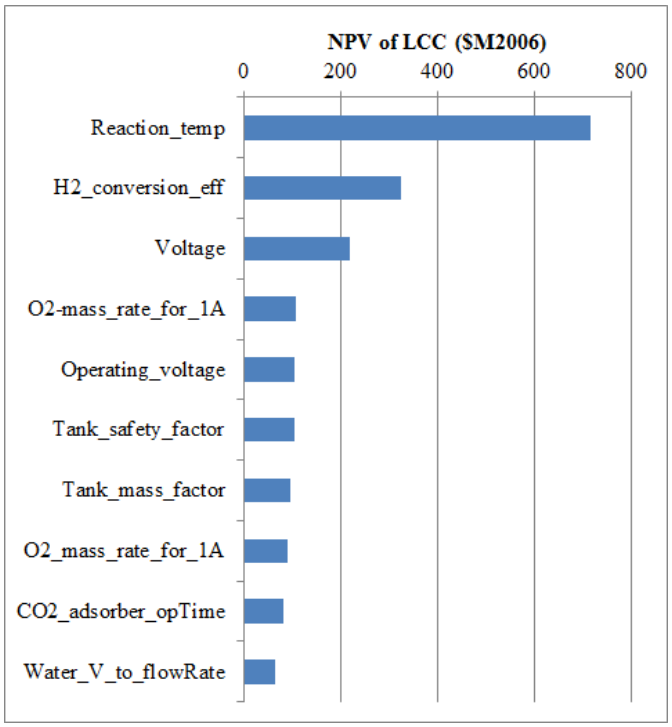

Figure 78: Tornado plot of the most sensitive model parameters for Architecture 1 (CH_4 with H_2 imported from Earth). The figure of merit is net present vale of the life cycle cost of the architecture.

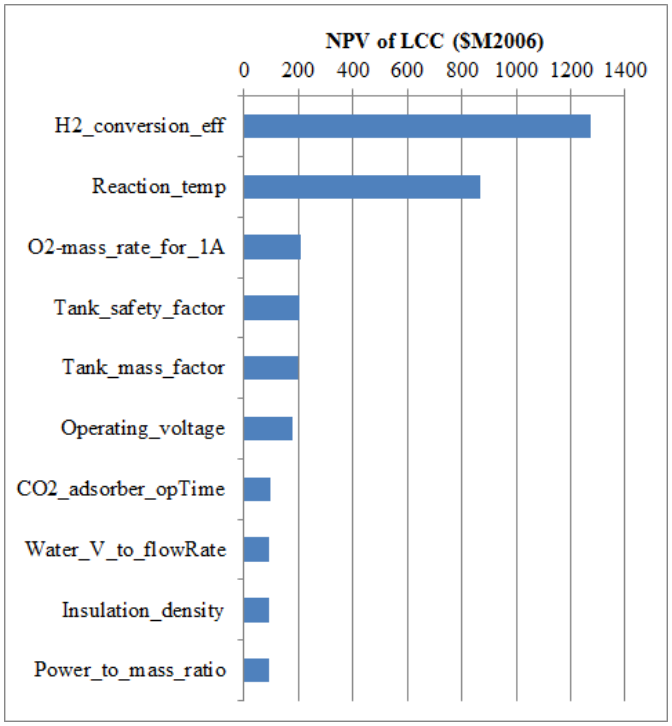

Figure 79: Tornado plot of the most sensitive model parameters for Architecture 2 (CH_4 with H_2O imported from Earth). The figure of merit is net present vale of the life cycle cost of the architecture.

oxygen electrolyzed per ampere of current, the safety factor and mass factor of the water tank, and the operating voltage of the water electrolyzer. In this, as in the other water importing architectures, parameters related to the water transport and processing are the most significant to the overall architecture.

Figure 80 shows the tornado plot for Architecture 3 (CH_4 with H_2O acquired at Mars). Again, the Sabatier reaction temperature and hydrogen conversion efficiency are the two most influential parameters. The third most important parameter is the concentration of water in the Martian regolith. The regolith collection and processing equipment is sized based on the amount of regolith to be processed, which in turn is determined by the fraction of water available. Thus, the mass of the water processing system depends upon the concentration fraction. Again, the two key power parameters for the water electrolyzer (the rate of oxygen electrolyzed per ampere of current and the operating voltage of the electrolyzer) also have significant impacts, as they

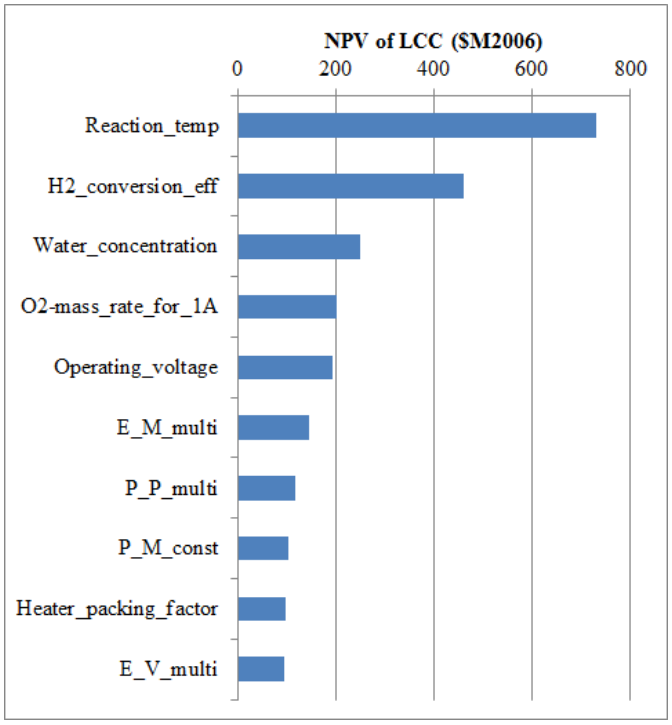

Figure 80: Tornado plot of the most sensitive model parameters for Architecture 3 (CH_4 with H_2O acquired at Mars). The figure of merit is net present vale of the life cycle cost of the architecture.

contribute to the power requirement and thus the power system mass.

For Architecture 4 (CH_4 brought from Earth, only O_2 produced at Mars), parameters of the carbon dioxide electrolyzer lead the list of most important parameters (Figure 81). By far the most significant is the voltage of the carbon dioxide electrolyzer, while the current parameter (the rate of oxygen electrolyzed per ampere of current) ranks second. The operating time of the carbon dioxide absorber and the packaging efficiency of the adsorbent follow, but with much smaller magnitudes than the two power parameters.

Two parameters related to the efficiency of processing hydrogen lead the tornado plot in Figure 82 for Architecture 5 (C_2H_4 with H_2 imported from Earth). The first is the efficiency with which hydrogen is converted to ethylene during the reverse water gas shift (RWGS). The second is the efficiency with which hydrogen is recovered

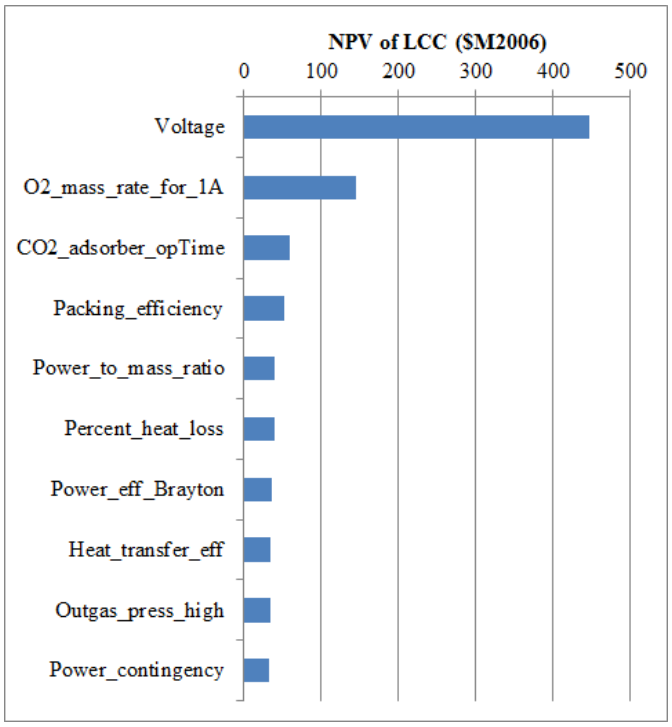

Figure 81: Tornado plot of the most sensitive model parameters for Architecture 4 (CH_4 brought from Earth, only O_2 produced at Mars). The figure of merit is net present vale of the life cycle cost of the architecture.

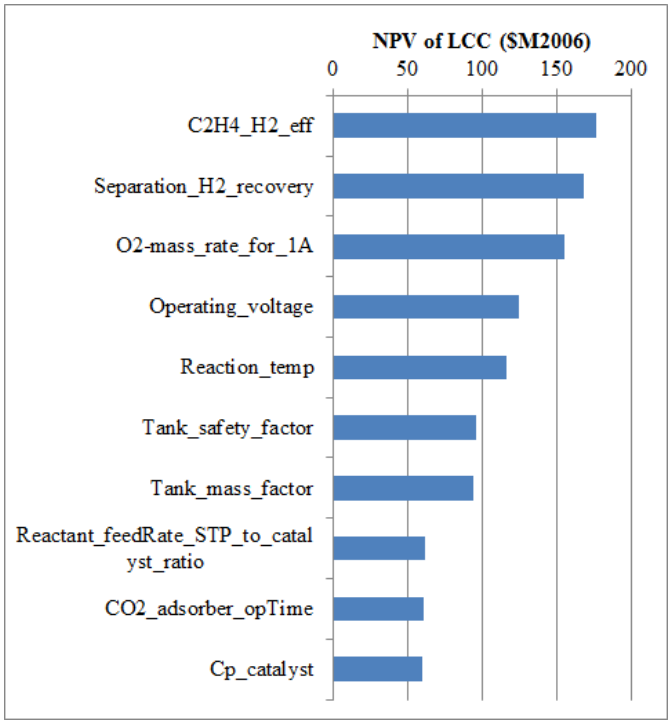

Figure 82: Tornado plot of the most sensitive model parameters for Architecture 5 (C_2H_4 with H_2 imported from Earth). The figure of merit is net present vale of the life cycle cost of the architecture.

through the membrane separator downstream of the condenser after the RWGS reaction. Both factors contribute to the amount of seed hydrogen required, which due to the low density of hydrogen, impacts the sizing of the transport systems. The two significant power parameters for the water electrolyzer again have notable impacts, as in Architectures 2 and 3.

The same parameters rank highly for Architecture 6 (C_2H_4 with H_2O imported from Earth), but the width of the CDFs is much greater, as shown in Figure 82. Again, this results from the impacts of requiring additional hydrogen: each additional kilogram of hydrogen requires an additional nine kilograms of water. Thus, the two parameters that impact the required amount of hydrogen have a signficant impact of the overall size, and thus cost, of the system.

As with Architecture 3, Architecture 7 (C_2H_4 with H_2O acquired at Mars) brings water concentration onto the list as a significant parameter; it places third behind the

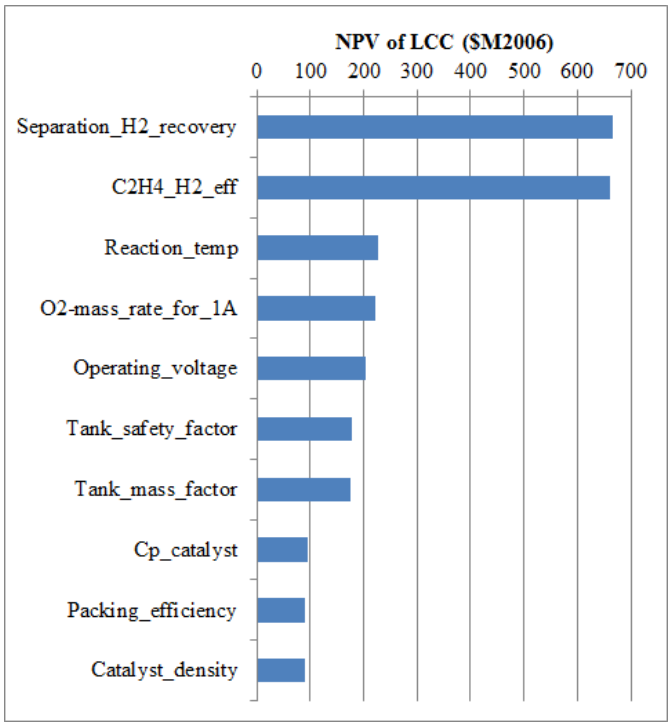

Figure 83: Tornado plot of the most sensitive model parameters for Architecture 6 (C_2H_4 with H_2O imported from Earth). The figure of merit is net present vale of the life cycle cost of the architecture.

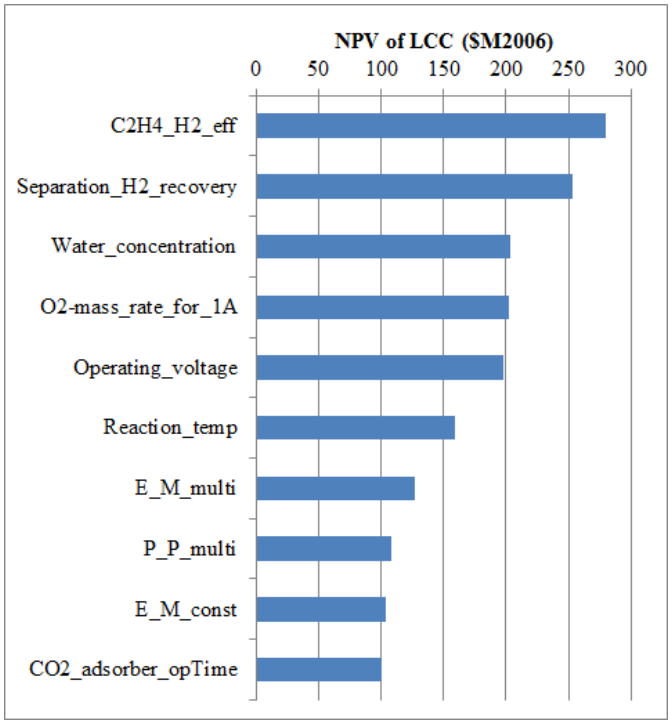

Figure 84: Tornado plot of the most sensitive model parameters for Architecture 7 (C_2H_4 with H_2O acquired at Mars). The figure of merit is net present vale of the life cycle cost of the architecture.

hydrogen efficiency parameters (which lead the chart for all three ethylene-producing architectures). Figure 84 shows that the water electrolyzer power parameters for voltage and current again play a key role, as does the reaction temperature of the RWGS reactor.

The tornado plot for Architecture 8 (C_2H_4 brought from Earth, only O_2 produced at Mars) is similar to that of Architecture 4; Figure 85 shows that the voltage of the carbon dioxide electrolyzer is clearly the most influential parameter, with only the rate of oxygen electrolyzed per ampere of current having even a fourth of the impact.

Of the four fuels considered in this research, methanol has the lowest O/F ratio, and thus parameters related to the hydrogen tank for Architecture 9 (CH_3OH with H_2 imported from Earth) rank highly on the corresponding tornado plot (see Figure 86. Additionally, the two power related parameters for the water electrolyzer also place in the top four, with the power-to-mass ratio, operating temperature, and fraction of

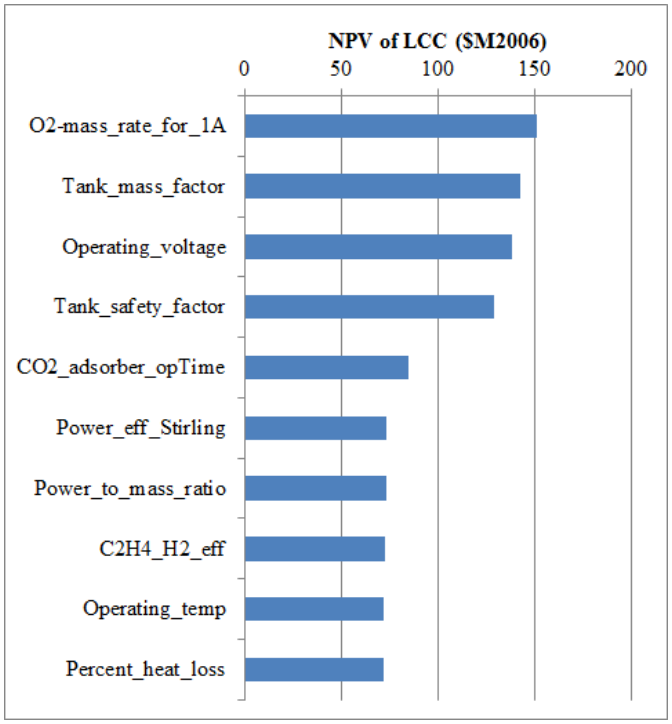

Figure 85: Tornado plot of the most sensitive model parameters for Architecture 8 (C_2H_4 brought from Earth, only O_2 produced at Mars). The figure of merit is net present vale of the life cycle cost of the architecture.

heat lost in the electrolysis process appearing on the list.

As above, the four most important variables in Architecture 10 (CH_3OH with H_2O imported from Earth) are the two key tank sizing parameters and the two water electrolyzer power parameters. Figure 87 shows the relative impact of these parameters as compared to others.

Figure 88 shows that five parameters stand out in Architecture 11 (CH_3OH with H_2O acquired at Mars). The most significant is the water concentration, previously an important factor for the other Mars water architectures. The two water electrolysis power parameters rank second and third. The other two parameters derive from the linear sizing of the Mars water acquisition system. The E_M_multi parameter is the multiplier in the equation for sizing the regolith excavator's mass, while the P_P_multi is the multiplier in the equation for estimating the regolith processing plant's power requirement. Also appearing on the list is P_V_const, the constant in the equation

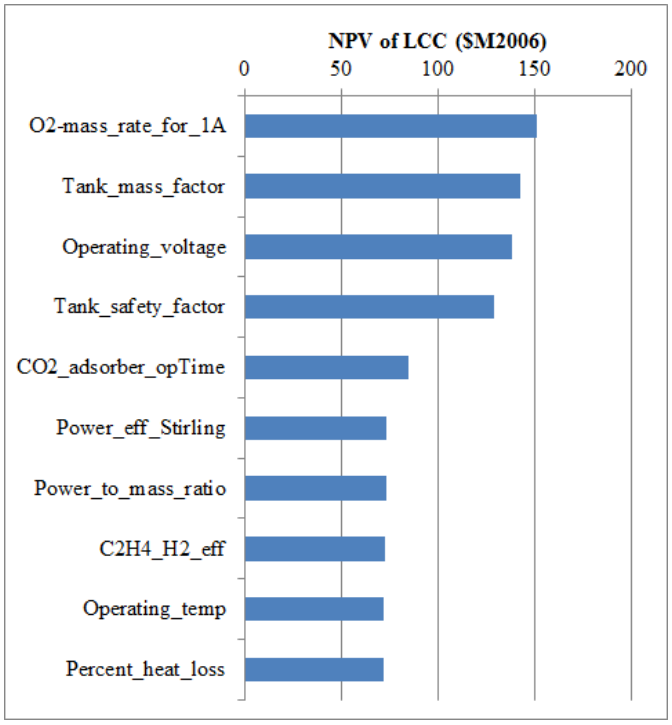

Figure 86: Tornado plot of the most sensitive model parameters for Architecture 9 (CH_3OH with H_2 imported from Earth). The figure of merit is net present vale of the life cycle cost of the architecture.

for calculating the regolith processing plant's volume.

As with the previous two oxygen only architectures, Architecture 12 (CH_3OH brought from Earth, only O_2 produced at Mars) has one parameter that rates far higher than the rest: the operating voltage of the carbon dioxide electrolyzer (Figure 89). Other than the efficiency of the oxygen cryocooler, all of the other top parameters are related to either the electrolyzer or the adsorber. Again, the two power parameters for the electrolyzer have greater impact than any other parameter.

Architecture 13 (H_2 brought from Earth, only O_2 produced at Mars), being an oxygen-only architecture, is dominated by the two power parameters for the carbon dioxide electrolyzer; see Figure 90.

Architecture 14 (H_2O imported from Earth and electrolyzed at Mars) is dependent upon water brought from Earth to provide all of the fuel and oxidizer for the MAV; thus, the sizing of the water tank and the water electrolyzer provide the most

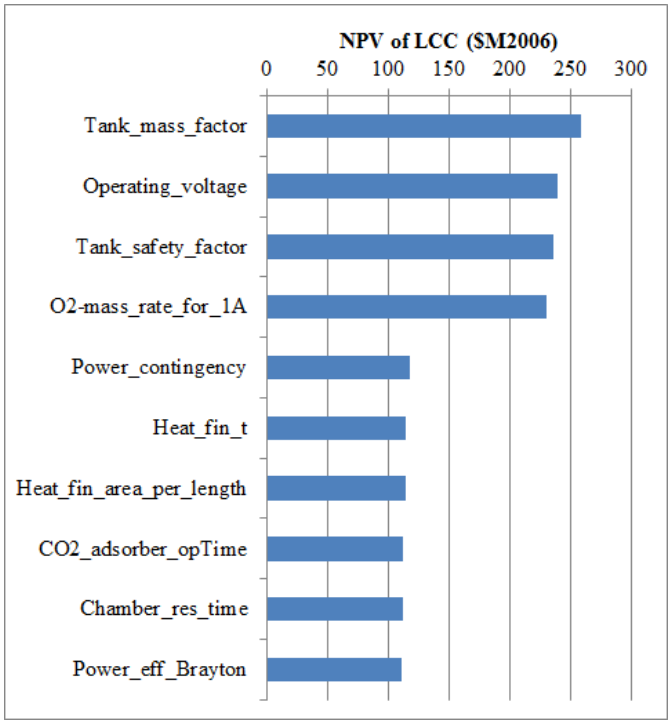

Figure 87: Tornado plot of the most sensitive model parameters for Architecture 10 (CH_3OH with H_2O imported from Earth). The figure of merit is net present vale of the life cycle cost of the architecture.

important parameters as shown in Figure 91.

As a Mars water based architecture, Architecture 15 (H_2O acquired at Mars and electrolyzed) is most influenced by the water concentration on Mars, as well as on the key parameters governing the regolith processing plant and water electrolyzer (Figure 92).

4.2.3 Identified Values

From the above plots, several parameters repeatedly emerge as the most significant across each architecture. Each of these parameters is discussed in further detail below, along with ranges of values extracted from a literature survey that are used in the architecture modeling results that follow.

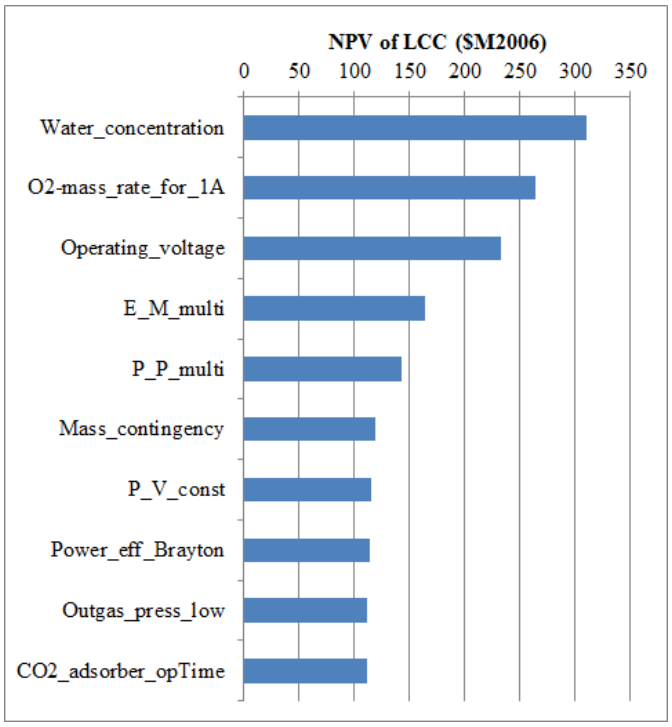

Figure 88: Tornado plot of the most sensitive model parameters for Architecture 11 (CH_3OH with H_2O acquired at Mars). The figure of merit is net present vale of the life cycle cost of the architecture.

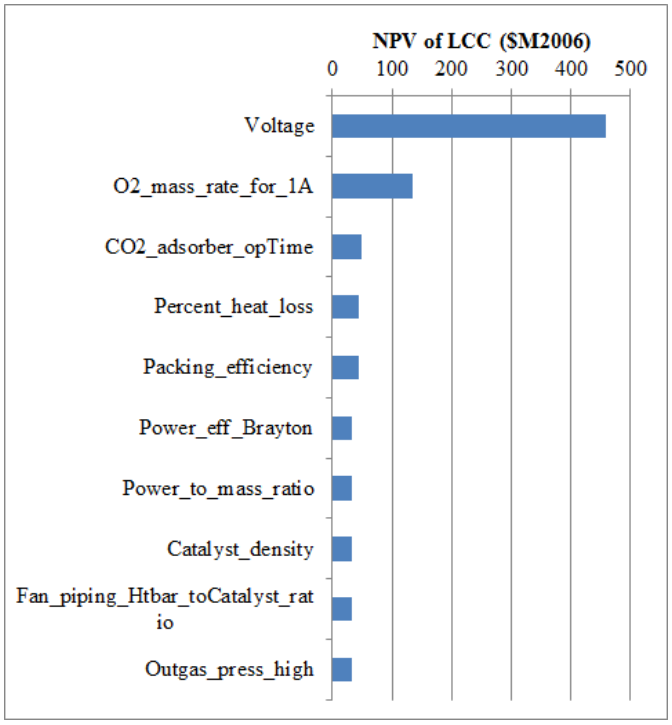

Figure 89: Tornado plot of the most sensitive model parameters for Architecture 12 (CH_3OH brought from Earth, only O_2 produced at Mars). The figure of merit is net present vale of the life cycle cost of the architecture.

4.2.3.1 Electrolyzer Operating Voltages

The operating voltage of the carbon dioxide electrolyzer is the leading parameter by a significant parameter for all four oxygen-only architectures for two reasons. First, the voltage is a critical parameter in determining the power requirements for the electrolyzer, and in turn, the entire ISPP system. This affects the sizing of the power plant, whose sizing parameter α is the single most important ISPP parameter across all fifteen architectures, due to its impact on total mass and life cycle cost.

Second, the operating voltage is very closely tied to the percent of carbon dioxide collected that is actually electrolyzed into oxygen. Figure 93 from Minh et al shows the relationship between carbon dioxide percent utilization and operating voltage [132]. As the voltage falls below the limit of 1.85 V, the utilization falls off sharply, reaching 0 at approximately 1.3 V. This contrasts with the theoretical results obtained by

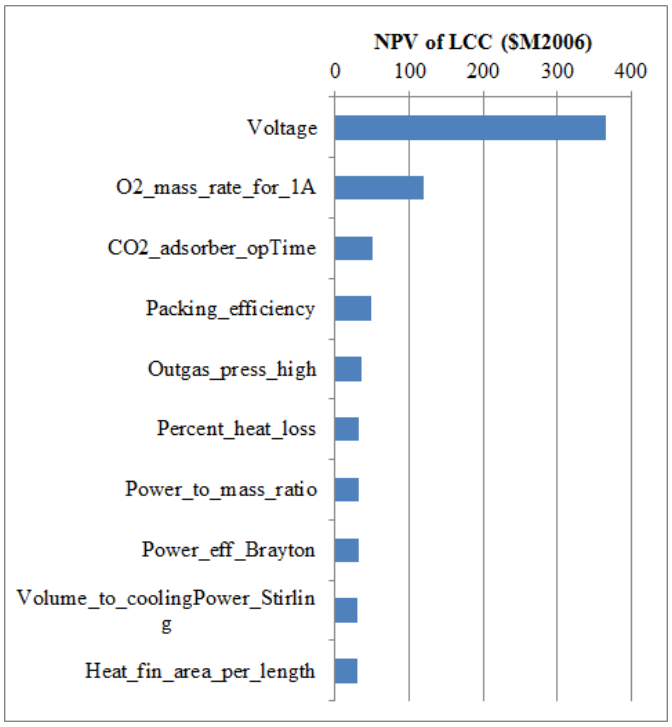

Figure 90: Tornado plot of the most sensitive model parameters for Architecture 13 (H_2 brought from Earth, only O_2 produced at Mars). The figure of merit is net present vale of the life cycle cost of the architecture.

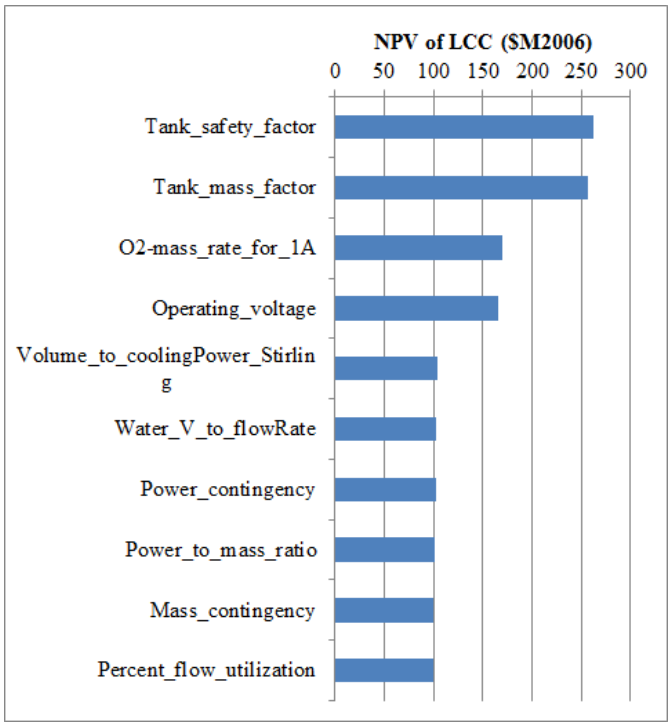

Figure 91: Tornado plot of the most sensitive model parameters for Architecture 14 (H_2O imported from Earth and electrolyzed at Mars). The figure of merit is net present vale of the life cycle cost of the architecture.

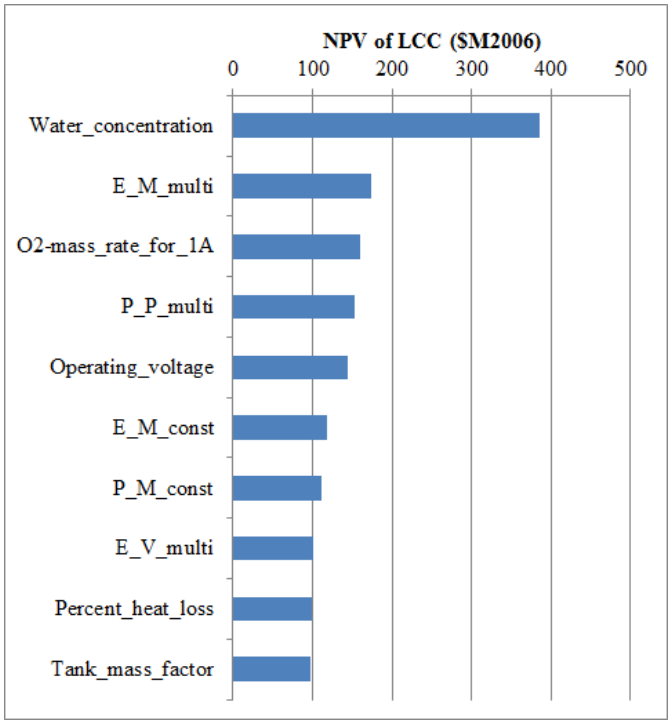

Figure 92: Tornado plot of the most sensitive model parameters for Architecture 15 (H_2O acquired at Mars and electrolyzed). The figure of merit is net present vale of the life cycle cost of the architecture.

Iacomini and Sridhar, whose calculations showed 50% utilization at voltages as low as 0.7 V [126]. Minh et al's results derive from experimental work, and are used in this research.

As the utilization decreases, the amount of carbon dioxide that must be acquired grows significantly, leading to a much larger catalyst bed in the adsorber and mass growth on the order of tonnes. Thus, it is critical that the voltage remain as high as possible; for the architecture modeling results, the voltage is constrained to between 1.7 V and 1.85 V. This range represents a variation between 50% and 100% of the maximum percent utilization possible (70%, according to the reference).

The power system and carbon dioxide adsorber masses are inversely proportional: higher voltages require higher power (and thus larger power systems), but smaller adsorber systems, while lower voltages have the opposite effect. The models and tools developed in this research permit the determination of which factor is more

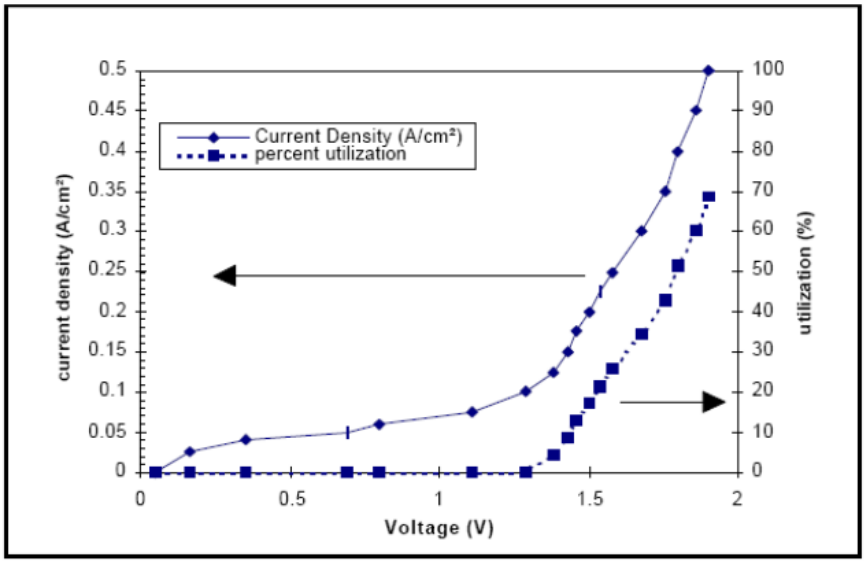

Figure 3. Performance curves of a 5 cm x 5 cm cell at 800°C.

Figure 93: Relationship between current density and carbon dioxide percent utilization to operating voltage of a CO_2 electrolyzer, reproduced from Reference [132].

significant. By varying the electrolyzer voltage across the range of 1.7 V to 1.85 V, while fixing other parameters at their nominal values, the combined mass of the ISPP sytem and power supply, and the power requirement, can be plotted against voltage to determine the optimal target voltage for future design. Each voltage was run ten times, with the mass growth uncertainty allowed to vary in each run; thus, there are columns of data (representing the spread caused by the mass growth uncertainty) at each voltage.

The results for the combined mass and the power requirement are shown in Figure 94. Regardless of whether a high, nominal, or low value of α is selected, the combined mass decreases as the voltage increases. This is due to the fact that across the range of voltages, the total power requirement (for the methane with Earth hydrogen architecture, the most demanding architecture that requires carbon dioxide electrolysis) only varies by approximately 500 We relative to the 47 kWe mean power requirement. While higher voltages do increase the power requirement for the electrolyzer,

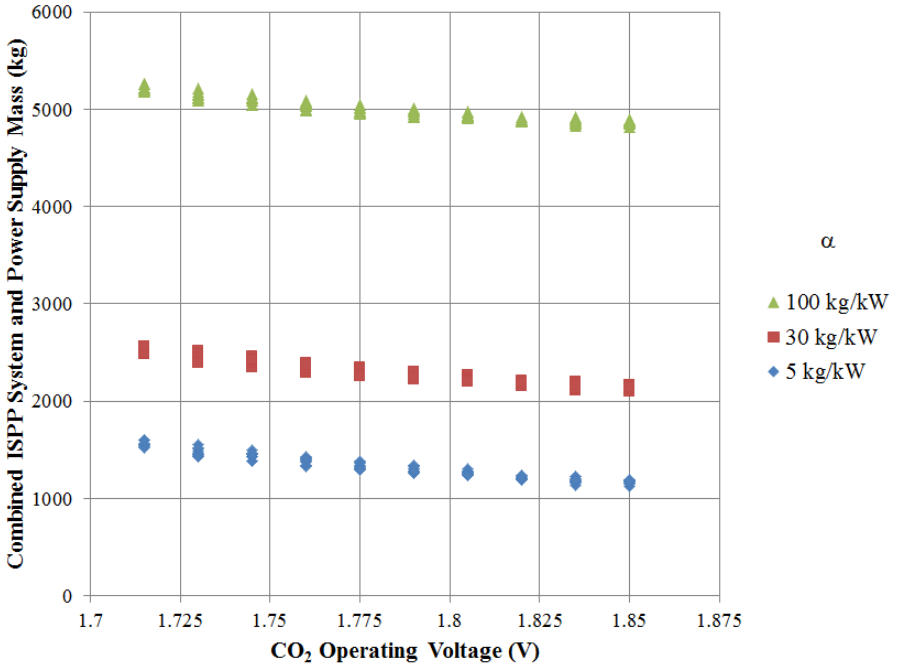

Figure 94: Combined mass of the ISPP system and power supply plotted against carbon dioxide operating voltage, for high, nominal, and low values of α.

the reduced size of the adsorber yields a lower power requirement for it. Thus, the preferred operating voltage is the maximum (1.85 V); however, in keeping with the stochastic nature of other model parameters in this study, the range for the primary analysis will be between 1.7 V and 1.85 V.

According to Thunnissen et al., the voltage for water electrolysis required is approximately 1.8 V [125]. Iacomini and Sridhar, surveying several electrolyzer voltage requirements, find results as low as 1.25 V [126]. These two values are used as the upper and lower bounds for the water electrolyzer voltage. For this system, lower voltages are better, but may be more difficult to achieve; hence the use of a range.

4.2.3.2 Rate of Oxygen Electrolyzed per Ampere of Current

In his treatise on ISRU for Mars, Rapp points to the rate of oxygen electrolyzed per ampere of current as a "basic quantity that relates the ion current to the oxygen gas

flow rate" in an electrolyzer [6]. With this parameter, the required oxygen production rate (determined by the ISPP system requirements), and the operating voltage (discussed above), the theoretical power requirement for an oxygen electrolyzer can be estimated using Equation 224. Rapp cites the work of Sridhar and Vaniman and estimates this quantity to have a value of 0.325 g/hr [37]; this value is also used by Thunnisen et al (of which Rapp was a co-author) [125]. Iacomini and Sridhar [126] cite a value computed by Clark [127] of 0.298 g/hr. These two values are used as the bounds for this parameter.

$$P_{theoretical} = \frac{\dot{m}_{O_{2required}}}{\dot{m}_I} * V_{electrolyzer} \tag{224}$$

4.2.3.3 Sabatier Reaction Temperature

Zubrin et al.'s work in 1994 on the development of a demonstration unit for the production of methane via the Sabatier process discussed the performance of two catalyst materials [115]. The original catalyst they considered, primarily consisting of nickel, could not provide sufficient reaction rates at temperatures below 623 K, and at colder temperatures would produce toxic products. The ruthenium-on-alumina catalyst they then used, on the other hand, could provide useful reaction rates at temperatures as low as 423 K. The reaction rate rose as the temperature increased from 423 K to 623 K, but the equilibrium constant (the ratio of products to reactants) fell as temperature increased. Figure 95, reproduced from Zubrin et al., shows the trade between reaction rate and equilibrium constant as a function of temperature.

The authors identify the high equilibrium constant as a factor that would push for lower temperatures, despite the lower conversion rate. Further, lower conversion rates require a small reactor and lower start-up power, potentially reducing system size. However, as discussed later in the paper, actual yields with their experimental

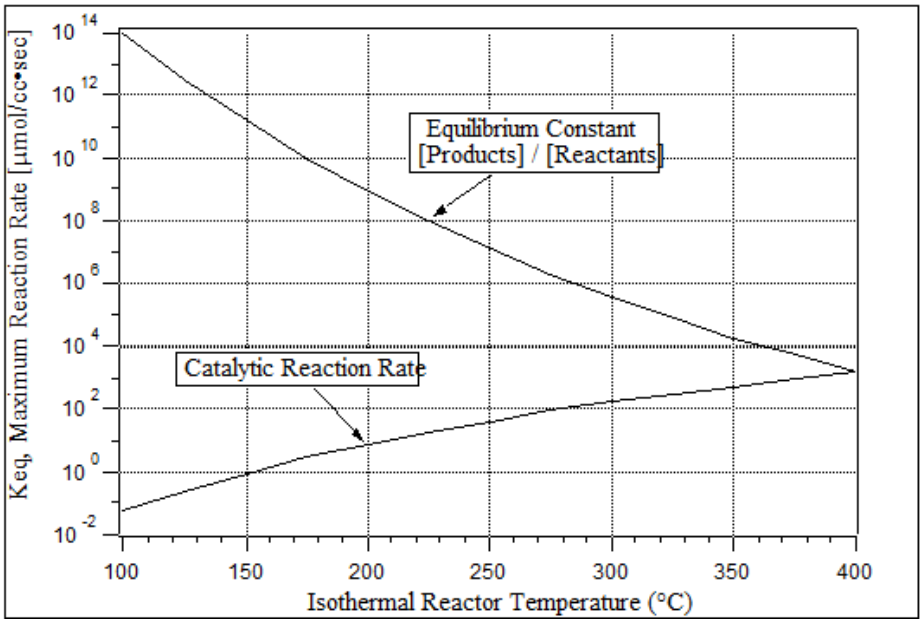

Figure 95: Catalytic reaction rate and equilibrium constant for Sabatier production of methane as a function of temperature [115].

setup were better with higher temperatures. The last of a series of test runs conducted evaluated hydrogen conversion percentage (to methane) as a function of temperature, showing improvement as temperatures approached 623 K (see Figure 96). The authors summarize their findings by pointing to the need for further optimization of multiple elements of the system, including better control of the temperature of reaction. As a result of the competing tensions pulling to both lower and higher temperatures, the Sabatier reaction temperature will be varied from 554 K (the lowest temperature with a better than 50% hydrogen conversion rate) to 645 K (the highest temperature proposed by Zubrin et al.); this also has implications for the H2 conversion efficiencies discussed below.

4.2.3.4 Hydrogen Conversion and Recovery Efficiencies

Due to the challenges involved in transporting hydrogen, as well as the high leverage it provides in any of the architectures that produce fuel locally, the abilities to convert and to recover hydrogen efficiently impact their corresponding architectures.

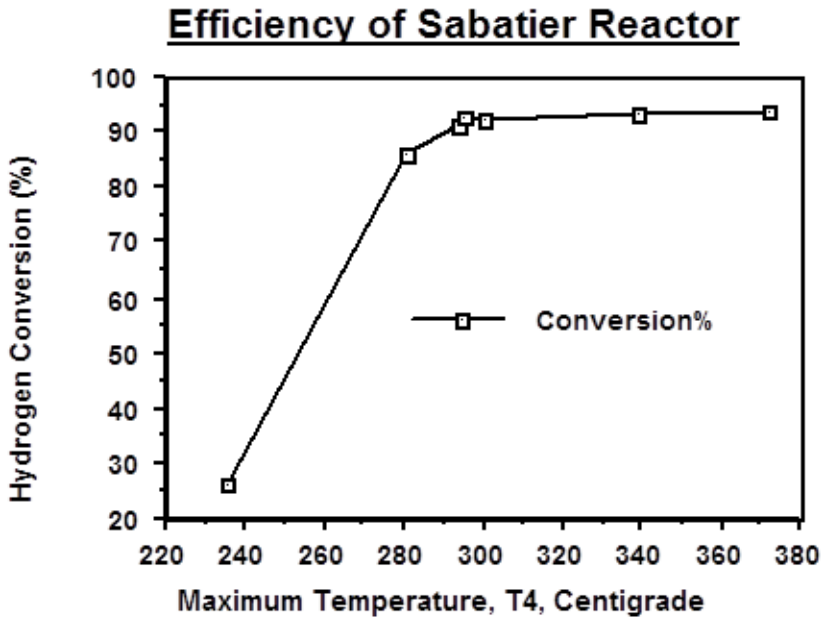

Figure 96: Hydrogen-to-methane conversion rate as a function of temperature for final test runs from Zubrin et al. [115].

For methane production, Zubrin et al. found that conversion rates of 94% were obtained at high temperatures; the authors further speculated that adjustments to the system could drive yields as high as 98% [115]. For this research, the hydrogen conversion efficiency will be derived from a second order polynomial fitting the hydrogen conversion data in Figure 96; see Equation 225.

$$\eta_{H_2 conversion} = -1.6156 * 10^{-5} * {T_{Sabatier}}^2 + 1.9980 * 10^{-2} * T_{Sabatier} - 5.2339 \quad (225)$$

Hydrogen recovery efficiencies (e.g. post-processing from the water electrolyzer) depend upon the necessary purity of the recovered hydrogen. Air Products hydrogen recovery membranes, for example, can recover 80% of hydrogen at 99% purity from high hydrogen streams ($> 85\%$), with recoveries approaching 97% for lower purity hydrogen [123]. In their work on a methanol production reactor, Zubrin et al. demonstrated complete hydrogen recovery with a two membrane loop, providing an upper

bound on the possible efficiency [34]. These lower (80%) and upper (100%) bounds will be used for the ranges of hydrogen recovery efficiency.

4.2.3.5 Water Concentration on Mars

In his initial ISPP proposal in 1978, Ash suggested that the availability of Martian water would permit the extraction of hydrogen necessary to produce methane [28]. However, as more details emerged in the post-Viking analysis of Mars, it was believed that there was not enough water available to faciliate methane production, and emphasis turned to options that did not rely on Martian water [4, 16, 29–33].

By the time of DRA 5.0, two possible concentrations of water in Martian regolith were considered as alternatives to bringing hydrogen from Earth, or producing oxygen exclusively: a lower bound of concentration of 3%, and an upper bound of 8% [10]. In the Addendum to DRA 5.0, the authors cited these figures as coming from measurements from Viking (for the 3% figure) and Mars Odyssey (for the 8% figure). They acknowledged the existence of more highly concentrated sources of water nearer to the Martian poles, but cited concerns about contamination and search for life in ignoring subsurface ice reservoirs.

Using data from more recent measurements provided by Phoenix (2008) and Curiosity (2012), Sanders suggests that at latitudes greater than 60 degrees, water concentrations can exceed 30% and even approach 60% within the top meter of the Martian surface [151]. As this research is indifferent to the particular latitude of the Mars mission, water concentraion ranges from the conservative 3% of DRA 5.0 to the 60% shown by Sanders.

4.2.3.6 Tank Safety and Mass Factors

In the NASA Technical Standard for Structural Design and Test Factors of Safety for Spaceflight Hardware, the ultimate design factor of safety given for the sizing of a metallic tank structure is 1.4 [152]. This standard applies for metallic structure

excluding fasteners, for which the ultimate design factor of safety is also given as 1.4. This provides a lower bound for the tank safety factor, particularly given that there is an additional mass margin applied (as for all masses sized in this research) based on the mass margins given in [153–155].

In their discussion of propellant tank sizing, Larson and Pranke suggest tank safety factors ranging from 2 to 4 [22]. They note that these factors are for tanks that typically contain "a lot of stored energy or hazardous propellant." However, for a tank transporting liquid water, neither of these characteristics apply. Thus, the value of 2 is used as the upper bound for the tank safety factor.

In the same discussion, Larson and Pranke offer a conservative estimate for tank mass factors (a parameter derived from their tank sizing that measures the efficiency of the tank design; a larger value corresponds to a more mass efficient tank) of 2500 m, while pointing out that a survey of tank mass factors clustered around a more optimistic 7500 m [22]. These values serve as the lower and upper bounds of tank mass factor for the primary trades comparing architectures in the next two sections.

Thus, several parameters have been identified as key drivers within the ISPP system modeling: the operating voltage of both the water and carbon dioxide electrolyzers, the rate of oxygen electrolyzed per ampere of current, the Sabatier reaction temperature (for methane production architectures), the efficiencies of hydrogen conversion and recovery, the concentration of water on Mars (for Mars water architectures), and the tank safety and mass factors. Three additional factors also influence the results across architectural comparisons: specific impulse, specific power (α), and launch cost. The effects of these are shown in the following two sections.

4.3 Architectural Comparisons

Each of the nineteen architectures has multiple common elements: a MAV, MDV, and MTV. Additionally, the fifteen architectures that utilize ISPP all have a surface

power system. The deterministic results for the ISPP elements, surface power system, and transportation elements for all nineteen architectures are shown in the figures in Appendix B. The nomenclature for the 19 architectures shown in the plots below is given in Table 57.

The mean masses (that is, the means of the CDFs) of each of the nineteen architectures are shown in Figures 97 (for α of 23 kg/kWe) and 98 (for α of 266 kg/kWe). A comparison of the nineteen architectures on the basis of total mass reveals that an architecture that uses full ISPP while bringing minimal quantities of mass from Earth has the lowest mass: ethylene with Mars water. This architecture has a specific impulse comparable to the similarly performing methane with Mars water (357 s as compared to 359 s), but due to the nature of the oxygen production resulting from the ethylene reactor as compared to the Sabatier reactor, it does not require as large an ISPP system. In addition, the lack of fuel cryocooling reduces the power burden relative to the methane architecture.

The ethylene with Mars water architecture also has a lower mass than the hydrogen with Mars water architecture despite the latter's smaller ISPP system and power plant and superior specific impulse; this results from the reduced volume of the MAV (692 m^3 compared to 1420 m^3 for the hydrogen MAV) due to the fuel density and the subsequent increases in size of the MDV and MTV required to deliver the system to Mars. This effect also drives the poor mass performance of the hydrogen with Earth water architecture, which has the greatest mass requirement.

The four architectures that bring water from Earth to supply hydrogen have similar masses of fluid to land as those that use no ISPP, while also requiring ISPP mass. As would be expected, each of the four architectures that acquire water on Mars have the lowest masses relative to their counterparts that use the same fuel but different acquisition methods. Thus, evaluating the nineteen architectures solely on a mass basis, the lowest mass architecture is ethylene with Mars water (for the low specific

Table 57: Architecture Nomenclature

Name	**Abbreviation**
Methane fuel with hydrogen brought from Earth	CH4-EH2
Ethylene fuel with hydrogen brought from Earth	C2H4-EH2
Methanol fuel with hydrogen brought from Earth	CH3OH-EH2
Methane fuel with water brought from Earth	CH4-EH2O
Ethylene fuel with water brought from Earth	C2H4-EH2O
Methanol fuel with water brought from Earth	CH3OH-EH2O
Hydrogen fuel with water brought from Earth	H2-EH2O
Methane fuel with water acquired on Mars	CH4-MH2O
Ethylene fuel with water acquired on Mars	C2H4-MH2O
Methanol fuel with water acquired on Mars	CH3OH-MH2O
Hydrogen fuel with water acquired on Mars	H2-MH2O
Methane fuel with no ISPP	CH4-none
Ethylene fuel with no ISPP	C2H4-none
Methanol fuel with no ISPP	CH3OH-none
Hydrogen fuel with no ISPP	H2-none
Methane fuel with only oxygen ISPP	CH4-oxonly
Ethylene fuel with only oxygen ISPP	C2H4-oxonly
Methanol fuel with only oxygen ISPP	CH3OH-oxonly
Hydrogen fuel with hydrogen brought from Earth	H2-EH2

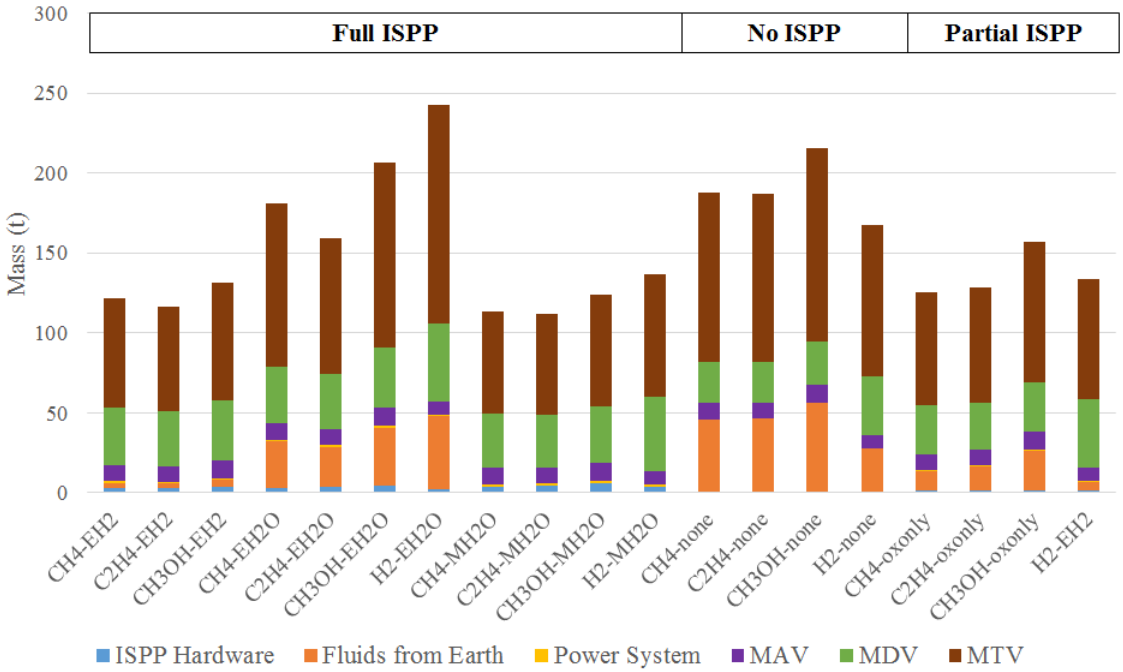

Figure 97: The deterministic masses for the nineteen architectures with low specific mass power system (α = 23 kg/kWe).

mass power systems).

With the high specific mass power system (Figure 98), a different ethylene approach has the lowest total mass: ethylene with Earth hydrogen. The ethylene with Earth hydrogen architecture's total mass relative to the ethylene with Mars water architecture's total mass is driven by the additional power required for the Mars water excavators and plant (11 kWe, see Figure 139 in Appendix B). At 266 kg/kWe, that additional power increases the size of the power system by 2.9 t, with subsequent increases in the MDV and MTV masses. Thus, the mass impact of the transportation requirements of bringing hydrogen from Earth are outweighed by the impact of the higher power.

Other architectures that have low mass in this scenario include the methane and ethylene architectures with Earth hydrogen, Mars water, and only oxygen ISPP. The performance of these six are driven by the volumetric impact on mass of high fuel density described above. Methanol has a higher density than either methane or

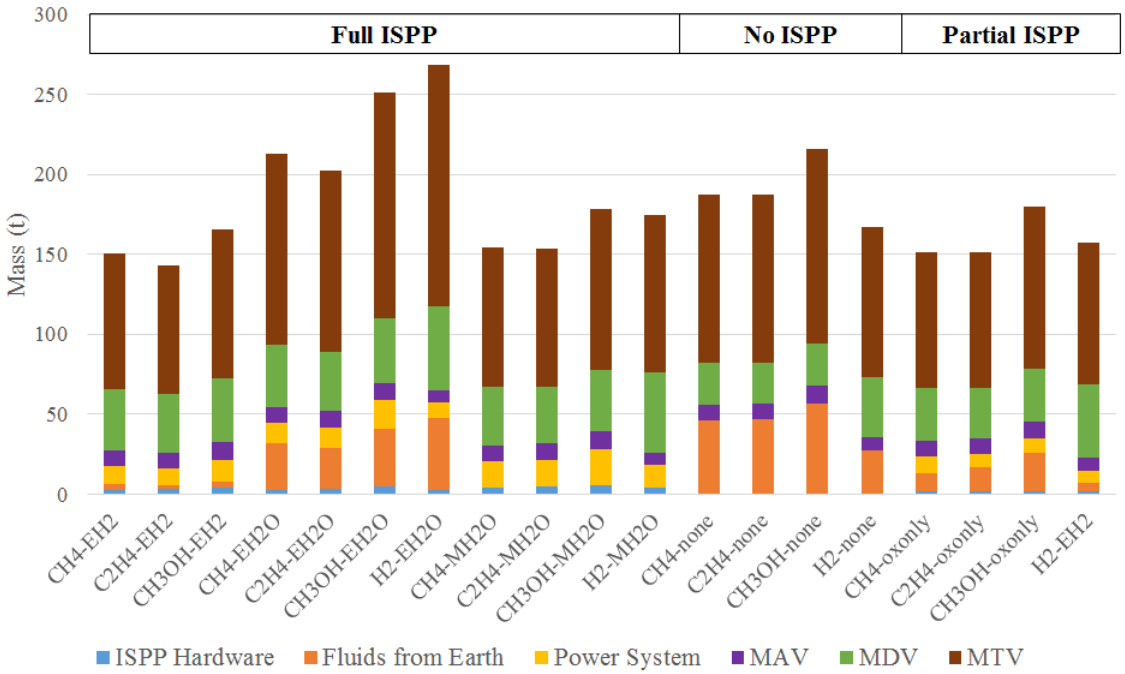

Figure 98: The deterministic masses for the nineteen architectures with high specific mass power system (α = 266 kg/kWe).

Table 58: Scenario grid based on α and launch cost.

	α = **23 kg/kWe**	α = **266 kg/kWe**
Launch Costs = \$2500/kg	Scenario 1	Scenario 2
Launch Costs = \$30000/kg	Scenario 3	Scenario 4

ethylene (see Table 38 in Chapter 3), but its lower specific impulse (330 s) yields a greater propellant requirement, which in turn requires more massive ISPP, power, and transportation elements. Thus, the analysis of the masses of the nineteen architectures at mean values reveals the interrelationship between specific impulse, fuel density, specific power, and total mass; there exists a balance between these variables that minimizes mass. That balance is achieved by methane and ethylene architectures with ISPP, which have the lowest mass for both low and high specific mass power systems. However, that balance does not include the impact of cost.

The mean costs of each of the nineteen architectures are shown in Figures 99

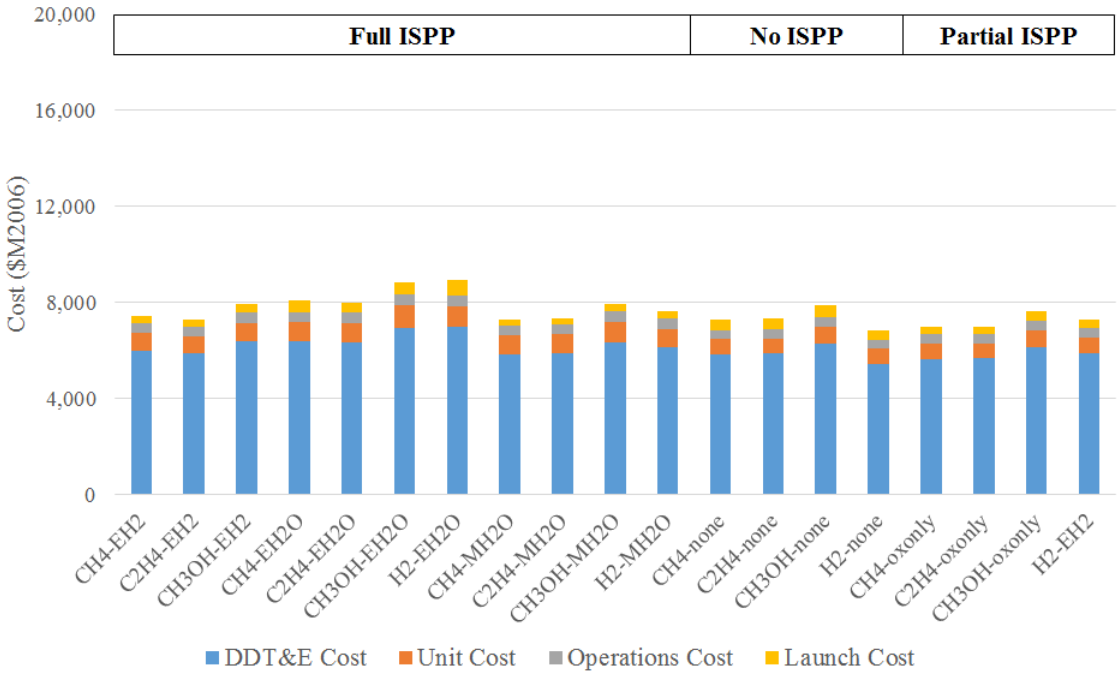

Figure 99: The deterministic costs for the nineteen architectures in Scenario 1 (α = 23 kg/kWe, LC = \$2500/kg).

through 102. Each figure corresponds to one of the four scenarios described in Section 4.4, shown in Table 58. As seen in Figure 99, when launch costs are low, DDT&E costs are by far the biggest contributor to the total cost in each architecture. In Scenario 1, with low launch costs and low specific mass power system, the mass advantage of using ISPP is countered by the investment required to develop that ISPP; the result is that the hydrogen with no ISPP architecture has the lowest mean cost. The next two lowest cost architectures are methane and ethylene with only oxygen ISPP. With low launch costs, the investment required to develop, deploy, and operate ISPP outweighs the savings in launch cost from lower mass, as well as the lower cost of the smaller MDV and MTV resulting from less mass landed on Mars. However, many of the ISPP concepts that performed well on mass, such as methane and ethylene using Earth hydrogen and Mars water, are only 7% to 8% more expensive than the hydrogen with no ISPP option.

In Scenario 2, when launch costs are low and specific power is high (shown in

Figure 100), all of the non-ISPP options are less expensive than any ISPP option. The increase in size, and thus cost, of the nuclear power system, in combination with the increased MDV and MTV sizes and costs, yield the higher costs. The best partial ISPP option, using ethylene, is 6% more expensive than the worst non-ISPP option, and 22% more expensive than hydrogen with no ISPP. Other architectures that perform well on a cost basis, such as ethylene with Earth hydrogen and ethylene with Mars water, are 31% and 47% more expensive than hydrogen with no ISPP, respectively.

The four architectures using Earth water, already the most mass prohibitive, are also among the most expensive; the reduced complexity (and thus development cost) of the associated ISPP is less than the increases cost of developing the larger MDV and MTV required to transport that water from Earth orbit. Of the eleven full ISPP architectures, methane and ethylene with Earth hydrogen are the lowest cost (35% and 31% greater than hydrogen with ISPP, respectively), although still worse than any partial or non-ISPP approach. As in the high specific mass power system mass comparison, this is driven by the additional power requirement for Mars water ISPP, which increases the masses (and costs) of the power and transportation systems. Further, the Mars water ISPP systems do not pay for themselves in this situation.

At the higher launch costs and low specific mass power system of Scenario 3, Figure 101 finds several ISPP options with lower costs than any non-ISPP option. Ethylene with Mars water is the least expensive approach, followed closely by methane with Mars water and methane with only oxygen ISPP. The next two least expensive architectures are ethylene with hydrogen from Earth and ethylene with only oxygen ISPP. Scenario 3 is the most favorable to ISPP, and thus the best performing architectures are those that also perform best on mass in Figure 97, with the exception of the two only oxygen ISPP architectures. An examination of why those two approaches appear among the least expensive, but not the least massive, architectures reveals

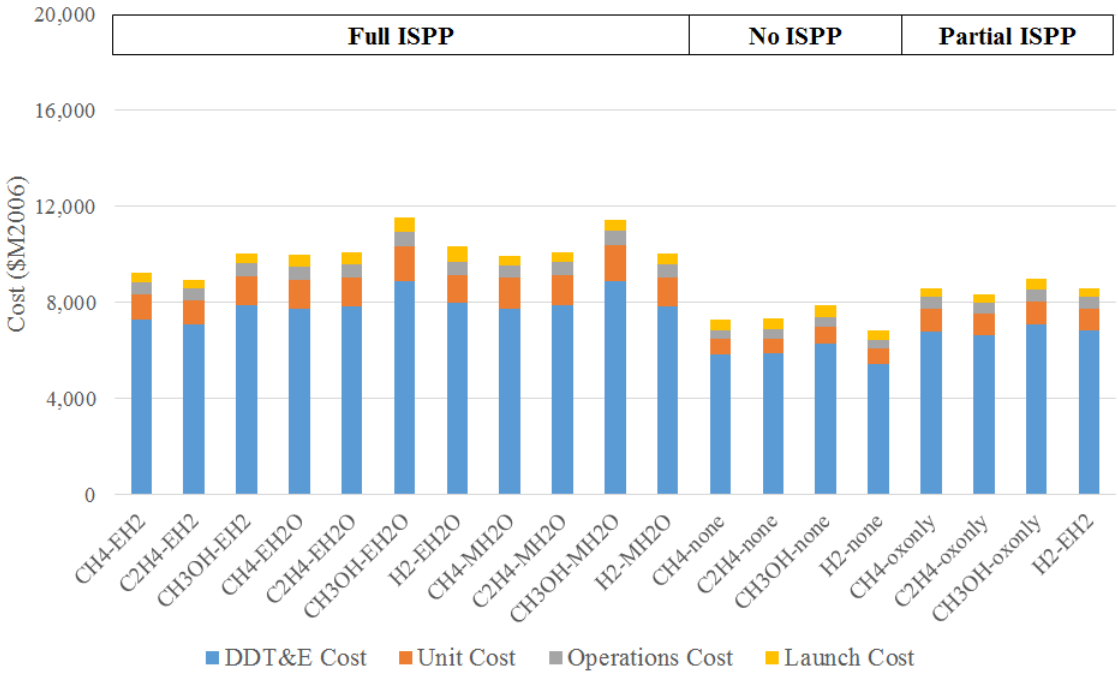

Figure 100: The deterministic masses for the nineteen architectures in Scenario 2 (α = 266 kg/kWe, LC = \$2500/kg).

that the combination of volume efficiency and minimal ISPP development drive their performance over full ISPP approaches using hydrogen or methanol.

Even in a scenario that is maximally favorable for ISPP, three of the four fuels have a non-ISPP option that is superior to the corresponding Earth water approach (only ethylene does slightly better for the Earth water than non-ISPP approach). This is driven by the high launch costs of the IMLEO required to transport the water; note that the Earth water architectures are also more massive than their non-ISPP counterparts (again, with the exception of ethylene) in Figure 97. The lack of a hydrogen tank (as in Earth hydrogen approaches) is balanced by the need for a water tank, while the lack of Mars water acquisition hardware (as in Mars water approaches) is outweighed by the greater IMLEO and costs of larger transportation systems.

Scenario 4, wherein ISPP benefits from the high launch costs but is penalized by the high specific mass power system (shown in Figure 102), finds several non-ISPP

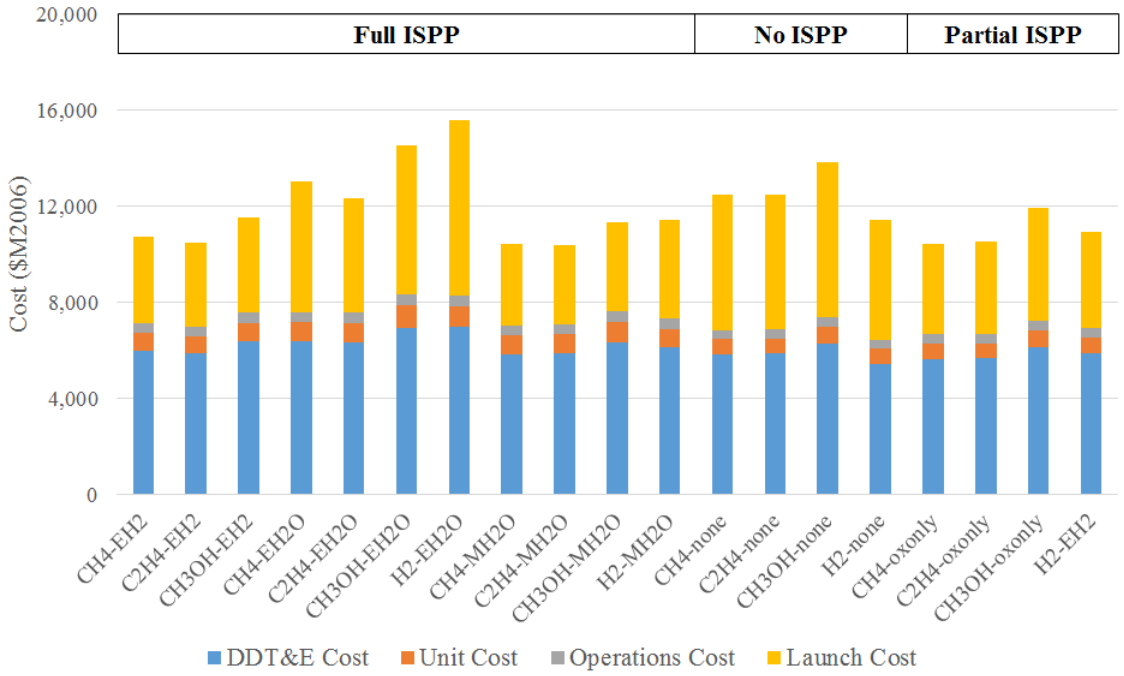

Figure 101: The deterministic masses for the nineteen architectures in Scenario 3 (α = 23 kg/kWe, LC = \$30000/kg).

options have lower total cost than the best ISPP options. Hydrogen with no ISPP is again the least expensive architecture, followed by methane and ethylene with no ISPP. The two best performing partial ISPP approaches (ethylene and methane) are 9% and 12% more expensive than hydrogen with no ISPP, respectively. As in the mass comparison shown in Figure 98 above, the ethylene and methane approaches using Earth hydrogen are superior to their Mars water counterparts due to the compounding effects of high specific mass power system; the effect is increased due to the proportional increases in costs of larger power systems, MDVs, and MTVs.

An examination of the results of the four scenario plots reveals several trends. At low values of specific power (Scenarios 1 and 3), Mars water ISPP is the best full ISPP approach. The best ISPP approach in general depends on the additional variable of launch cost: a partial approach using only oxygen ISPP is less expensive in Scenario 1 with low launch costs, while Mars water ISPP performs better at high launch costs in Scenario 3. Similarly, the best overall approach between the two scenarios depends

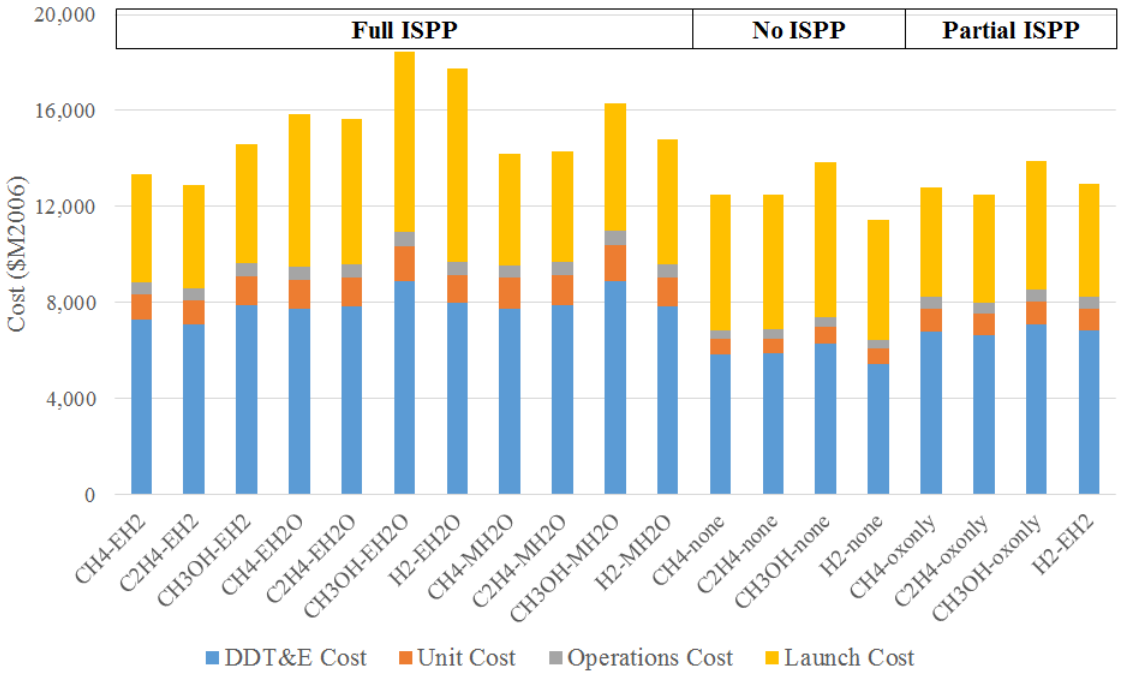

Figure 102: The deterministic masses for the nineteen architectures in Scenario 4 (α = 266 kg/kWe, LC = \$30000/kg).

on launch costs: in Scenario 1, hydrogen with no ISPP is the least expensive, while in Scenario 3, ethylene with Mars water is the best.

At high values of specific power (Scenarios 2 and 4), hydrogen with no ISPP is the best architecture, and the methane and ethylene with no ISPP approaches are the two next best. In these scenarios, partial ISPP is better than full ISPP when comparing across the same fuel. Of the full ISPP approaches, ISPP with Earth hydrogen is better than ISPP with Mars water, which in turn is superior to ISPP with Earth water, due to the impact of larger, more expensive MDVs and MTVs and greater power requirements.

Among the full ISPP approaches, ethylene is superior to methane when bringing hydrogen from Earth, but this trend reverses when hydrogen is extracted from Mars water. Among the partial ISPP approaches, methane is superior to ethylene when power is efficient (Scenarios 1 and 3), but this trend reverses when power is inefficient (Scenarios 2 and 4); this is driven by the additional power requirements of the carbon

dioxide electrolyzer and methane cryocooler becoming magnified in Scenarios 2 and 4 over the superior Isp of methane.

These singular results for each approach only partially capture the effects of model uncertainty, and they do not examine scenarios with α and launch cost in between the extrema defined in Table 58. The results in Section 4.4 examine the full range of stochastic results to address both issues.

4.4 Stochastic Results

Five scenarios are considered in the primary analysis. Each scenario captures a region of the space defined by the variation in launch cost (between \$2500/kg and \$30000/kg, as described by Arney [147]) and in specific power (between 23 kg/kWe and 266 kg/kWe, as discussed in Section 2.3.2). The first four form the "corners" of that space: low launch cost and low specific mass power system, high launch cost and low specific mass power system, low launch cost and high specific mass power system, and high launch cost and high specific mass power system. The fifth scenario allows both parameters to vary uniformly between their lower and upper bounds; this yields an understanding of the overall trade space of the nineteen architectures.

4.4.1 The Impact of Low Launch Cost and Low Specific Mass Power System on ISPP

The first scenario considers the effect of both low launch costs (at \$2500/kg) and highly efficient, low specific mass nuclear power (at 23 kg/kWe) on the comparison of the nineteen architectures. A one thousand run Monte Carlo, using the distributions described above, was used to generate CDFs of multiple metrics, including the figure of merit of this research (the net present value of the life cycle cost of the architecture). The relative robustness integrals of the nineteen architectures were computed for the figure of merit to identify the preferred architecture.

Figure 103 illustrates the CDFs of the nineteen architectures for the net present

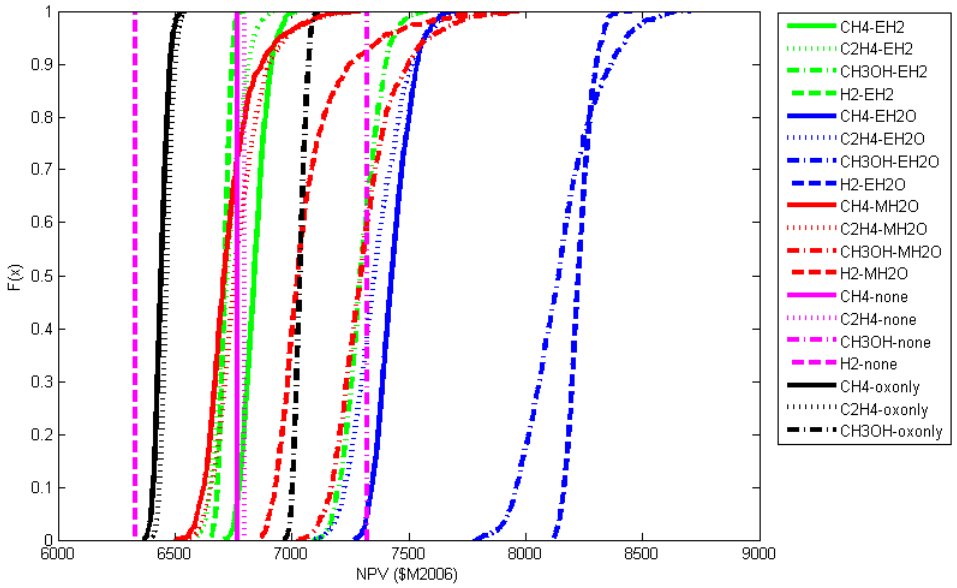

Figure 103: The net present value of the life cycle cost of the nineteen architectures with low launch costs and low specific mass power system.

value of the life cycle cost. The form of each line corresponds to the fuel type (solid for methane, small dash for ethylene, small and large dash for methanol, and large dash for hydrogen), and the color corresponds to the type of ISPP approach (green for hydrogen supplied from Earth, blue for water supplied from Earth, red for water acquired at Mars, magenta for no ISPP, and black for only oxygen ISPP). Table 59 gives the means and standard deviations of several figures of merit of each architecture.

In this scenario, based on the relative robustness integral of the net present value of the life cycle cost, a non-ISPP approach using hydrogen as fuel outperformed two partial ISPP architectures: methane and ethylene. The low launch costs damp the savings achieved by reduced mass from ISPP, while the additional complexity of ISPP increases the development costs more than the reduction due to smaller in-space transportation systems. These two partial ISPP architectures in turn performed better than hydrogen with only oxygen ISPP, as well as the two best performing full ISPP architectures: ethylene using Earth hydrogen and ethylene using Martian water.

Table 59: Mean ± Standard Deviation of Figures of Merit for Scenario 1 (Low Launch Costs and Low Specific Mass Power System)

Architecture	**IMLEO (t)**	**ISPP Power (kWe)**	**NPV of LCC ($M2006)**
CH4-EH2	127 ± 1	42 ± 2	6843 ± 50
C2H4-EH2	121 ± 2	38 ± 3	6728 ± 64
CH3OH-EH2	137 ± 2	50 ± 4	7302 ± 79
H2-EH2	140 ± 1	29 ± 1	6712 ± 24
CH4-EH2O	189 ± 3	47 ± 3	7439 ± 74
C2H4-EH2O	176 ± 7	50 ± 4	7362 ± 118
CH3OH-EH2O	216 ± 11	67 ± 6	8159 ± 156
H2-EH2O	253 ± 1	34 ± 3	8233 ± 51
CH4-MH2O	119 ± 2	62 ± 8	6734 ± 108
C2H4-MH2O	116 ± 2	63 ± 7	6766 ± 104
CH3OH-MH2O	129 ± 3	84 ± 11	7312 ± 144
H2-MH2O	143 ± 4	54 ± 11	7070 ± 149
CH4-none	196 ± 0	0 ± 0	6768 ± 0
C2H4-none	195 ± 0	0 ± 0	6799 ± 0
CH3OH-none	225 ± 0	0 ± 0	7325 ± 0
H2-none	175 ± 0	0 ± 0	6332 ± 0
CH4-oxonly	131 ± 1	38 ± 2	6443 ± 28
C2H4-oxonly	134 ± 1	31 ± 2	6464 ± 26
CH3OH-oxonly	164 ± 1	32 ± 2	7036 ± 25

The gap between the first two partial ISPP options is driven by the volumetric effect of a hydrogen MAV impacted the MDV and MTV size, while the additional costs of developing full ISPP account for the difference between the partial and full ISPP approaches. The four Earth-water-based architectures were by far the worst, with methanol from Earth water and hydrogen from Earth water having the highest net present values of their life cycle costs. As in comparison in Section 4.3, the larger MDV and MTV required for the transport of water from Earth increases costs more than the decrease of less complex ISPP; this effect is found even for lower launch costs.

Figure 104 shows the relative robustness integrals, normalized such that the best scoring architecture (hydrogen with no ISPP) has a score of 1 and the worst scoring architecture (hydrogen from Earth water) has a score of 0. The relative robustness integral collapses the two dimensionality of the CDF results into a single dimension ratio while still preserving the effects of the shape of each distribution. Thus, it can be seen that after the hydrogen with no ISPP approach and two partial ISPP options emerge as the leaders, the hydrogen with only oxygen ISPP and the two ethylene options (with Earth hydrogen and with Mars water) follow. The DRA 5.0 like option (methane with oxygen only) finishes second among the nineteen architectures; the balance of smaller in-space transportation (with associated lower cost) and minimal ISPP investment lead to its less expensive performance. This preference ordering and the relative spacing are consistent across multiple runs of the same scenario.

Figure 105, Figure 106, and Figure 107 show the launch costs, DDT&E costs, and unit production costs of the nineteen architectures, respectively. At the low launch costs considered in this scenario, the DDT&E costs dominate the total cost; they are an order of magnitude larger than the launch and unit costs. As the DDT&E costs are driven by both the number and size of the elements required, the combination of high mass (the large landed payload of the water) and high technology (the ISPP

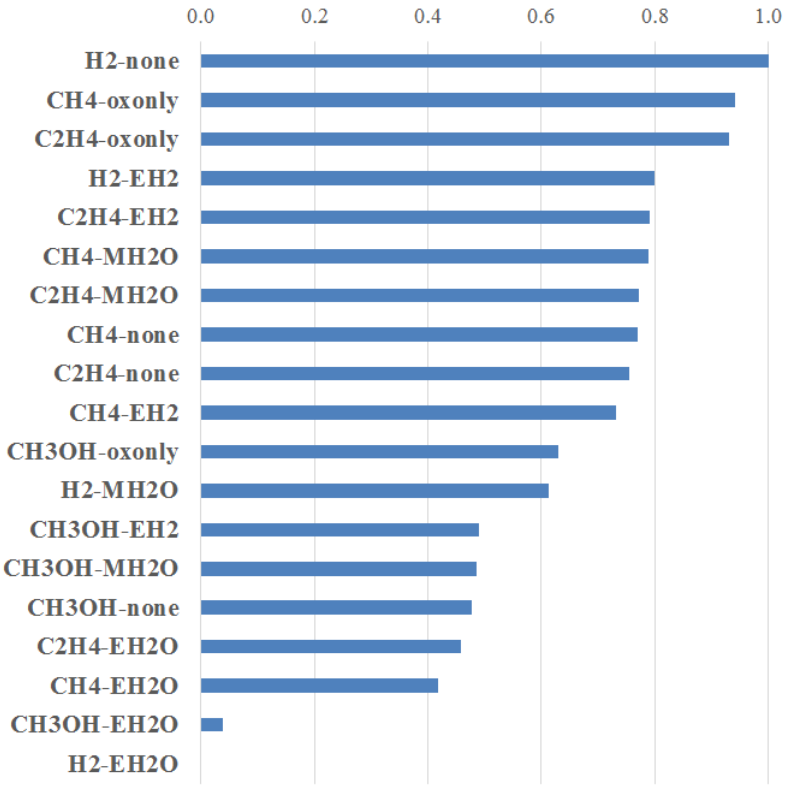

Figure 104: Relative robustness integrals of the net present value of the life cycle cost of the nineteen architectures with low launch costs and low specific mass power system.

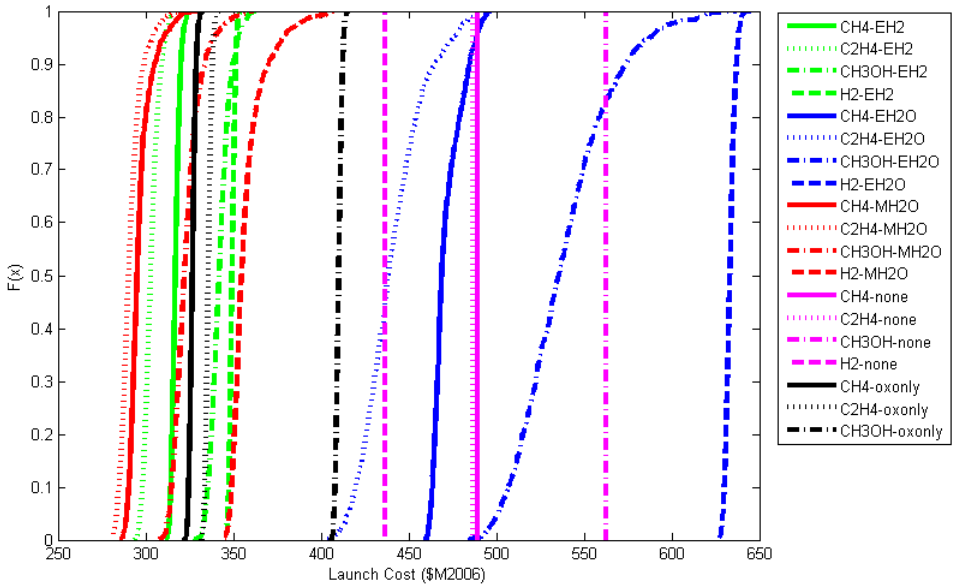

Figure 105: The launch cost of the nineteen architectures with low launch costs and low specific mass power system.

systems to produce fuel and oxidizer) required by the Earth water approaches leads to significantly higher development costs than the other types of architectures. This, in turn, leads to the poor performance in net present value of life cycle cost. By comparison, the balance struck of low landed mass and an intermediate amount of technology required by the oxygen only architectures (oxidizer production, but not fuel production), drives the high performance of the ethylene with only oxygen ISPP and methane with only oxygen ISPP architectures. The high performance of the hydrogen stage (with its low O/F ratio) yields the smallest oxygen demand of the partial ISPP options; this leads to its fourth place finish among the nineteen architectures. The larger landed mass requirement of the methanol with only oxygen ISPP architecture yields its middling performance relative to the three high performing only oxygen ISPP architectures.

One limitation of this analysis is that the full impact of the volume of elements on the architecture. Although the volumes of the ISPP elements, surface power system,

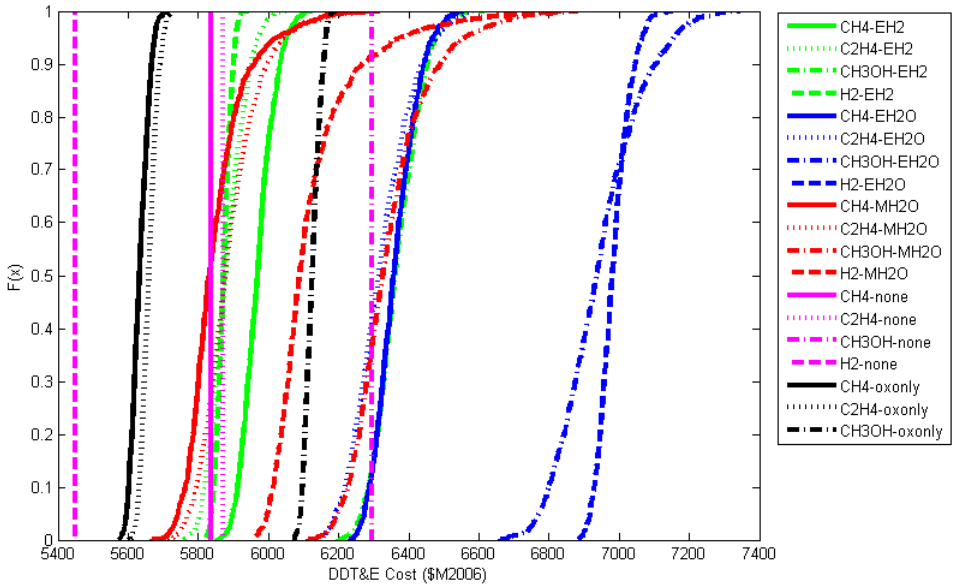

Figure 106: The DDT&E cost of the nineteen architectures with low launch costs and low specific mass power system.

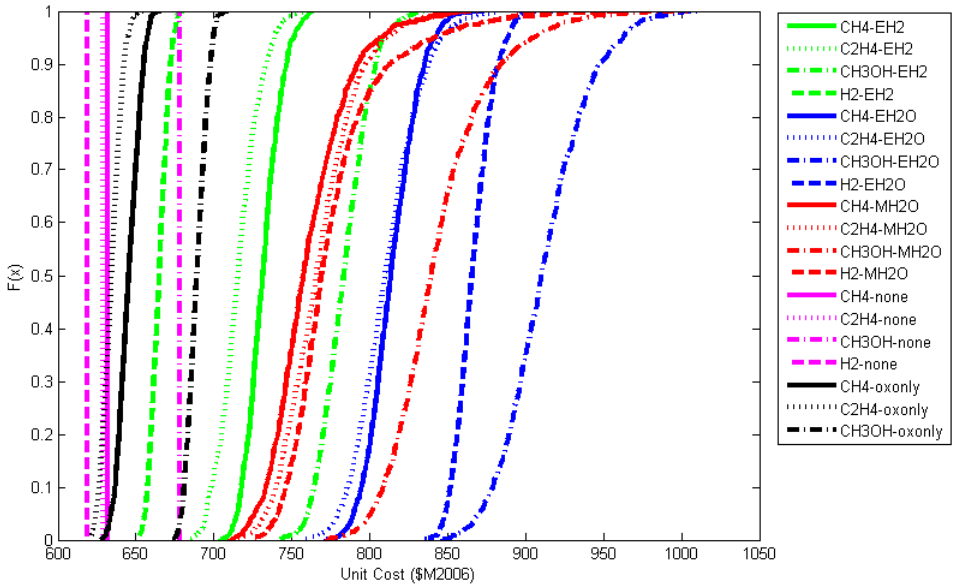

Figure 107: The unit cost of the nineteen architectures with low launch costs and low specific mass power system.

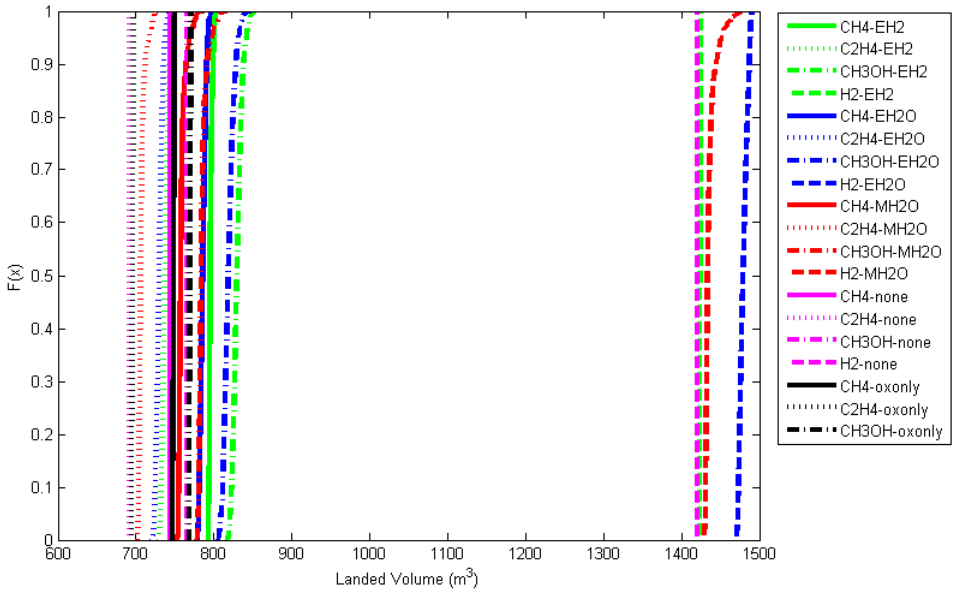

Figure 108: The landed volume (ISPP system, surface power system, and MAV) of the nineteen architectures with low launch costs and low specific mass power system.

and MAV are used in the sizing of the MDV and MTV, there is no check that the volumes can be built and launched aboard a particular launch vehicle from Earth. Thus, the effects of the high volume of the hydrogen fuel architectures is not fully quantified, and the figure of merit may underestimate the costs needed to develop and support such high volume systems. The landed volumes for the nineteen architectures are shown in Figure 108.

4.4.2 The Impact of Low Launch Cost and High Specific Mass Power System on ISPP

The second scenario considers the impact of a scenario that would be most unfavorable to ISPP: both low launch costs that reduce the value of saving mass, and high mass power systems that reduce the mass savings and increase the technology development requirements. As before, a one thousand run Monte Carlo, using the distributions described above, was used to generate CDFs of multiple metrics, including the figure of merit of this research (the net present value of the life cycle cost of the architecture).

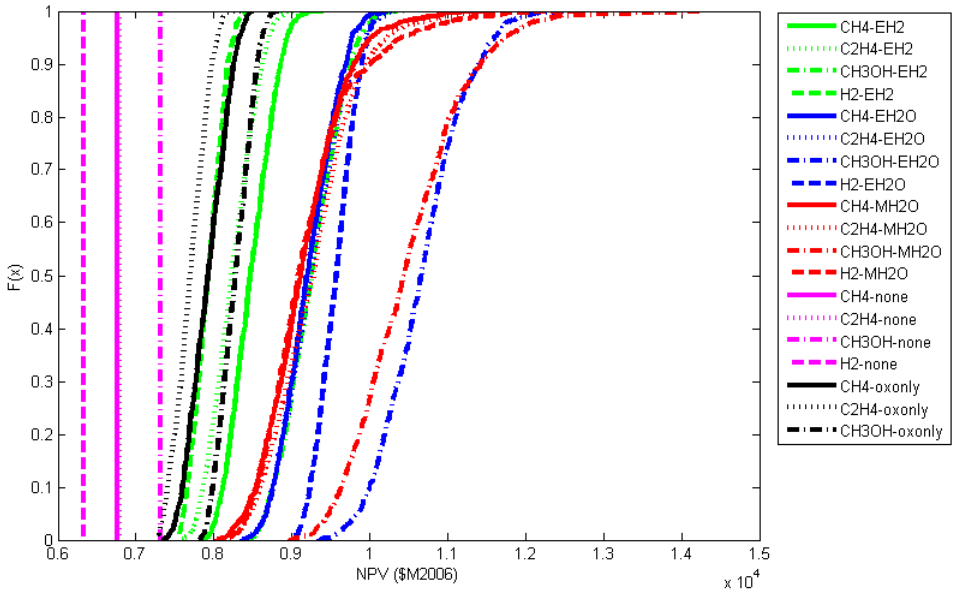

Figure 109: The net present value of the life cycle cost of the nineteen architectures with low launch costs and high specific mass power system.

The relative robustness integrals of the nineteen architectures were computed for the figure of merit to identify the preferred architecture.

Figure 109 illustrates the CDFs of the nineteen architectures for the net present value of the life cycle cost. The form of each line corresponds to the fuel type (solid for methane, small dash for ethylene, small and large dash for methanol, and large dash for hydrogen), and the color corresponds to the type of ISPP approach (green for hydrogen supplied from Earth, blue for water supplied from Earth, red for water acquired at Mars, magenta for no ISPP, and black for only oxygen ISPP). Table 60 gives the means and standard deviations of several figures of merit of each architecture.

In this scenario, all the ISPP architectures are dominated by the non-ISPP architectures. The best ISPP architecture is ethylene with only oxygen ISPP, followed by methane with only oxygen ISPP and hydrogen with only oxygen ISPP. As expected in a scenario unfavorable to ISPP, the architectures are ordered by the relative robustness integral according to the degree of ISPP used (the least expensive having no

Table 60: Mean ± Standard Deviation of Figures of Merit for Scenario 2 (Low Launch Costs and High Specific Mass Power System)

Architecture	IMLEO (t)	ISPP Power (kWe)	NPV of LCC ($M2006)
CH4-EH2	157 ± 2	42 ± 2	8488 ± 285
C2H4-EH2	149 ± 3	38 ± 3	8233 ± 273
CH3OH-EH2	173 ± 4	51 ± 4	9266 ± 377
H2-EH2	164 ± 1	29 ± 1	7916 ± 197
CH4-EH2O	222 ± 5	47 ± 3	9227 ± 341
C2H4-EH2O	212 ± 9	50 ± 4	9273 ± 400
CH3OH-EH2O	263 ± 13	67 ± 6	10677 ± 537
H2-EH2O	281 ± 3	34 ± 3	9557 ± 251
CH4-MH2O	161 ± 7	62 ± 8	9148 ± 557
C2H4-MH2O	160 ± 7	64 ± 7	9272 ± 541
CH3OH-MH2O	186 ± 10	84 ± 11	10524 ± 778
H2-MH2O	183 ± 11	54 ± 12	9234 ± 697
CH4-none	196 ± 0	0 ± 0	6768 ± 0
C2H4-none	195 ± 0	0 ± 0	6799 ± 0
CH3OH-none	225 ± 0	0 ± 0	7325 ± 0
H2-none	175 ± 0	0 ± 0	6332 ± 0
CH4-oxonly	158 ± 1	38 ± 2	7913 ± 249
C2H4-oxonly	158 ± 1	31 ± 2	7678 ± 220
CH3OH-oxonly	188 ± 1	32 ± 2	8255 ± 213

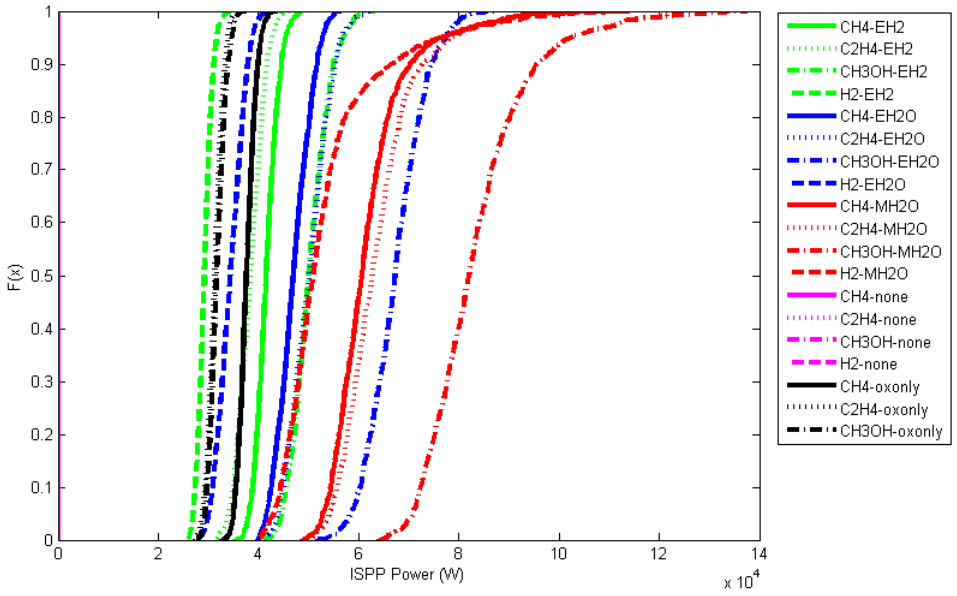

Figure 110: The ISPP power of the nineteen architectures with low launch costs and high specific mass power system.

Table 61: Propellant Requirements by Fuel Type

Name	CH_4	C_2H_4	CH_3OH	H_2
Fuel	11509 kg	15028 kg	24630 kg	5098 kg
Oxidizer	34525 kg	31558 kg	32018 kg	22433 kg
Total	46034 kg	46586 kg	56648 kg	27531 kg

ISPP, the most expensive requiring the largest ISPP systems). In this scenario, the two worst architectures are those based on methanol fuel (excepting the non-ISPP methanol architecture). This results from the high power needs of the methanol architectures, shown in Figure 110. This power need, in turn, is a function of the high quantity of propellant required, because the specific impulse is the lowest of the four fuel types; see Table 61. Additionally, the large quantity of fuel required relative to oxygen (due to the low O/F ratio) leads to larger ISPP systems relative to the other fuel types.

Figure 111 shows the relative robustness integrals, normalized such that the best

scoring architecture (hydrogen with no ISPP) has a score of 1 and the worst scoring architecture (methanol from Earth water) has a score of 0. The four non-ISPP architectures again are ahead of the ISPP architectures. Of the ISPP architectures, those using only oxygen ISPP are some of the better options. The DRA 5.0 like option (methane with oxygen only) finishes as the sixth best of the nineteen architectures, as it is a partial ISPP approach and thus is less expensive than any full ISPP approach. Additionally, the architectures using Mars water perform poorly due to the high power demands shown in Figure 110. The architectures using Earth water perform poorly due to the much larger and more power intensive water electrolyzers required (driving up DDT&E costs of both the ISPP systems and the power system); see Appendix B for the greater masses and powers of the water electrolyzers for those architectures. Additionally, the Earth water approaches are penalized for the impact of the larger ISPP and power systems on the in-space transportation. The preference ordering and the relative spacing are consistent across multiple runs of the same scenario.

4.4.3 The Impact of High Launch Cost and Low Specific Mass Power System on ISPP

The third scenario considers the impact of a scenario that would be most favorable to ISPP: high launch costs that increase the value of saving mass, and low mass power systems that facilitate meeting the requirements for ISPP. Again, a one thousand run Monte Carlo, using the distributions described above, was used to generate CDFs of multiple metrics, including the figure of merit of this research (the net present value of the life cycle cost of the architecture). The relative robustness integrals of the nineteen architectures were computed for the figure of merit to identify the preferred architecture.

Figure 112 illustrates the CDFs of the nineteen architectures for the net present value of the life cycle cost. The form of each line corresponds to the fuel type (solid

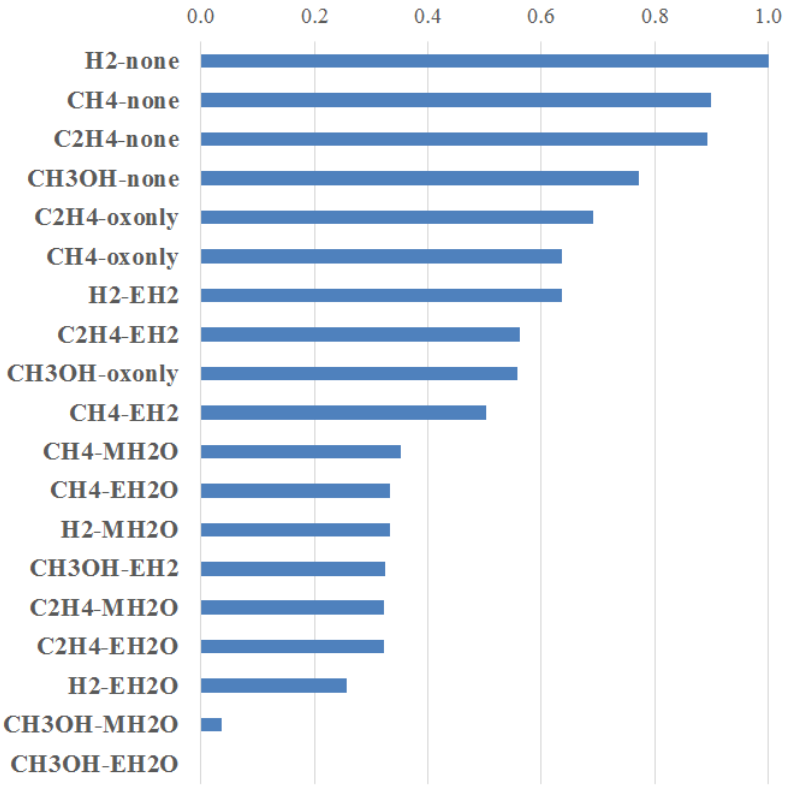

Figure 111: Relative robustness integrals of the net present value of the life cycle cost of the nineteen architectures with low launch costs and high specific mass power system.

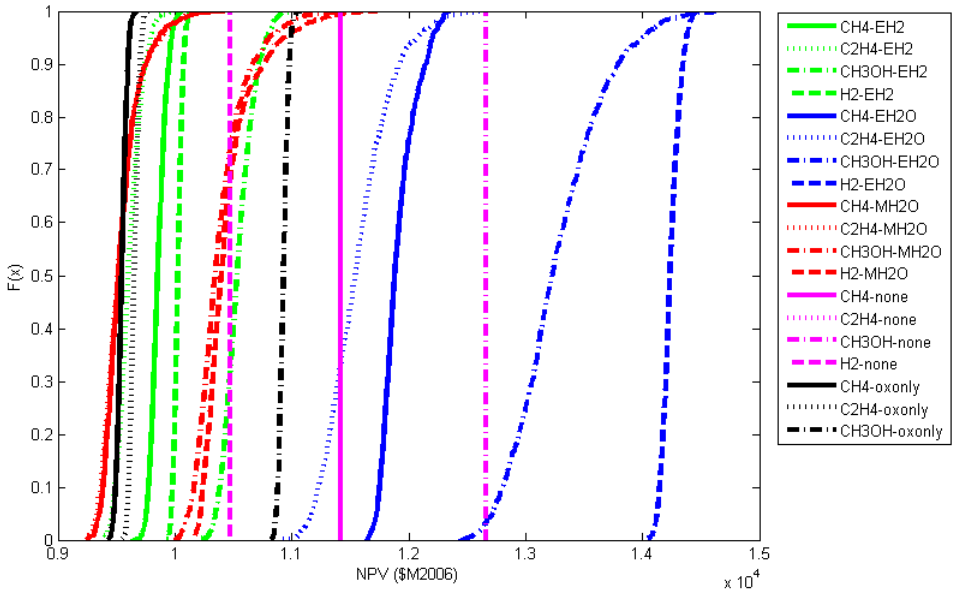

Figure 112: The net present value of the life cycle cost of the nineteen architectures with high launch costs and high specific mass power system.

for methane, small dash for ethylene, small and large dash for methanol, and large dash for hydrogen), and the color corresponds to the type of ISPP approach (green for hydrogen supplied from Earth, blue for water supplied from Earth, red for water acquired at Mars, magenta for no ISPP, and black for only oxygen ISPP). Table 62 gives the means and standard deviations of several figures of merit of each architecture.

The ethylene and methane ISPP architectures that do not use Earth water are the top performing architectures. These six architectures are among the seven with the least IMLEO (see Figure 114 and Table 62), as two of them require only hardware from Earth, while the other four require some of the smallest masses of fluids brought from Earth (either in liquid hydrogen to support full ISPP, or in the form of fuel already brought with the lander), as shown in Figure 113. With the launch cost per IMLEO set at $30000/kg, the architecture launch costs (Figure 115) are of a similar order to the DDT&E costs (Figure 116). Thus, low IMLEO has a significant impact on the life cycle cost.

Table 62: Mean ± Standard Deviation of Figures of Merit for Scenario 3 (High Launch Costs and High Specific Mass Power System)

Architecture	IMLEO (t)	ISPP Power (kWe)	NPV of LCC ($M2006)
CH4-EH2	127 ± 1	42 ± 2	9857 ± 67
C2H4-EH2	121 ± 2	38 ± 3	9608 ± 94
CH3OH-EH2	137 ± 2	51 ± 4	10557 ± 129
H2-EH2	140 ± 1	29 ± 1	10029 ± 37
CH4-EH2O	189 ± 3	47 ± 3	11912 ± 140
C2H4-EH2O	177 ± 7	50 ± 4	11559 ± 288
CH3OH-EH2O	216 ± 10	67 ± 6	13297 ± 387
H2-EH2O	253 ± 1	34 ± 3	14244 ± 76
CH4-MH2O	119 ± 3	62 ± 8	9554 ± 171
C2H4-MH2O	116 ± 2	63 ± 7	9524 ± 152
CH3OH-MH2O	129 ± 3	84 ± 11	10381 ± 215
H2-MH2O	143 ± 4	54 ± 11	10460 ± 238
CH4-none	196 ± 0	0 ± 0	11415 ± 0
C2H4-none	195 ± 0	0 ± 0	11419 ± 0
CH3OH-none	225 ± 0	0 ± 0	12664 ± 0
H2-none	175 ± 0	0 ± 0	10473 ± 0
CH4-oxonly	131 ± 1	38 ± 2	9543 ± 42
C2H4-oxonly	134 ± 1	31 ± 2	9651 ± 37
CH3OH-oxonly	164 ± 1	32 ± 2	10930 ± 39

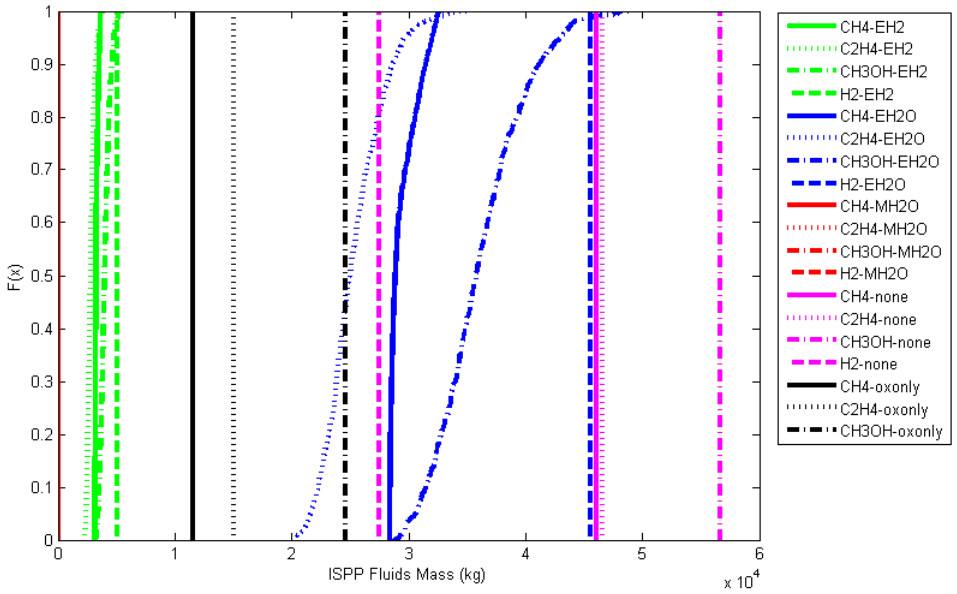

Figure 113: The fluids mass brought from Earth (either feedstock or propellant) of the nineteen architectures with high launch costs and low specific mass power system.

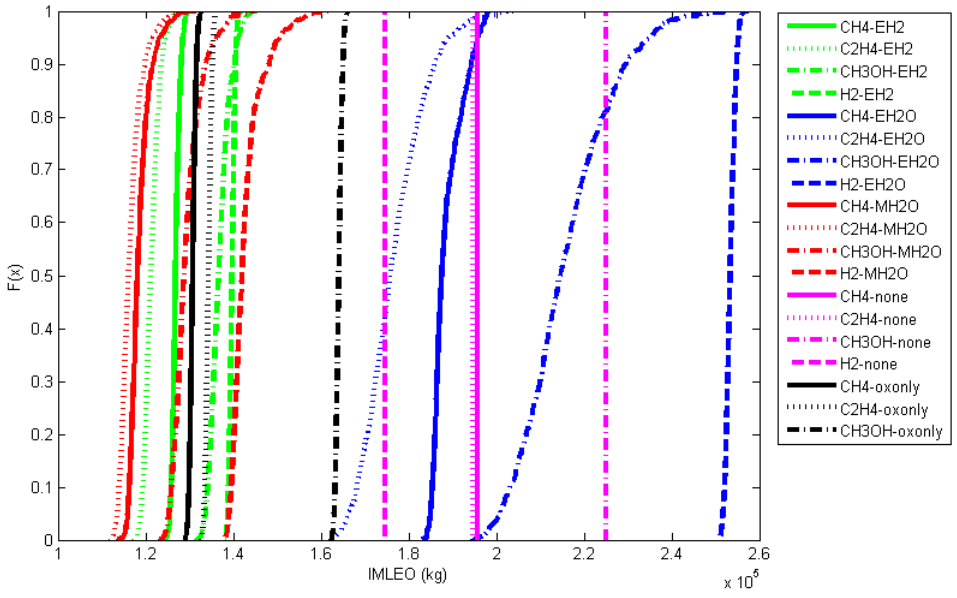

Figure 114: The initial mass in low Earth orbit of the nineteen architectures with high launch costs and low specific mass power system.

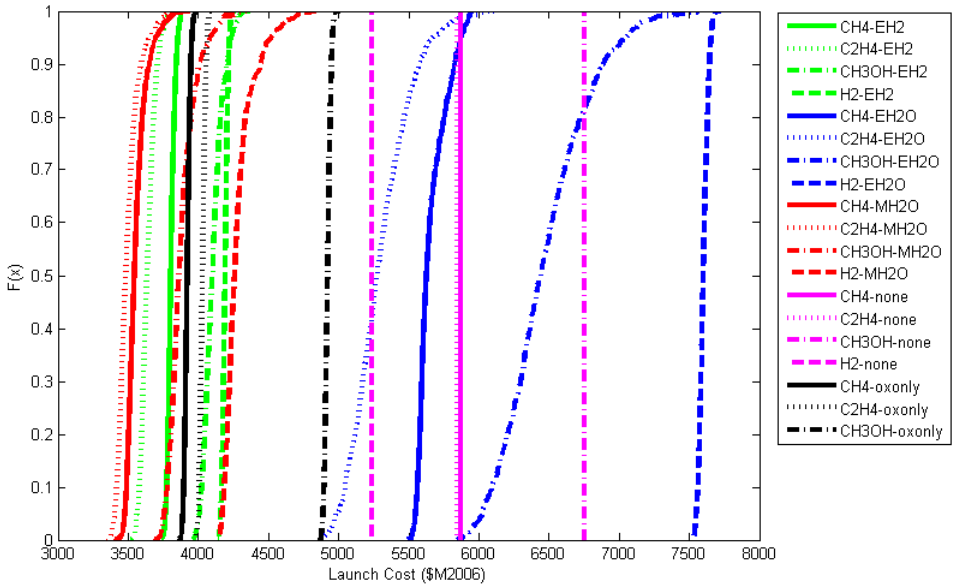

Figure 115: The launch cost of the nineteen architectures with high launch costs and low specific mass power system.

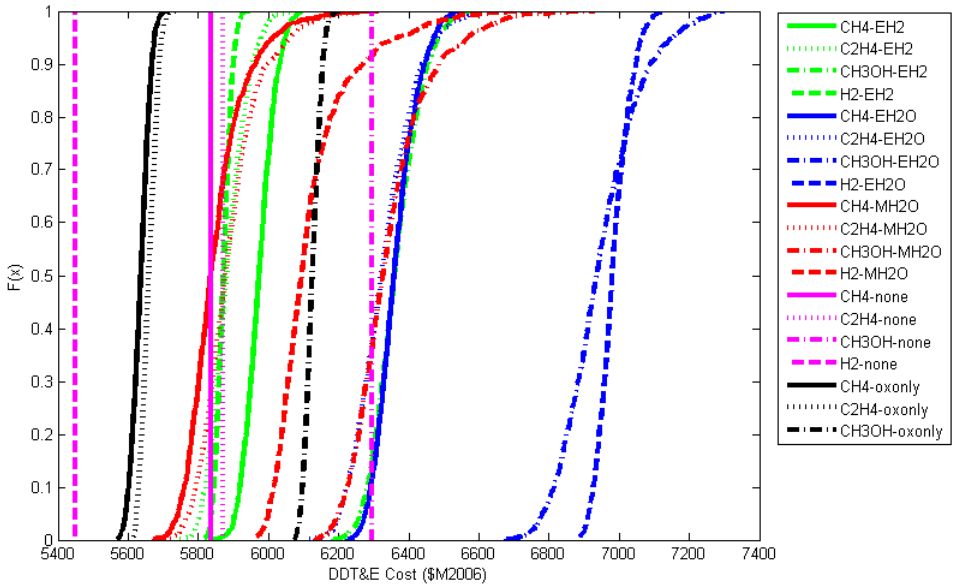

Figure 116: The DDT&E cost of the nineteen architectures with high launch costs and low specific mass power system.

Figure 117 shows the relative robustness integrals, normalized such that the best scoring architecture (ethylene with Mars water) has a score of 1 and the worst scoring architecture (hydrogen from Earth water) has a score of 0. With low IMLEO at a premium in this scenario, options that involve bringing no fluids (i.e. using Mars water) or hydrogen from Earth perform well, with only the methanol with Earth hydrogen architecture falling in the lower half. The high IMLEO approaches using ISPP, which bring Earth water, populate the lowest portion of the graph, including two of the consistently worst options, methanol with Earth water and hydrogen with Earth water. The DRA 5.0 like option (methane with oxygen only) finishes second of the nineteen architectures; as in the first scenario, the balance of mass reduction due to ISPP and limited ISPP requirements lead to its low cost relative to other ISPP approaches. This preference ordering and the relative spacing are consistent across multiple runs of the same scenario.

4.4.4 The Impact of High Launch Cost and High Specific Mass Power System on ISPP

The fourth scenario considers the impact high launch costs that increase the value of saving mass, and inefficient, high mass power systems that reward lower power approaches. Once more, a one thousand run Monte Carlo simulation, using the distributions described above, was used to generate CDFs of multiple metrics, including the figure of merit of this research (the net present value of the life cycle cost of the architecture). The relative robustness integrals of the nineteen architectures were computed for the figure of merit to identify the preferred architecture.

Figure 118 illustrates the CDFs of the nineteen architectures for the net present value of the life cycle cost. The form of each line corresponds to the fuel type (solid for methane, small dash for ethylene, small and large dash for methanol, and large dash for hydrogen), and the color corresponds to the type of ISPP approach (green for

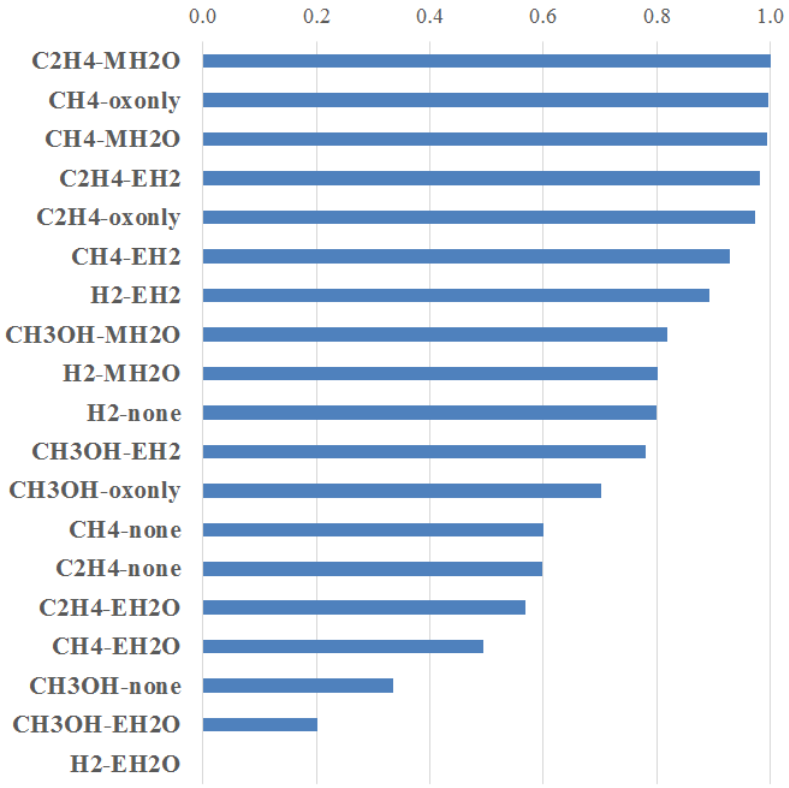

Figure 117: Relative robustness integrals of the net present value of the life cycle cost of the nineteen architectures with high launch costs and low specific mass power system.

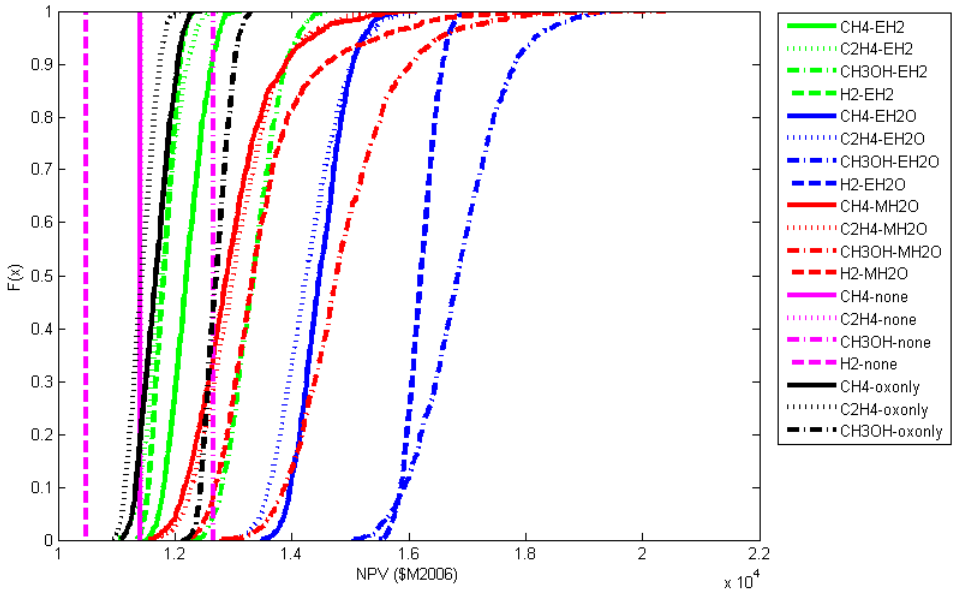

Figure 118: The net present value of the life cycle cost of the nineteen architectures with high launch costs and high specific mass power system.

hydrogen supplied from Earth, blue for water supplied from Earth, red for water acquired at Mars, magenta for no ISPP, and black for only oxygen ISPP). Table 63 gives the means and standard deviations of several figures of merit of each architecture.

In this scenario, three architectures that use no ISPP perform the best; methanol is absent due to its large initial mass being penalized by the high launch costs. Three partial ISPP approaches, using ethylene, methane, and hydrogen, are the best ISPP options. These are followed by the ethylene and methane with Earth hydrogen architectures. As in the previous scenario, the high launch costs (Figure 120) are comparable to the DDT&E costs (Figure 121), although the launch costs are generally less than the DDT&E costs given the high specific mass of the power system. Thus, this scenario rewards architectures that balance minimizing mass with minimizing power required on the ISPP system; this is why the Mars water approaches are more expensive than their corresponding Earth hydrogen approaches.

Figure 119 shows the relative robustness integrals, normalized such that the best

Table 63: Mean ± Standard Deviation of Figures of Merit for Scenario 4 (High Launch Costs and High Specific Mass Power System)

Architecture	IMLEO (t)	ISPP Power (kWe)	NPV of LCC ($M2006)
CH4-EH2	157 ± 2	42 ± 2	12230 ± 300
C2H4-EH2	149 ± 3	38 ± 3	11811 ± 322
CH3OH-EH2	172 ± 4	50 ± 4	13340 ± 445
H2-EH2	164 ± 1	29 ± 1	11805 ± 212
CH4-EH2O	222 ± 5	47 ± 3	14473 ± 409
C2H4-EH2O	211 ± 9	50 ± 4	14270 ± 536
CH3OH-EH2O	262 ± 12	67 ± 6	16855 ± 729
H2-EH2O	281 ± 3	34 ± 3	16213 ± 290
CH4-MH2O	161 ± 8	62 ± 8	12990 ± 738
C2H4-MH2O	160 ± 7	64 ± 8	13077 ± 689
CH3OH-MH2O	185 ± 10	84 ± 11	14912 ± 919
H2-MH2O	183 ± 11	54 ± 11	13534 ± 842
CH4-none	196 ± 0	0 ± 0	11415 ± 0
C2H4-none	195 ± 0	0 ± 0	11419 ± 0
CH3OH-none	225 ± 0	0 ± 0	12664 ± 0
H2-none	175 ± 0	0 ± 0	10473 ± 0
CH4-oxonly	158 ± 2	38 ± 2	11674 ± 254
C2H4-oxonly	158 ± 1	31 ± 2	11442 ± 229
CH3OH-oxonly	188 ± 1	32 ± 2	12710 ± 228

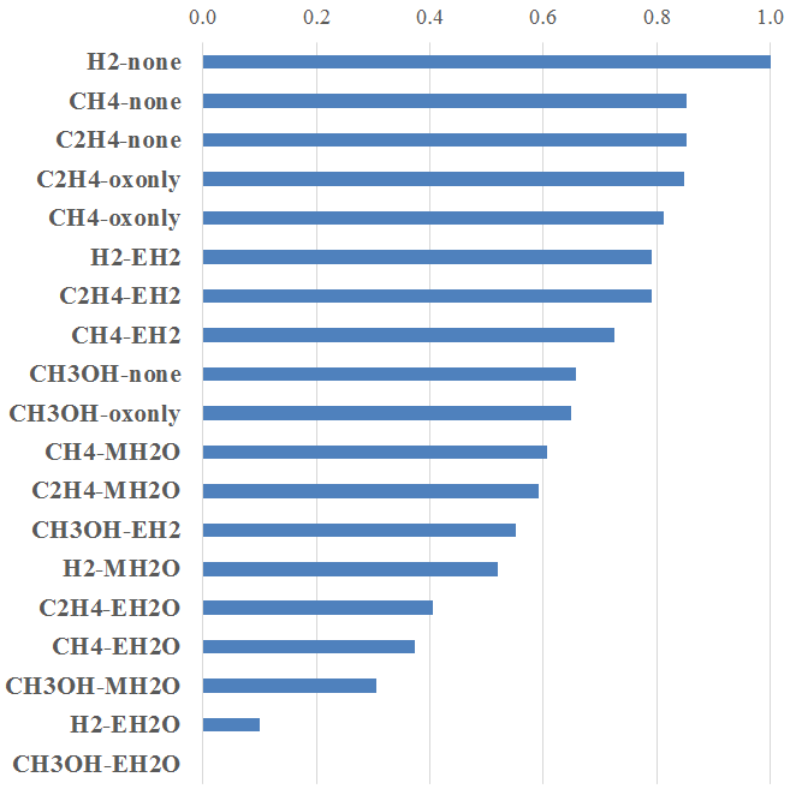

Figure 119: Relative robustness integrals of the net present value of the life cycle cost of the nineteen architectures with high launch costs and high specific mass power system.

scoring architecture (hydrogen with no ISPP) has a score of 1 and the worst scoring architecture (methanol with Earth water) has a score of 0. The DRA 5.0 like option (methane with oxygen only) finishes in the middle of the nineteen architectures, as it has the highest power requirement of the partial ISPP approaches, which is penalized via the more massive and expensive power system and in-space transportation. This preference ordering and the relative spacing are consistent across multiple runs of the same scenario.

4.4.5 Mars Ascent Vehicle—In Situ Propellant Production

The fifth scenario applies uniform distributions to both the launch cost (varying between \$2500/kg and \$30000/kg) and specific mass (varying between 23 kg/kWe and 266 kg/kWe) to explore the interior trade space between the four "corners"

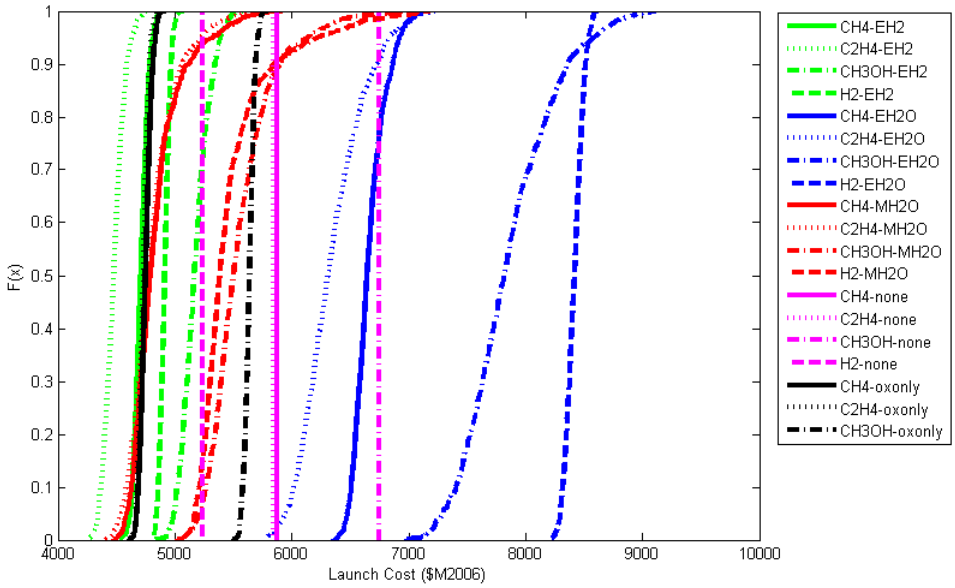

Figure 120: The launch cost of the nineteen architectures with high launch costs and high specific mass power system.

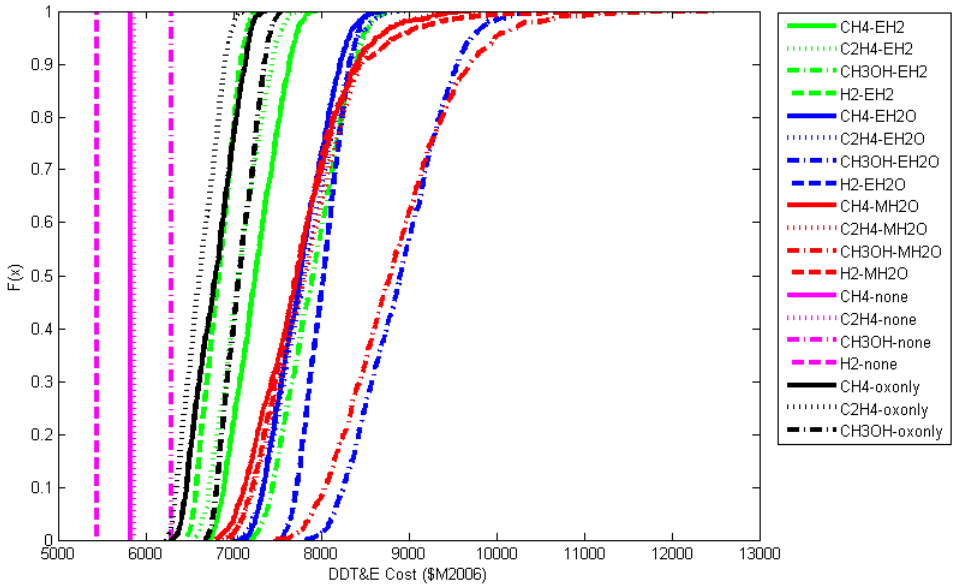

Figure 121: The DDT&E cost of the nineteen architectures with high launch costs and high specific mass power system.

considered in the scenarios above. Having considered the bounding cases previously to understand the performance of the nineteen architectures at those extremes, it is now possible to understand how combinations of launch cost and specific mass between those points impacts a launch cost and specific mass agnostic comparison. A one thousand run Monte Carlo simulation was performed using the previous distributions on ISPP system parameters, as well as the distributions on launch cost and specific mass, to generate the CDFs of the nineteen architectures that yielded the relative robustness integrals. As in the other scenarios, the resulting preference ordering and relative spacing are consistent across multiple runs of the fifth scenario.

Figure 122 illustrates the CDFs of the nineteen architectures for the net present value of the life cycle cost. The form of each line corresponds to the fuel type (solid for methane, small dash for ethylene, small and large dash for methanol, and large dash for hydrogen), and the color corresponds to the type of ISPP approach (green for hydrogen supplied from Earth, blue for water supplied from Earth, red for water acquired at Mars, magenta for no ISPP, and black for only oxygen ISPP). Table 64 gives the means and standard deviations of several figures of merit of each architecture.

Unlike in the previous four scenarios, where only ISPP related parameters were varied across the Monte Carlo simulation, here the two architectural parameter variations yield distributions of the non-ISPP architectures (as opposed to the vertical lines seen on previous plots). As a result, the relative robustness integral plot, as shown in Figure 123, is particularly useful in distinguishing the performance of the nineteen architectures. That plot shows that the hydrogen with no ISPP architecture outperforms the ethylene architecture with only oxygen ISPP and methane with only oxygen ISPP architectures. These two architecture were the best ISPP architecture in Scenarios 1, 2, and 4, and methane with only oxygen ISPP was the second best ISPP architecture in Scenario 3. The next two ISPP architectures, ethylene with Earth hydrogen and hydrogen with only oxygen ISPP, also performed well in the previous

Table 64: Mean ± Standard Deviation of Figures of Merit for Scenario 5 (Randomly Sampled Launch Costs and Specific Mass)

Architecture	IMLEO (t)	ISPP Power (kWe)	NPV of LCC ($M2006)
CH4-EH2	143 ± 9	42 ± 2	9346 ± 1132
C2H4-EH2	136 ± 8	38 ± 3	9144 ± 1080
CH3OH-EH2	156 ± 11	50 ± 4	10200 ± 1268
H2-EH2	152 ± 7	29 ± 1	9144 ± 1128
CH4-EH2O	207 ± 10	47 ± 3	10869 ± 1643
C2H4-EH2O	194 ± 12	50 ± 4	10645 ± 1514
CH3OH-EH2O	240 ± 17	67 ± 6	12275 ± 1919
H2-EH2O	268 ± 8	34 ± 3	12083 ± 1951
CH4-MH2O	141 ± 13	62 ± 8	9640 ± 1351
C2H4-MH2O	140 ± 13	64 ± 8	9763 ± 1330
CH3OH-MH2O	158 ± 17	84 ± 11	10823 ± 1681
H2-MH2O	164 ± 13	54 ± 11	10084 ± 1439
CH4-none	196 ± 0	0 ± 0	9138 ± 1361
C2H4-none	195 ± 0	0 ± 0	9146 ± 1356
CH3OH-none	225 ± 0	0 ± 0	9999 ± 1554
H2-none	175 ± 0	0 ± 0	8406 ± 1180
CH4-oxonly	145 ± 8	38 ± 2	8987 ± 1124
C2H4-oxonly	147 ± 7	31 ± 2	8780 ± 1071
CH3OH-oxonly	177 ± 7	32 ± 2	9754 ± 1290

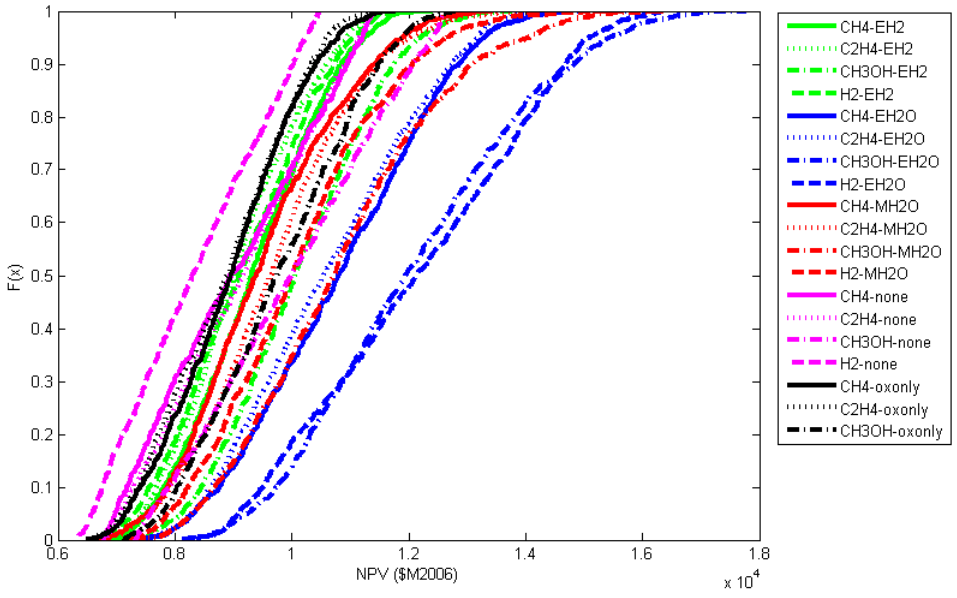

Figure 122: The net present value of the life cycle cost of the nineteen architectures with randomly sampled launch costs and specific mass.

scenarios.

Thus, all five scenarios indicated that architectures using only oxygen production (except for the methanol) are among the best performing ISPP architectures under the ranges of assumptions used in this research, and the options are competitive with, though sometimes worse performing, than the best non-ISPP architecture. This is to be expected, as the net present value of the life cycle cost is influenced by the landed mass requirements on Mars, and thus the IMLEO. However, as can be seen by examining the relative robustness integrals for IMLEO in Figure 124, the ordering of architectures is different: an analysis based solely on mass leads to a conclusion that many ISPP architectures perform better than any non-ISPP approach. The analysis on a cost basis reveals that the savings in launch costs from smaller systems do not necessarily outweigh the investments required to develop, manufacture, and operate the requisite ISPP and power systems. The DRA 5.0 like option (methane with oxygen only) finishes as the third best architecture.

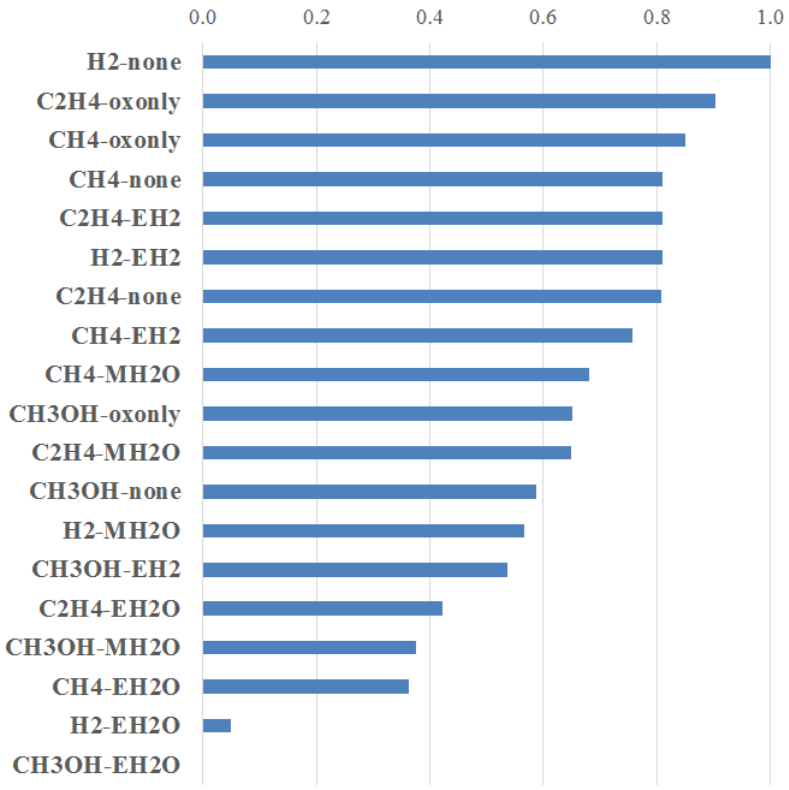

Figure 123: Relative robustness integrals of the net present value of the life cycle cost of the nineteen architectures with randomly sampled launch costs and specific mass.

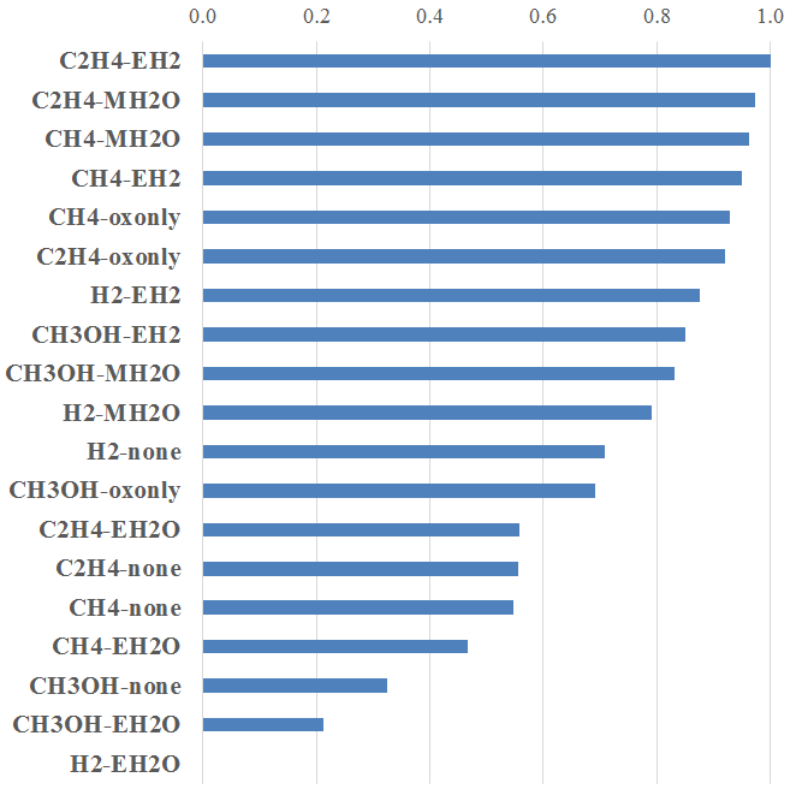

Figure 124: Relative robustness integrals of the initial mass in low Earth orbit of the nineteen architectures with randomly sampled launch costs and specific mass.

4.4.6 Comparison of Threshold Evaluation with Relative Robustness Integrals

As discussed in Section 2.5, an alternative method to assess the CDFs of each architecture is to evaluate the value of the figure of merit at particular probability thresholds. For a figure of merit that is being minimized (such as the net present value of the life cycle cost), the architecture with the lowest value of that figure of merit at a given threshold would be the preferred architecture at that threshold. For example, in Figure 122, at the 90% level, the hydrogen with no ISPP architecture (H2-none) has a net present value of the life cycle cost of 1.0 E04 $M2006, while the methanol with Earth water architecture (CH3OH-EH2O) has a net present value of the life cycle cost of 1.5 E04 $M2006.

The order of preference of architectures, and the magnitude of the differences between any two architectures, depends on the chosen threshold for evaluation. This can be seen from inspection of Figure 122, as any point where two CDFs cross indicate a change in ordering. Figure 125 shows the normalized values of each architecture's net present value of the life cycle cost evaluated at the 50%, 90%, and 95% thresholds (where a score of 1 is the lowest net present value of the life cycle cost of the nineteen architectures, while a score of 0 is the highest net present value of the life cycle cost), as well as the normalized relative robustness integral shown in Figure 123. In this plot, a horizontal line indicates an architecture that maintains the same normalized score at each threshold, as well as in the normalized relative robustness integral. Two parallel lines (or line segments) indicates two architectures that maintain a constant spacing across multiple thresholds; for example, ethylene with only oxygen (C2H4-oxonly) outperforms ethylene with Earth hydrogen (C2H4-EH2) at each threshold, and also in the relative robustness integral. Two lines that intersect indicate two architectures whose preference ordering change depending on the threshold; for example, methanol with no ISPP (CH3OH-none) slightly outperforms methanol with Earth hydrogen

(CH3OH-EH2) at the 50% threshold, underperforms at the 90% threshold, then returns to outperforming at the 95% threshold. The relative robustness integral, which evaluates the preference ordering across all thresholds, indicates that methanol with no ISPP outperforms methanol with Earth hydrogen over the range of Monte Carlo results.

Figures 126 to 129 show the comparison of threshold performance to the relative robustness integral in the previous four scenarios. In each scenario, there are intersecting lines indicating a change in preference ordering as a function of the particular threshold chosen. The relative robustness integral allows for identification of the preference ordering independent of the particular threshold.

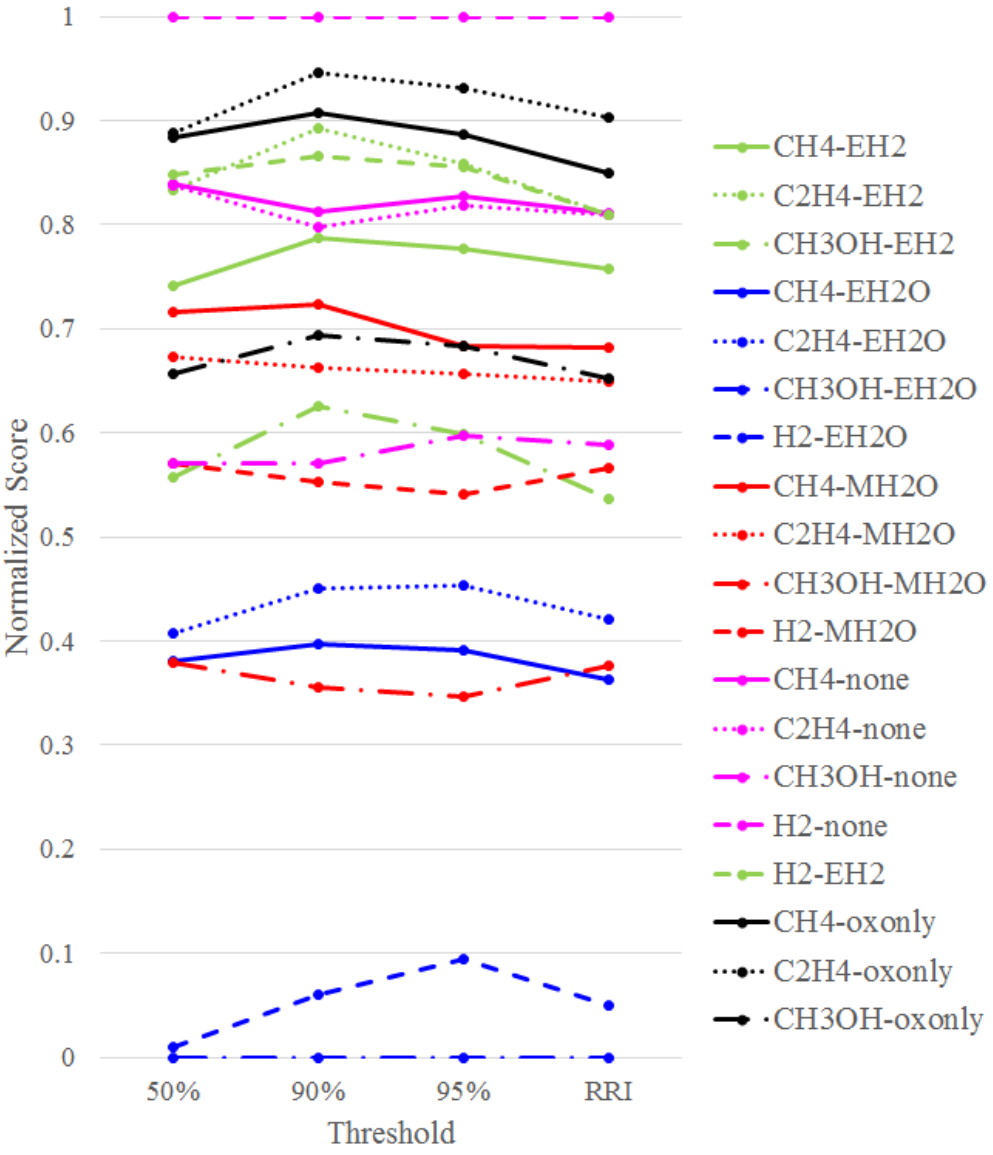

Figure 125: Normalized net present value of the life cycle cost of the nineteen architectures at the 50%, 90%, and 95% thresholds, as well as normalized relative robustness integrals, for Scenario 5.

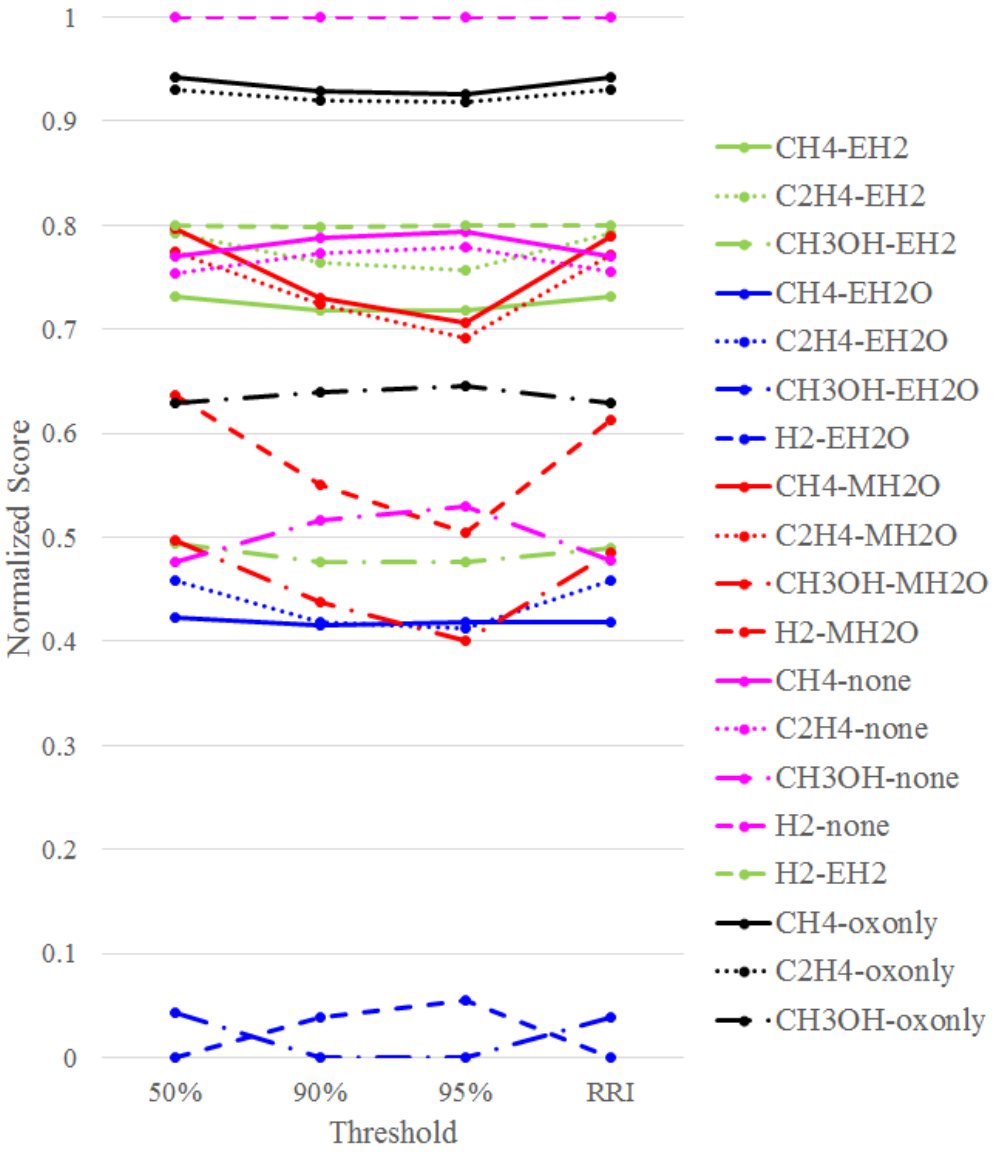

Figure 126: Normalized net present value of the life cycle cost of the nineteen architectures at the 50%, 90%, and 95% thresholds, as well as normalized relative robustness integrals, for Scenario 1 (low launch costs and low specific mass power system).

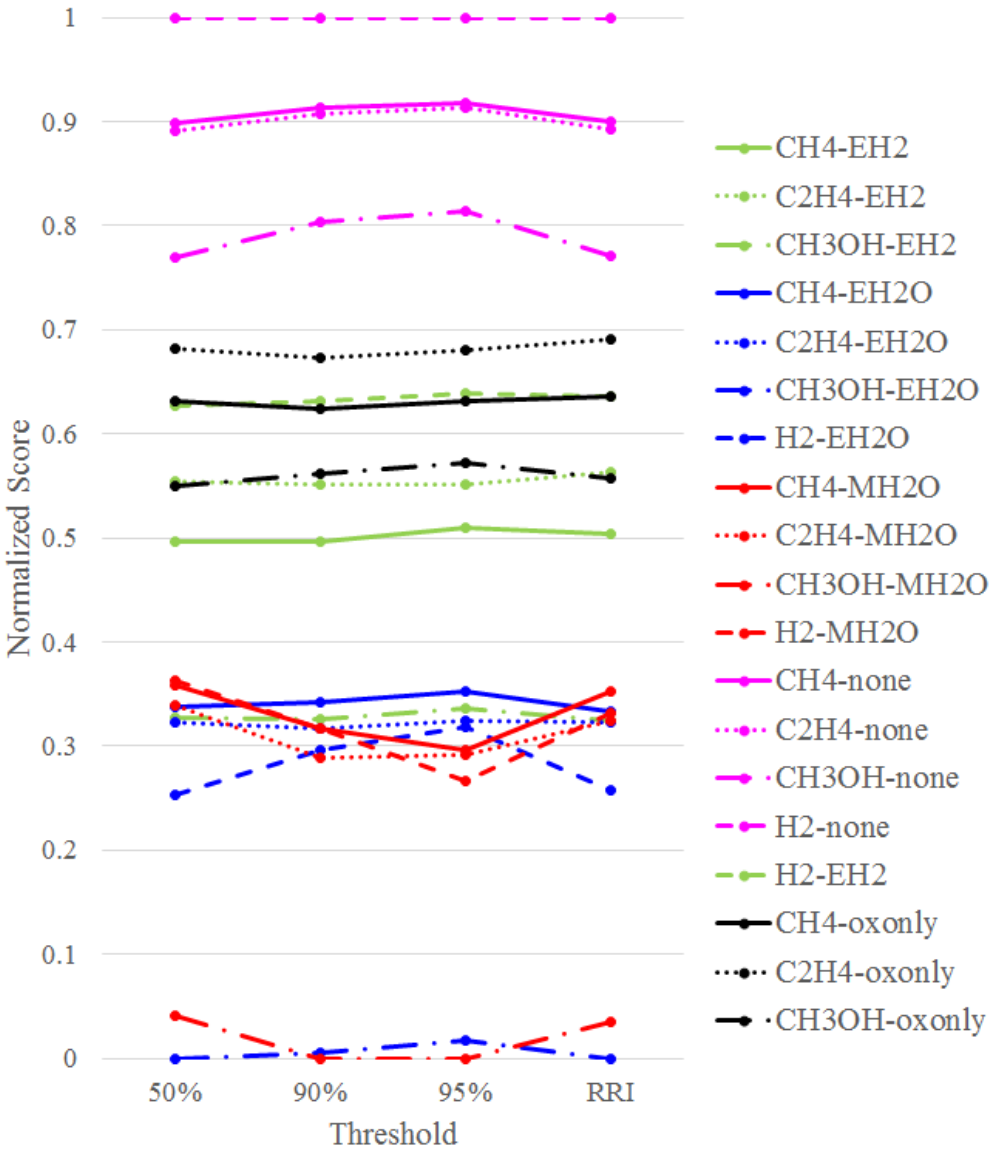

Figure 127: Normalized net present value of the life cycle cost of the nineteen architectures at the 50%, 90%, and 95% thresholds, as well as normalized relative robustness integrals, for Scenario 2 (low launch costs and high specific mass power system).

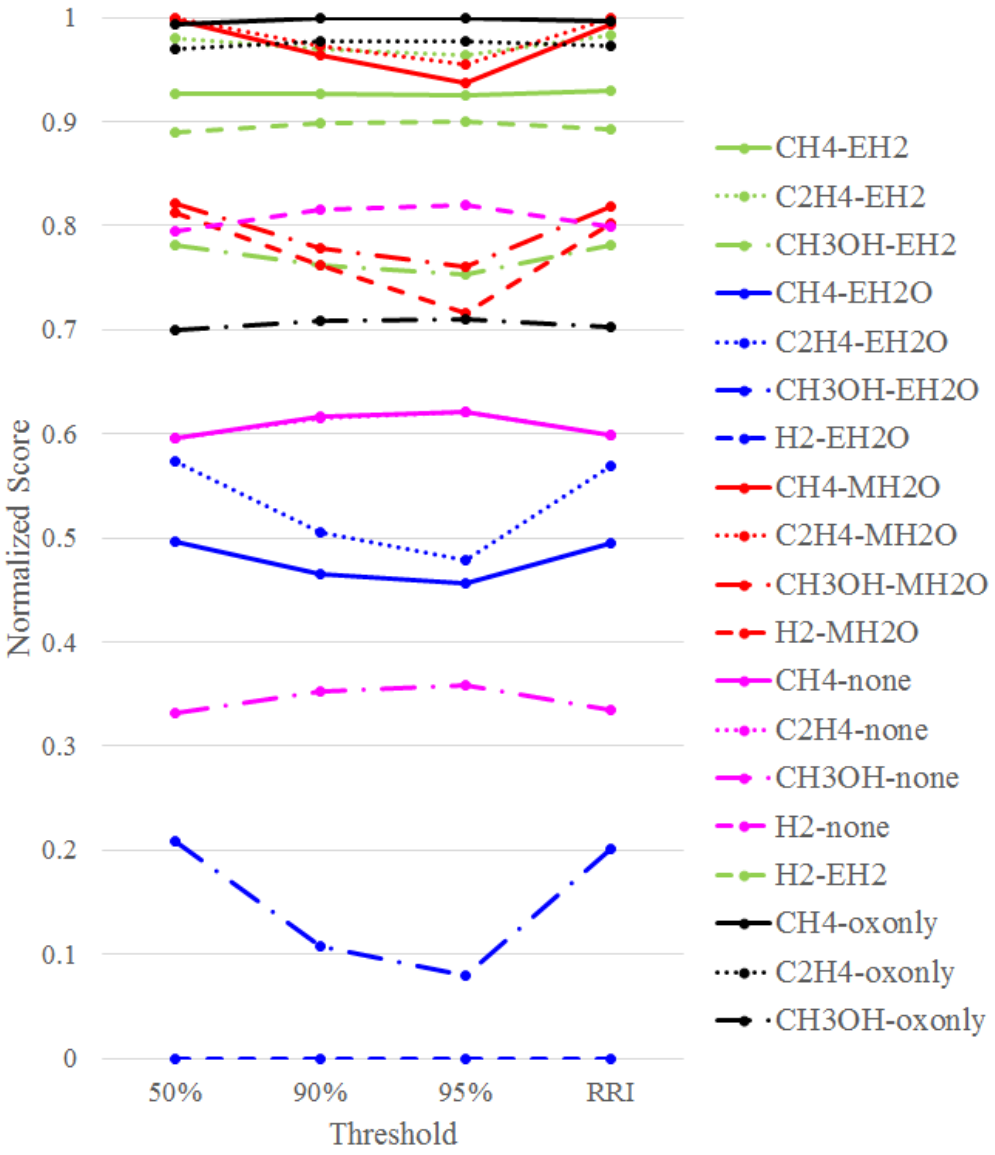

Figure 128: Normalized net present value of the life cycle cost of the nineteen architectures at the 50%, 90%, and 95% thresholds, as well as normalized relative robustness integrals, for Scenario 3 (high launch costs and low specific mass power system).

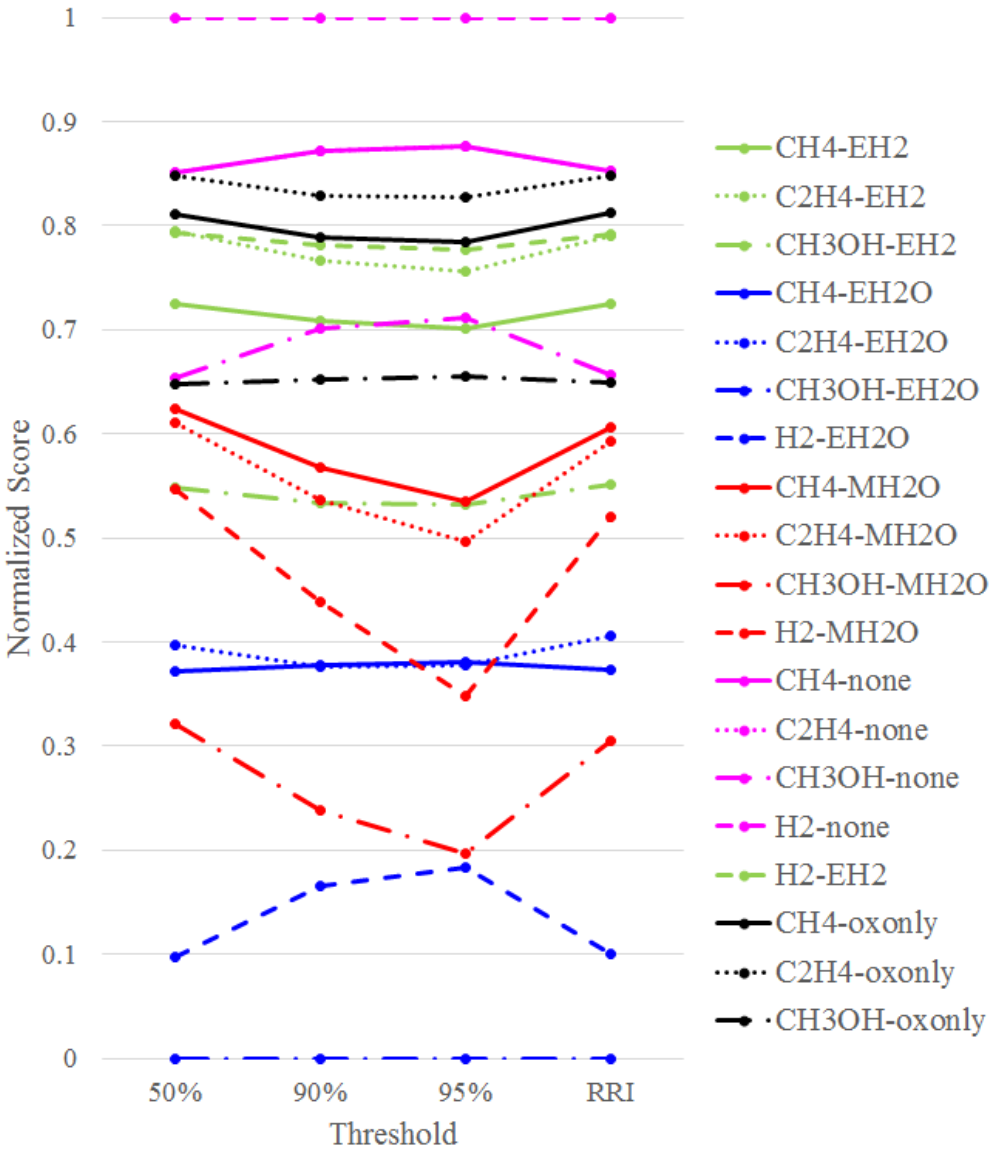

Figure 129: Normalized net present value of the life cycle cost of the nineteen architectures at the 50%, 90%, and 95% thresholds, as well as normalized relative robustness integrals, for Scenario 4 (high launch costs and high specific mass power system).

CHAPTER V

CONCLUSIONS AND FUTURE WORK

5.1 Conclusions

Making decisions on the best selection of systems and technologies for future missions is a challenging task, and the inherent uncertainty in evaluating architectures that do not yet physically exist increases the difficulty. The research described here offers a method for modeling and analyzing multiple competing mission architectures to support decision makers in understanding what technologies could be enabling for future Mars missions. Within the limitations of the techniques used and under the performance and cost assumptions in the model, several trends emerge.

Previous literature has shown the value of ISPP for a Mars Ascent Vehicle from a mass basis; in this evaluation, a non-ISPP option emerged as the best architecture on a cost basis under a scenario with variable launch cost and power system mass. Although ISPP generally reduces the mass that must be landed on Mars, and thus that must be launched from Earth, the requisite costs to implement ISPP may outweigh the savings realized from fewer launches. This trend is most clear in scenarios that are particular unfavorable a priori to ISPP: those with low launch costs and high technology requirements for the ISPP and supporting systems. In circumstances that would be expected to be favorable for ISPP (high launch cost and highly efficient surface power systems), nine ISPP architectures are superior to the modeled non-ISPP approaches.

The performance on the power system is highly influential in determining the relative value of ISPP and non-ISPP options. At low specific powers corresponding to

efficient power systems, ISPP options are competitive with non-ISPP options, particularly when launch costs are high. However, as power becomes less mass efficient, even the best full ISPP options are more expensive than non-ISPP options due to the large investment required in the power system, and the associated impact on larger, more expensive transportation systems. Thus, the value of ISPP is strongly tied to the capabilities of the surface power system that powers it.

Launch costs are also significant contributors to the value of ISPP. The relative robustness integrals show that when launch costs are much less than development costs, only partial ISPP approaches are competitive on a cost basis to non-ISPP approaches. However, high launch costs, especially in conjunction with efficient power, lead to ISPP options being preferred. Previous studies have assumed this effect to justify the use of ISPP. As launch costs from commercial competition decrease, the benefit of ISPP from a cost perspective will not trade well with a non-ISPP approach, under the assumptions of this research.

Architectures that utilize Martian water to provide the hydrogen for fuel production show promise in the scenarios with highly efficient surface power systems. Of critical importance to these architectures is the water concentration in the regolith. This drives the power requirements of those architectures, which becomes significant as the launch costs and power system specific mass increase. These architectures have their costs driven by the power system requirements and the multiple technologies required to enable them. Given the sensitivity of these architectures to the concentration of water available, the selection of a site with easy and copious access to water is enabling to ISPP.

Every proposed ISPP architecture relies on electrolysis, whether of water, carbon dioxide, or both. The performance of those electrolyzers, especially their power requirements, contribute to the power requirements of each architecture, which has a

significant impact on the net present value of the life cycle cost. Thus, the development of high efficiency electrolyzers is enabling to all forms of ISPP.

Additionally, the efficiency of recovering hydrogen after water electrolysis, and the efficiency of converting hydrogen to fuel, affect the quantity of hydrogen required from either Earth or water input into the system. Given the volumetric and thermal requirements for transporting hydrogen, and the power requirements for creating it via water electrolysis, minimizing the excess hydrogen required due to losses is enabling to those ISPP architectures that create fuel.

In these scenarios, approaches that performed partial ISPP often outperformed their counterparts that performed full ISPP. Given the initial investments required in systems and technology to perform any ISPP (e.g. surface nuclear power, cryogenic liquefaction, electrolysis), the additional systems that enable fuel and oxidizer production, and the growth in the initial systems to accommodate fuel production require more investment than the savings achieved by further reducing landed mass, and thus IMLEO.

Architectures that use water brought from Earth performed worse than corresponding architectures with any other approach. The combination of high initial mass and investments in ISPP technology yield poor performance that, in this model, overcomes the benefits in avoiding the transportation of liquid hydrogen or not developing Mars water acquisition.

Ethylene and hydrogen are the two most promising fuels considered, particularly in conjunction with approaches that produce both fuel and oxidizer in-situ. Ethylene provides similar specific impulse to methane, without requiring the same degree of thermal management. Hydrogen provides more specific impulse than the other three fuels (in this research, 100 more seconds than the next best, methane), yielding the lowest propellant requirements for either ISPP or delivery from Earth. Both propellants, however, have challenges deserving of further exploration: the design and

operation of an ethylene engine requires detailed analysis to verify that a real system could be built, and the volumetric requirements for storing hydrogen may yield ascent vehicles, even empty ones, larger than can be launched within current and proposed launch vehicle shrouds. Methane is also promising in some architectures, but very sensitive to the temperature of the reaction; thus, precise temperature monitoring and control are required for peak performance. Methanol had poor performance among all of the scenarios, excepting for the non-ISPP approach in scenarios that did not favor any ISPP; even there it is the lowest performing fuel. The lower specific impulse of methanol, resulting in greater propellant production and larger vehicles, yields higher costs than similar architectures with other fuels.

Of the ISPP approaches considered in this research, three performed well across all five scenarios: ethylene with only oxygen ISPP, ethylene with hydrogen from Earth, and methane with only oxygen. In the fifth scenario, which considered the ISPP architectures across wide ranges of launch cost and power system specific mass, ethylene with only oxygen ISPP was found to be the best ISPP approach. This conclusion depends on the assumptions made in the modeling and analysis of these approaches.

5.2 Future Work

Based on the results of this research, several areas of further study have been identified. Although the approach described and applied within this research advances the state of the art by evaluating in-situ propellant production on a cost basis rather than a strictly mass basis, several other key factors are omitted: the impact of technical risk on the development of ISPP systems, the reliabilities of autonomous resource collection and processing systems as compared with autonomous propellant storage systems, the potential positive and negative impacts to crew safety of having available

and relying upon in-situ resource utilization technologies, and the challenges associated with maintainability of the considered options. In addition, the architecture modeling, risk and reliability modeling, and modeling of ISRU and power systems are areas for future study.

5.2.1 Epistemic Uncertainty Modeling

Two key assumptions of epistemic uncertainty modeling in this research merit further analysis. Uniform distributions are assumed to be adequate to allow a relative comparison of different architectures. While this allows for stochastic modeling when little information is available on certain parameters, future research and development of in-situ propellant production systems will lead to more refined estimates of the values of these parameters. This will allow for the use of other distributions, which in turn may impact the resulting values of the figures of merit.

Due to the large number of parameters, combinatorial analysis of the parameter intervals was discarded, and instead sampling of each parameter was used to model its epistemic uncertainty. This approach neglects the possibility of extreme values of figures of merit when multiple parameters are at their respective limits. This research assumes that the omitting of extreme values did not impact the relative comparison of architectures. Future research would explore the impact of that assumption on the resulting ranges of figures of merit and robustness integral evaluations. One possible technique would be to use the extreme values of the parameters identified in this research as most impactful on the figures of merit; this would limit the expansion of computations required while further exploring the impact of variables previously identified as significant to the results of the model.

5.2.2 Architectural Modeling

The surface power system is a significant contributor, both on the bases of mass and cost, to an ISPP approach. As such, more detailed modeling of the mass, volume, and

cost of the system as a function of varying power demands is critical to fully understanding the ISPP trade. This research assumes a linear relationship between power required and power system mass and cost, with the specific power identified as a key parameter. If future detailed analysis finds a sub-linear trend (that is, power system mass and cost increases at a less-than-linear rate with power required), the high power ISPP approaches will trade better with lower power approaches; conversely, a super-linear trend (where power system mass and cost increases at a greater-than-linear rate with power required) will further increase the importance of minimizing power requirements to minimize cost.

One of the assumptions used in modeling the transportation systems was that the choice of ISRU approach did not impact any of the other surface systems (e.g. habitation). As a result, the transportation systems needed to bring those other systems are not considered in the figures of merit used in this evaluation. However, the ability to access or produce water on the surface of Mars may impact the logistical requirements of those other systems, which in turn could change their sizing, and thus, the associated transportation systems. Future research would model an entire DRA 5.0 analogous architecture to capture those impacts.

The level of fidelity of the models of the the MDV and the MTV are based on parametrization of data given in DRA 5.0. While these models accommodate the impact of changes in the required mass, power, and volume on the surface of Mars, they can be improved with more detailed modeling. Future research would model the transportation systems with higher fidelity to determine if any of the trends shown in this research are impacted.

The conceptual design of an ethylene ascent vehicle is needed to evaluate the feasibility of its promising ISPP results. Ethylene stages may have significant challenges in the design of their propulsion system due to the different chemistry as compared to currently used hydrocarbon engines; the technology investments and engineering

work required to meet those challenges may erode the savings realized by using a high performance, non-cryogenic-on-Mars fuel. Additionally, this modeling assumes that because the liquefaction of ethylene does not require cryogenic refrigeration, the fluid thermal management functionality can be fully offloaded to the MAV; this assumption requires detailed design of the integrated ISPP/MAV system to understand the capabilities needed to achieve this.

The design of hydrogen ascent vehicles is more mature; hydrogen stages for launch and in-space environments have been built before. However, these stages have not had to maintain hydrogen storage for months to years of time; the thermal management required by the vehicle to mitigate significant levels of boiloff is a key technical challenge in designing such a vehicle. Due to its sparse nature relative to denser fuels, hydrogen also requires larger tanks, which in turn could strain entry system and launch vehicle designs to accommodate the larger volumes of these vehicles. Thus, detailed design of a hydrogen MAV, as well as studies of its integration into the transportation elements required to bring it from Earth, is needed before hydrogen's other benefits in ISPP can lead to it being accepted as the preferred approach.

5.2.3 Risk and Reliability

The modeling of the ISPP systems assumes that they are able to deliver their demanded products in the time available. Thus, this assumption does not consider possible needs for spare parts and maintenance on those systems, nor the possibility of downtime due to that maintenance. Accounting for those requirements would impact the mass, power, and volume requirements to be transported to the surface. Future research would consider these impacts through analysis of sparing and maintenance requirements as considered in other advanced space systems, yielding updated estimates of requirements differentiated across the ISPP approaches.

These systems also must operate for months without direct human supervision,

in harsh environments. Thus, the need for highly autonomous systems (as required in any robotic exploration of another planet) is particularly acute here; without the successful operation of the ISPP system, the crew would be unable to ascend from the surface. Therefore, the autonomous operation of complex systems working in the Martian environment, and the impact of implementing that autonomy from hardware, software, and operational perspectives, is needed to evaluate the challenges of performing ISPP.

5.2.4 Other ISRU Approaches

This research considers the most commonly considered ISPP approaches discussed in the literature, and evaluates them on a cost basis under uncertainty to determine how to select among them. However, it is not an exhaustive exploration of the in-situ resource utilization trade space. Alternative fuels and oxidizers that could be produced or acquired at Mars (e.g. carbon dioxide from the atmosphere and magnesium from the regolith) may be useful, contingent upon future work modeling the systems required to make those products. Other systems on Mars can also benefit from the ISRU technologies considered here; for example, the ability to acquire water on Mars can reduce the requirements on crew logistics and life support system closure, which in turn could yield further savings in mass and cost required to perform a human mission to Mars.

APPENDIX A

CODE

A.1 ISPP Models

The MATLAB code used to model each ISPP system is given below. System models are based on the work done by DePasquale et al. in their modeling of different ISPP systems [42].

A.1.1 Carbon Dioxide Acquisition

```
%This program uses the ISRU tool from Spaceworks engineering to estimate
%parameters of a CO2 adsorption system.
%
%Input is a three element vector
%  input(1) = CO2 required in kg
%  input(2) = number of days for production in days
%  input(3) = daily time for CH4 manufacture in hr
%
%Parameters is an optional vector (length 25) containing alternative values
%to the default parameters values. If ommited, the default values will be
%used.
%
%Cost_vector is an optional vector (length 10) containing constants and
%exponents for DDT&E and production cost for each subcomponent (specific to
%a given model). If ommitted, the neutral values will be used.
%
%Output is a five element vector
```

```
%  output(1) = Total system mass in kg
%  output(2) = Total system power required in W
%  output(3) = Total system volume in m^3
%  output(4) = DDT&E cost in 2006 $M for 2015 launch date from NAFCOM CERs
%  output(5) = Production cost in 2006 $M for 2015 launch date from NAFCOM
    CERs

function output = ISRU_CO2Adsorber(input, parameters, cost_vector)

%Input processing
CO2_demand = input(1); %kg
days_of_operation = input(2); %day
daily_operation_time = input(3); %hr

%Parameters
if nargin < 2
    CO2_fraction_atm = 0.95;
    Usable_atm_fraction = 0.87;
    Outgas_temp_high = 523.16; %K
    Outgas_press_high = 600; %torr
    Outgas_press_low = 6; %torr
    Packing_efficiency = 0.8;
    Catalyst_density = 642.86; %kg/m^3, zeolite
    Tank_L_to_D_ratio = 3.6;
    Tank_safety_factor = 2;
    Tank_mass_factor = 5000; %m
    Tank_insulation_density = 1.27; %kg/m^2
    Tank_insulation_thickness = 0.063; %m
    Heat_fin_density = 2700; %kg/m^3
```

```
    Heat_fin_t = 0.0003; %m
    Heat_fin_area_per_length = 7.65; %m^-1
    Fan_piping_HTbar_toCatalyst_ratio = 0.1;
    Radiator_area_parameter = 1.27 * 10^-7; %m^2 / (K*s)
    CO2_adsorber_opTime = 12; %hr
    Night_temp = 200; %K
    Radiator_density = 3.3; %kg/m^2
    Cp_catalyst = 1.0101; %kJ/(kg * K)
    Valve_open_temp = 273; %K
    Heat_transfer_eff = 0.9;
    Mass_contingency = 0.1;
    Power_contingency = 0.1;
else
    CO2_fraction_atm = parameters(1);
    Usable_atm_fraction = parameters(2);
    Outgas_temp_high = parameters(3); %K
    Outgas_press_high = parameters(4); %torr
    Outgas_press_low = parameters(5); %torr
    Packing_efficiency = parameters(6);
    Catalyst_density = parameters(7); %kg/m^3, zeolite
    Tank_L_to_D_ratio = parameters(8);
    Tank_safety_factor = parameters(9);
    Tank_mass_factor = parameters(10); %m
    Tank_insulation_density = parameters(11); %kg/m^2
    Tank_insulation_thickness = parameters(12); %m
    Heat_fin_density = parameters(13); %kg/m^3
    Heat_fin_t = parameters(14); %m
    Heat_fin_area_per_length = parameters(15); %m^-1
    Fan_piping_HTbar_toCatalyst_ratio = parameters(16);
```

```
    Radiator_area_parameter = parameters(17); %m^2 / (K*s)
    CO2_adsorber_opTime = parameters(18); %hr
    Night_temp = parameters(19); %K
    Radiator_density = parameters(20); %kg/m^2
    Cp_catalyst = parameters(21); %kJ/(kg * K)
    Valve_open_temp = parameters(22); %K
    Heat_transfer_eff = parameters(23);
    Mass_contingency = parameters(24);
    Power_contingency = parameters(25);
end

%Cost
if nargin < 3
    DDTE_const_struct = 0.4267;
    DDTE_exp_struct = 0.6376;
    DDTE_const_therm = 2.4798;
    DDTE_exp_therm = 0.4194;
    Unit_const_struct = 0.0795;
    Unit_exp_struct = 0.7313;
    Unit_const_therm = 0.4611;
    Unit_exp_therm = 0.489;
    DDTE_multi = 0.4471;
    Unit_multi = 0.5086;
else
    DDTE_const_struct = cost_vector(1);
    DDTE_exp_struct = cost_vector(2);
    DDTE_const_therm = cost_vector(3);
    DDTE_exp_therm = cost_vector(4);
    Unit_const_struct = cost_vector(5);
```

```
    Unit_exp_struct = cost_vector(6);
    Unit_const_therm = cost_vector(7);
    Unit_exp_therm = cost_vector(8);
    DDTE_multi = cost_vector(9);
    Unit_multi = cost_vector(10);
end

%%%%%%%%%%%%%%%%%%%%%%%%%%%%%%%%%%%%%%%%%%%%%%%%%%%%%%%%%%%%%%%%%%%%%%%%%%%%
%Calculations
%%%%%%%%%%%%%%%%%%%%%%%%%%%%%%%%%%%%%%%%%%%%%%%%%%%%%%%%%%%%%%%%%%%%%%%%%%%%

%Production rates
CO2_rate_required = CO2_demand / days_of_operation / CO2_adsorber_opTime; %
    kg/hr
Atm_rate_required = CO2_rate_required / (CO2_fraction_atm *
    Usable_atm_fraction); %kg/hr

%Catalyst sizing
CO2_loading_high = (0.0201 * log(Outgas_press_low) + 0.1337); %g/g
CO2_loading_low = (0.001 * exp(0.0046 * Outgas_press_high)); %g/g
Loading_difference = CO2_loading_high - CO2_loading_low; %g/g
Catalyst_mass = CO2_rate_required * (daily_operation_time / 1) /
    Loading_difference / Packing_efficiency; %kg,
Catalyst_volume = Catalyst_mass / Catalyst_density; %m^3

%Tank sizing
Tank_internal_radius = (Catalyst_volume / (pi * (4/3 + Tank_L_to_D_ratio *
    2))) ^ (1/3); %m
Tank_internal_length = Tank_internal_radius * 2 * Tank_L_to_D_ratio; %m
```

```
Tank_internal_pressure = 133.322368 * Outgas_press_high; %Pa
Tank_internal_mass = (Tank_internal_pressure + 101350) * Tank_safety_factor
    * Catalyst_volume / 9.81 / Tank_mass_factor; %kg
Tank_internal_surface_area = (4 * pi * sqrt(2)/2 * Tank_internal_radius^2)
   + (2 * pi * Tank_internal_radius * (Tank_internal_length - 2 *
   Tank_internal_radius)); %m^2
Insulation_mass = Tank_internal_surface_area * Tank_insulation_density; %kg
Tank_external_volume = 4/3 * pi * (Tank_internal_radius +
   Tank_insulation_thickness)^3 + pi * (Tank_internal_radius +
   Tank_insulation_thickness)^2 * (Tank_internal_length + 2 *
   Tank_insulation_thickness); %m^3
Tank_external_mass = (Tank_internal_pressure + 101350) * Tank_safety_factor
    * Tank_external_volume / 9.81 / Tank_mass_factor; %kg

%Internal parts and radiator sizing
Heat_fin_mass = Tank_internal_length * Heat_fin_area_per_length * pi *
   Tank_internal_radius^2 * Heat_fin_t * Heat_fin_density; %kg
Fan_piping_andHTbar_mass = Fan_piping_HTbar_toCatalyst_ratio *
   Catalyst_mass; %kg
Radiator_area = Radiator_area_parameter * (Outgas_temp_high - Night_temp) *
    CO2_adsorber_opTime * 3600; %m^2
Radiator_mass = Radiator_density * Radiator_area; %kg

%Power calculations
Heat_to_warm_V = Catalyst_mass * Cp_catalyst * (Outgas_temp_high -
   Valve_open_temp); %kJ
CO2_mass_per_night = CO2_rate_required * daily_operation_time; %kg
Heat_of_adsorption_high = -1334 * CO2_loading_low^2 - 14.793 *
   CO2_loading_low + 44.823; %kJ/mol
```

```
Heat_of_adsorption_low = -1334 * CO2_loading_high^2 - 14.793 *
    CO2_loading_high + 44.823; %kJ/mol
Delta_heat_of_adsorption = Heat_of_adsorption_high - Heat_of_adsorption_low
    ; %kJ/mol
CO2_per_night = 0.044 * CO2_mass_per_night; %mol
Heat_of_adsorption = Delta_heat_of_adsorption * CO2_per_night; %kJ
Heating_power = (Heat_to_warm_V + Heat_of_adsorption) /
    daily_operation_time * 1000/3600 / 0.5; %W %Adding 50% duty cycle
    factor to raise power bounds
Heat_leak = Heating_power * (1 - Heat_transfer_eff); %W

%Final mass calculations
T_mass = (Catalyst_mass + Heat_fin_mass + Fan_piping_andHTbar_mass +
    Radiator_mass) * (1 + MassMargin('T')); %kg
S_mass = (Tank_internal_mass + Insulation_mass + Tank_external_mass) * (1 +
     MassMargin('S')); %kg

%Cost calculations
DDTE_cost = (DDTE_const_struct * S_mass ^ DDTE_exp_struct +
    DDTE_const_therm * T_mass ^ DDTE_exp_therm) / DDTE_multi;
Unit_cost = (Unit_const_struct * S_mass ^ Unit_exp_struct +
    Unit_const_therm * T_mass ^ Unit_exp_therm) / Unit_multi;

%Output calculations
%OUTPUT_system_mass = (Catalyst_mass + Tank_internal_mass + Insulation_mass
     + Tank_external_mass + Heat_fin_mass + Fan_piping_andHTbar_mass +
    Radiator_mass) * (1 + Mass_contingency); %kg
OUTPUT_system_mass = S_mass + T_mass; %kg
```

```
OUTPUT_system_power = (Heating_power + Heat_leak) * (1 + Mass_contingency);
    %W
OUTPUT_system_volume = Tank_external_volume; %m^3


%Final output
output = [OUTPUT_system_mass; OUTPUT_system_power; OUTPUT_system_volume;
   DDTE_cost; Unit_cost];
```

A.1.2 Mars Water Acquisition

```
%This program uses data from DRA 5.0 Addendum to estimate
%parameters of a Mars water acquisition system that produces H2 and O2.
%
%Input is a two element vector
%  input(1) = Total hydrogen demanded in kg
%  input(2) = total time for production in hr
%
%Parameters is an optional vector (length 17) containing alternative values
%to the default parameters values. If ommited, the default values will be
%used.
%
%Cost_vector is an optional vector (length 4) containing cost factors and
%multipliers for DDTE and Unit cost. If ommitted, the neutral values will
   be used.
%
%Output is a six element vector
%  output(1) = Total system mass in kg
%  output(2) = Total system power required in W
%  output(3) = Total system volume in m^3
%  output(4) = Water produced for electrolysis in kg
```

```
%  output(5) = DDT&E cost in 2006 $M for 2015 launch date from NAFCOM CERs
%  output(6) = Production cost in 2006 $M for 2015 launch date from NAFCOM
    CERs

function output = ISRU_MarsH2O(input, parameters, cost_vector);

%Input processing
H2_demand = input(1); %kg
total_production_time = input(2); %hr

%Parameters
if nargin < 2
    H2_retain_eff = 0.95;
    Water_retain_eff = 0.99;
    Water_concentration = 0.03;
    Regolith_useful_frac = 0.95;
    E_M_multi = 10.191; %hr
    E_M_const = 398.26; %kg
    E_P_multi = 0.0155; %hr
    E_P_const = 0.334; %kW
    E_V_multi = 0.1532; %hr
    E_V_const = -0.3157; %m^3
    P_M_multi = 3; %hr
    P_M_const = 384; %kg
    P_P_multi = 0.3423; %hr
    P_P_const = 5.5398; %kW
    P_V_multi = 0.0626; %hr
    P_V_const = 2.2334; %m^3
    Power_contingency = 0.1;
```

```
else
    H2_retain_eff = parameters(1);
    Water_retain_eff = parameters(2);
    Water_concentration = parameters(3);
    Regolith_useful_frac = parameters(4);
    E_M_multi = parameters(5); %hr
    E_M_const = parameters(6); %kg
    E_P_multi = parameters(7); %hr
    E_P_const = parameters(8); %kW
    E_V_multi = parameters(9); %hr
    E_V_const = parameters(10); %m^3
    P_M_multi = parameters(11); %hr
    P_M_const = parameters(12); %kg
    P_P_multi = parameters(13); %hr
    P_P_const = parameters(14); %kW
    P_V_multi = parameters(15); %hr
    P_V_const = parameters(16); %m^3
    Power_contingency = parameters(17);
end

%Cost vector
if nargin < 3
    DDTE_factor = 0.05515; %based on Lunar ISRU Spaceworks presentation
        from Dom
    Unit_factor = 0.01622; %based on Lunar ISRU Spaceworks presentation
        from Dom
    DDTE_multi = 0.4543;
    Unit_multi = 0.5240;
else
```

```
    DDTE_factor = cost_vector(1); %based on Lunar ISRU Spaceworks
        presentation from Dom
    Unit_factor = cost_vector(2); %based on Lunar ISRU Spaceworks
        presentation from Dom
    DDTE_multi = cost_vector(3);
    Unit_multi = cost_vector(4);
end

%%%%%%%%%%%%%%%%%%%%%%%%%%%%%%%%%%%%%%%%%%%%%%%%%%%%%%%%%%%%%%%%%%%%%%%%%%%%
%Calculations
%%%%%%%%%%%%%%%%%%%%%%%%%%%%%%%%%%%%%%%%%%%%%%%%%%%%%%%%%%%%%%%%%%%%%%%%%%%%

%Rate calculations
H2_rate_theory = H2_demand / total_production_time; %kg/hr
H2_rate_actual = H2_rate_theory / H2_retain_eff; %kg/hr
Water_rate_actual = H2_rate_actual / 0.112 / Water_retain_eff; %kg/hr
Regolith_rate_actual = Water_rate_actual / Water_concentration /
    Regolith_useful_frac; %kg/hr
Water_out = Water_rate_actual * total_production_time; %kg

%Sizing
Excavator_mass = E_M_multi * Regolith_rate_actual + E_M_const; %kg
Excavator_power = (E_P_multi * Regolith_rate_actual + E_P_const) * 1000; %W
Excavator_volume = E_V_multi * Regolith_rate_actual + E_V_const; %m^3
Plant_mass = P_M_multi * Regolith_rate_actual + P_M_const; %kg
Plant_power = (P_P_multi * Regolith_rate_actual + P_P_const) * 1000; %W
Plant_volume = P_V_multi * Regolith_rate_actual + P_V_const; %m^3

%Output calculations
```

```
OUTPUT_system_mass = Excavator_mass * (1 + MassMargin('S')) + Plant_mass *
    (1 + MassMargin('T')); %kg
OUTPUT_system_power = (Excavator_power + Plant_power) * (1 +
    Power_contingency); %W
OUTPUT_system_volume = Excavator_volume + Plant_volume; %m^3


%Cost calculations
DDTE_cost = DDTE_factor * OUTPUT_system_mass; %$M2006
Unit_cost = Unit_factor * OUTPUT_system_mass; %$M2006
DDTE_cost = DDTE_cost / DDTE_multi; %$M2006
Unit_cost = Unit_cost / Unit_multi; %$M2006


%Final output
output = [OUTPUT_system_mass; OUTPUT_system_power; OUTPUT_system_volume;
    Water_out; DDTE_cost; Unit_cost];
```

A.1.3 Sabatier Reactor

```
%This program uses the ISRU tool from Spaceworks engineering to estimate
%parameters of a Sabatier system.
%
%Input is a two element vector
%  input(1) = CH4 demanded in kg
%  input(2) = total time for production in hr
%
%Parameters is an optional vector (length 28) containing alternative values
%to the default parameters values. If ommited, the default values will be
%used.
%
%Cost_vector is an optional vector (length 14) containing constants and
```

```
%exponents for DDT&E and production cost for each subcomponent (specific to
%a given model). If ommitted, the neutral values will be used.
%
%Output is an eight element vector
%  output(1) = Total system mass in kg
%  output(2) = Total system power required in W
%  output(3) = Total system volume in m^3
%  output(4) = Hydrogen required for Sabatier system in kg
%  output(5) = CO2 required for Sabatier system in kg
%  output(6) = Water produced for electrolysis in kg
%  output(7) = Exit temperature of Sabatier products in K
%  output(8) = DDT&E cost in 2006 $M for 2015 launch date from NAFCOM CERs
%  output(9) = Production cost in 2006 $M for 2015 launch date from NAFCOM
    CERs



function output = ISRU_Sabatier(input, parameters, cost_vector);


%Input processing
CH4_demand = input(1); %kg
production_time = input(2); %hr


%Parameters
if nargin < 2
    H2_conversion_eff = 0.98;
    Reaction_temp = 523; %K         %Matters for other fuel
    ChamberV_to_GasV_ratio = 8;
    Chamber_residence_time_multiplier = 3;
    Chamber_LtoD_ratio = 3.5;
```

```
    Reaction_chamber_t = 2; %cm
    Chamber_wall_density = 7850; %kg/m^3, steel
    Catalyst_density = 1; %g/cc, Ru-Al        %Matters for other fuel
    Insulation_density = 50; %kg/m^2
    Other_parts_fraction = 0.2;
    Heatup_temp = 473; %K         %Matters for other fuel
    Daytime_temp = 240; %K
    Heatup_time = 2; %hr         %Matters for other fuel
    Heat_transfer_eff = 0.9;
    Cp_of_catalyst = 238; %J/(kg*K), Ru       %Matters for other fuel
    Cp_of_wall = 900; %J/(kg*K), Al
    Heating_wire_diameter = 0.25 / 100; %m
    Wire_resistivity = 1.08*10^-6; %Ohm/m
    Wire_density = 8400; %kg/m^3, Nichrome
    Heater_packing_factor = 3;
    Cp_of_water = 4.1813; %J/(g*K)        %Matters for other fuel
    Cp_of_CH4 = 2.2; %J/(g*K)        %Matters for other fuel
    Heat_transfer_coefficient = 700; %W/(m^2*K)      %Matters for other
       fuel
    Water_boil_temp = 373; %K
    Condenser_t = 2; %cm
    Condenser_density = 7850; %kg/m^3, Steel
    Condenser_massFactor = 2;
    Mass_contingency = 0.1;
else
    %H2_conversion_eff = parameters(1);
    H2_conversion_eff = -1.6156 * 10^-5 * parameters(2)^2 + 1.99798997 *
       10^-2 * parameters(2) - 5.2339228;
    Reaction_temp = parameters(2); %K
```

```
    ChamberV_to_GasV_ratio = parameters(3);
    Chamber_residence_time_multiplier = parameters(4);
    Chamber_LtoD_ratio = parameters(5);
    Reaction_chamber_t = parameters(6); %cm
    Chamber_wall_density = parameters(7); %kg/m^3, steel
    Catalyst_density = parameters(8); %g/cc, Ru-Al
    Insulation_density = parameters(9); %kg/m^2
    Other_parts_fraction = parameters(10);
    Heatup_temp = parameters(11); %K
    Daytime_temp = parameters(12); %K
    Heatup_time = parameters(13); %hr
    Heat_transfer_eff = parameters(14);
    Cp_of_catalyst = parameters(15); %J/(kg*K), Ru
    Cp_of_wall = parameters(16); %J/(kg*K), Al
    Heating_wire_diameter = parameters(17); %m
    Wire_resistivity = parameters(18); %Ohm/m
    Wire_density = parameters(19); %kg/m^3, Nichrome
    Heater_packing_factor = parameters(20);
    Cp_of_water = parameters(21); %J/(g*K)
    Cp_of_CH4 = parameters(22); %J/(g*K)
    Heat_transfer_coefficient = parameters(23); %W/(m^2*K)
    Water_boil_temp = parameters(24); %K
    Condenser_t = parameters(25); %cm
    Condenser_density = parameters(26); %kg/m^3, Steel
    Condenser_massFactor = parameters(27);
    Mass_contingency = parameters(28);
end

%Cost vector
```

```
if nargin < 3
    DDTE_const_therm = 2.7497;
    DDTE_exp_therm = 0.3988;
    DDTE_const_struct = 1.2704;
    DDTE_exp_struct = 0.6847;
    DDTE_const_elect = 0.588;
    DDTE_exp_elect = 0.742;
    Unit_const_therm = 0.5276;
    Unit_exp_therm = 0.4526;
    Unit_const_struct = 0.0925;
    Unit_exp_struct = 0.7645;
    Unit_const_elect = 0.0365;
    Unit_exp_elect = 1.1107;
    DDTE_multi = 0.4543;
    Unit_multi = 0.5240;
else
    DDTE_const_therm = cost_vector(1);
    DDTE_exp_therm = cost_vector(2);
    DDTE_const_struct = cost_vector(3);
    DDTE_exp_struct = cost_vector(4);
    DDTE_const_elect = cost_vector(5);
    DDTE_exp_elect = cost_vector(6);
    Unit_const_therm = cost_vector(7);
    Unit_exp_therm = cost_vector(8);
    Unit_const_struct = cost_vector(9);
    Unit_exp_struct = cost_vector(10);
    Unit_const_elect = cost_vector(11);
    Unit_exp_elect = cost_vector(12);
    DDTE_multi = cost_vector(13);
```

```
    Unit_multi = cost_vector(14);
end



%%%%%%%%%%%%%%%%%%%%%%%%%%%%%%%%%%%%%%%%%%%%%%%%%%%%%%%%%%%%%%%%%%%%%%%%%%%%%%%%
%Calculations
%%%%%%%%%%%%%%%%%%%%%%%%%%%%%%%%%%%%%%%%%%%%%%%%%%%%%%%%%%%%%%%%%%%%%%%%%%%%%%%%

%%Flow rates
CH4_rate_kghr = CH4_demand/production_time; %kg/hr
CH4_rate = CH4_rate_kghr * 1000/3600; %g/s
Reactant_flow_rate = CH4_rate * 3.25/H2_conversion_eff; %g/s

%%Reaction chamber sizing
if Reaction_temp < 523
    Catalytic_reaction_rate_mol = 4.192595*10^-9*exp(0.04521818*
        Reaction_temp); %micromol/(cc*sec)
else
    Catalytic_reaction_rate_mol = 6.5084*10^-4*exp(0.02220601*Reaction_temp
        ); %micromol/(cc*sec)
end
Catalytic_reaction_rate = Catalytic_reaction_rate_mol *44.094/10^6; %g/(cc*
    sec)
Reaction_enthalpy = (-0.000029*(Reaction_temp-273)^2+0.057211*(
    Reaction_temp-273)+163.590212)/44.094; %kJ/g
Gas_volume_atReaction = Reactant_flow_rate/Catalytic_reaction_rate; %cc
Required_chamber_volume = Gas_volume_atReaction * ChamberV_to_GasV_ratio; %
    cc
```

```
Chamber_volume_RTM = Required_chamber_volume *
    Chamber_residence_time_multiplier; %cc
Catalyst_volume = Chamber_volume_RTM - Gas_volume_atReaction; %cc

%%Sabatier sizing
Reaction_chamber_diameter = (4*Chamber_volume_RTM/(pi*Chamber_LtoD_ratio))
    ^(1/3); %cm
Reaction_chamber_radius = Reaction_chamber_diameter / 2; %cm
Reaction_chamber_length = Reaction_chamber_diameter * Chamber_LtoD_ratio; %
    cm
Reaction_chamber_circumference = Reaction_chamber_diameter * pi; %cm
Reaction_chamber_outerV = pi * Reaction_chamber_length * (
    Reaction_chamber_radius + Reaction_chamber_t)^2; %cc
Reaction_chamber_innerV = pi * Reaction_chamber_length * (
    Reaction_chamber_radius)^2; %cc
Wall_volume = (Reaction_chamber_outerV - Reaction_chamber_innerV) / 100^3;
    %m^3
Wall_mass = Wall_volume * Chamber_wall_density; %kg;
Catalyst_mass = Catalyst_volume * Catalyst_density / 1000; %kg
Reaction_chamber_area = Reaction_chamber_circumference *
    Reaction_chamber_length / 100^2; %m^2
Insulation_mass = Reaction_chamber_area * Insulation_density; %kg
Other_parts_mass = Wall_mass * Other_parts_fraction; %kg

%%Heater sizing
Required_deltaT = Heatup_temp - Daytime_temp; %K
Catalyst_heating_power = Catalyst_mass * Cp_of_catalyst * (Required_deltaT
    /(Heatup_time*3600)) / Heat_transfer_eff; %W
```

```
Wall_heating_power = Wall_mass/2 * Cp_of_wall * (Required_deltaT/(
    Heatup_time*3600)) / Heat_transfer_eff; %W
Total_heating_power = Catalyst_heating_power + Wall_heating_power; %W
Heating_wire_crosssecA = pi * (Heating_wire_diameter/2)^2; %m^2
Wire_loop_count = Reaction_chamber_length/(Heating_wire_diameter*100);
Wire_length = Wire_loop_count / 100 * Reaction_chamber_circumference; %m
Wire_resistance = Wire_resistivity * Wire_length/Heating_wire_crosssecA; %
    Ohm
Wire_current = sqrt(Total_heating_power/Wire_resistance); %Amp
Wire_voltage = Wire_resistance * Wire_current; %V
Wire_volume = Wire_length * Heating_wire_crosssecA; %m^3
Wire_mass = Wire_volume * Wire_density; %kg
Heater_mass = Wire_mass * Heater_packing_factor; %kg

%%Condenser Sizing
Condenser_diam = Reaction_chamber_diameter / 2; %cm
Cp_average = (2.25 * Cp_of_water + Cp_of_CH4) / 3.25; %J/(g*K)
Sabatier_exit_temp = Reaction_temp; %K
Heat_to_reject = Reactant_flow_rate * Cp_average * (Sabatier_exit_temp -
    Water_boil_temp); %W
Condenser_length = Heat_to_reject/(Heat_transfer_coefficient/100^2 *
    Condenser_diam * pi * (Sabatier_exit_temp - Water_boil_temp)); %cm
Condenser_outerV = pi * (Condenser_diam/2 + Condenser_t)^2 *
    Condenser_length; %cc
Condenser_innerV = pi * (Condenser_diam/2)^2 * Condenser_length; %cc
Condenser_volume = (Condenser_outerV - Condenser_innerV) / 100^3; %m^3
Condenser_mass = Condenser_volume * Condenser_density *
    Condenser_massFactor; %kg
```

```
%%Output Calculations
Hydrogen_required = 0.5027 * CH4_demand / H2_conversion_eff; %kg
CO2_required = 5.46 * Hydrogen_required; %kg
H2O_produced = 4.4683 * Hydrogen_required * H2_conversion_eff; %kg
Warmup_power = Total_heating_power; %W
Power_of_reaction = Reactant_flow_rate * Reaction_enthalpy * 1000; %W
H2_from_water = H2O_produced * 0.112 / 0.98; %kg
H2_actual = Hydrogen_required - H2_from_water;

%%Final mass calculations
S_mass = (Wall_mass + Insulation_mass) * (1 + MassMargin('S')); %kg
T_mass = (Catalyst_mass + Heater_mass + Condenser_mass) * (1 + MassMargin('
    T')); %kg
E_mass = Other_parts_mass * (1 + MassMargin('E')); %kg

%%Cost calculations
DDTE_cost = DDTE_const_therm * T_mass ^ DDTE_exp_therm + DDTE_const_struct
    * S_mass ^ DDTE_exp_struct + DDTE_const_elect * E_mass ^ DDTE_exp_elect
    ;
Unit_cost = Unit_const_therm * T_mass ^ Unit_exp_therm + Unit_const_struct
    * S_mass ^ Unit_exp_struct + Unit_const_elect * E_mass ^ Unit_exp_elect
    ;
DDTE_cost = DDTE_cost / DDTE_multi;
Unit_cost = Unit_cost / Unit_multi;

OUTPUT_system_power = max(0,Warmup_power - Power_of_reaction); %W
%OUTPUT_system_mass = (Wall_mass + Catalyst_mass + Insulation_mass +
    Other_parts_mass + Heater_mass + Condenser_mass) * (1 +
    Mass_contingency); %kg
```

```
OUTPUT_system_mass = T_mass + S_mass + E_mass; %kg
OUTPUT_system_volume = (Condenser_outerV + Reaction_chamber_outerV) /
    100^3; %m^3


%Final output
output = [OUTPUT_system_mass; OUTPUT_system_power; OUTPUT_system_volume;
    H2_actual; CO2_required; H2O_produced; Sabatier_exit_temp; DDTE_cost;
    Unit_cost];
```

A.1.4 Reverse Water Gas Shift and Ethylene Reactor

```
%This program uses the ISRU tool from Spaceworks engineering to estimate
%parameters of a RWGS system that produces C2H4 and O2.
%
%Input is a three element vector
%  input(1) = Total propellant demanded in kg
%  input(2) = O/F ratio of C2H4 and O2
%  input(3) = total time for production in hr
%
%Parameters is an optional vector (length 38) containing alternative values
%to the default parameters values. If ommited, the default values will be
%used.
%
%Cost_vector is an optional vector (length 14) containing constants and
%exponents for DDT&E and production cost for each subcomponent (specific to
%a given model). If ommitted, the neutral values will be used.
%
%Output is an eight element vector
%  output(1) = Total system mass in kg
%  output(2) = Total system power required in W
```

```
%  output(3) = Total system volume in m^3
%  output(4) = H2 required in kg
%  output(5) = CO2 required for Sabatier system in kg
%  output(6) = Water produced for electrolysis in kg
%  output(7) = DDT&E cost in 2006 $M for 2015 launch date from NAFCOM CERs
%  output(8) = Production cost in 2006 $M for 2015 launch date from NAFCOM
    CERs

function output = ISRU_RWGS_C2H4(input, parameters, cost_vector);

%Input processing
prop_demand = input(1); %kg
OF = input(2); %n/a
production_time = input(3); %hr

%Parameters
if nargin < 2
    Reaction_temp = 873; %K
    Chamber_inlet_press = 1; %atm
    Chamber_res_time = 0.025; %sec
    Chamber_L_to_D_ratio = 2;
    Chamber_wall_t = 2; %cm
    Chamber_wall_density = 7850; %kg/m^3, steel
    Unit_to_chamber_size_multi = 1.5;
    Ratio_quartz_to_catalyst = 3;
    Reactant_feedRate_STP_to_catalyst_ratio = 80; %cc/min/(g * cat)
    Catalyst_loading = 0.1;
    Catalyst_selectivity = 1;
    CO2_conversion_eff = 0.97;
```

```
    Cp_hydrogen = 14.57; %J/(g*K)
    Cp_CO2 = 1.102; %J/(g*K)
    Insulation_t = 2; %cm
    Insulation_density = 50; %kg/m^2
    Reactor_shell_conductivity = 14; %W/m/K
    Insulation_conductivity = 0.033; %W/m/K
    Other_parts_mass_ratio = 0.2;
    HT_eff = 0.8;
    Wire_D = 0.25; %cm
    Wire_resistivity = 1.08 * 10^-6; %Ohm*m
    Wire_density = 8400; %kg/m^3, nichrome
    Heater_packing_factor = 3;
    Separation_purity = 0.97;
    Separation_CO2_recovery = 0.92;
    Separation_H2_recovery = 0.95;
    Condenser_separator_mass_ratio_to_reactor = 0.7;
    Membrane_mass_ratio_to_reactor = 0.4;
    Pump_mass_multi = 1;
    Pump_power_multi = 1;
    Volume_RWGS_multi_reactor_V = 2.5;
    C2H4_reactor_mass_multi = 1;
    C2H4_reactor_V_multi = 1;
    C2H4_H2_eff = 0.9;
    C2H4_CO2_eff = 0.9;
    Mass_contingency = 0.1;
    Power_contingency = 0.1;
else
    Reaction_temp = parameters(1); %K
    Chamber_inlet_press = parameters(2); %atm
```

```
Chamber_res_time = parameters(3); %sec

Chamber_L_to_D_ratio = parameters(4);

Chamber_wall_t = parameters(5); %cm

Chamber_wall_density = parameters(6); %kg/m^3, steel

Unit_to_chamber_size_multi = parameters(7);

Ratio_quartz_to_catalyst = parameters(8);

Reactant_feedRate_STP_to_catalyst_ratio = parameters(9); %cc/min/(g *
    cat)

Catalyst_loading = parameters(10);

Catalyst_selectivity = parameters(11);

CO2_conversion_eff = parameters(12);

Cp_hydrogen = parameters(13); %J/(g*K)

Cp_CO2 = parameters(14); %J/(g*K)

Insulation_t = parameters(15); %cm

Insulation_density = parameters(16); %kg/m^2

Reactor_shell_conductivity = parameters(17); %W/m/K

Insulation_conductivity = parameters(18); %W/m/K

Other_parts_mass_ratio = parameters(19);

HT_eff = parameters(20);

Wire_D = parameters(21); %cm

Wire_resistivity = parameters(22); %Ohm*m

Wire_density = parameters(23); %kg/m^3, nichrome

Heater_packing_factor = parameters(24);

Separation_purity = parameters(25);

Separation_CO2_recovery = parameters(26);

Separation_H2_recovery = parameters(27);

Condenser_separator_mass_ratio_to_reactor = parameters(28);

Membrane_mass_ratio_to_reactor = parameters(29);

Pump_mass_multi = parameters(30);
```

```
    Pump_power_multi = parameters(31);
    Volume_RWGS_multi_reactor_V = parameters(32);
    C2H4_reactor_mass_multi = parameters(33);
    C2H4_reactor_V_multi = parameters(34);
    C2H4_H2_eff = parameters(35);
    C2H4_CO2_eff = parameters(36);
    Mass_contingency = parameters(37);
    Power_contingency = parameters(38);
end

%Cost vector
if nargin < 3
    DDTE_const_therm = 2.7497;
    DDTE_exp_therm = 0.3988;
    DDTE_const_struct = 1.2704;
    DDTE_exp_struct = 0.6847;
    DDTE_const_elect = 0.588;
    DDTE_exp_elect = 0.742;
    Unit_const_therm = 0.5276;
    Unit_exp_therm = 0.4526;
    Unit_const_struct = 0.0925;
    Unit_exp_struct = 0.7645;
    Unit_const_elect = 0.0365;
    Unit_exp_elect = 1.1107;
    DDTE_multi = 0.4543;
    Unit_multi = 0.5240;
else
    DDTE_const_therm = cost_vector(1);
    DDTE_exp_therm = cost_vector(2);
```

```
    DDTE_const_struct = cost_vector(3);
    DDTE_exp_struct = cost_vector(4);
    DDTE_const_elect = cost_vector(5);
    DDTE_exp_elect = cost_vector(6);
    Unit_const_therm = cost_vector(7);
    Unit_exp_therm = cost_vector(8);
    Unit_const_struct = cost_vector(9);
    Unit_exp_struct = cost_vector(10);
    Unit_const_elect = cost_vector(11);
    Unit_exp_elect = cost_vector(12);
    DDTE_multi = cost_vector(13);
    Unit_multi = cost_vector(14);
end

%%%%%%%%%%%%%%%%%%%%%%%%%%%%%%%%%%%%%%%%%%%%%%%%%%%%%%%%%%%%%%%%%%%%%%%%%%%%
%Calculations
%%%%%%%%%%%%%%%%%%%%%%%%%%%%%%%%%%%%%%%%%%%%%%%%%%%%%%%%%%%%%%%%%%%%%%%%%%%%

%Flow rates
H2_required_theory = max(2*2.02/28.05/(1+OF)*prop_demand,2.02/32*OF/(1+OF)*
    prop_demand); %kg
CO2_required_theory = max(2*44.01/28.05/(1+OF)*prop_demand,44.01/32*OF/(1+
    OF)*prop_demand); %kg
Water_demand = H2_required_theory / 2.02 * 2 * 18.02; %kg
Equilibrium_constant = exp(-4.33 + (4577.8 / Reaction_temp));
Transform = 1 + 1 / sqrt(Equilibrium_constant);
Eq_CO2_converted_per_pass = 1 - 1 / Transform;
Eq_H2_converted_per_pass = 1 - 1 / Transform;
%%%%%%%H2_required_theory = 0.112 * Water_demand; %kg
```

```
H2_required_actual = H2_required_theory / Eq_H2_converted_per_pass; %kg
H2_separation_losses = H2_required_actual * (1 - Eq_H2_converted_per_pass)
    * (1 - Separation_H2_recovery); %kg
%%%%%%%%CO2_required_theory = 21.73 * H2_required_theory; %kg
CO2_required_actual = CO2_required_theory / Eq_CO2_converted_per_pass; %kg
CO2_separation_losses = CO2_required_actual * (1 -
    Eq_CO2_converted_per_pass) * (1 - Separation_CO2_recovery); %kg
H2_feed_after_recycle = H2_required_theory / C2H4_H2_eff +
    H2_separation_losses; %kg
CO2_feed_after_recycle = CO2_required_theory / C2H4_CO2_eff +
    CO2_separation_losses; %kg
H2_flow_rate = H2_required_actual / production_time / 60; %kg/min
CO2_flow_rate = CO2_required_actual / production_time / 60; %kg/min
H2_V_flow_rate_reactT = (H2_flow_rate / (1.008 * 2 / 1000) * 0.08205784 *
    Reaction_temp * 1000) / Chamber_inlet_press; %cc / min
CO2_V_flow_rate_reactT = (CO2_flow_rate / ((12.01 + (2 * 16)) / 1000) *
    0.08205784 * Reaction_temp * 1000) / Chamber_inlet_press; %cc / min
Total_V_flow_rate_reactT = H2_V_flow_rate_reactT + CO2_V_flow_rate_reactT;
    %cc / min
H2_V_flow_rate_STP = (H2_flow_rate / (1.008 * 2 / 1000) * 0.08205784 * 273
    * 1000) / 1; %cc / min
CO2_V_flow_rate_STP = (CO2_flow_rate / ((12.01 + (2 * 16)) / 1000) *
    0.08205784 * 273 * 1000) / 1; %cc / min
Total_V_flow_rate_STP = H2_V_flow_rate_STP + CO2_V_flow_rate_STP; %cc / min

%Reaction chamber sizing
Chamber_V = Total_V_flow_rate_reactT * Chamber_res_time / 60; %cc
Reactor_V = Chamber_V * Unit_to_chamber_size_multi; %cc
Reactor_D = (4 * Reactor_V / (pi * Chamber_L_to_D_ratio)) ^ (1/3); %cm
```

```
Reactor_r = Reactor_D / 2; %cm
Reactor_L = Reactor_D * Chamber_L_to_D_ratio; %cm
Reactor_C = 2 * pi * Reactor_r; %cm
Outer_V = pi * (Reactor_r + Chamber_wall_t) ^ 2 * Reactor_L; %cc
Inner_V = pi * Reactor_r ^ 2 * Reactor_L; %cc
Shell_V = (Outer_V - Inner_V) / 100^3; %m^3
Shell_mass = Shell_V * Chamber_wall_density; %kg
Catalyst_mass = Total_V_flow_rate_STP /
    Reactant_feedRate_STP_to_catalyst_ratio / 1000; %kg
Catalyst_andSupport_mass = Catalyst_mass / Catalyst_loading; %kg
Catalyst_andQuartz_mass = Catalyst_andSupport_mass * (1 +
    Ratio_quartz_to_catalyst); %kg
Reactor_area = Reactor_C * Reactor_L / 100^2; %m^2
Insulation_mass = Reactor_area * Insulation_density; %kg
Other_parts_mass = Shell_mass * Other_parts_mass_ratio; %kg
Reactor_total_mass = Shell_mass + Catalyst_andQuartz_mass + Insulation_mass
     + Other_parts_mass; %kg

%Reaction power requirements
RWGS_reaction_enthalpy = 816.93; %kJ/kg
C2H4_reaction_enthalpy = -330.962; %kJ/kg, assuming -49.4 kcal/(k)mole from
     Zubrin paper (MW*kcal/kmol/4.184(kJ/kcal))
Reaction_thermal_power = RWGS_reaction_enthalpy * (H2_flow_rate +
    CO2_flow_rate) * 1000 / 60; %W
C2H4_thermal_power = C2H4_reaction_enthalpy * (H2_flow_rate + CO2_flow_rate
    ) * 1000 / 60; %W, assuming all flow into C2H4 reactor
%%%PARAMETERIZE DAYTIME TEMP
CO2_heating_requirement = (Reaction_temp - 240) * Cp_CO2; %kJ/kg, Daytime
    temp of 240K
```

```
H2_heating_requirement = (Reaction_temp - 240) * Cp_hydrogen; %kJ/kg,
    Daytime temp of 240K
%%%PARAMETERIZE DAYTIME TEMP
Thermal_power_heating = (CO2_heating_requirement * CO2_flow_rate +
    H2_heating_requirement * H2_flow_rate) * 1000/60; %W
Delta_T = Reaction_temp - 240; %K, Daytime temp of 240K
Heat_loss = (((log(Reactor_r + Chamber_wall_t)/Reactor_r) * (1 / (2 * pi *
    Reactor_shell_conductivity / 100 * Reactor_L))) + ((log(Reactor_r +
    Chamber_wall_t + Insulation_t) / (Reactor_r + Chamber_wall_t)) * (1 /
    (2 * pi * Insulation_conductivity / 100 * Reactor_L)))); %W
Total_thermal_power_required = (Reaction_thermal_power +
    Thermal_power_heating + Heat_loss + C2H4_thermal_power) / HT_eff; %W,
    power modified by C2H4 reactor


%Heater sizing
Wire_diameter = Wire_D / 100; %m
Wire_crosssecA = pi * (Wire_diameter / 2) ^ 2; %m^2
Wire_loops = Reactor_L / Wire_D;
Wire_length = Wire_loops * Reactor_C / 100; %m
Wire_resistance = Wire_resistivity * Wire_length / Wire_crosssecA; %Ohm
Wire_current = sqrt(Total_thermal_power_required / Wire_resistance); %A
Wire_voltage = Wire_current * Wire_resistance; %V
Nichrome_V = Wire_crosssecA * Wire_length; %m^3
Nichrome_mass = Wire_density * Nichrome_V; %kg
Heater_mass = Heater_packing_factor * Nichrome_mass; %kg


%Pump sizing
Pump_flow_rate = Total_V_flow_rate_STP * 60 / 100^3; %m^3/hr; is mass of CO
    + H2?
```

```
if Pump_flow_rate > 0
    Pump_mass = 2.922398 * Pump_flow_rate + 5.605963; %kg
end
if Pump_flow_rate > 6
    Pump_mass = 0.518374 * Pump_flow_rate + 21.196411; %kg
end
if Pump_flow_rate > 26
    Pump_mass = 1.20803 * Pump_flow_rate + 4.52366; %kg
end
if Pump_flow_rate > 80
    Pump_mass = 0.796 * (Pump_flow_rate - 80) + 101; %kg
end
if Pump_flow_rate > 178
    Pump_mass = 1.102 * Pump_flow_rate - 16.8333; %kg
end
Pump_mass = Pump_mass * Pump_mass_multi; %kg, Source F9
if Pump_flow_rate > 0
    Pump_power = 56.74299 * Pump_flow_rate + 19.27133; %W
end
if Pump_flow_rate > 7.8
    Pump_power = 7.61593 * Pump_flow_rate + 405.87326; %W
end
if Pump_flow_rate > 26.8
    Pump_power = 29.2898 * Pump_flow_rate - 173.2902; %W
end
if Pump_flow_rate > 80
    Pump_power = 28.041 * (Pump_flow_rate - 80) + 2170; %W
end
if Pump_flow_rate > 178
```

```
    Pump_power = 17.6909 * Pump_flow_rate + 1768.9692; %W
end
Pump_power = Pump_power * Pump_power_multi; %W, Source F9

%Condenser and membrane sizing
Condenser_mass = Reactor_total_mass *
    Condenser_separator_mass_ratio_to_reactor; %kg
Membrane_mass = Reactor_total_mass * Membrane_mass_ratio_to_reactor; %kg

%C2H4 Reactor Sizing
C2H4_reactor_mass = Reactor_total_mass * C2H4_reactor_mass_multi; %kg
C2H4_reactor_V = Reactor_V * C2H4_reactor_V_multi; %cc

%%Output Calculations
OUTPUT_system_power = (Total_thermal_power_required + Pump_power) * (1 +
    Power_contingency); %W
OUTPUT_system_mass = (Reactor_total_mass + Heater_mass + Pump_mass +
    Condenser_mass + Membrane_mass + C2H4_reactor_mass) * (1 + MassMargin('
    T')); %kg
OUTPUT_system_volume = (Reactor_V + C2H4_reactor_V) / 100^3 *
    Volume_RWGS_multi_reactor_V; %m^3

%Cost calculations (from Sabatier)
DDTE_cost = DDTE_const_therm * OUTPUT_system_mass ^ DDTE_exp_therm; %$M2006
Unit_cost = Unit_const_therm * OUTPUT_system_mass ^ Unit_exp_therm; %$M2006
DDTE_cost = DDTE_cost / DDTE_multi;
Unit_cost = Unit_cost / Unit_multi;

%Final output
```

```
output = [OUTPUT_system_mass; OUTPUT_system_power; OUTPUT_system_volume;
   H2_feed_after_recycle; CO2_feed_after_recycle; Water_demand; DDTE_cost;
    Unit_cost];
```

A.1.5 Reverse Water Gas Shift and Methanol Reactor

```
%This program uses the ISRU tool from Spaceworks engineering to estimate
%parameters of a RWGS system that produces CH3OH and O2.
%
%Input is a three element vector
%  input(1) = Total propellant demanded in kg
%  input(2) = O/F ratio of CH3OH and O2
%  input(3) = total time for production in hr
%
%Parameters is an optional vector (length 38) containing alternative values
%to the default parameters values. If ommited, the default values will be
%used.
%
%Cost_vector is an optional vector (length 14) containing constants and
%exponents for DDT&E and production cost for each subcomponent (specific to
%a given model). If ommitted, the neutral values will be used.
%
%Output is an eight element vector
%  output(1) = Total system mass in kg
%  output(2) = Total system power required in W
%  output(3) = Total system volume in m^3
%  output(4) = H2 required in kg
%  output(5) = CO2 required for Sabatier system in kg
%  output(6) = Water produced for electrolysis in kg
%  output(7) = DDT&E cost in 2006 $M for 2015 launch date from NAFCOM CERs
```

```
%  output(8) = Production cost in 2006 $M for 2015 launch date from NAFCOM
    CERs

function output = ISRU_RWGS_CH3OH(input, parameters, cost_vector);

%Input processing
prop_demand = input(1); %kg
OF = input(2); %n/a
production_time = input(3); %hr

%Parameters
if nargin < 2
    Reaction_temp = 873; %K
    Chamber_inlet_press = 1; %atm
    Chamber_res_time = 0.025; %sec
    Chamber_L_to_D_ratio = 2;
    Chamber_wall_t = 2; %cm
    Chamber_wall_density = 7850; %kg/m^3, steel
    Unit_to_chamber_size_multi = 1.5;
    Ratio_quartz_to_catalyst = 3;
    Reactant_feedRate_STP_to_catalyst_ratio = 80; %cc/min/(g * cat)
    Catalyst_loading = 0.1;
    Catalyst_selectivity = 1;
    CO2_conversion_eff = 0.97;
    Cp_hydrogen = 14.57; %J/(g*K)
    Cp_CO2 = 1.102; %J/(g*K)
    Insulation_t = 2; %cm
    Insulation_density = 50; %kg/m^2
    Reactor_shell_conductivity = 14; %W/m/K
```

```
    Insulation_conductivity = 0.033; %W/m/K
    Other_parts_mass_ratio = 0.2;
    HT_eff = 0.8;
    Wire_D = 0.25; %cm
    Wire_resistivity = 1.08 * 10^-6; %Ohm*m
    Wire_density = 8400; %kg/m^3, nichrome
    Heater_packing_factor = 3;
    Separation_purity = 0.97;
    Separation_CO2_recovery = 0.92;
    Separation_H2_recovery = 0.95;
    Condenser_separator_mass_ratio_to_reactor = 0.7;
    Membrane_mass_ratio_to_reactor = 0.4;
    Pump_mass_multi = 1;
    Pump_power_multi = 1;
    Volume_RWGS_multi_reactor_V = 2.5;
    CH3OH_reactor_mass_multi = 1;
    CH3OH_reactor_V_multi = 1;
    CH3OH_H2_eff = 0.9;
    CH3OH_CO2_eff = 0.9;
    Mass_contingency = 0.1;
    Power_contingency = 0.1;
else
    Reaction_temp = parameters(1); %K
    Chamber_inlet_press = parameters(2); %atm
    Chamber_res_time = parameters(3); %sec
    Chamber_L_to_D_ratio = parameters(4);
    Chamber_wall_t = parameters(5); %cm
    Chamber_wall_density = parameters(6); %kg/m^3, steel
    Unit_to_chamber_size_multi = parameters(7);
```

```
Ratio_quartz_to_catalyst = parameters(8);
Reactant_feedRate_STP_to_catalyst_ratio = parameters(9); %cc/min/(g *
    cat)
Catalyst_loading = parameters(10);
Catalyst_selectivity = parameters(11);
CO2_conversion_eff = parameters(12);
Cp_hydrogen = parameters(13); %J/(g*K)
Cp_CO2 = parameters(14); %J/(g*K)
Insulation_t = parameters(15); %cm
Insulation_density = parameters(16); %kg/m^2
Reactor_shell_conductivity = parameters(17); %W/m/K
Insulation_conductivity = parameters(18); %W/m/K
Other_parts_mass_ratio = parameters(19);
HT_eff = parameters(20);
Wire_D = parameters(21); %cm
Wire_resistivity = parameters(22); %Ohm*m
Wire_density = parameters(23); %kg/m^3, nichrome
Heater_packing_factor = parameters(24);
Separation_purity = parameters(25);
Separation_CO2_recovery = parameters(26);
Separation_H2_recovery = parameters(27);
Condenser_separator_mass_ratio_to_reactor = parameters(28);
Membrane_mass_ratio_to_reactor = parameters(29);
Pump_mass_multi = parameters(30);
Pump_power_multi = parameters(31);
Volume_RWGS_multi_reactor_V = parameters(32);
CH3OH_reactor_mass_multi = parameters(33);
CH3OH_reactor_V_multi = parameters(34);
CH3OH_H2_eff = parameters(35);
```

```
    CH3OH_CO2_eff = parameters(36);
    Mass_contingency = parameters(37);
    Power_contingency = parameters(38);
end

%Cost vector
if nargin < 3
    DDTE_const_therm = 2.7497;
    DDTE_exp_therm = 0.3988;
    DDTE_const_struct = 1.2704;
    DDTE_exp_struct = 0.6847;
    DDTE_const_elect = 0.588;
    DDTE_exp_elect = 0.742;
    Unit_const_therm = 0.5276;
    Unit_exp_therm = 0.4526;
    Unit_const_struct = 0.0925;
    Unit_exp_struct = 0.7645;
    Unit_const_elect = 0.0365;
    Unit_exp_elect = 1.1107;
    DDTE_multi = 0.4543;
    Unit_multi = 0.5240;
else
    DDTE_const_therm = cost_vector(1);
    DDTE_exp_therm = cost_vector(2);
    DDTE_const_struct = cost_vector(3);
    DDTE_exp_struct = cost_vector(4);
    DDTE_const_elect = cost_vector(5);
    DDTE_exp_elect = cost_vector(6);
    Unit_const_therm = cost_vector(7);
```

```
    Unit_exp_therm = cost_vector(8);
    Unit_const_struct = cost_vector(9);
    Unit_exp_struct = cost_vector(10);
    Unit_const_elect = cost_vector(11);
    Unit_exp_elect = cost_vector(12);
    DDTE_multi = cost_vector(13);
    Unit_multi = cost_vector(14);
end

%%%%%%%%%%%%%%%%%%%%%%%%%%%%%%%%%%%%%%%%%%%%%%%%%%%%%%%%%%%%%%%%%%%%%%%%%%%%
%Calculations
%%%%%%%%%%%%%%%%%%%%%%%%%%%%%%%%%%%%%%%%%%%%%%%%%%%%%%%%%%%%%%%%%%%%%%%%%%%%

%Flow rates
H2_required_theory = 2*2.02/32.04*prop_demand/(1+OF); %kg
CO2_required_theory = max(2*44.01/32*OF/(1+OF)*prop_demand
    ,3*44.01/32.04/(1+OF)*prop_demand); %kg
Water_demand = CO2_required_theory * 18.02 / 44.01; %kg
Equilibrium_constant = exp(-4.33 + (4577.8 / Reaction_temp));
Transform = 1 + 1 / sqrt(Equilibrium_constant);
Eq_CO2_converted_per_pass = 1 - 1 / Transform;
Eq_H2_converted_per_pass = 1 - 1 / Transform;
%%%%%%%%H2_required_theory = 0.112 * Water_demand; %kg
H2_required_actual = H2_required_theory / Eq_H2_converted_per_pass; %kg
H2_separation_losses = H2_required_actual * (1 - Eq_H2_converted_per_pass)
    * (1 - Separation_H2_recovery); %kg
%%%%%%%%CO2_required_theory = 21.73 * H2_required_theory; %kg
CO2_required_actual = CO2_required_theory / Eq_CO2_converted_per_pass; %kg
```

```
CO2_separation_losses = CO2_required_actual * (1 -
    Eq_CO2_converted_per_pass) * (1 - Separation_CO2_recovery); %kg
H2_feed_after_recycle = H2_required_theory / CH3OH_H2_eff +
    H2_separation_losses; %kg
CO2_feed_after_recycle = CO2_required_theory / CH3OH_CO2_eff +
    CO2_separation_losses; %kg
H2_flow_rate = H2_required_actual / production_time / 60; %kg/min
CO2_flow_rate = CO2_required_actual / production_time / 60; %kg/min
H2_V_flow_rate_reactT = (H2_flow_rate / (1.008 * 2 / 1000) * 0.08205784 *
    Reaction_temp * 1000) / Chamber_inlet_press; %cc / min
CO2_V_flow_rate_reactT = (CO2_flow_rate / ((12.01 + (2 * 16)) / 1000) *
    0.08205784 * Reaction_temp * 1000) / Chamber_inlet_press; %cc / min
Total_V_flow_rate_reactT = H2_V_flow_rate_reactT + CO2_V_flow_rate_reactT;
    %cc / min
H2_V_flow_rate_STP = (H2_flow_rate / (1.008 * 2 / 1000) * 0.08205784 * 273
    * 1000) / 1; %cc / min
CO2_V_flow_rate_STP = (CO2_flow_rate / ((12.01 + (2 * 16)) / 1000) *
    0.08205784 * 273 * 1000) / 1; %cc / min
Total_V_flow_rate_STP = H2_V_flow_rate_STP + CO2_V_flow_rate_STP; %cc / min

%Reaction chamber sizing
Chamber_V = Total_V_flow_rate_reactT * Chamber_res_time / 60; %cc
Reactor_V = Chamber_V * Unit_to_chamber_size_multi; %cc
Reactor_D = (4 * Reactor_V / (pi * Chamber_L_to_D_ratio)) ^ (1/3); %cm
Reactor_r = Reactor_D / 2; %cm
Reactor_L = Reactor_D * Chamber_L_to_D_ratio; %cm
Reactor_C = 2 * pi * Reactor_r; %cm
Outer_V = pi * (Reactor_r + Chamber_wall_t) ^ 2 * Reactor_L; %cc
Inner_V = pi * Reactor_r ^ 2 * Reactor_L; %cc
```

```
Shell_V = (Outer_V - Inner_V) / 100^3; %m^3
Shell_mass = Shell_V * Chamber_wall_density; %kg
Catalyst_mass = Total_V_flow_rate_STP /
    Reactant_feedRate_STP_to_catalyst_ratio / 1000; %kg
Catalyst_andSupport_mass = Catalyst_mass / Catalyst_loading; %kg
Catalyst_andQuartz_mass = Catalyst_andSupport_mass * (1 +
    Ratio_quartz_to_catalyst); %kg
Reactor_area = Reactor_C * Reactor_L / 100^2; %m^2
Insulation_mass = Reactor_area * Insulation_density; %kg
Other_parts_mass = Shell_mass * Other_parts_mass_ratio; %kg
Reactor_total_mass = Shell_mass + Catalyst_andQuartz_mass + Insulation_mass
     + Other_parts_mass; %kg

%Reaction power requirements
RWGS_reaction_enthalpy = 816.93; %kJ/kg
CH3OH_reaction_enthalpy = -176.01; %kJ/kg, assuming -23 kcal/(k)mole from
    Zubrin paper
Reaction_thermal_power = RWGS_reaction_enthalpy * (H2_flow_rate +
    CO2_flow_rate) * 1000 / 60; %W
CH3OH_thermal_power = CH3OH_reaction_enthalpy * (H2_flow_rate +
    CO2_flow_rate) * 1000 / 60; %W, assuming all flow into CH3OH reactor
%%%PARAMETERIZE DAYTIME TEMP
CO2_heating_requirement = (Reaction_temp - 240) * Cp_CO2; %kJ/kg, Daytime
    temp of 240K
H2_heating_requirement = (Reaction_temp - 240) * Cp_hydrogen; %kJ/kg,
    Daytime temp of 240K
%%%PARAMETERIZE DAYTIME TEMP
Thermal_power_heating = (CO2_heating_requirement * CO2_flow_rate +
    H2_heating_requirement * H2_flow_rate) * 1000/60; %W
```

```
Delta_T = Reaction_temp - 240; %K, Daytime temp of 240K
Heat_loss = (((log(Reactor_r + Chamber_wall_t)/Reactor_r) * (1 / (2 * pi *
    Reactor_shell_conductivity / 100 * Reactor_L))) + ((log(Reactor_r +
    Chamber_wall_t + Insulation_t) / (Reactor_r + Chamber_wall_t)) * (1 /
    (2 * pi * Insulation_conductivity / 100 * Reactor_L)))); %W
Total_thermal_power_required = (Reaction_thermal_power +
    Thermal_power_heating + Heat_loss + CH3OH_thermal_power) / HT_eff; %W,
    power modified by CH3OH reactor

%Heater sizing
Wire_diameter = Wire_D / 100; %m
Wire_crosssecA = pi * (Wire_diameter / 2) ^ 2; %m^2
Wire_loops = Reactor_L / Wire_D;
Wire_length = Wire_loops * Reactor_C / 100; %m
Wire_resistance = Wire_resistivity * Wire_length / Wire_crosssecA; %Ohm
Wire_current = sqrt(Total_thermal_power_required / Wire_resistance); %A
Wire_voltage = Wire_current * Wire_resistance; %V
Nichrome_V = Wire_crosssecA * Wire_length; %m^3
Nichrome_mass = Wire_density * Nichrome_V; %kg
Heater_mass = Heater_packing_factor * Nichrome_mass; %kg

%Pump sizing
Pump_flow_rate = Total_V_flow_rate_STP * 60 / 100^3; %m^3/hr; is mass of CO
     + H2?
if Pump_flow_rate > 0
    Pump_mass = 2.922398 * Pump_flow_rate + 5.605963; %kg
end
if Pump_flow_rate > 6
    Pump_mass = 0.518374 * Pump_flow_rate + 21.196411; %kg
```

```
end
if Pump_flow_rate > 26
    Pump_mass = 1.20803 * Pump_flow_rate + 4.52366; %kg
end
if Pump_flow_rate > 80
    Pump_mass = 0.796 * (Pump_flow_rate - 80) + 101; %kg
end
if Pump_flow_rate > 178
    Pump_mass = 1.102 * Pump_flow_rate - 16.8333; %kg
end
Pump_mass = Pump_mass * Pump_mass_multi; %kg, Source F9
if Pump_flow_rate > 0
    Pump_power = 56.74299 * Pump_flow_rate + 19.27133; %W
end
if Pump_flow_rate > 7.8
    Pump_power = 7.61593 * Pump_flow_rate + 405.87326; %W
end
if Pump_flow_rate > 26.8
    Pump_power = 29.2898 * Pump_flow_rate - 173.2902; %W
end
if Pump_flow_rate > 80
    Pump_power = 28.041 * (Pump_flow_rate - 80) + 2170; %W
end
if Pump_flow_rate > 178
    Pump_power = 17.6909 * Pump_flow_rate + 1768.9692; %W
end
Pump_power = Pump_power * Pump_power_multi; %W, Source F9

%Condenser and membrane sizing
```

```
Condenser_mass = Reactor_total_mass *
    Condenser_separator_mass_ratio_to_reactor; %kg
Membrane_mass = Reactor_total_mass * Membrane_mass_ratio_to_reactor; %kg

%CH3OH Reactor Sizing
CH3OH_reactor_mass = Reactor_total_mass * CH3OH_reactor_mass_multi; %kg
CH3OH_reactor_V = Reactor_V * CH3OH_reactor_V_multi; %cc

%%Output Calculations
OUTPUT_system_power = (Total_thermal_power_required + Pump_power) * (1 +
    Power_contingency); %W
OUTPUT_system_mass = (Reactor_total_mass + Heater_mass + Pump_mass +
    Condenser_mass + Membrane_mass + CH3OH_reactor_mass) * (1 + MassMargin
    ('T')); %kg
OUTPUT_system_volume = (Reactor_V + CH3OH_reactor_V) / 100^3 *
    Volume_RWGS_multi_reactor_V; %m^3

%Cost calculations (from Sabatier)
DDTE_cost = DDTE_const_therm * OUTPUT_system_mass ^ DDTE_exp_therm; %$M2006
Unit_cost = Unit_const_therm * OUTPUT_system_mass ^ Unit_exp_therm; %$M2006
DDTE_cost = DDTE_cost / DDTE_multi;
Unit_cost = Unit_cost / Unit_multi;

%Final output
output = [OUTPUT_system_mass; OUTPUT_system_power; OUTPUT_system_volume;
    H2_feed_after_recycle; CO2_feed_after_recycle; Water_demand; DDTE_cost;
     Unit_cost];
```

A.1.6 Water Electrolysis

```
%This program uses the ISRU tool from Spaceworks engineering to estimate
%parameters of a water electrolysis system.
%
%Input is a two element vector
%  input(1) = Water available in kg
%  input(2) = total time for production in hr
%
%Parameters is an optional vector (length 16) containing alternative values
%to the default parameters values. If ommited, the default values will be
%used.
%
%Cost_vector is an optional vector (length 14) containing constants and
%exponents for DDT&E and production cost for each subcomponent (specific to
%a given model). If ommitted, the neutral values will be used.
%
%Output is a seven element vector
%  output(1) = Total system mass in kg
%  output(2) = Total system power required in W
%  output(3) = Total system volume in m^3
%  output(4) = Hydrogen produced for recycling in kg
%  output(5) = Oxygen produced in kg
%  output(6) = Exit temp of oxygen in K
%  output(7) = DDT&E cost in 2006 $M for 2015 launch date from NAFCOM CERs
%  output(8) = Production cost in 2006 $M for 2015 launch date from NAFCOM
   CERs

function output = ISRU_H2OElectrolyzer(input, parameters, cost_vector)

%Input processing
```

```
H2O_available = input(1); %kg
production_time = input(2); %hr

%Parameters
if nargin < 2
    Percent_flow_utilization = 0.03; %Not sure I understand this
    Operating_voltage = 1.5; %V
    Operating_temp = 298; %K
    O2_mass_rate_for_1A = 0.000298; %A/(kg/hr)
    Water_flow_velocity = 0.168; %m/s
    Water_V_to_flowRate = 0.016; %m^3/(kg/s)
    Volume_struct_fraction = 0.1;
    Percent_heat_loss = 0.15;
    Power_to_mass_ratio = 23; %W/kg, 23 from original tool, Pauly is 10.9
    Water_density = 1000; %kg/m^3
    Tank_fill_fraction = 0.9;
    Tank_mass_factor = 5000; %m
    Tank_safety_factor = 2;
    Percent_H2_recycled = 0.98;
    Mass_contingency = 0.1;
    Power_contingency = 0.1;
else
    Percent_flow_utilization = parameters(1); %Not sure I understand this
    Operating_voltage = parameters(2); %V
    Operating_temp = parameters(3); %K
    O2_mass_rate_for_1A = parameters(4); %kg/hr
    Water_flow_velocity = parameters(5); %m/s
    Water_V_to_flowRate = parameters(6); %m^3/(kg/s)
    Volume_struct_fraction = parameters(7);
```

```
    Percent_heat_loss = parameters(8);
    Power_to_mass_ratio = parameters(9); %W/kg, 23 from original tool,
       Pauly is 10.9
    Water_density = parameters(10); %kg/m^3
    Tank_fill_fraction = parameters(11);
    Tank_mass_factor = parameters(12); %m
    Tank_safety_factor = parameters(13);
    Percent_H2_recycled = parameters(14);
    Mass_contingency = parameters(15);
    Power_contingency = parameters(16);
end

%Cost vector
if nargin < 3
    DDTE_const_therm = 0.5357;
    DDTE_exp_therm = 0.6705;
    DDTE_const_elect = 0.2677;
    DDTE_exp_elect = 0.8403;
    Unit_const_therm = 0.2619;
    Unit_exp_therm = 0.7003;
    Unit_const_elect = 0.1017;
    Unit_exp_elect = 0.8886;
    DDTE_multi_alltherm = 0.4494;
    DDTE_multi_8020_therm = 0.2866;
    DDTE_multi_8020_elect = 0.1667;
    Unit_multi_alltherm = 0.5198;
    Unit_multi_8020_therm = 0.3506;
    Unit_multi_8020_elect = 0.1711;
else
```

```
    DDTE_const_therm = cost_vector(1);
    DDTE_exp_therm = cost_vector(2);
    DDTE_const_elect = cost_vector(3);
    DDTE_exp_elect = cost_vector(4);
    Unit_const_therm = cost_vector(5);
    Unit_exp_therm = cost_vector(6);
    Unit_const_elect = cost_vector(7);
    Unit_exp_elect = cost_vector(8);
    DDTE_multi_alltherm = cost_vector(9);
    DDTE_multi_8020_therm = cost_vector(10);
    DDTE_multi_8020_elect = cost_vector(11);
    Unit_multi_alltherm = cost_vector(12);
    Unit_multi_8020_therm = cost_vector(13);
    Unit_multi_8020_elect = cost_vector(14);
end
%%%%%%%%%%%%%%%%%%%%%%%%%%%%%%%%%%%%%%%%%%%%%%%%%%%%%%%%%%%%%%%%%%%%%%%%%%%%
%Calculations
%%%%%%%%%%%%%%%%%%%%%%%%%%%%%%%%%%%%%%%%%%%%%%%%%%%%%%%%%%%%%%%%%%%%%%%%%%%%

%Production rates
Water_input_rate = H2O_available / production_time; %kg/hr
O2_production_rate = Water_input_rate * 8/9; %kg/hr
Liquid_flow_rate = Water_input_rate / Percent_flow_utilization; %kg/s %What
    ?

%Power calculations
Current_required = O2_production_rate / O2_mass_rate_for_1A; %A
Power_process = Current_required * Operating_voltage; %W
Power_heat_leak = Power_process * Percent_heat_loss; %W
```

```
Total_power = Power_process + Power_heat_leak; %W

%Water tank sizing
Volume_water = Liquid_flow_rate * Water_V_to_flowRate; %m^3
Volume_storage_tank = Volume_water / Tank_fill_fraction; %m^3
Tank_radius = (0.75 * Volume_storage_tank / pi) ^ (1/3); %m
Tank_area = 4 * pi * Tank_radius ^ 2; %m^2
Pressure_on_tank_bottom = H2O_available * 9.81 / (Tank_area / 2); %Pa
Tank_mass = (Pressure_on_tank_bottom + 101350) * Tank_safety_factor /
    Tank_mass_factor / 9.81 * (1 + MassMargin('S')); %kg

%Output calculations
Electrolyzer_mass = Total_power / Power_to_mass_ratio * (1 + MassMargin('T
    ')); %kg
Hydrogen_produced = Percent_H2_recycled * 0.1119 * H2O_available; %kg
Oxygen_produced = 0.8881 * H2O_available; %kg

%Cost calculations
DDTE_cost = DDTE_const_therm * (Electrolyzer_mass + Tank_mass) ^
    DDTE_exp_therm / DDTE_multi_alltherm;
Unit_cost = Unit_const_therm * (Electrolyzer_mass + Tank_mass) ^
    Unit_exp_therm / Unit_multi_alltherm;

%OUTPUT_system_mass = (Electrolyzer_mass + Tank_mass) * (1 +
    Mass_contingency); %kg
OUTPUT_system_mass = Electrolyzer_mass + Tank_mass; %kg
OUTPUT_system_power = Total_power * (1 + Power_contingency); %W
OUTPUT_system_volume = Volume_storage_tank * (1 + Volume_struct_fraction);
    %m^3
```

```
output = [OUTPUT_system_mass; OUTPUT_system_power; OUTPUT_system_volume;
   Hydrogen_produced; Oxygen_produced; Operating_temp; DDTE_cost;
   Unit_cost];
```

A.1.7 Carbon Dioxide Electrolysis

```
%This program uses the ISRU tool from Spaceworks engineering to estimate
%parameters of a CO2 electrolysis system.
%
%Input is a two element vector
%  input(1) = Oxygen demanded in kg
%  input(2) = total time for production in hr
%
%Parameters is an optional vector (length 7) containing alternative values
%to the default parameters values. If ommited, the default values will be
%used.
%
%Cost_vector is an optional vector (length 14) containing constants and
%exponents for DDT&E and production cost for each subcomponent (specific to
%a given model). If ommitted, the neutral values will be used.
%
%Output is a six element vector
%  output(1) = Total system mass in kg
%  output(2) = Total system power required in W
%  output(3) = Total system volume in m^3
%  output(4) = CO2 required in kg
%  output(5) = DDT&E cost in 2006 $M for 2015 launch date from NAFCOM CERs
%  output(6) = Production cost in 2006 $M for 2015 launch date from NAFCOM
   CERs
```

```
function output = ISRU_CO2Electrolysis(input, parameters, cost_vector);

%Input processing
O2_demand = input(1); %kg
production_time = input(2); %hr

%Parameters
if nargin < 2
    Voltage = 1.85; %V
    O2_mass_rate_for_1A = 0.000298; %kg/hr, Rapp has 0.000325
    Percent_heat_loss = 0.25;
    Power_to_mass_ratio = 297.3; %kg/W??? default is 29.73
    t_to_L_ratio = 0.1;
    Mass_contingency = 0.1;
    Power_contingency = 0.1;
else
    Voltage = parameters(1); %V
    O2_mass_rate_for_1A = parameters(2); %kg/hr
    Percent_heat_loss = parameters(3);
    Power_to_mass_ratio = parameters(4); %kg/W???
    t_to_L_ratio = parameters(5);
    Mass_contingency = parameters(6);
    Power_contingency = parameters(7);
end

%Cost vector
if nargin < 3
    DDTE_const = 2.4894;
```

```
    DDTE_exp = 0.4189;
    Unit_const = 0.4241;
    Unit_exp = 0.5007;
    DDTE_multi = 0.4437;
    Unit_multi = 0.5059;
else
    DDTE_const = cost_vector(1);
    DDTE_exp = cost_vector(2);
    Unit_const = cost_vector(3);
    Unit_exp = cost_vector(4);
    DDTE_multi = cost_vector(5);
    Unit_multi = cost_vector(6);
end

%%%%%%%%%%%%%%%%%%%%%%%%%%%%%%%%%%%%%%%%%%%%%%%%%%%%%%%%%%%%%%%%%%%%%%%%%%%%
%Calculations
%%%%%%%%%%%%%%%%%%%%%%%%%%%%%%%%%%%%%%%%%%%%%%%%%%%%%%%%%%%%%%%%%%%%%%%%%%%%

%Production rate
O2_production_rate = O2_demand / production_time; %kg/hr

%Power calculations
%Percent_utilization = 0.4045 * Voltage^4 - 1.0273 * Voltage^3 + 0.863 *
    Voltage^2 - 0.2766 * Voltage + 0.0283;
Percent_utilization = 7.12157e-5 * exp(5 * Voltage); %Eureqa analysis of
    raw data cutting at V = 1.3
Current_required = O2_production_rate / O2_mass_rate_for_1A; %A
Power_process = Voltage * Current_required; %W
Power_heat_leak = Power_process * Percent_heat_loss; %W
```

```
Total_power = Power_process + Power_heat_leak; %W

%Volume calculations
%Current_density = 0.2362 * Voltage^4 - 0.6285 * Voltage^3 + 0.5656 *
    Voltage^2 - 0.1426 * Voltage + 0.0406; %A/cm^2
Current_density = 0.0022268 * exp(2.92651 * Voltage); %Eureqa analysis of
    raw data cutting at V = 1.3
Wafer_area = Current_required / Current_density * 0.0001; %m^2
Thickness = sqrt(Wafer_area) * t_to_L_ratio; %m

%Output calculations
CO2_required = 2.7506 * O2_demand / Percent_utilization; %kg

%OUTPUT_system_mass = Total_power / Power_to_mass_ratio * (1 +
    Mass_contingency); %kg
OUTPUT_system_mass = Total_power / Power_to_mass_ratio * (1 + MassMargin('T
    ')); %kg
OUTPUT_system_power = Total_power * (1 + Power_contingency); %W
OUTPUT_system_volume = Wafer_area * Thickness; %m^2

%Cost calculation
DDTE_cost = DDTE_const * OUTPUT_system_mass ^ DDTE_exp / DDTE_multi;
Unit_cost = Unit_const * OUTPUT_system_mass ^ Unit_exp / Unit_multi;

output = [OUTPUT_system_mass; OUTPUT_system_power; OUTPUT_system_volume;
    CO2_required; DDTE_cost; Unit_cost];
```

A.1.8 Methane Cryocooler

```
%This program uses the ISRU tool from Spaceworks engineering to estimate
```

```
%parameters of a CH4 cryocooler (either Stirling or Brayton).
%
%Input is a two element vector
%  input(1) = Methane to cool in kg
%  input(2) = total time for production in hr
%  input(3) = Methane incoming temperature in K
%
%Parameters is an optional vector (length 10) containing alternative values
%to the default parameters values. If ommited, the default values will be
%used.
%
%Cost_vector is an optional vector (length 6) containing constants and
%exponents for DDT&E and production cost for each subcomponent (specific to
%a given model). If ommitted, the neutral values will be used.
%

%Output is a three element vector
%  output(1) = Total system mass in kg
%  output(2) = Total system power required in W
%  output(3) = Total system volume in m^3
%  output(4) = DDT&E cost in 2006 $M for 2015 launch date from NAFCOM CERs
%  output(5) = Production cost in 2006 $M for 2015 launch date from NAFCOM
    CERs

function output = ISRU_CH4Cryocooler(input, parameters, cost_vector);

%Input processing
CH4_mass = input(1); %kg
production_time = input(2); %hr
```

```
CH4_input_temp = input(3); %K


%Parameters
if nargin < 2
    Daytime_temp = 240; %K
    Tank_temp = 112; %K
    Cycle_eff = 0.98;
    CH4_latent_heat = 512; %J/g
    Power_eff_Stirling = 0.07;
    Power_eff_Brayton = 0.07;
    Volume_to_coolingPower_Stirling = 7.10 * 10^-5; %m^3/W
    Volume_to_coolingPower_Brayton = 7.10 * 10^-5; %m^3/W
    Mass_contingency = 0.1;
    Power_contingency = 0.1;
else
    Daytime_temp = parameters(1); %K
    Tank_temp = parameters(2); %K
    Cycle_eff = parameters(3);
    CH4_latent_heat = parameters(4); %J/g
    Power_eff_Stirling = parameters(5);
    Power_eff_Brayton = parameters(6);
    Volume_to_coolingPower_Stirling = parameters(7); %m^3/W
    Volume_to_coolingPower_Brayton = parameters(8); %m^3/W
    Mass_contingency = parameters(9);
    Power_contingency = parameters(10);
end


%Cost
if nargin < 3
```

```
    DDTE_const = 2.5158;
    DDTE_exp = 0.4193;
    Unit_const = 0.4407;
    Unit_exp = 0.4957;
    DDTE_multi = 0.4292;
    Unit_multi = 0.4962;
else
    DDTE_const = cost_vector(1);
    DDTE_exp = cost_vector(2);
    Unit_const = cost_vector(3);
    Unit_exp = cost_vector(4);
    DDTE_multi = cost_vector(5);
    Unit_multi = cost_vector(6);
end

%%%%%%%%%%%%%%%%%%%%%%%%%%%%%%%%%%%%%%%%%%%%%%%%%%%%%%%%%%%%%%%%%%%%%%%%%%%%
%Calculations
%%%%%%%%%%%%%%%%%%%%%%%%%%%%%%%%%%%%%%%%%%%%%%%%%%%%%%%%%%%%%%%%%%%%%%%%%%%%

%Production rate
CH4_production_rate = CH4_mass / production_time; %kg/hr

%Power calculations
Cooldown_enthalpy = -209 + 2.08 * CH4_input_temp; %J/g
Ambient_enthalpy = -209 + 2.08 * Daytime_temp; %J/g
Enthalpy_cryocool = -209 + 2.08 * Tank_temp; %J/g
Cooldown_deltah = Cooldown_enthalpy - Ambient_enthalpy; %J/g
Liquifaction_deltah = Ambient_enthalpy - Enthalpy_cryocool; %J/g
```

```
Total_deltah = Liquifaction_deltah + CH4_latent_heat + Cooldown_deltah; %J/
    g
Liquifaction_heat_load = Total_deltah * CH4_production_rate / Cycle_eff *
    1000/3600; %W
Stirling_power = Liquifaction_heat_load / Power_eff_Stirling; %W
Brayton_power = Liquifaction_heat_load / Power_eff_Brayton; %W

%Mass and volume calculations
%Stirling_mass = (Liquifaction_heat_load^0.7 * ((Daytime_temp - Tank_temp)/
    Tank_temp)^1.45) * (1 + Mass_contingency); %kg
%Brayton_mass = (172 * Tank_temp^-0.85 * Liquifaction_heat_load^0.52) * (1
    + Mass_contingency); %kg
Stirling_mass = (Liquifaction_heat_load^0.7 * ((Daytime_temp - Tank_temp)/
    Tank_temp)^1.45) * (1 + MassMargin('T')); %kg
Brayton_mass = (172 * Tank_temp^-0.85 * Liquifaction_heat_load^0.52) * (1 +
     MassMargin('T')); %kg
Stirling_volume = Liquifaction_heat_load * Volume_to_coolingPower_Stirling;
     %m^3
Brayton_volume = Liquifaction_heat_load * Volume_to_coolingPower_Brayton; %
    m^3

%Output calculations
if Stirling_mass < Brayton_mass
    OUTPUT_system_mass = Stirling_mass; %kg
    OUTPUT_system_power = Stirling_power * (1 + Power_contingency); %W
    OUTPUT_system_volume = Stirling_volume; %m^3
else
    OUTPUT_system_mass = Brayton_mass; %kg
    OUTPUT_system_power = Brayton_power * (1 + Power_contingency); %W
```

```
    OUTPUT_system_volume = Brayton_volume; %m^3
end

%Cost
DDTE_cost = DDTE_const * OUTPUT_system_mass ^ DDTE_exp / DDTE_multi;
Unit_cost = Unit_const * OUTPUT_system_mass ^ Unit_exp / Unit_multi;

output = [OUTPUT_system_mass; OUTPUT_system_power; OUTPUT_system_volume;
    DDTE_cost; Unit_cost];
```

A.1.9 Oxygen Cryocooler

```
%This program uses the ISRU tool from Spaceworks engineering to estimate
%parameters of an O2 cryocooler (either Stirling or Brayton).
%
%Input is a two element vector
%  input(1) = Oxygen to cool in kg
%  input(2) = total time for production in hr
%  input(3) = Temperature of incoming oxygen in K
%
%Parameters is an optional vector (length 10) containing alternative values
%to the default parameters values. If ommited, the default values will be
%used.
%
%Cost_vector is an optional vector (length 6) containing constants and
%exponents for DDT&E and production cost for each subcomponent (specific to
%a given model). If ommitted, the neutral values will be used.
%
%Output is a three element vector
%  output(1) = Total system mass in kg
```

```
%  output(2) = Total system power required in W
%  output(3) = Total system volume in m^3
%  output(4) = DDT&E cost in 2006 $M for 2015 launch date from NAFCOM CERs
%  output(5) = Production cost in 2006 $M for 2015 launch date from NAFCOM
    CERs

function output = ISRU_O2Cryocooler(input, parameters, cost_vector);

%Input processing
O2_mass = input(1); %kg
production_time = input(2); %hr
O2_input_temp = input(3); %K

%Parameters
if nargin < 2
    Daytime_temp = 240; %K
    Tank_temp = 90; %K
    Cycle_eff = 0.98;
    O2_latent_heat = 213; %J/g
    Power_eff_Stirling = 0.07;
    Power_eff_Brayton = 0.07;
    Volume_to_coolingPower_Stirling = 7.10 * 10^-5; %m^3/W
    Volume_to_coolingPower_Brayton = 7.10 * 10^-5; %m^3/W
    Mass_contingency = 0.1;
    Power_contingency = 0.1;
else
    Daytime_temp = parameters(1); %K
    Tank_temp = parameters(2); %K
    Cycle_eff = parameters(3);
```

```
    O2_latent_heat = parameters(4); %J/g
    Power_eff_Stirling = parameters(5);
    Power_eff_Brayton = parameters(6);
    Volume_to_coolingPower_Stirling = parameters(7); %m^3/W
    Volume_to_coolingPower_Brayton = parameters(8); %m^3/W
    Mass_contingency = parameters(9);
    Power_contingency = parameters(10);
end

%Cost
if nargin < 3
    DDTE_const = 2.5158;
    DDTE_exp = 0.4193;
    Unit_const = 0.4407;
    Unit_exp = 0.4957;
    DDTE_multi = 0.4292;
    Unit_multi = 0.4962;
else
    DDTE_const = cost_vector(1);
    DDTE_exp = cost_vector(2);
    Unit_const = cost_vector(3);
    Unit_exp = cost_vector(4);
    DDTE_multi = cost_vector(5);
    Unit_multi = cost_vector(6);
end

%%%%%%%%%%%%%%%%%%%%%%%%%%%%%%%%%%%%%%%%%%%%%%%%%%%%%%%%%%%%%%%%%%%%%%%%%%%%%%%
%Calculations
%%%%%%%%%%%%%%%%%%%%%%%%%%%%%%%%%%%%%%%%%%%%%%%%%%%%%%%%%%%%%%%%%%%%%%%%%%%%%%%
```

```
%Production rate
O2_production_rate = O2_mass / production_time; %kg/hr

%Power calculations
Cooldown_enthalpy = -82.6 + 0.912 * O2_input_temp; %J/g
Ambient_enthalpy = -82.6 + 0.912 * Daytime_temp; %J/g
Enthalpy_cryocool = -82.6 + 0.912 * Tank_temp; %J/g
Cooldown_deltah = Cooldown_enthalpy - Ambient_enthalpy; %J/g
Liquifaction_deltah = Ambient_enthalpy - Enthalpy_cryocool; %J/g
Total_deltah = Liquifaction_deltah + O2_latent_heat + Cooldown_deltah; %J/g
Liquifaction_heat_load = Total_deltah * O2_production_rate / Cycle_eff *
    1000/3600; %W
Stirling_power = Liquifaction_heat_load / Power_eff_Stirling; %W
Brayton_power = Liquifaction_heat_load / Power_eff_Brayton; %W

%Mass and volume calculations
%Stirling_mass = (Liquifaction_heat_load^0.7 * ((Daytime_temp - Tank_temp)/
    Tank_temp)^1.45) * (1 + Mass_contingency); %kg
Stirling_mass = (Liquifaction_heat_load^0.7 * ((Daytime_temp - Tank_temp)/
    Tank_temp)^1.45) * (1 + MassMargin('T')); %kg
%Brayton_mass = (172 * Tank_temp^-0.85 * Liquifaction_heat_load^0.52) * (1
    + Mass_contingency); %kg
Brayton_mass = (172 * Tank_temp^-0.85 * Liquifaction_heat_load^0.52) * (1 +
     MassMargin('T')); %kg
Stirling_volume = Liquifaction_heat_load * Volume_to_coolingPower_Stirling;
     %m^3
Brayton_volume = Liquifaction_heat_load * Volume_to_coolingPower_Brayton; %
    m^3
```

```
%Output calculations
if Stirling_mass < Brayton_mass
    OUTPUT_system_mass = Stirling_mass; %kg
    OUTPUT_system_power = Stirling_power * (1 + Power_contingency); %W
    OUTPUT_system_volume = Stirling_volume; %m^3
else
    OUTPUT_system_mass = Brayton_mass; %kg
    OUTPUT_system_power = Brayton_power * (1 + Power_contingency); %W
    OUTPUT_system_volume = Brayton_volume; %m^3
end

%Cost
DDTE_cost = DDTE_const * OUTPUT_system_mass ^ DDTE_exp / DDTE_multi;
Unit_cost = Unit_const * OUTPUT_system_mass ^ Unit_exp / Unit_multi;

output = [OUTPUT_system_mass; OUTPUT_system_power; OUTPUT_system_volume;
   DDTE_cost; Unit_cost];
```

A.1.10 Hydrogen Cryocooler

```
%This program is based on the CH4 cryocooler to estimate
%parameters of a surface LH2 cryocooler (either Stirling or Brayton).
%
%It is estimated that due to the decreasing supply of H2 available, this
%function will oversize the cryocooler.
%
%Input is a two element vector
%  input(1) = Hydrogen to cool in kg
%  input(2) = production time in hr
```

```
%
%Parameters is an optional vector (length 10) containing alternative values
%to the default parameters values. If ommited, the default values will be
%used.
%
%Cost_vector is an optional vector (length 6) containing constants and
%exponents for DDT&E and production cost for each subcomponent (specific to
%a given model). If ommitted, the neutral values will be used.
%
%Output is a three element vector
%  output(1) = Total system mass in kg
%  output(2) = Total system power required in W
%  output(3) = Total system volume in m^3
%  output(4) = DDT&E cost in 2006 $M for 2015 launch date from NAFCOM CERs
%  output(5) = Production cost in 2006 $M for 2015 launch date from NAFCOM
    CERs

function output = ISRU_H2Cryocooler(input, parameters, cost_vector);

%Input processing
H2_mass = input(1); %kg
production_time = input(2); %hr

%Parameters
if nargin < 2
    Daytime_temp = 240; %K
    Tank_temp = 20; %K
    Cycle_eff = 0.98;
    H2_latent_heat = 454.3; %J/g
```

```
    Power_eff_Stirling = 0.07;
    Power_eff_Brayton = 0.07;
    Volume_to_coolingPower_Stirling = 7.10 * 10^-5; %m^3/W
    Volume_to_coolingPower_Brayton = 7.10 * 10^-5; %m^3/W
    Mass_contingency = 0.1;
    Power_contingency = 0.1;
else
    Daytime_temp = parameters(1); %K
    Tank_temp = parameters(2); %K
    Cycle_eff = parameters(3);
    H2_latent_heat = parameters(4); %J/g
    Power_eff_Stirling = parameters(5);
    Power_eff_Brayton = parameters(6);
    Volume_to_coolingPower_Stirling = parameters(7); %m^3/W
    Volume_to_coolingPower_Brayton = parameters(8); %m^3/W
    Mass_contingency = parameters(9);
    Power_contingency = parameters(10);
end

%Cost
if nargin < 3
    DDTE_const = 2.5158;
    DDTE_exp = 0.4193;
    Unit_const = 0.4407;
    Unit_exp = 0.4957;
    DDTE_multi = 0.4292;
    Unit_multi = 0.4962;
else
    DDTE_const = cost_vector(1);
```

```
    DDTE_exp = cost_vector(2);
    Unit_const = cost_vector(3);
    Unit_exp = cost_vector(4);
    DDTE_multi = cost_vector(5);
    Unit_multi = cost_vector(6);
end

%%%%%%%%%%%%%%%%%%%%%%%%%%%%%%%%%%%%%%%%%%%%%%%%%%%%%%%%%%%%%%%%%%%%%%%%%%%%
%Calculations
%%%%%%%%%%%%%%%%%%%%%%%%%%%%%%%%%%%%%%%%%%%%%%%%%%%%%%%%%%%%%%%%%%%%%%%%%%%%

%Production rate
H2_production_rate = H2_mass / production_time; %kg/hr

%Power calculations
Ambient_enthalpy = -141.67 + 13 * Daytime_temp; %J/g, Interpolation from
    Figure 4 of CC2
Enthalpy_cryocool = -141.67 + 13 * Tank_temp; %J/g
Liquifaction_deltah = Ambient_enthalpy - Enthalpy_cryocool; %J/g
Total_deltah = Liquifaction_deltah + H2_latent_heat; %J/g
Liquifaction_heat_load = Total_deltah * H2_production_rate / Cycle_eff *
    1000/3600; %W
Stirling_power = Liquifaction_heat_load / Power_eff_Stirling; %W
Brayton_power = Liquifaction_heat_load / Power_eff_Brayton; %W

%Mass and volume calculations
% Stirling_mass = (Liquifaction_heat_load^0.7 * ((Daytime_temp - Tank_temp)
    /Tank_temp)^1.45) * (1 + Mass_contingency); %kg
```

```
% Brayton_mass = (172 * Tank_temp^-0.85 * Liquifaction_heat_load^0.52) * (1
    + Mass_contingency); %kg
Stirling_mass = (Liquifaction_heat_load^0.7 * ((Daytime_temp - Tank_temp)/
   Tank_temp)^1.45) * (1 + MassMargin('T')); %kg
Brayton_mass = (172 * Tank_temp^-0.85 * Liquifaction_heat_load^0.52) * (1 +
    MassMargin('T')); %kg
Stirling_volume = Liquifaction_heat_load * Volume_to_coolingPower_Stirling;
    %m^3
Brayton_volume = Liquifaction_heat_load * Volume_to_coolingPower_Brayton; %
   m^3

%Output calculations
if Stirling_mass < Brayton_mass
    OUTPUT_system_mass = Stirling_mass; %kg
    OUTPUT_system_power = Stirling_power * (1 + Power_contingency); %W
    OUTPUT_system_volume = Stirling_volume; %m^3
else
    OUTPUT_system_mass = Brayton_mass; %kg
    OUTPUT_system_power = Brayton_power * (1 + Power_contingency); %W
    OUTPUT_system_volume = Brayton_volume; %m^3
end

%Cost
DDTE_cost = DDTE_const * OUTPUT_system_mass ^ DDTE_exp / DDTE_multi;
Unit_cost = Unit_const * OUTPUT_system_mass ^ Unit_exp / Unit_multi;

output = [OUTPUT_system_mass; OUTPUT_system_power; OUTPUT_system_volume;
   DDTE_cost; Unit_cost];
```

A.1.11 Water Tank

```
%This program uses the ISRU tool from Spaceworks engineering to estimate
%parameters of a water storage tank system.
%
%Input is a three element vector
%  input(1) = H2O to be stored in kg
%
%Parameters is an optional vector (length 5) containing alternative values
%to the default parameters values. If ommited, the default values will be
%used.
%
%Cost_vector is an optional vector (length 14) containing constants and
%exponents for DDT&E and production cost for each subcomponent (specific to
%a given model). If ommitted, the neutral values will be used.
%
%Output is a three element vector
%  output(1) = Total system mass in kg
%  output(2) = Total system power required in W
%  output(3) = Total system volume in m^3
%  output(4) = DDT&E cost in 2006 $M for 2015 launch date from NAFCOM CERs
%  output(5) = Production cost in 2006 $M for 2015 launch date from NAFCOM
    CERs

function output = ISRU_H2OTank(input, parameters, cost_vector);

%Input processing
H2O_mass = input(1); %kg
```

```
%Parameters
if nargin < 2
    H2O_density = 1000; %kg/m^3
    Tank_fill_frac = 0.9;
    Tank_mass_factor = 5000; %m
    Tank_safety_factor = 2;
    Insulation_density = 1.27; %kg/m^2
else
    H2O_density = parameters(1); %kg/m^3
    Tank_fill_frac = parameters(2);
    Tank_mass_factor = parameters(3); %m
    Tank_safety_factor = parameters(4);
    Insulation_density = parameters(5); %kg/m^2
end

%Cost vector
if nargin < 3
    DDTE_const_therm = 2.7497;
    DDTE_exp_therm = 0.3988;
    DDTE_const_struct = 1.2704;
    DDTE_exp_struct = 0.6847;
    DDTE_const_elect = 0.588;
    DDTE_exp_elect = 0.742;
    Unit_const_therm = 0.5276;
    Unit_exp_therm = 0.4526;
    Unit_const_struct = 0.0925;
    Unit_exp_struct = 0.7645;
    Unit_const_elect = 0.0365;
    Unit_exp_elect = 1.1107;
```

```
    DDTE_multi = 0.4543;
    Unit_multi = 0.5240;
else
    DDTE_const_therm = cost_vector(1);
    DDTE_exp_therm = cost_vector(2);
    DDTE_const_struct = cost_vector(3);
    DDTE_exp_struct = cost_vector(4);
    DDTE_const_elect = cost_vector(5);
    DDTE_exp_elect = cost_vector(6);
    Unit_const_therm = cost_vector(7);
    Unit_exp_therm = cost_vector(8);
    Unit_const_struct = cost_vector(9);
    Unit_exp_struct = cost_vector(10);
    Unit_const_elect = cost_vector(11);
    Unit_exp_elect = cost_vector(12);
    DDTE_multi = cost_vector(13);
    Unit_multi = cost_vector(14);
end

%%%%%%%%%%%%%%%%%%%%%%%%%%%%%%%%%%%%%%%%%%%%%%%%%%%%%%%%%%%%%%%%%%%%%%%%%%%%
%Calculations
%%%%%%%%%%%%%%%%%%%%%%%%%%%%%%%%%%%%%%%%%%%%%%%%%%%%%%%%%%%%%%%%%%%%%%%%%%%%

Volume_water = H2O_mass / H2O_density; %m^3
Volume_tank = Volume_water / Tank_fill_frac; %m^3
Tank_R = (Volume_tank * 0.75 / pi) ^ (1/3); %m
Tank_A = 4 * pi * Tank_R^2; %m^2
Tank_P_bot = H2O_mass * 9.80665 / (Tank_A * 2); %Pa
```

```
Tank_mass = (Tank_P_bot + 101350) * Tank_safety_factor / Tank_mass_factor *
     Volume_tank; %kg
Tank_insulation_mass = Tank_A * Insulation_density; %kg

%Output calculations
%OUTPUT_system_mass = (Tank_mass + Tank_insulation_mass) * (1 +
    Mass_contingency); %kg
OUTPUT_system_mass = (Tank_mass + Tank_insulation_mass) * (1 + MassMargin('
    S')); %kg
OUTPUT_system_power = 0; %W
OUTPUT_system_volume = Volume_tank; %m^3

%Cost calculations
%Cost calculations (from Sabatier)
DDTE_cost = DDTE_const_struct * OUTPUT_system_mass ^ DDTE_exp_struct; %
    $M2006
Unit_cost = Unit_const_struct * OUTPUT_system_mass ^ Unit_exp_struct; %
    $M2006
DDTE_cost = DDTE_cost / DDTE_multi;
Unit_cost = Unit_cost / Unit_multi;

%Final output
output = [OUTPUT_system_mass; OUTPUT_system_power; OUTPUT_system_volume;
    DDTE_cost; Unit_cost];
```

A.1.12 Hydrogen Tank

```
%This program uses the ISRU tool from Spaceworks engineering to estimate
%parameters of an LH2 storage tank system.
%
```

```
%Input is a three element vector
%  input(1) = H2 to be stored in kg
%
%Parameters is an optional vector (length 8) containing alternative values
%to the default parameters values. If ommited, the default values will be
%used.
%
%Cost_vector is an optional vector (length 14) containing constants and
%exponents for DDT&E and production cost for each subcomponent (specific to
%a given model). If ommitted, the neutral values will be used.
%
%Output is a three element vector
%  output(1) = Total system mass in kg
%  output(2) = Total system power required in W
%  output(3) = Total system volume in m^3

function output = ISRU_H2Tank(input, parameters, cost_vector);

%Input processing
H2_mass = input(1); %kg

%Parameters
if nargin < 2
    H2_density = 71; %kg/m^3
    H2_temp = 20; %K
    Tank_mass_factor = 5000; %m
    Tank_safety_factor = 2;
    Tank_barrel_L_to_D = 1;
    Insulation_density = 1.27; %kg/m^2
```

```
    Tank_dome_factor = sqrt(2)/2;
    Mass_contingency = 0.1;
else
    H2_density = parameters(1); %kg/m^3
    H2_temp = parameters(2); %K
    Tank_mass_factor = parameters(3); %m
    Tank_safety_factor = parameters(4);
    Tank_barrel_L_to_D = parameters(5);
    Insulation_density = parameters(6); %kg/m^2
    Tank_dome_factor = parameters(7);
    Mass_contingency = parameters(8);
end

%Cost vector
if nargin < 3
    DDTE_const_therm = 2.7497;
    DDTE_exp_therm = 0.3988;
    DDTE_const_struct = 1.2704;
    DDTE_exp_struct = 0.6847;
    DDTE_const_elect = 0.588;
    DDTE_exp_elect = 0.742;
    Unit_const_therm = 0.5276;
    Unit_exp_therm = 0.4526;
    Unit_const_struct = 0.0925;
    Unit_exp_struct = 0.7645;
    Unit_const_elect = 0.0365;
    Unit_exp_elect = 1.1107;
    DDTE_multi = 0.4543;
    Unit_multi = 0.5240;
```

```
else
    DDTE_const_therm = cost_vector(1);
    DDTE_exp_therm = cost_vector(2);
    DDTE_const_struct = cost_vector(3);
    DDTE_exp_struct = cost_vector(4);
    DDTE_const_elect = cost_vector(5);
    DDTE_exp_elect = cost_vector(6);
    Unit_const_therm = cost_vector(7);
    Unit_exp_therm = cost_vector(8);
    Unit_const_struct = cost_vector(9);
    Unit_exp_struct = cost_vector(10);
    Unit_const_elect = cost_vector(11);
    Unit_exp_elect = cost_vector(12);
    DDTE_multi = cost_vector(13);
    Unit_multi = cost_vector(14);
end

%%%%%%%%%%%%%%%%%%%%%%%%%%%%%%%%%%%%%%%%%%%%%%%%%%%%%%%%%%%%%%%%%%%%%%%%%%%%
%Calculations
%%%%%%%%%%%%%%%%%%%%%%%%%%%%%%%%%%%%%%%%%%%%%%%%%%%%%%%%%%%%%%%%%%%%%%%%%%%%

%Volume calculations
Tank_internal_V = H2_mass / H2_density; %m^3
Tank_diameter = (Tank_internal_V / (0.25 * pi * Tank_barrel_L_to_D + pi / 6
    * Tank_dome_factor)) ^ (1/3); %m
Tank_radius = Tank_diameter / 2; %m
Tank_top_dome_V = (4/3 * pi * Tank_dome_factor * Tank_radius^3) / 2; %m^3
Tank_bottom_dome_V = Tank_top_dome_V; %m^3
```

```
Tank_barrel_V = Tank_internal_V - Tank_top_dome_V - Tank_bottom_dome_V; %m
    ^3

%Mass calculations
Pressure = (0.0003 * H2_temp^4 - 0.0226 * H2_temp^3 + 0.665 * H2_temp^2 -
    8.6511 * H2_temp + 41.55) * 10^5; %Pa
Tank_barrel_length = Tank_diameter * Tank_barrel_L_to_D; %m
Tank_mass = (Pressure + 101350) * Tank_safety_factor * Tank_internal_V /
    9.81 / Tank_mass_factor; %kg
Tank_surface_area = (4 * pi * Tank_dome_factor * Tank_radius^2) + (2 * pi *
     Tank_radius * Tank_barrel_length); %m^2
Tank_insulation_mass = Tank_surface_area * Insulation_density; %kg

%Output calculations
%OUTPUT_system_mass = (Tank_mass + Tank_insulation_mass) * (1 +
    Mass_contingency); %kg
OUTPUT_system_mass = (Tank_mass + Tank_insulation_mass) * (1 + MassMargin('
    S')); %kg
OUTPUT_system_power = 0; %W
OUTPUT_system_volume = Tank_internal_V; %m^3

%Cost calculations
%Cost calculations (from Sabatier)
DDTE_cost = DDTE_const_struct * OUTPUT_system_mass ^ DDTE_exp_struct; %
    $M2006
Unit_cost = Unit_const_struct * OUTPUT_system_mass ^ Unit_exp_struct; %
    $M2006
DDTE_cost = DDTE_cost / DDTE_multi;
Unit_cost = Unit_cost / Unit_multi;
```

```
%Final output
output = [OUTPUT_system_mass; OUTPUT_system_power; OUTPUT_system_volume;
   DDTE_cost; Unit_cost];
```

A.2 Other Code

A.2.1 Methane Mars Ascent Vehicle

```
%CH4 fueled MAV for LVSSS


function output = MAV_Chris(input,stage);
OF_ratio = input(1);


if stage == 1
   %DeltaVReq = -32.7280 * OF_ratio^2 + 225.6452 * OF_ratio + 5103.1227; %
      m/s
   M_inert = 819.3409 * OF_ratio^2 - 6075.3184 * OF_ratio + 17259.08; %kg
   M_prop = 8401.1665 * OF_ratio^2 -61074.2464 * OF_ratio + 158545.9003; %
      kg
   M_pay = 5115; %kg
   IMF = M_inert / (M_inert + M_prop);
   Isp = -12.44356 * OF_ratio ^ 2 + 88.51149 * OF_ratio + 186.22378; %sec
   DDTE_cost = (13.9714 * OF_ratio^2 - 108.06 * OF_ratio + 459.6143) /
      0.3909; %$M 2006
   Unit_cost = (3.3429 * OF_ratio^2 - 25.94 * OF_ratio + 93.9886) /
      0.3623; %$M 2006
else
   M_inert_2 = 115.135 * OF_ratio^2 - 865.3443 * OF_ratio + 6012.4976; %kg
   M_prop_2 = 1003.1557 * OF_ratio^2 - 7204.5482 * OF_ratio + 27851.3917;
      %kg
```

```
    M_pay = 5805;
    M_inert_1 = 430.1632 * OF_ratio^2 - 3178.3405 * OF_ratio + 11704.7342;
       %kg
    M_prop_1 = 3696.9103 * OF_ratio^2 - 26570.9935 * OF_ratio + 83494.6374;
        %kg
    M_inert = M_inert_1 + M_inert_2;
    M_prop = M_prop_1 + M_prop_2;
    IMF = M_inert / (M_inert + M_prop);
    Isp = -12.44356 * OF_ratio ^ 2 + 88.51149 * OF_ratio + 186.22378; %sec
    TranscostOUT = TransCost([1000,M_inert-1000,2,10,0,1,1000,M_prop]);
    DDTE_cost = TranscostOUT(1); %$M 2006
    Unit_cost = TranscostOUT(2); %$M 2006
end
%%%GEOMETRY%%%
F_dens = 422.6; %kg/m^3
O_dens = 1140; %kg/m^3
F_vol = (M_prop/(1+OF_ratio)) / F_dens / 0.95; %m^3
O_vol = (M_prop * OF_ratio / (1+OF_ratio)) / O_dens / 0.95; %m^3
Max_R = 5; %m
%Fuel Tank
if (F_vol*3/4/pi)^(1/3) > Max_R
    F_R = Max_R; %m
    F_L = (F_vol - 4/3*pi*F_R^3)/(pi*F_R^2); %m
else
    F_R = (F_vol*3/4*pi)^(1/3); %m
    F_L = F_R; %m
end
%O2 Tank
if (O_vol*3/4*pi)^(1/3) > Max_R
```

```
    O_R = Max_R; %m
    O_L = (O_vol - 4/3*pi*O_R^3)/(pi*O_R^2); %m
else
    O_R = (O_vol*3/4*pi)^(1/3); %m
    O_L = O_R; %m
end
Total_R = max(F_R,O_R); %m
Total_L = F_L + O_L + 1.5 + 3.5; %m, 1.5 for skirts and intertank, 3.5 for
    capsule
%%%GEOMETRY%%%
output = [M_inert; M_prop; M_pay; IMF; Isp; Total_R; Total_L; DDTE_cost;
    Unit_cost];
```

A.2.2 Ethylene Mars Ascent Vehicle

```
%Ethylene fueled MAV for LVSSS


function output = MAV_Chris_C2H4(input,stage);
OF_ratio = input(1);


if stage == 1
    %DeltaVReq = -32.7280 * OF_ratio^2 + 225.6452 * OF_ratio + 5103.1227; %
        m/s
    M_inert = 674.7835 * OF_ratio^2 - 3377.1277 * OF_ratio + 9605.1455; %kg
    M_prop = 7054.329 * OF_ratio^2 -34320.1126 * OF_ratio + 83358.1576; %kg
    M_pay = 5115; %kg
    IMF = M_inert / (M_inert + M_prop);
    Isp = -18.30709 * OF_ratio ^ 2 + 87.48312 * OF_ratio + 253.50665; %sec
    %%%%%%NEED TO DO%%%%%%%%
```

```
    DDTE_cost = (13.9714 * OF_ratio^2 - 108.06 * OF_ratio + 459.6143) /
        0.3909; %$M 2006
    Unit_cost = (3.3429 * OF_ratio^2 - 25.94 * OF_ratio + 93.9886) /
        0.3623; %$M 2006
else
    M_inert_2 = 149.6173 * OF_ratio^2 - 781.2539 * OF_ratio + 5320.8744; %
        kg
    M_prop_2 = 1297.1305 * OF_ratio^2 - 6289.4745 * OF_ratio + 21530.788; %
        kg
    M_pay = 5805;
    M_inert_1 = 536.4412 * OF_ratio^2 - 2727.8747 * OF_ratio + 8942.9576; %
        kg
    M_prop_1 = 4581.6316 * OF_ratio^2 - 22243.9497 * OF_ratio + 59142.0274;
         %kg
    M_inert = M_inert_1 + M_inert_2;
    M_prop = M_prop_1 + M_prop_2;
    IMF = M_inert / (M_inert + M_prop);
    Isp = -12.44356 * OF_ratio ^ 2 + 88.51149 * OF_ratio + 186.22378; %sec
    TranscostOUT = TransCost([1000,M_inert-1000,2,10,0,1,1000,M_prop]);
    DDTE_cost = TranscostOUT(1); %$M 2006
    Unit_cost = TranscostOUT(2); %$M 2006
end
%%%%%%%%%%%%%%%%%%%%%%%%
%%%GEOMETRY%%%
F_dens = 568; %kg/m^3
O_dens = 1140; %kg/m^3
F_vol = (M_prop/(1+OF_ratio)) / F_dens / 0.95; %m^3
O_vol = (M_prop * OF_ratio / (1+OF_ratio)) / O_dens / 0.95; %m^3
Max_R = 5; %m
```

```
%Fuel Tank
if (F_vol*3/4/pi)^(1/3) > Max_R
    F_R = Max_R; %m
    F_L = (F_vol - 4/3*pi*F_R^3)/(pi*F_R^2); %m
else
    F_R = (F_vol*3/4*pi)^(1/3); %m
    F_L = F_R; %m
end
%O2 Tank
if (O_vol*3/4*pi)^(1/3) > Max_R
    O_R = Max_R; %m
    O_L = (O_vol - 4/3*pi*O_R^3)/(pi*O_R^2); %m
else
    O_R = (O_vol*3/4*pi)^(1/3); %m
    O_L = O_R; %m
end
Total_R = max(F_R,O_R); %m
Total_L = F_L + O_L + 1.5 + 3.5; %m, 1.5 for skirts and intertank, 3.5 for
    capsule
%%%GEOMETRY%%%
output = [M_inert; M_prop; M_pay; IMF; Isp; Total_R; Total_L; DDTE_cost;
    Unit_cost];
```

A.2.3 Methanol Mars Ascent Vehicle

```
%Methanol fueled MAV for LVSSS


function output = MAV_Chris_CH3OH(input,stage);
OF_ratio = input(1);
```

```
if stage == 1;
    %DeltaVReq = -32.7280 * OF_ratio^2 + 225.6452 * OF_ratio + 5103.1227; %
        m/s
    M_inert = 2362.3019 * OF_ratio^2 - 7046.8812 * OF_ratio + 12436.1822; %
        kg
    M_prop = 25683.4786 * OF_ratio^2 -74035.6345 * OF_ratio + 112933.4429;
        %kg
    M_pay = 5115; %kg
    IMF = M_inert / (M_inert + M_prop);
    Isp = -25.91663 * OF_ratio ^ 2 + 71.76811 * OF_ratio + 274.5178; %sec
    %%%%%%NEED TO DO%%%%%%%%
    DDTE_cost = (13.9714 * OF_ratio^2 - 108.06 * OF_ratio + 459.6143) /
        0.3909; %$M 2006
    Unit_cost = (3.3429 * OF_ratio^2 - 25.94 * OF_ratio + 93.9886) /
        0.3623; %$M 2006
else
    M_inert_2 = 299.8875 * OF_ratio^2 - 942.7401 * OF_ratio + 5439.8083; %
        kg
    M_prop_2 = 2614.2575 * OF_ratio^2 - 7420.3477 * OF_ratio + 22081.232; %
        kg
    M_pay = 5805;
    M_inert_1 = 1198.8736 * OF_ratio^2 - 3624.8274 * OF_ratio + 9647.5884;
        %kg
    M_prop_1 = 10376.5199 * OF_ratio^2 - 29491.4197 * OF_ratio + 63988.449;
         %kg
    M_inert = M_inert_1 + M_inert_2;
    M_prop = M_prop_1 + M_prop_2;
    IMF = M_inert / (M_inert + M_prop);
    Isp = -12.44356 * OF_ratio ^ 2 + 88.51149 * OF_ratio + 186.22378; %sec
```

```
    TranscostOUT = TransCost([1600,M_inert-1600,2,10,0,1,1000,M_prop]);
    DDTE_cost = TranscostOUT(1); %$M 2006
    Unit_cost = TranscostOUT(2); %$M 2006
end
%%%%%%%%%%%%%%%%%%%%%%%%
%%%GEOMETRY%%%
F_dens = 786.5; %kg/m^3
O_dens = 1140; %kg/m^3
F_vol = (M_prop/(1+OF_ratio)) / F_dens / 0.95; %m^3
O_vol = (M_prop * OF_ratio / (1+OF_ratio)) / O_dens / 0.95; %m^3
Max_R = 5; %m
%Fuel Tank
if (F_vol*3/4/pi)^(1/3) > Max_R
    F_R = Max_R; %m
    F_L = (F_vol - 4/3*pi*F_R^3)/(pi*F_R^2); %m
else
    F_R = (F_vol*3/4*pi)^(1/3); %m
    F_L = F_R; %m
end
%O2 Tank
if (O_vol*3/4*pi)^(1/3) > Max_R
    O_R = Max_R; %m
    O_L = (O_vol - 4/3*pi*O_R^3)/(pi*O_R^2); %m
else
    O_R = (O_vol*3/4*pi)^(1/3); %m
    O_L = O_R; %m
end
Total_R = max(F_R,O_R); %m
```

```
Total_L = F_L + O_L + 1.5 + 3.5; %m, 1.5 for skirts and intertank, 3.5 for
    capsule
%%%GEOMETRY%%%
output = [M_inert; M_prop; M_pay; IMF; Isp; Total_R; Total_L; DDTE_cost;
    Unit_cost];
```

A.2.4 Hydrogen Mars Ascent Vehicle

```
%LH2 fueled MAV for LVSSS


function output = MAV_Chris_H2(input,stage);
OF_ratio = input(1);


if stage == 1;
    %DeltaVReq = -32.7280 * OF_ratio^2 + 225.6452 * OF_ratio + 5103.1227; %
        m/s
    M_inert = 60.9351 * OF_ratio^2 - 751.9506 * OF_ratio + 6458.6537; %kg
    M_prop = 364.7965 * OF_ratio^2 -3944.2987 * OF_ratio + 35378.3593; %kg
    M_pay = 5115; %kg
    IMF = M_inert / (M_inert + M_prop);
    Isp = -2.01385 * OF_ratio ^ 2 + 19.30519 * OF_ratio + 396.5039; %sec
    %%%%%%NEED TO DO%%%%%%%%
    DDTE_cost = (13.9714 * OF_ratio^2 - 108.06 * OF_ratio + 459.6143) /
        0.3909; %$M 2006
    Unit_cost = (3.3429 * OF_ratio^2 - 25.94 * OF_ratio + 93.9886) /
        0.3623; %$M 2006
else
    M_inert_2 = 14.1652 * OF_ratio^2 - 187.7436 * OF_ratio + 4588.0218; %kg
    M_prop_2 = 80.3790 * OF_ratio^2 - 828.4688 * OF_ratio + 12071.2546; %kg
    M_pay = 5805;
```

```
    M_inert_1 = 39.9118 * OF_ratio^2 - 500.5041 * OF_ratio + 5840.0178; %kg
    M_prop_1 = 236.5494 * OF_ratio^2 - 2467.6305 * OF_ratio + 26052.3452; %
        kg
    M_inert = M_inert_1 + M_inert_2;
    M_prop = M_prop_1 + M_prop_2;
    IMF = M_inert / (M_inert + M_prop);
    Isp = -12.44356 * OF_ratio ^ 2 + 88.51149 * OF_ratio + 186.22378; %sec
    TranscostOUT = TransCost([1000,M_inert-1000,3,10,0,1,1000,M_prop]);
    DDTE_cost = TranscostOUT(1); %$M 2006
    Unit_cost = TranscostOUT(2); %$M 2006
end
%%%%%%%%%%%%%%%%%%%%%%%%

%%%GEOMETRY%%%
F_dens = 71; %kg/m^3
O_dens = 1140; %kg/m^3
F_vol = (M_prop/(1+OF_ratio)) / F_dens / 0.95; %m^3
O_vol = (M_prop * OF_ratio / (1+OF_ratio)) / O_dens / 0.95; %m^3
Max_R = 5; %m
%Fuel Tank
if (F_vol*3/4/pi)^(1/3) > Max_R
    F_R = Max_R; %m
    F_L = (F_vol - 4/3*pi*F_R^3)/(pi*F_R^2); %m
else
    F_R = (F_vol*3/4*pi)^(1/3); %m
    F_L = F_R; %m
end
%O2 Tank
if (O_vol*3/4*pi)^(1/3) > Max_R
```

```
    O_R = Max_R; %m
    O_L = (O_vol - 4/3*pi*O_R^3)/(pi*O_R^2); %m
else
    O_R = (O_vol*3/4*pi)^(1/3); %m
    O_L = O_R; %m
end
Total_R = max(F_R,O_R); %m
Total_L = F_L + O_L + 1.5 + 3.5; %m, 1.5 for skirts and intertank, 3.5 for
    capsule
%%%GEOMETRY%%%
output = [M_inert; M_prop; M_pay; IMF; Isp; Total_R; Total_L; DDTE_cost;
    Unit_cost];
```

A.2.5 Mars Descent Vehicle

```
%beta = 4.2857 * 10^-3 from DRA 5 (p. 33) 300m^2/69.8T->kg
%beta = 2.3734 * 10^-3 from DRA 5 Addendum (p. 182)
%Prop_mass_frac = 0.1977 from 13.8/(110.2-40.4) on p.33
%Eng_mass_frac = 0.0235 from 16.4 * 0.1 / (69.8) on p.33
%Sys_mass_frac = 0.2115 from 16.4 * 0.9 / (69.8) on p.33


function output = MDV(V_vector, R_max, MAV_R, MAV_L, prop_type, payload,
    beta, Prop_mass_frac, Eng_mass_frac, Sys_mass_frac)
if V_vector == [0];
    R_vector = [0];
    L_vector = [0];
else
    R_vector = zeros(length(V_vector),1);
    L_vector = zeros(length(V_vector),1);
```

```
    shapeflag_vector = zeros(length(V_vector),1); %0 for sphere, 1 for
        cylinder
    for i = 1:length(V_vector)
        V = V_vector(i);
        R_sphere = (3/4/pi*V)^(1/3);
        if R_sphere > R_max
            R_vector(i) = R_max;
            h_barrel = (V - 4/3*pi*R_max^3)/(pi*R_max^2);
            L_vector(i) = h_barrel + 2 * R_max;
            SA = 4*pi*R_max^2 + 2*pi*R_max*h_barrel;
            shapeflag_vector(i) = 1;
        else
            R_vector(i) = R_sphere;
            L_vector(i) = R_vector(i);
            SA = 4*pi*R_sphere^2;
            shapeflag_vector(i) = 0;
        end
    end
end
if nargin < 7
    beta = 4.2857*10^-3;
end
R_star = max(max(R_vector),MAV_R);
L_total = sum(L_vector) + MAV_L;
ProjArea = 2 * R_star * L_total;
Mass_MDV = ProjArea / beta;
Power = 0;
MDV_volume = 2/3*pi*R_star^3 + pi * R_star^2 * (L_total - R_star);
```

```
%%%%%Transcost Costing%%%%%
if nargin < 8
    Prop_mass_frac = 0.1977;
end
if nargin < 9
    Eng_mass_frac = 0.0235;
end
if nargin < 10
    Sys_mass_frac = 0.2115;
end

M_prop = Mass_MDV * Prop_mass_frac; %kg
M_sys = Mass_MDV * Sys_mass_frac; %kg

M_eng = (M_sys + payload) * 3.711 * 1.2 / 80 / 3.711; %kg, Mars gravity
    3.711 Earth, T/W sys = 1.2, T/W_eng = 200
TranscostOUT = TransCost([M_eng,M_sys-M_eng,prop_type,10,0,1,100,M_prop]);
DDTE = TranscostOUT(1);
Unit = TranscostOUT(2);

output = [Mass_MDV;Power;MDV_volume;DDTE;Unit];
```

A.2.6 Mars Transfer Vehicle

```
function output = MTV(payload, IMF, Isp, deltaV, margin, prop_type,
    Eng_mass_frac);

MR = exp(deltaV / 9.80665 / Isp);
M_prop = payload * (1 - IMF) * (MR - 1) / (1 - IMF * MR) * (1 + margin(1));
     %kg
```

```
M_sys = IMF / (1 - IMF) * M_prop; %kg
if nargin < 7
    Eng_mass_frac = 0.0235;
end
M_eng = (M_sys + payload + M_prop) * 0.2 / 20; %Earth gravity, T/Wsys of
    0.2, T/W_eng of 20
TranscostOUT = TransCost([M_eng,M_sys-M_eng,prop_type,10,0,1,1000,M_prop]);
DDTE = TranscostOUT(1);
Unit = TranscostOUT(2);

output = [M_sys, M_prop, payload, DDTE, Unit];
```

A.2.7 Transcost

```
%mass_engine and mass_vehicle are in kg
%
%Set type = 1 for storable, type = 2 for cryogenic other, type = 3 for H2
%
%Rate newness on a scale from 0 (minor variation of existing project) to 10
%(first generation system, new concept approach, involving new techniques
%and new technologies).
%
%Rate strength of team on a scale from 0 (team has superior experience with
%this type of project) to 10 (new team with no relevant direct company
%experience)
%
%n is number of engines
%
%nq is number of quality engine firings; set to 1 for storable
%
```

```
%mass_propellant is in kg
%
%Outputs DDTE and Unit cost in $M2006

function output = TransCost(input);
mass_engine = input(1); %kg
mass_vehicle = input(2); %kg
prop_type = input(3);
newness = input(4);
teamness = input(5);
n = input(6);
nq = input(7);
mass_propellant = input(8); %kg

%Teamness transform
teamness = teamness * 0.8;

%Factor calculations
f1 = 0.4 + newness / 10;
f2 = 0.026 * log(nq) * log(nq);
f3 = 0.4 + teamness / 10;
if prop_type == 3
    kstar = 1.9726 * mass_propellant ^ -0.2705 / (mass_vehicle /
        mass_propellant);
else
    kstar = 5.2014 * mass_propellant ^ -0.4036 / (mass_vehicle /
        mass_propellant);
end
```

```
%Work-year calculations
if prop_type == 1
    H_E_D = 16.3 * mass_engine ^ 0.54 * f1 * f3;
    H_V_D = 100 * mass_vehicle ^ 0.555 * f1 * f3 * kstar;
    H_E_U = 1.9 * mass_engine ^ 0.535 * n;
    H_V_U = 1.4388 * mass_vehicle ^ 0.5932;
else
    H_E_D = 277 * mass_engine ^ 0.48 * f1 * f2 * f3;
    H_V_D = 100 * mass_vehicle ^ 0.555 * f1 * f3 * kstar;
    H_E_U = 3.15 * mass_engine ^ 0.535 * n;
    H_V_U = 1.4182 * mass_vehicle ^ 0.6464;
end

%Convert work-years to $M2006
DDTE_cost = (H_E_D + H_V_D) * 259200 / 10^6; %$M2006
Unit_cost = (H_E_U + H_V_U) * 259200 / 10^6; %$M2006

output = [DDTE_cost;Unit_cost];
```

A.2.8 Integrated Architecture Example

This example is for the architecture producing ethylene from hydrogen brought from Earth.

```
function output = OMNI_C2H4_EH2(input,pertname,dist_type,parameter_value,
    use_mod_dvx,npv_vect,paramequalsthis);

%pername = 'all' to run on all variables permitted by control vectors,
%input any number for pertvector(1)

%pertvector(1) = parameter number within .m file
```

```
%pertvector(2) = low for trid
%pertvector(3) = high for trid

% timerseed = clock;
% rand('state',input(1)*timerseed(6));

%Input processing
OF_ratio = input(1);
total_production_time = input(2); %hr
days_of_operation = input(3); %days
R_max = input(4); %m
MTV_Isp = input(5); %sec
MTV_IMF = input(6);
MTV_deltaV = input(7); %m/s
MTV_margin = input(8);
Launch_cost = input(9); %$/kg to LEO
if length(input) < 10,
    alpha = 0;
else
    alpha = input(10);
end
if length(input) < 11,
    V_alpha = 0;
else
    V_alpha = input(11);
end

ndr = npv_vect(1);
startyear = npv_vect(2);
```

```
usebeta_flag = npv_vect(3);



%MAV Computation
MAV_output = MAV_Chris_C2H4(OF_ratio,2);
Prop_demanded = MAV_output(2);%kg

%Parameters
Piping_fraction = 0.2;
if nargin < 4
    parameter_value = 0;
else
    if strcmp(pertname, 'all') == 1
        parameter_value = 0;
    end
end
if nargin < 5
    use_mod_dvx = 0;
end
%%%%%%%%%%%%%%%%%%%%%%%%%%%%%%%%%%%%%%%%%%%%%%%%%%%%%%%%%%%%%%%%%%%%%%%%%%%%
%Calculations
%%%%%%%%%%%%%%%%%%%%%%%%%%%%%%%%%%%%%%%%%%%%%%%%%%%%%%%%%%%%%%%%%%%%%%%%%%%%

%Input calculations
daily_operation_time = total_production_time / days_of_operation; %hr
C2H4_demanded = Prop_demanded / (1 + OF_ratio); %kg
O2_demanded = Prop_demanded - C2H4_demanded; %kg

%%%%%%%%%%%%%%%%%%%%%%%%%%%%%%%%%%%%%%%%%%%%%%%%%%%%%%%%%%%%%%%%%%%%%%%%%%%%
```

```
%Technology Definitions
%%%%%%%%%%%%%%%%%%%%%%%%%%%%%%%%%%%%%%%%%%%%%%%%%%%%%%%%%%%%%%%%%%%%%%%%%%%%
ISRU_RWGS_C2H4 = Technology('ISRU_RWGS_C2H4');
ISRU_RWGS_C2H4.ParameterVector =
    [873;1;0.025;2;2;7850;1.5;3;80;0.1;1;0.97;14.57;1.102;2;50;14;0.033;0.2;0.8;0.25;1.08


ISRU_RWGS_C2H4.ControlVector =
    [1;1;1;1;1;1;1;1;1;1;1;1;0;0;1;1;1;1;1;1;1;1;1;1;1;1;1;1;1;1;1;1;1;1;1;1;1;1;1;1;1];


ISRU_RWGS_C2H4.CostVector =
    [2.7497;0.3988;1.2704;0.6847;0.588;0.742;0.5276;0.4526;0.0925;0.7645;0.0365;1.1107;0.


ISRU_RWGS_C2H4.DistributionVectrix = ISRU_RWGS_C2H4_dvx(use_mod_dvx);


ISRU_H2OElectrolyzer = Technology('ISRU_H2OElectrolyzer');
ISRU_H2OElectrolyzer.ParameterVector =
    [0.03;1.5;298;0.000298;0.168;0.016;0.1;0.15;230;1000;0.9;5000;2;0.98;0.1;0.1];
     %modified 23 to 230
ISRU_H2OElectrolyzer.ControlVector = [1;1;1;1;1;1;1;1;1;1;0;1;1;0;1;1];
ISRU_H2OElectrolyzer.CostVector =
    [0.5357;0.6705;0.2677;0.8403;0.2619;0.7003;0.1017;0.8886;0.4494;0.2866;0.1667;0.5198;


ISRU_H2OElectrolyzer.DistributionVectrix = ISRU_H2OElectrolyzer_dvx(
    use_mod_dvx);


ISRU_CO2Adsorber = Technology('ISRU_CO2Adsorber');
ISRU_CO2Adsorber.ParameterVector =
    [0.95;0.87;523.16;600;6;0.8;642.86;3.6;2;5000;1.27;0.063;2700;0.0003;7.65;0.1;1.27*10
```

```
ISRU_CO2Adsorber.ControlVector =
    [0;0;1;1;1;1;1;1;1;1;1;1;1;1;1;1;1;1;0;1;1;1;1;1;1];
ISRU_CO2Adsorber.CostVector =
    [0.4267;0.6376;2.4798;0.4194;0.0795;0.7313;0.4611;0.489;0.4471;0.5086];
ISRU_CO2Adsorber.DistributionVectrix = ISRU_CO2Adsorber_dvx(use_mod_dvx);

ISRU_H2Cryocooler = Technology('ISRU_H2Cryocooler');
ISRU_H2Cryocooler.ParameterVector =
    [240;20;0.98;454.3;0.07;0.07;7.1*10^-5;7.1*10^-5;0.1;0.1];
ISRU_H2Cryocooler.ControlVector = [0;0;0;0;1;1;1;1;1;1];
ISRU_H2Cryocooler.CostVector = [2.5158;0.4193;0.4407;0.4957;0.4292;0.4962];
ISRU_H2Cryocooler.DistributionVectrix = ISRU_H2Cryocooler_dvx(use_mod_dvx);

ISRU_O2Cryocooler = Technology('ISRU_O2Cryocooler');
ISRU_O2Cryocooler.ParameterVector =
    [240;90;0.98;213;0.07;0.07;7.1*10^-5;7.1*10^-5;0.1;0.1];
ISRU_O2Cryocooler.ControlVector = [0;0;0;0;1;1;1;1;1;1];
ISRU_O2Cryocooler.CostVector = [2.5158;0.4193;0.4407;0.4957;0.4292;0.4962];
ISRU_O2Cryocooler.DistributionVectrix = ISRU_O2Cryocooler_dvx(use_mod_dvx);

ISRU_H2Tank = Technology('ISRU_H2Tank');
ISRU_H2Tank.ParameterVector = [71;20;5000;2;1;1.27;sqrt(2)/2;0.1];
ISRU_H2Tank.ControlVector = [0;0;1;1;1;1;1;1];
ISRU_H2Tank.CostVector =
    [2.7497;0.3988;1.2704;0.6847;0.588;0.742;0.5276;0.4526;0.0925;0.7645;0.0365;1.1107;0.

ISRU_H2Tank.DistributionVectrix = ISRU_H2Tank_dvx(use_mod_dvx);
%%%%%%%%%%%%%%%%%%%%%%%%%%%%%%%%%%%%%%%%%%%%%%%%%%%%%%%%%%%%%%%%%%%%%%%%%%%%
```

```
%Pertvector handling
if nargin > 1
    if strcmp(pertname, 'none') ~= 1
        if strcmp(pertname, 'all') ~= 1
            param_handle = strcat(pertname,'.ParameterVector');
            control_handle = strcat(pertname,'.ControlVector');
            dvx_handle = strcat(pertname,'.DistributionVectrix');
            control2 = zeros(length(eval(control_handle)),1);
            control2(parameter_value) = 1;
            if isnan(paramequalsthis) ~= 1
                neoparam = zeros(length(eval(control_handle)),1);
                neoparam(parameter_value) = paramequalsthis;
                random_para_vector = neoparam .* control2 + comp(control2) .*
                     eval(param_handle);
            else
                random_para_vector = (UseDVX(eval(dvx_handle),dist_type,eval(
                    param_handle)))' .* control2 + comp(control2) .* eval(
                    param_handle);
            end
        end
    end
end



%C2H4 RWGS calculation
if nargin > 1
    if strcmp(pertname, 'all') == 1
        ISRU_RWGS_C2H4.ParameterVector = UseDVX(ISRU_RWGS_C2H4.
            DistributionVectrix,dist_type,ISRU_RWGS_C2H4.ParameterVector);
```

```
        %ISRU_RWGS_C2H4.ParameterVector = ((ones(length(ISRU_RWGS_C2H4.
            ControlVector),1) .* trid([pertvector(2),1,pertvector(3)],length
            (ISRU_RWGS_C2H4.ControlVector),1)) .* ISRU_RWGS_C2H4.
            ControlVector + comp(ISRU_RWGS_C2H4.ControlVector)) .*
            ISRU_RWGS_C2H4.ParameterVector;
    else
        if strcmp(pertname, 'ISRU_RWGS_C2H4') == 1
            ISRU_RWGS_C2H4.ParameterVector = random_para_vector;
        end
    end
end
ISRU_RWGS_C2H4.InputVector = [Prop_demanded;OF_ratio;total_production_time
    ];
H2_required = ISRU_RWGS_C2H4.OutputVector(4); %kg
CO2_required_C2H4 = ISRU_RWGS_C2H4.OutputVector(5); %kg
H2O_electrolyzer = ISRU_RWGS_C2H4.OutputVector(6); %kg


%Water electrolysis calculation
if nargin > 1
    if strcmp(pertname, 'all') == 1
        ISRU_H2OElectrolyzer.ParameterVector = UseDVX(ISRU_H2OElectrolyzer.
            DistributionVectrix,dist_type,ISRU_H2OElectrolyzer.
            ParameterVector);
        %ISRU_H2OElectrolyzer.ParameterVector = ((ones(length(
            ISRU_H2OElectrolyzer.ControlVector),1) .* trid([pertvector(2),1,
            pertvector(3)],length(ISRU_H2OElectrolyzer.ControlVector),1)) .*
             ISRU_H2OElectrolyzer.ControlVector + comp(ISRU_H2OElectrolyzer.
            ControlVector)) .* ISRU_H2OElectrolyzer.ParameterVector;
```

```
    else
        if strcmp(pertname, 'ISRU_H2OElectrolyzer') == 1
            ISRU_H2OElectrolyzer.ParameterVector = random_para_vector;
        end
    end
end
ISRU_H2OElectrolyzer.InputVector = [H2O_electrolyzer, total_production_time
    ];
O2_from_Sab = ISRU_H2OElectrolyzer.OutputVector(5); %kg
O2_from_other = O2_demanded - O2_from_Sab; %kg
O2_exit_temp = ISRU_H2OElectrolyzer.OutputVector(6); %K

%CO2 adsorber calculation
if nargin > 1
    if strcmp(pertname, 'all') == 1
        ISRU_CO2Adsorber.ParameterVector = UseDVX(ISRU_CO2Adsorber.
            DistributionVectrix,dist_type,ISRU_CO2Adsorber.ParameterVector);
        %ISRU_CO2Adsorber.ParameterVector = ((ones(length(ISRU_CO2Adsorber.
            ControlVector),1) .* trid([pertvector(2),1,pertvector(3)],length
            (ISRU_CO2Adsorber.ControlVector),1)) .* ISRU_CO2Adsorber.
            ControlVector + comp(ISRU_CO2Adsorber.ControlVector)) .*
            ISRU_CO2Adsorber.ParameterVector;
    else
        if strcmp(pertname, 'ISRU_CO2Adsorber') == 1
            ISRU_CO2Adsorber.ParameterVector = random_para_vector;
        end
    end
end
```

```
ISRU_CO2Adsorber.InputVector = [CO2_required_C2H4, days_of_operation,
    daily_operation_time];

%Cyrocooler calculations
if nargin > 1
    if strcmp(pertname, 'all') == 1
        ISRU_O2Cryocooler.ParameterVector = UseDVX(ISRU_O2Cryocooler.
            DistributionVectrix,dist_type,ISRU_O2Cryocooler.ParameterVector)
            ;
        %ISRU_O2Cryocooler.ParameterVector = ((ones(length(ISRU_O2Cryocooler
            .ControlVector),1) .* trid([pertvector(2),1,pertvector(3)],
            length(ISRU_O2Cryocooler.ControlVector),1)) .* ISRU_O2Cryocooler
            .ControlVector + comp(ISRU_O2Cryocooler.ControlVector)) .*
            ISRU_O2Cryocooler.ParameterVector;
        ISRU_H2Cryocooler.ParameterVector = UseDVX(ISRU_H2Cryocooler.
            DistributionVectrix,dist_type,ISRU_H2Cryocooler.ParameterVector)
            ;
        %ISRU_H2Cryocooler.ParameterVector = ((ones(length(ISRU_H2Cryocooler
            .ControlVector),1) .* trid([pertvector(2),1,pertvector(3)],
            length(ISRU_H2Cryocooler.ControlVector),1)) .* ISRU_H2Cryocooler
            .ControlVector + comp(ISRU_H2Cryocooler.ControlVector)) .*
            ISRU_H2Cryocooler.ParameterVector;
    else
        if strcmp(pertname, 'ISRU_O2Cryocooler') == 1
            ISRU_O2Cryocooler.ParameterVector = random_para_vector;
        end
        if strcmp(pertname, 'ISRU_H2Cryocooler') == 1
            ISRU_H2Cryocooler.ParameterVector = random_para_vector;
        end
```

```
    end
end
ISRU_O2Cryocooler.InputVector = [O2_demanded; total_production_time;
    O2_exit_temp];
ISRU_H2Cryocooler.InputVector = [H2_required; total_production_time];

%H2 Tank Sizing
if nargin > 1
    if strcmp(pertname, 'all') == 1
        ISRU_H2Tank.ParameterVector = UseDVX(ISRU_H2Tank.DistributionVectrix
            ,dist_type,ISRU_H2Tank.ParameterVector);
        %ISRU_H2Tank.ParameterVector = ((ones(length(ISRU_H2Tank.
            ControlVector),1) .* trid([pertvector(2),1,pertvector(3)],length
            (ISRU_H2Tank.ControlVector),1)) .* ISRU_H2Tank.ControlVector +
            comp(ISRU_H2Tank.ControlVector)) .* ISRU_H2Tank.ParameterVector;
    else
        if strcmp(pertname, 'ISRU_H2Tank') == 1
            ISRU_H2Tank.ParameterVector = random_para_vector;
        end
    end
end
ISRU_H2Tank.InputVector = [H2_required];


%Output calculations
Piping_struct_mass = (ISRU_RWGS_C2H4.OutputVector(1) + ISRU_H2OElectrolyzer
    .OutputVector(1) + ISRU_CO2Adsorber.OutputVector(1) + ISRU_O2Cryocooler
    .OutputVector(1) + ISRU_H2Cryocooler.OutputVector(1) + ISRU_H2Tank.
    OutputVector(1)) * Piping_fraction; %kg
```

```
OUTPUT_system_mass = Piping_struct_mass * (1 / Piping_fraction) * (1 +
    Piping_fraction); %kg
OUTPUT_system_power = ISRU_RWGS_C2H4.OutputVector(2) + ISRU_H2OElectrolyzer
    .OutputVector(2) + ISRU_CO2Adsorber.OutputVector(2) + ISRU_O2Cryocooler
    .OutputVector(2) + ISRU_H2Cryocooler.OutputVector(2) + ISRU_H2Tank.
    OutputVector(2); %W
OUTPUT_system_volume = ISRU_RWGS_C2H4.OutputVector(3) +
    ISRU_H2OElectrolyzer.OutputVector(3) + ISRU_CO2Adsorber.OutputVector(3)
     + ISRU_O2Cryocooler.OutputVector(3) + ISRU_H2Cryocooler.OutputVector
    (3) + ISRU_H2Tank.OutputVector(3); %m^3
OUTPUT_system_DDTE_cost = ISRU_RWGS_C2H4.OutputVector(end-1) +
    ISRU_H2OElectrolyzer.OutputVector(end-1) + ISRU_CO2Adsorber.
    OutputVector(end-1) + ISRU_O2Cryocooler.OutputVector(end-1) +
    ISRU_H2Cryocooler.OutputVector(end-1) + ISRU_H2Tank.OutputVector(end-1)
    ;
OUTPUT_system_Unit_cost = ISRU_RWGS_C2H4.OutputVector(end) +
    ISRU_H2OElectrolyzer.OutputVector(end) + ISRU_CO2Adsorber.OutputVector(
    end) + ISRU_O2Cryocooler.OutputVector(end) + ISRU_H2Cryocooler.
    OutputVector(end) + ISRU_H2Tank.OutputVector(end);
OUTPUT_system_wetmass = H2_required; %kg

%%%%%%%%%%%%%%%%%%%%%%%%%%%%%%%%%%%%%%%%%%%%%%%%%%%%%%%%%%%%%%%%%%%%%%%%%%%
%ARCHITECTURE
%%%%%%%%%%%%%%%%%%%%%%%%%%%%%%%%%%%%%%%%%%%%%%%%%%%%%%%%%%%%%%%%%%%%%%%%%%%
%For MDV
Power_output = PowerSystem(OUTPUT_system_power,alpha,V_alpha);
```

```
Volume_vector = [ISRU_RWGS_C2H4.OutputVector(3);ISRU_H2OElectrolyzer.
    OutputVector(3);ISRU_CO2Adsorber.OutputVector(3);ISRU_O2Cryocooler.
    OutputVector(3);ISRU_H2Cryocooler.OutputVector(3);ISRU_H2Tank.
    OutputVector(3);Power_output(3)];
MDV_output = MDV(Volume_vector,R_max,MAV_output(6),MAV_output(7),2,
    OUTPUT_system_mass + OUTPUT_system_wetmass + MAV_output(1) +
    Power_output(1));

%For MTV
total_payload = OUTPUT_system_mass + OUTPUT_system_wetmass + MAV_output(1)
    + Power_output(1) + MDV_output(1);
MTV_output = MTV(total_payload,MTV_IMF,MTV_Isp,MTV_deltaV,MTV_margin,2);

%OMNI totals
OMNI_mass = MTV_output(1) + MTV_output(2) + total_payload * (1 + MTV_margin
    ); %kg
OMNI_power = OUTPUT_system_power; %W
OMNI_volume = sum(Volume_vector) + MAV_output(6)^2 * pi * MAV_output(7); %m
    ^3 landed volume
OMNI_DDTE = OUTPUT_system_DDTE_cost + Power_output(end-1) + MAV_output(end
    -1) + MDV_output(end-1) + MTV_output(end-1); %$M2006
OMNI_Unit = OUTPUT_system_Unit_cost + Power_output(end) + MAV_output(end) +
     MDV_output(end) + MTV_output(end); %$M2006
OMNI_Launchcost = OMNI_mass * Launch_cost / 10^6; %$M2006
OMNI_Ops = 0.3011 * (OMNI_DDTE + OMNI_Unit) ^ 0.785; %$M2006
OMNI_LCC = OMNI_DDTE + OMNI_Unit + OMNI_Launchcost; %$M2006

%NPV
```

```
npv_out = NPV(ndr,startyear,usebeta_flag,OMNI_DDTE,OMNI_Unit,OMNI_Ops,
    OMNI_Launchcost);
OMNI_NPV = sum(npv_out);

%Final output


output = [OMNI_mass OMNI_power OMNI_volume OMNI_LCC OMNI_Launchcost
    OMNI_DDTE OMNI_Unit;
          OUTPUT_system_mass OUTPUT_system_power OUTPUT_system_volume
              OUTPUT_system_wetmass OMNI_NPV OUTPUT_system_DDTE_cost
              OUTPUT_system_Unit_cost;
          parameter_value paramequalsthis NaN NaN NaN NaN NaN];
```

APPENDIX B

ARCHITECTURE RESULTS

The mean masses, powers, volumes, and costs of the elements of each of the nineteen architectures are given in the figures below. For each figure, the masses of the possible ISPP hardware elements, including any fluids brought from Earth (such as fuel when making only oxidizer), are summed in the ISPP row. The DDT&E, Unit, Operations, and Launch costs (at the lower and upper bounds of $2500/kg and $30000/kg for the aggregate ISPP hardware is given on this row. The next two rows give the data for the surface power system at the lower and upper bounds of αs of 23 kg/kWe and 266 kg/kWe. The ISPP hardware and fluids, power system, MAV inert mass, and MAV payload are then used as the inputs into the sizing of the MDV; there are two rows of data for the MDV based on the two values of α. The MDV and its payloads are the payload for the MTV; there are rows for the MTV inert mass and propellant mass for the two values of α.

Figure 130 gives the results for the methane with Earth hydrogen architecture.

Figure 131 gives the results for the ethylene with Earth hydrogen architecture.

Figure 132 gives the results for the methanol with Earth hydrogen architecture.

Figure 133 gives the results for the hydrogen with Earth hydrogen architecture.

Figure 134 gives the results for the methane with Earth water architecture.

Figure 135 gives the results for the ethylene with Earth water architecture.

Figure 136 gives the results for the methanol with Earth water architecture.

Figure 137 gives the results for the hydrogen with Earth water architecture.

Figure 138 gives the results for the methane with Mars water architecture.

Figure 139 gives the results for the ethylene with Mars water architecture.

	Mass (kg)	Power (kWe)	Volume (m^3)	DDTE ($M2006)	Unit ($M2006)	Ops ($M2006)	LC ($M2006) 2.5k	LC ($M2006) 30k
CO2 Adsorber	203	1	0					
Mars Water Excavators	0	0	0					
Mars Water Plant	0	0	0					
Sabatier Reactor	35	0	0					
Ethylene Reactor	0	0	0					
Methanol Reactor	0	0	0					
Water Electrolyzer	624	12	2					
CO2 Electrolyzer	303	8	0					
Methane Cryocooler	96	7	0					
Oxygen Cryocooler	133	9	0					
Hydrogen Cryocooler	330	5	0					
Water Tank	0	0	0					
Hydrogen Tank	673	0	46					
Piping and Structure	479	0	0					
Fluids from Earth	3292	0	0					
ISPP	6168			638	138	56	15	185
Power System 23	960		4	98	29	13	2	29
Power System 266	11101		48	1129	329	92	28	333
MAV Inert	9889		737	2514	168	148	25	297
Payload	5825					0	15	175
MDV Stage 23	36153			666	135	57	90	1085
MDV Stage 266	38622			742	142	62	97	1159
MTV Inert 23	22014			2057	264	132	55	660
MTV Inert 266	27332			2237	302	142	68	820
MTV Prop 23	46353						116	1391
MTV Prop 266	57339						143	1720

Figure 130: Mean results for the methane with Earth hydrogen architecture.

	Mass (kg)	Power (kWe)	Volume (m^3)	DDTE ($M2006)	Unit ($M2006)	Ops ($M2006)	LC ($M2006) 2.5k	LC ($M2006) 30k
CO2 Adsorber	139	1	0					
Mars Water Excavators	0	0	0					
Mars Water Plant	0	0	0					
Sabatier Reactor	0	0	0					
Ethylene Reactor	441	7	0					
Methanol Reactor	0	0	0					
Water Electrolyzer	940	18	2					
CO2 Electrolyzer	0	0	0					
Methane Cryocooler	0	0	0					
Oxygen Cryocooler	127	9	0					
Hydrogen Cryocooler	303	4	0					
Water Tank	0	0	0					
Hydrogen Tank	580	0	40					
Piping and Structure	506	0	0					
Fluids from Earth	2817	0	0					
ISPP	5853			558	135	51	15	176
Power System 23	882		4	90	26	13	2	26
Power System 266	10184		44	1034	298	85	25	306
MAV Inert	9955		692	2555	169	150	25	299
Payload	5825					0	15	175
MDV Stage 23	34142			658	130	57	85	1024
MDV Stage 266	36496			730	137	61	91	1095
MTV Inert 23	21049			2021	256	130	53	631
MTV Inert 266	25874			2192	292	139	65	776
MTV Prop 23	44320						111	1330
MTV Prop 266	54480						136	1634

Figure 131: Mean results for the ethylene with Earth hydrogen architecture.

	Mass (kg)	Power (kWe)	Volume (m^3)	DDTE ($M2006)	Unit ($M2006)	Ops ($M2006)	LC ($M2006) 2.5k	LC ($M2006) 30k
CO2 Adsorber	289	1	1					
Mars Water Excavators	0	0	0					
Mars Water Plant	0	0	0					
Sabatier Reactor	0	0	0					
Ethylene Reactor	0	0	0					
Methanol Reactor	752	15	0					
Water Electrolyzer	1013	19	2					
CO2 Electrolyzer	0	0	0					
Methane Cryocooler	0	0	0					
Oxygen Cryocooler	128	9	0					
Hydrogen Cryocooler	368	6	0					
Water Tank	0	0	0					
Hydrogen Tank	818	0	57					
Piping and Structure	674	0	0					
Fluids from Earth	4064	0	0					
ISPP	8106			660	155	58	20	243
Power System 23	1159		5	119	34	16	3	35
Power System 266	13410		58	1364	396	106	34	402
MAV Inert	11050		766	2777	181	160	28	332
Payload	5825					0	15	175
MDV Stage 23	37118			693	138	59	93	1114
MDV Stage 266	39790			778	146	64	99	1194
MTV Inert 23	23775			2120	277	135	59	713
MTV Inert 266	29965			2324	320	146	75	899
MTV Prop 23	50061						125	1502
MTV Prop 266	63094						158	1893

Figure 132: Mean results for the methanol with Earth hydrogen architecture.

	Mass (kg)	Power (kWe)	Volume (m^3)	DDTE ($M2006)	Unit ($M2006)	Ops ($M2006)	LC ($M2006) 2.5k	LC ($M2006) 30k
CO2 Adsorber	255	1	0					
Mars Water Excavators	0	0	0					
Mars Water Plant	0	0	0					
Sabatier Reactor	0	0	0					
Ethylene Reactor	0	0	0					
Methanol Reactor	0	0	0					
Water Electrolyzer	0	0	0					
CO2 Electrolyzer	589	15	0					
Methane Cryocooler	0	0	0					
Oxygen Cryocooler	106	6	0					
Hydrogen Cryocooler	413	7	0					
Water Tank	0	0	0					
Hydrogen Tank	0	0	0					
Piping and Structure	273	0	0					
Fluids from Earth	5098	0	0					
ISPP	6734			256	61	28	17	202
Power System 23	674		3	69	20	10	2	20
Power System 266	7819		34	798	234	70	20	235
MAV Inert	8143		1420	2324	155	139	20	244
Payload	5825					0	15	175
MDV Stage 23	43025			750	149	63	108	1291
MDV Stage 266	45958			812	157	67	115	1379
MTV Inert 23	24255			2474	280	151	61	728
MTV Inert 266	28428			2641	310	159	71	853
MTV Prop 23	51072						128	1532
MTV Prop 266	59857						150	1796

Figure 133: Mean results for the hydrogen with Earth hydrogen architecture.

	Mass (kg)	Power (kWe)	Volume (m^3)	DDTE ($M2006)	Unit ($M2006)	Ops ($M2006)	LC ($M2006) 2.5k	LC ($M2006) 30k
CO2 Adsorber	76	0	0					
Mars Water Excavators	0	0	0					
Mars Water Plant	0	0	0					
Sabatier Reactor	36	0	0					
Ethylene Reactor	0	0	0					
Methanol Reactor	0	0	0					
Water Electrolyzer	1355	26	3					
CO2 Electrolyzer	0	0	0					
Methane Cryocooler	96	7	0					
Oxygen Cryocooler	133	9	0					
Hydrogen Cryocooler	330	5	0					
Water Tank	258	0	34					
Hydrogen Tank	0	0	0					
Piping and Structure	458	0	0					
Fluids from Earth	29445	0	0					
ISPP	32187			502	138	48	80	966
Power System 23	1086		5	109	32	15	3	33
Power System 266	12533		55	1270	371	101	31	376
MAV Inert	9889		737	2514	168	148	25	297
Payload	5825					0	15	175
MDV Stage 23	35985			830	139	67	90	1080
MDV Stage 266	38568			892	146	70	96	1157
MTV Inert 23	32757			2408	339	151	82	983
MTV Inert 266	38555			2571	376	159	96	1157
MTV Prop 23	68973						172	2069
MTV Prop 266	81181						203	2435

Figure 134: Mean results for the methane with Earth water architecture.

	Mass (kg)	Power (kWe)	Volume (m^3)	DDTE ($M2006)	Unit ($M2006)	Ops ($M2006)	LC ($M2006) 2.5k	LC ($M2006) 30k
CO2 Adsorber	141	1	0					
Mars Water Excavators	0	0	0					
Mars Water Plant	0	0	0					
Sabatier Reactor	0	0	0					
Ethylene Reactor	438	7	0					
Methanol Reactor	0	0	0					
Water Electrolyzer	1577	30	4					
CO2 Electrolyzer	0	0	0					
Methane Cryocooler	0	0	0					
Oxygen Cryocooler	127	9	0					
Hydrogen Cryocooler	304	4	0					
Water Tank	225	0	30					
Hydrogen Tank	0	0	0					
Piping and Structure	562	0	0					
Fluids from Earth	25254	0	0					
ISPP	28628			500	149	49	72	859
Power System 23	1156		5	118	34	16	3	35
Power System 266	13278		57	1366	392	106	33	398
MAV Inert	9955		692	2555	169	150	25	299
Payload	5825					0	15	175
MDV Stage 23	34214			807	135	65	86	1026
MDV Stage 266	36779			876	142	69	92	1103
MTV Inert 23	30577			2343	325	147	76	917
MTV Inert 266	36699			2520	364	157	92	1101
MTV Prop 23	54382						136	1631
MTV Prop 266	77274						193	2318

Figure 135: Mean results for the ethylene with Earth water architecture.

	Mass (kg)	Power (kWe)	Volume (m^3)	DDTE ($M2006)	Unit ($M2006)	Ops ($M2006)	LC ($M2006) 2.5k	LC ($M2006) 30k
CO2 Adsorber	291	1	1					
Mars Water Excavators	0	0	0					
Mars Water Plant	0	0	0					
Sabatier Reactor	0	0	0					
Ethylene Reactor	0	0	0					
Methanol Reactor	758	15	0					
Water Electrolyzer	1904	36	5					
CO2 Electrolyzer	0	0	0					
Methane Cryocooler	0	0	0					
Oxygen Cryocooler	128	9	0					
Hydrogen Cryocooler	366	6	0					
Water Tank	313	0	42					
Hydrogen Tank	0	0	0					
Piping and Structure	751	0	0					
Fluids from Earth	36185	0	0					
ISPP	40696			591	175	55	102	1221
Power System 23	1545		7	158	45	20	4	46
Power System 266	17856		77	1824	534	134	45	536
MAV Inert	11050		766	2777	181	160	28	332
Payload	5825					0	15	175
MDV Stage 23	37259			883	143	70	93	1118
MDV Stage 266	40190			942	152	73	100	1206
MTV Inert 23	37453			2541	369	158	94	1124
MTV Inert 266	45537			2750	417	169	114	1366
MTV Prop 23	78862						197	2366
MTV Prop 266	95883						240	2876

Figure 136: Mean results for the methanol with Earth water architecture.

	Mass (kg)	Power (kWe)	Volume (m^3)	DDTE ($M2006)	Unit ($M2006)	Ops ($M2006)	LC ($M2006) 2.5k	LC ($M2006) 30k
CO2 Adsorber	0	0	0					
Mars Water Excavators	0	0	0					
Mars Water Plant	0	0	0					
Sabatier Reactor	0	0	0					
Ethylene Reactor	0	0	0					
Methanol Reactor	0	0	0					
Water Electrolyzer	1108	21	3					
CO2 Electrolyzer	0	0	0					
Methane Cryocooler	0	0	0					
Oxygen Cryocooler	106	6	0					
Hydrogen Cryocooler	413	7	0					
Water Tank	383	0	54					
Hydrogen Tank	0	0	0					
Piping and Structure	402	0	0					
Fluids from Earth	45521	0	0					
ISPP	47933			409	111	41	120	1438
Power System 23	791		3	80	23	11	2	24
Power System 266	9117		40	912	270	78	23	274
MAV Inert	8143		1420	2324	155	139	20	244
Payload	5825					0	15	175
MDV Stage 23	49321			1010	169	78	123	1480
MDV Stage 266	52402			1056	176	80	131	1572
MTV Inert 23	43973			3162	408	185	110	1319
MTV Inert 266	48692			3298	435	192	122	1461
MTV Prop 23	92588						231	2778
MTV Prop 266	102525						256	3076

Figure 137: Mean results for the hydrogen with Earth water architecture.

	Mass (kg)	Power (kWe)	Volume (m^3)	DDTE ($M2006)	Unit ($M2006)	Ops ($M2006)	LC ($M2006) 2.5k	LC ($M2006) 30k
CO2 Adsorber	76	0	0					
Mars Water Excavators	724	1	2					
Mars Water Plant	560	11	3					
Sabatier Reactor	35	0	0					
Ethylene Reactor	0	0	0					
Methanol Reactor	0	0	0					
Water Electrolyzer	1436	27	3					
CO2 Electrolyzer	0	0	0					
Methane Cryocooler	95	7	0					
Oxygen Cryocooler	133	9	0					
Hydrogen Cryocooler	329	5	0					
Water Tank	0	0	0					
Hydrogen Tank	0	0	0					
Piping and Structure	678	0	0					
Fluids from Earth	0	0	0					
ISPP	4066			539	169	52	10	122
Power System 23	1427		6	147	43	19	4	43
Power System 266	16422		71	1680	489	125	41	493
MAV Inert	9889		737	2514	168	148	25	297
Payload	5825					0	15	175
MDV Stage 23	34327			648	130	56	86	1030
MDV Stage 266	37126			759	140	63	93	1114
MTV Inert 23	20590			2004	253	129	51	618
MTV Inert 266	27948			2260	307	143	70	838
MTV Prop 23	43355						108	1301
MTV Prop 266	58847						147	1765

Figure 138: Mean results for the methane with Mars water architecture.

	Mass (kg)	Power (kWe)	Volume (m^3)	DDTE ($M2006)	Unit ($M2006)	Ops ($M2006)	LC ($M2006) 2.5k	LC ($M2006) 30k
CO2 Adsorber	139	1	0					
Mars Water Excavators	685	1	2					
Mars Water Plant	554	10	3					
Sabatier Reactor	0	0	0					
Ethylene Reactor	438	7	0					
Methanol Reactor	0	0	0					
Water Electrolyzer	1633	31	4					
CO2 Electrolyzer	0	0	0					
Methane Cryocooler	0	0	0					
Oxygen Cryocooler	127	9	0					
Hydrogen Cryocooler	303	4	0					
Water Tank	0	0	0					
Hydrogen Tank	0	0	0					
Piping and Structure	775	0	0					
Fluids from Earth	0	0	0					
ISPP	4654			544	180	53	12	140
Power System 23	1465		6	151	43	19	4	44
Power System 266	16986		74	1742	510	129	42	510
MAV Inert	9955		692	2555	169	150	25	299
Payload	5825					0	15	175
MDV Stage 23	32724			649	127	56	82	982
MDV Stage 266	35496			763	136	63	89	1065
MTV Inert 23	20208			1989	250	128	51	606
MTV Inert 266	27782			2255	305	143	69	833
MTV Prop 23	42549						106	1276
MTV Prop 266	58498						146	1755

Figure 139: Mean results for the ethylene with Mars water architecture.

	Mass (kg)	Power (kWe)	Volume (m^3)	DDTE ($M2006)	Unit ($M2006)	Ops ($M2006)	LC ($M2006) 2.5k	LC ($M2006) 30k
CO2 Adsorber	289	1	1					
Mars Water Excavators	775	1	3					
Mars Water Plant	576	13	4					
Sabatier Reactor	0	0	0					
Ethylene Reactor	0	0	0					
Methanol Reactor	764	15	0					
Water Electrolyzer	1997	38	5					
CO2 Electrolyzer	0	0	0					
Methane Cryocooler	0	0	0					
Oxygen Cryocooler	128	9	0					
Hydrogen Cryocooler	366	6	0					
Water Tank	0	0	0					
Hydrogen Tank	0	0	0					
Piping and Structure	979	0	0					
Fluids from Earth	0	0	0					
ISPP	5874			621	207	59	15	176
Power System 23	1928		8	198	57	23	5	58
Power System 266	22427		97	2257	655	158	56	673
MAV Inert	11050		766	2777	181	160	28	332
Payload	5825					0	15	175
MDV Stage 23	35386			678	133	58	88	1062
MDV Stage 266	38540			814	144	66	96	1156
MTV Inert 23	22458			2073	267	133	56	674
MTV Inert 266	32260			2393	336	150	81	968
MTV Prop 23	47288						118	1419
MTV Prop 266	67926						170	2038

Figure 140: Mean results for the methanol with Mars water architecture.

Figure 140 gives the results for the methanol with Mars water architecture.

Figure 141 gives the results for the hydrogen with Mars water architecture.

Figure 142 gives the results for the methane with only oxygen architecture.

Figure 143 gives the results for the ethylene with only oxygen architecture.

Figure 144 gives the results for the methanol with only oxygen architecture.

Figure 145 gives the results for the methane with no ISPP architecture.

Figure 146 gives the results for the ethylene with no ISPP architecture.

Figure 147 gives the results for the methanol with no ISPP architecture.

Figure 148 gives the results for the hydrogen with no ISPP architecture.

	Mass (kg)	Power (kWe)	Volume (m^3)	DDTE ($M2006)	Unit ($M2006)	Ops ($M2006)	LC ($M2006) 2.5k	LC ($M2006) 30k
CO2 Adsorber	0	0	0					
Mars Water Excavators	825	1	3					
Mars Water Plant	594	14	4					
Sabatier Reactor	0	0	0					
Ethylene Reactor	0	0	0					
Methanol Reactor	0	0	0					
Water Electrolyzer	1248	24	3					
CO2 Electrolyzer	0	0	0					
Methane Cryocooler	0	0	0					
Oxygen Cryocooler	106	6	0					
Hydrogen Cryocooler	415	7	0					
Water Tank	0	0	0					
Hydrogen Tank	0	0	0					
Piping and Structure	637	0	0					
Fluids from Earth	0	0	0					
ISPP	3825			431	145	44	10	115
Power System 23	1222		5	125	36	16	3	37
Power System 266	14180		61	1462	424	112	35	425
MAV Inert	8143		1420	2324	155	139	20	244
Payload	5825					0	15	175
MDV Stage 23	46662			746	156	63	117	1400
MDV Stage 266	50254			849	166	69	126	1508
MTV Inert 23	24777			2496	284	152	62	743
MTV Inert 266	31644			2759	332	165	79	949
MTV Prop 23	52171						130	1565
MTV Prop 266	66630						167	1999

Figure 141: Mean results for the hydrogen with Mars water architecture.

	Mass (kg)	Power (kWe)	Volume (m^3)	DDTE ($M2006)	Unit ($M2006)	Ops ($M2006)	LC ($M2006) 2.5k	LC ($M2006) 30k
CO2 Adsorber	387	2	1					
Mars Water Excavators	0	0	0					
Mars Water Plant	0	0	0					
Sabatier Reactor	0	0	0					
Ethylene Reactor	0	0	0					
Methanol Reactor	0	0	0					
Water Electrolyzer	0	0	0					
CO2 Electrolyzer	911	23	0					
Methane Cryocooler	65	3	0					
Oxygen Cryocooler	133	9	0					
Hydrogen Cryocooler	0	0	0					
Water Tank	0	0	0					
Hydrogen Tank	0	0	0					
Piping and Structure	298	0	0					
Fluids from Earth	11509	0	0					
ISPP	13303			247	60	27	33	399
Power System 23	865		4	88	26	12	2	26
Power System 266	10023		44	1025	294	85	25	301
MAV Inert	9889		737	2514	168	148	25	297
Payload	5825					0	15	175
MDV Stage 23	30732			703	124	59	77	922
MDV Stage 266	33122			767	131	63	83	994
MTV Inert 23	22683			2082	269	133	57	680
MTV Inert 266	27464			2245	303	142	69	824
MTV Prop 23	47762						119	1433
MTV Prop 266	57828						145	1735

Figure 142: Mean results for the methane with only oxygen ISPP architecture.

	Mass (kg)	Power (kWe)	Volume (m^3)	DDTE ($M2006)	Unit ($M2006)	Ops ($M2006)	LC ($M2006) 2.5k	LC ($M2006) 30k
CO2 Adsorber	352	2	1					
Mars Water Excavators	0	0	0					
Mars Water Plant	0	0	0					
Sabatier Reactor	0	0	0					
Ethylene Reactor	0	0	0					
Methanol Reactor	0	0	0					
Water Electrolyzer	0	0	0					
CO2 Electrolyzer	830	21	0					
Methane Cryocooler	0	0	0					
Oxygen Cryocooler	126	8	0					
Hydrogen Cryocooler	0	0	0					
Water Tank	0	0	0					
Hydrogen Tank	0	0	0					
Piping and Structure	262	0	0					
Fluids from Earth	15028	0	0					
ISPP	16598			207	51	24	41	498
Power System 23	720		3	73	21	11	2	22
Power System 266	8327		36	851	247	73	21	250
MAV Inert	9955		692	2555	169	150	25	299
Payload	5825					0	15	175
MDV Stage 23	29032			720	120	59	73	871
MDV Stage 266	31214			773	127	63	78	936
MTV Inert 23	23314			2104	273	135	58	699
MTV Inert 266	27369			2242	303	142	68	821
MTV Prop 23	49091						123	1473
MTV Prop 266	57628						144	1729

Figure 143: Mean results for the ethylene with only oxygen ISPP architecture.

	Mass (kg)	Power (kWe)	Volume (m^3)	DDTE ($M2006)	Unit ($M2006)	Ops ($M2006)	LC ($M2006) 2.5k	LC ($M2006) 30k
CO2 Adsorber	357	2	1					
Mars Water Excavators	0	0	0					
Mars Water Plant	0	0	0					
Sabatier Reactor	0	0	0					
Ethylene Reactor	0	0	0					
Methanol Reactor	0	0	0					
Water Electrolyzer	0	0	0					
CO2 Electrolyzer	842	21	0					
Methane Cryocooler	0	0	0					
Oxygen Cryocooler	128	9	0					
Hydrogen Cryocooler	0	0	0					
Water Tank	0	0	0					
Hydrogen Tank	0	0	0					
Piping and Structure	265	0	0					
Fluids from Earth	24630	0	0					
ISPP	26222			208	51	24	66	787
Power System 23	730		3	73	21	11	2	22
Power System 266	8442		37	861	249	74	21	253
MAV Inert	11050		766	2777	181	160	28	332
Payload	5825					0	15	175
MDV Stage 23	30771			791	126	64	77	923
MDV Stage 266	33063			838	133	67	83	992
MTV Inert 23	28477			2278	310	144	71	854
MTV Inert 266	32620			2404	338	151	82	979
MTV Prop 23	59961						150	1799
MTV Prop 266	68065						170	2042

Figure 144: Mean results for the methanol with only oxygen architecture.

	Mass (kg)	Power (kWe)	Volume (m^3)	DDTE ($M2006)	Unit ($M2006)	Ops ($M2006)	LC ($M2006) 2.5k	LC ($M2006) 30k
CO2 Adsorber	0	0	0					
Mars Water Excavators	0	0	0					
Mars Water Plant	0	0	0					
Sabatier Reactor	0	0	0					
Ethylene Reactor	0	0	0					
Methanol Reactor	0	0	0					
Water Electrolyzer	0	0	0					
CO2 Electrolyzer	0	0	0					
Methane Cryocooler	0	0	0					
Oxygen Cryocooler	0	0	0					
Hydrogen Cryocooler	0	0	0					
Water Tank	0	0	0					
Hydrogen Tank	0	0	0					
Piping and Structure	0	0	0					
Fluids from Earth	46034	0	0					
ISPP	46034			0	0	0	115	1381
Power System 23	0		0	0	0	0	0	0
Power System 266	0		0	0	0	0	0	0
MAV Inert	9889		737	2514	168	148	25	297
Payload	5825					0	15	175
MDV Stage 23	26172			877	117	68	65	785
MDV Stage 266	26172			877	117	68	65	785
MTV Inert 23	33994			2444	347	153	85	1020
MTV Inert 266	33994			2444	347	153	85	1020
MTV Prop 23	71577						179	2147
MTV Prop 266	71577						179	2147

Figure 145: Mean results for the methane with no ISPP architecture.

	Mass (kg)	Power (kWe)	Volume (m^3)	DDTE ($M2006)	Unit ($M2006)	Ops ($M2006)	LC ($M2006) 2.5k	LC ($M2006) 30k
CO2 Adsorber	0	0	0					
Mars Water Excavators	0	0	0					
Mars Water Plant	0	0	0					
Sabatier Reactor	0	0	0					
Ethylene Reactor	0	0	0					
Methanol Reactor	0	0	0					
Water Electrolyzer	0	0	0					
CO2 Electrolyzer	0	0	0					
Methane Cryocooler	0	0	0					
Oxygen Cryocooler	0	0	0					
Hydrogen Cryocooler	0	0	0					
Water Tank	0	0	0					
Hydrogen Tank	0	0	0					
Piping and Structure	0	0	0					
Fluids from Earth	46586	0	0					
ISPP	46586			0	0	0	116	1398
Power System 23	0		0	0	0	0	0	0
Power System 266	0		0	0	0	0	0	0
MAV Inert	9955		692	2555	169	150	25	299
Payload	5825					0	15	175
MDV Stage 23	25087			878	115	68	63	753
MDV Stage 266	25807			878	115	68	65	774
MTV Inert 23	33800			2439	346	152	85	1014
MTV Inert 266	33800			2439	346	152	85	1014
MTV Prop 23	71170						178	2135
MTV Prop 266	71170						178	2135

Figure 146: Mean results for the ethylene with no ISPP architecture.

	Mass (kg)	Power (kWe)	Volume (m^3)	DDTE ($M2006)	Unit ($M2006)	Ops ($M2006)	LC ($M2006) 2.5k	LC ($M2006) 30k
CO2 Adsorber	0	0	0					
Mars Water Excavators	0	0	0					
Mars Water Plant	0	0	0					
Sabatier Reactor	0	0	0					
Ethylene Reactor	0	0	0					
Methanol Reactor	0	0	0					
Water Electrolyzer	0	0	0					
CO2 Electrolyzer	0	0	0					
Methane Cryocooler	0	0	0					
Oxygen Cryocooler	0	0	0					
Hydrogen Cryocooler	0	0	0					
Water Tank	0	0	0					
Hydrogen Tank	0	0	0					
Piping and Structure	0	0	0					
Fluids from Earth	56648	0	0					
ISPP	56648			0	0	0	142	1699
Power System 23	0		0	0	0	0	0	0
Power System 266	0		0	0	0	0	0	0
MAV Inert	11050		766	2777	181	160	28	332
Payload	5825					0	15	175
MDV Stage 23	26643			935	120	71	67	799
MDV Stage 266	26643			935	120	71	67	799
MTV Inert 23	39065			2585	379	160	98	1172
MTV Inert 266	39065			2585	379	160	98	1172
MTV Prop 23	82254						206	2468
MTV Prop 266	82254						206	2468

Figure 147: Mean results for the methanol with no ISPP architecture.

	Mass (kg)	Power (kWe)	Volume (m^3)	DDTE ($M2006)	Unit ($M2006)	Ops ($M2006)	LC ($M2006) 2.5k	LC ($M2006) 30k
CO2 Adsorber	0	0	0					
Mars Water Excavators	0	0	0					
Mars Water Plant	0	0	0					
Sabatier Reactor	0	0	0					
Ethylene Reactor	0	0	0					
Methanol Reactor	0	0	0					
Water Electrolyzer	0	0	0					
CO2 Electrolyzer	0	0	0					
Methane Cryocooler	0	0	0					
Oxygen Cryocooler	0	0	0					
Hydrogen Cryocooler	0	0	0					
Water Tank	0	0	0					
Hydrogen Tank	0	0	0					
Piping and Structure	0	0	0					
Fluids from Earth	27531	0	0					
ISPP	27531			0	0	0	69	826
Power System 23	0		0	0	0	0	0	0
Power System 266	0		0	0	0	0	0	0
MAV Inert	8143		1420	2324	155	139	20	244
Payload	5825					0	15	175
MDV Stage 23	37495			791	141	65	94	1125
MDV Stage 266	37495			791	141	65	94	1125
MTV Inert 23	30298			2334	323	147	76	909
MTV Inert 266	30298			2334	323	147	76	909
MTV Prop 23	63795						159	1914
MTV Prop 266	63795						159	1914

Figure 148: Mean results for the hydrogen with no ISPP architecture.

REFERENCES

[1] Drake, B., "Human Exploration of Mars Design Reference Architecture 5.0," Tech. Rep. NASA-SP-2009-566, NASA, 2009.

[2] Drake, B., "Reference Mission Verson 3.0: Addendum to the Human Exploration of Mars: The Reference Mission of the NASA Mars Exploration Study Team," Tech. Rep. SP-6107-ADD, NASA, June 1998.

[3] Hoffman, S. and Kaplan, D., "Human Exploration of Mars: The Reference Mission of the NASA Mars Exploration Study Team," Tech. Rep. NASA-SP-6107, NASA, 1997.

[4] Zubrin, R., Daker, D., and Gwynne, O., "Mars Direct: A Simple, Robust, and Cost Effective Architecture for the Space Exploration Initiaitve," *29th Aerospace Sciences Meeting*, No. AIAA-91-329, Jan. 1991.

[5] Rapp, D., *Human Mission to Mars: Enabling Technologies for Exploring the Red Planet*, Praxis, Chichester, UK, 2008.

[6] Rapp, D., *Use of Extraterrestrial Resources for Human Space Missions to Moon or Mars*, Praxis Publishing, Chichester, UK, 2013.

[7] Arney, D., Jones, C., Klovstad, J., Komar, D., Earle, K., Moses, R., and Shyface, H., "Sustaining Human Presence on Mars Using ISRU and a Reusable Lander," *AIAA SPACE 2015 Conference and Exposition*, No. AIAA 2015-4479, 2015.

[8] Mueller, R., Sibille, L., Sanders, G., Jones, C., and Mantovani, J., "Opportunities and Strategies for Testing and Infusion of ISRU in the Evolvable Mars Campaign," *AIAA SPACE 2015 Conference and Exposition*, No. AIAA 2015-4459, 2015.

[9] Jones, C., Wilhite, A., Hickman, J., and Wagner, J., "Mars Ascent Vehicle–Optimization of Propulsion with In-Situ Propellant Production," *59th International Astronautical Congress*, No. IAC-08.D1.2.8, Oct. 2008.

[10] Drake, B., "Human Exploration of Mars Design Reference Architecture 5.0: Addendum," Tech. Rep. NASA-SP-2009-566-ADD, NASA, July 2009.

[11] Zubrin, R., Frankie, B., and Kito, T., "Mars In-Situ Resource Utilization Based on the Reverse Water Gas Shift: Experiments and Mission Applications," *33rd Joint Propulsion Conference and Exhibit*, No. AIAA-1997-2767, July 1997.

[12] Zubrin, R. and Wagner, R., *The Case for Mars: The Plan to Settle the Red Planet and Why We Must*, Touchstone, New York, 1996.

[13] Rapp, D., Andringa, J., Easter, R., Smith, J., Wilson, T., Clark, D., and Payne, K., "Preliminary System Analysis of In Situ Resource Utilization for Mars Human Exploration," *IEEE Aerospace Conference*, No. 1538, 2005.

[14] Rapp, D., "Initial Mass in Low Earth Orbit Required to Transfer Space Vehicles to Mars Orbit or Mars Surface," Accessed at http://www.spaceclimate.net/IMLEO.pdf on March 7, 2013.

[15] Pauly, K., "A Comparison of In Situ Resource Utilization Options for the First Human Mars Missions," *Mars Society Papers*, No. MAR-98-063, 1998.

[16] Frisbee, R., "Mass and Power Estimates for Mars In-Situ Propellant Production Systems," *AIAA/SAE/ASME/ASEE 23rd Joint Propulsion Conference*, No. AIAA-87-1900, 1987.

[17] of the President of the United States, O., "National Space Policy of the United States of America," June 2010.

[18] O'Keefe, S., "The Vision for Space Exploration," Feb. 2004.

[19] Review of US Human Spaceflight Plans Committee, Augustine, N., "Seeking a Human Spaceflight Program Worthy of a Great Nation," Oct. 2009.

[20] Zubrin, R., *Entering Space: Creating a Spacefaring Civilization*, Jeremy P. Tarcher/Putnam, New York, 1999.

[21] Chai, P., Currey, S., and Jones, C., "Review of Recent U.S. Human Space Exploration Plans Beyond Low Earth Orbit," *AIAA SPACE 2013 Conference and Exposition*, No. AIAA 2013-5314, Sept. 2013.

[22] Larson, W. and Pranke, L., *Human Spaceflight: Mission Analysis and Design*, McGraw-Hill, New York, 1999.

[23] Koelle, D., *Handbook of Cost Engineering for Space Transportation Systems*, No. TCS-TR-190, TCS TransCostSystems, 3rd ed., 2010.

[24] McAfee, J., Culver, G., and Naderi, M., "NASA/Air Force Cost Model (NAFCOM): Capabilities and Results," *2011 JANNAF MSS/LPS/SPS Meeting*, Dec. 2011.

[25] Portree, D., "Humans to Mars: Fifty Years of Mission Planning, 1950-2000," Tech. Rep. NASA SP-2001-4521, NASA, Feb. 2001.

[26] Reck, G., "Report of the 90-Day Study on Human Exploration of the Moon and Mars," Tech. Rep. NASA-TM-102999, NASA, Nov. 1989.

[27] NASA, "NASA's Exploration Systems Architecture Study," Tech. Rep. NASA-TM-2005-214062, NASA, Nov. 2005.

[28] Ash, R., Dowler, W., and Varsi, G., "Feasibility of Rocket Propellant Production on Mars," *Acta Astronautica*, Vol. 5, No. 9, Sept. 1978, pp. 705–724.

[29] Ramohalli, K., Lawton, E., and Ash, R., "Recent Concepts in Missions to Mars: Extraterrestrial Processes," *Journal of Propulsion and Power*, Vol. 5, No. 2, March 1989, pp. 181–187.

[30] Ramohalli, K., Dowler, W., French, J., and Ash, R., "Some Aspects of Space Propulsion with Extraterrestrial Resources," *Journal of Spacecraft and Rockets*, Vol. 24, No. 3, 1987, pp. 236–244.

[31] Ramohalli, K., Downer, W., French, J., and Ash, R., "Novel Extraterrestrial Processing for Space Propulsion," *36th International Astronautical Congress*, No. IAF Paper 85-166, 1985.

[32] Ash, R., Huang, J.-K., Johnson, P., and Sivertson Jr., W., "Elements of Oxygen Production Systems Using Martian Atmosphere," *22nd Joint Propulsion Conference*, No. AIAA-86-1586, June 1986.

[33] Frisbee, R., French Jr., J., and Lawton, E., "A New Look at Oxygen Production on Mars-ISPP," *AIAA 25th Aerospace Sciences Meeting*, No. AIAA-87-0236, Jan. 1987.

[34] Zubrin, R., Kito, T., and Frankie, B., "Report on the Construction and Operation of a Mars In Situ Propellant Production Unit Utilizing the Reverse Water Gas Shift," *34th AIAA/ASME/SAE/ASEE Joint Propulsion Conference and Exhibit*, No. AIAA-98-3303, July 1998.

[35] Zubrin, R., Frankie, B., Muscatello, T., and Kito, T., "Progress in the Development of Mars In Situ Propellant Production Systems," *37th Aerospace Sciences Meeting and Exhibit*, No. AIAA-99-0855, Jan. 1999.

[36] Sridhar, K., "Mars Sample Return Mission with In-Situ Resource Utilization," *Journal of Propulsion and Power*, Vol. 11, No. 6, Nov. 1995, pp. 1356–1362.

[37] Sridhar, K. and Vaniman, B., "Oxygen Production on Mars Using Solid Oxide Electrolysis," *25th International Conference on Environmental Systems*, No. 951737, 1995.

[38] Sridhar, K., Finn, J., and Kliss, M., "In-situ Resource Utilization Technologies for Mars Life Support Systems," *Advances in Space Research*, Vol. 25, No. 2, 2000, pp. 249–255.

[39] Sridhar, K. and Foerstner, R., "Regenerative Solid Oxide Fuel Cells for Mars Exploration," *Journal of Propulsion and Power*, Vol. 16, No. 6, Nov. 2000, pp. 1105–1111.

[40] Sridhar, K., Gottmann, M., and Baird, R., "Update on the Oxygen Generator System for the 2001 Mars Surveyor Mission," *38th Aerospace Sciences Meeting and Exhibit*, No. AIAA-2000-1068, Jan. 2000.

[41] Sridhar, K., Iacomini, C., and Finn, J., "Combined H2O/CO2 Solid Oxide Electrolysis for Mars In-Situ Resource Utilization," *Journal of Propulsion and Power*, Vol. 20, No. 5, Sept. 2004, pp. 892–901.

[42] DePasquale, D., *Mars In-Situ Resource Utilization Sizer: Technical Modeling Summary*, SpaceWorks Engineering, Inc., Jan. 2008.

[43] "Space Radioisotope Power Systems: Multi-Mission Radioisotope Thermoelectric Generator," 2008.

[44] James, G., Chamitoof, G., and Barker, D., "Surviving on Mars Without Nuclear Energy," *Mars Society Papers*, No. MAR-98-058, 1998.

[45] Wead, J., *On to Mars: Colonizing a New World*, chap. Mars Surface Power Technology Options, Collector's Guide Publishing Inc., 2002, pp. 146–154.

[46] "Lecture 12: Planets and Radiation," .

[47] Appelbaum, J. and Flood, D., "Solar Radiation on Mars," Tech. Rep. NASA TM 102299, NASA, 1989.

[48] Landis, G., Hyatt, D., and Team, M. A. S., "The Solar Spectrum on the Martian Surface and Its Effect on Photovoltaic Performance," *IEEE 4th World Conference on Photovolatic Energy Conversion*, 2006.

[49] Landis, G. and Jenkins, P., "Measurement of the Settling Rate of Atmospheric Dust on Mars by the MAE Instrument on Mars Pathfinder," *Journal of Geophysical Research*, Vol. 105, 2000.

[50] Landis, G. and Jenkins, P., "Dust on Mars: Materials Adherence Experiment Results from Mars Pathfinder," *Conference Record of the 26th IEEE Photovoltaic Specialists Conference*, 1997.

[51] Crisp., D., Pathare, A., and Ewell, R., "The Performance of Gallium Arsenide/Germanium Solar Cells at the Martian Surface," *Acta Astronautica*, Vol. 54, No. 2, 2004.

[52] Gaier, J. and Perez-Davis, M., "Effect of Particle Size of Martian Dust on the Degradation of Photovoltaic Cell Performance," Tech. Rep. NASA TM 105232, NASA, 1991.

[53] Gaier, J., Perez-Davis, M., Rutledge, S., and Hotes, D., "Aeolian Removal of Dust from Radiator Surface on Mars," Tech. Rep. NASA TM 103205, NASA, 1990.

[54] Landis, G., "Dust Obscuration of Mars Solar Arrays," *Acta Astronautica*, Vol. 38, No. 11, 1996.

[55] James, G., Chamitoff, G., and Barker, D., "Resource Utilization and Site Selection for a Self-Sufficient Martian Outpost," Tech. Rep. NASA TM-98-206538, NASA, 1998.

[56] Landis, G. and Appelbaum, J., "Design Considerations for Mars Photovoltaic Power Systems," *Proceedings of the European Space Power Conference*, No. ESA SP-320, 1990.

[57] Haberle, R., McKay, C., Pollack, J., Gwynne, O., Atkinson, D., Appelbaum, J., Landis, G., Zurek, R., and Flood, D., *Resources of Near-Earth Space*, University of Arizona Press, 1993.

[58] Littman, F., "First Mars Outpost Power Systems," *IEEE Aerospace and Electronic Systems Magazine*, 1993.

[59] Kerslake, T. and Kohout, L., "Solar Electric Power System Analyses for Mars Surface MIssions," Tech. Rep. NASA-TM-1999-209288, NASA, 1999.

[60] Balint, T., "Nuclear Systems for Mars Exploration," *Proceedings of 2004 IEEE Aerospace Conference*, 2004.

[61] Petri, D., Cataldo, R., and Bozek, J., "Power System Requirements and Definition for Lunar and Mars Outposts: A Review of the Space Exploration Initiative's NASA 90 Day Study," *4th International Energy Conversion Engineering Conference and Exhibit (IECEC)*, No. AIAA 2006-4103, 2006.

[62] Cooper, C., Horstetter, C., Hoffman, J., and Crawley, E., "Assessment of Architectural Options for Surface Power Generation and Energy Storage on Human Mars Missions," *Acta Astronautica*, Vol. 66, No. 7, 2010.

[63] NASA, "Spread Your Wings, It's Time to Fly," Website, July 2006.

[64] Bailey, S. and Raffaelle, R., *Handbook of Photovoltaic Science and Engineering*, chap. Space Solar Cells and Arrays, John Wiley and Sons, Ltd., 2003, pp. 413–448.

[65] Aftergood, S., "Background on Space Nuclear Power," *Science and Global Security*, Vol. 1, 1989.

[66] Smith, J., "SP-100 Nuclear Space Power Systems with Application to Space Commercialization," Tech. Rep. NASA TM 101403, NASA, 1989.

[67] Marriott, A. and Fujita, T., "Evolution of SP100 System Designs," *AIP Conference Proceedings*, Vol. 301, 1994.

[68] Gebicke, M., "The SP-100 Nuclear Reactor Program: Should It Be Continued? Statement of Mark E. Gebicke, Director, NASA Issues, National Security and International Affairs Division," Tech. Rep. GAO/T-NSIAD-92-15, General Accounting Office, 1992.

[69] Cropp, L., Gallup, D., and Marshall, A., "Mass and Performance Estimates for 5 to 1000 kW(e) Nuclear Reactor Power Systems for Space Applications," Tech. Rep. SAND90-0312, Sandia National Laboratories, 1990.

[70] Lindeburg, M., *Engineer-in-Training Reference Manual*, Professional Publications, Inc., 8th ed., 2002.

[71] Mason, L., "Surface Nuclear Power for Human Mars Missions," Tech. Rep. NASA/TM-1999-208894, NASA, Jan. 1999.

[72] Mason, L., "A Comparison of Brayton and Stirling Space Nuclear Power Systems for Power Levels from 1 Kilowatt to 10 Megawatts," Tech. Rep. NASA/TM-2001-210593, NASA, Jan. 2001.

[73] Mason, L., "Power Technology Options for Nuclear Electric Propulsion," *37th Intersociety Energy Conversion Engineering Conference*, 2002.

[74] Taylor, R., "Prometheus Project: Final Report," Tech. Rep. 982-R120461, NASA and JPL, 2005.

[75] Palac, D., Mason, L., Houts, M., and Harlow, S., "Fission Surface Power Technology Development Status," *AIAA SPACE 2009 Conference and Exposition*, No. AIAA 2009-6535, 2009.

[76] Palac, D., Mason, L., Houts, M., and Harlow, S., "Fission Surface Power Technology Development Update," *AIAA SPACE 2010 Conference and Exposition*, No. AIAA 2010-8711, 2010.

[77] Kohout, L., "Power System Trade Studies for the Lunar Surface Access Module," Tech. Rep. NASA/TM-2008-215179, NASA, 2008.

[78] Shahan, Z., "Sharp Regains Solar Cell Efficiency Record," Web Article, May 2013, http://solarlove.org/sharp-regains-solar-cell-efficiency-record/.

[79] Wertz, J. and Larson, W., *Space Mission Analysis and Design*, Microcosm Press and Kluwer Academic Publishers, El Segundo, CA, 3rd ed., 1999.

[80] of Energy Fuel Cell Technologies Office, U. D., "Comparison of Fuel Cell Technologies," May 2014.

[81] Donahue, B., "Architecture Selection: The Key Decision for Human Mars Mission Planning," *37th Joint Propulsion Conference and Exhibit*, No. AIAA-2001-3371, July 2001.

[82] Duke, M., Keaton, P., Weaver, D., Roberts, B., Griggs, G., and Huber, W., "Mission Objectives and Comparison of Strategies for Mars Exploration," *Aerospace Design Conference*, No. AIAA-1993-0956, Feb. 1993.

[83] *2008 NASA Cost Estimating Handbook*, Washington, DC, 2008.

[84] Newnan, D., Eschenback, T., and Lavelle, J., *Engineering Economic Analysis*, Oxford University Press, New York, 9th ed., 2004.

[85] Office of Mangement and Budget, *OMB Circular No. A-94 Appendix C*, White House, Dec. 2009.

[86] Reeves, J., DePasquale, D., and Lim, E., "Affordability Engineering: Bridging the Gap Between Design and Cost," *AIAA SPACE 2010 Conference and Exposition*, No. AIAA 2010-8904, 2010.

[87] Hamaker, J. and Dodd, G., "Expendable vs Reusable Propulsion Systems Cost Sensitivity," *AIAA/ASME/SAE/ASEE 25th Joint Propulsion Conference*, No. AIAA 89-2402, July 1989.

[88] Vanderplaats, G., *Numerical Optimization Techniques for Engineering Design: With Applications*, McGraw-Hill, New York, 1984.

[89] Alexandrov, N., "Multilevel and Multiobjective Optimization in Multidisciplinary Design," *6th Symposium on Multidisciplinary Analysis and Optimization*, No. AIAA-96-4122, Sept. 1996.

[90] Cox, M. and Siebert, B., "The Use of a Monte Carlo Method for Evaluating Uncertainty and Expanded Uncertainty," *Metrologia*, Vol. 43, 2006, pp. 178–188.

[91] Durga Rao, K., Kushwaha, H., Verma, A., and Srividya, A., "Quantification of Epistemic and Aleatory Uncertainties in Level-1 Probabilistic Safety Assessment Studies," *Reliability Engineering and System Safety*, Vol. 92, No. 7, July 2007.

[92] Wubbeler, G., Krystek, M., and Elster, C., "Evaluation of Measurement Uncertainty and its Numerical Calculation by a Monte Carlo Method," *Meas. Sci. Technol.*, Vol. 19, 2008, pp. 1–4.

[93] Papadopoulos, C. and Yeung, H., "Uncertainty Estimation and Monte Carlo Simulation Method," *Flow Measurement and Instrumentation*, Vol. 12, 2001, pp. 291–298.

[94] Ferson, S. and Ginzburg, L., "Different Methods are Needed to Propagate Ignorance and Variability," *Treatment of Aleatory and Epistemic Uncertainty*, Vol. 54, No. 2, Nov. 1996, pp. 133–144.

[95] Roy, C. and Oberkampf, W., "A Comprehensive Framework for Verification, Validation, and Uncertainty Quantification in Scientific Computing," *Computer Methods in Applied Mechanics and Engineering*, Vol. 200, No. 25, 2011.

[96] Hofer, E., Kloos, M., Krzykacz-Hausmann, B., Peschke, J., and Woltereck, M., "An Approximate Epistemic Uncertainty Analysis Approach in the Presence of Epistemic and Aleatory Uncertainties," *Reliability Engineering and System Safety*, Vol. 77, 2002.

[97] Tammineni, S., Scanlan, J., and Reed, P., "Knowledge Based System for Cost Optimization," *48th AIAA/ASME/ASCE/AHS/ASC Structures, Structural Dynamics, and Materials Conference*, No. AIAA-2007-1907, April 2007.

[98] Chen, W., Allen, J., Tsui, K.-L., and Mistree, F., "A Procedure for Robust Design: Minimizing Variations Caused by Noise Factors and Control Factors," *Journal of Mechanical Design*, Vol. 118, Dec. 1996.

[99] Mistree, F., Hughes, O., and Bras, B., *Structural Optimzation: Staus and Promise*, chap. The Compromise Decision Support Problem and the Adaptive Linear Programming Algorithm, AIAA, 1993, pp. 247–286.

[100] Simon, H., *Sciences of the Artificial*, MIT Press, 1982.

[101] Muster, D. and Mistree, F., "The Decision-Support Problem Technique in Engineering Design," *International Journal of Applied Engineering Education*, Vol. 4, 1988.

[102] Du, X. and Chen, W., "Efficient Uncertainty Analysis Methods for Multidisciplinary Robust Design," *AIAA Journal*, Vol. 40, No. 3, 2002.

[103] Schultz, M., Mitchell, K., Harper, B., and Bridges, T., "Decision Making Under Uncertainty," Tech. Rep. ERDC TR-10-12, US Army Corps of Engineers, 2010.

[104] Hamby, D., "A Comparison of Sensitivity Analysis Techniques," *Health Physics*, Vol. 68, No. 2, 1995.

[105] Chen, W., Jin, R., and Sudjianto, A., "Analytical Variant-Based Global Sensitivity Analysis in Simulation-Based Design Under Uncertainty," *Journal of Mechanical Design*, Vol. 127, No. 5, Sept. 2005.

[106] Parnell, G., Bresnick, T., Tani, S., and E., J., *Handbook of Decision Analysis*, Wiley, 2013.

[107] Chang, C., "Special Adsorbent for Carbon Dioxide Acquisition on Mars," 2001.

[108] Rapp, D., Karlmann, P., Clark, D., and Carr, C., "Adsorption Compressor for Acquisition and Compression of Atmospheric CO2 on Mars," *33rd Joint Propulsion Conference and Exhibit*, No. AIAA-1997-2763, July 1997.

[109] Mulloth, L. and Finn, J., "Carbon Dioxide Adsorption on a 5A Zeolite Designed for CO2 Removal in Spacecraft Cabins," Tech. Rep. NASA/TM-1998-208752, NASA, Nov. 1998.

[110] England, C., "Mars Atmosphere Resource Recovery System (MARSS)," *39th Aerospace Sciences Meeting and Exhibit*, No. AIAA-2001-0942, Jan. 2001.

[111] Notardonato, W., "Densification of In Situ Produced Propellants for the Human Exploration of Mars," *38th AIAA/ASME/SAE/ASEE Joint Propulsion Conference and Exhibit*, No. AIAA-2002-4296, July 2002.

[112] Kim, J. and White, R., "Comparison of Heat-Fin Materials and Design of a Common-Pressure-Vessel Nickel-Hydrogen Battery," *Journal of the Electrochemical Society*, Vol. 139, No. 12, Dec. 1992, pp. 3492–3499.

[113] Lunde, P. and Kester, F., "Rates of Methane Formation from Carbon Dioxide and Hydrogen over a Ruthenium Catalyst," *Journal of Catalysis*, Vol. 30, No. 3, Sept. 1973, pp. 423–429.

[114] WireTronic Inc., "Nichrome 80 and Other Resistance Alloys - Technical Data & Properties," .

[115] Zubrin, R., Price, S., Mason, L., and Clark, L., "Report on the Construction and Operation of a Mars In-Situ Propellant Production Plant," *30th AIAA/ASME/SAE/ASEE Joint Propulsion Conference*, No. AIAA-94-2844, June 1994.

[116] Air Liquide, "Space Cryogenic Insulation: Insulation Systems for Cryogenic Tanks, Lines or Equipments on Space Launchers," .

[117] Ross, R., *Metallic Materials Specification Handbook*, Chapman & Hall, 4th ed., 1981.

[118] Incropera, F. and DeWitt, D., *Fundamentals of Heat and Mass Transfer*, John Wiley & Sons, Inc., 2002.

[119] Globus, R., "Regenerative Life Support: Methods of Water Production," Website, July 2002.

[120] Kim, J., Lee, S., Lee, S., Choi, M., and Lee, K., "Performance of Catalytic Reactors for the Hydrogenation of CO2 to Hydrocarbons," *Catalysis Today*, Vol. 115, April 2006, pp. 228–234.

[121] Holladay, J., Brooks, K., Wegeng, R., Hu, J., Sanders, J., and Baird, S., "Microreactor Development for Martian In Situ Propellant Production," *Catalysis Today*, Vol. 120, 2007, pp. 35–44.

[122] Chen, C., Cheng, W., and Lin, S., "Study of Reverse Water Gas Shift Reaction by TPD, TPR, and CO2 Hydrogenation over Potassium-Promoted Cu/SiO2 Catalyst," *Applied Catalysis A: General*, Vol. 238, 2003, pp. 55–67.

[123] Air Products, "Advanced Prism Membrane Systems for Cost Effective Cas Separations," .

[124] Kolb, G., Pennemann, H., and Zapf, R., "Water-gas Shift Reaction in Micro-Channels–Results from Catalyst Screening and Optimisation," *Catalysis Today*, Vol. 110, 2005, pp. 121–131.

[125] Thunnissen, D., Rapp, D., Voorhees, C., Dawson, S., and Guernsey, C., "A 2007 Mars Sample Return Mission Utilizing In-Situ Propellant Production," *37th AIAA Aerospace Sciences Meeting and Exhibit*, No. AIAA-99-0851, 1999.

[126] Iacomini, C. and Sridhar, K., "Electrolyzer Power Requirements for Oxidizer Production on Mars," *Journal of Propulsion and Power*, Vol. 21, No. 6, Nov. 2005, pp. 1062–1068.

[127] Clark, D., "In-Situ Propellant Production on Mars: A Sabatier/Electrolysis Demonstration Plant," *33rd Joint Propulsion Conference and Exhibit*, No. AIAA-1997-2764, July 1997.

[128] Conner, W., Greenough, B., and Cook, G., "Design and Development of a Water Vapor Electrolysis Unit," Tech. Rep. NASA-CR-607, NASA, Sept. 1966.

[129] Onda, K., Murakami, T., Hikosaka, T., Kobayashi, M., Notu, R., and Ito, K., "Performance Analysis of Polymer-Electrolyte Water Electrolysis Cell at a Smll-Unit Test Cell and Performance Prediction of Large Stacked Cell," *Journal of the Electrochemical Society*, Vol. 149, No. 8, Aug. 2002, pp. A1069–A1078.

[130] Funk, J. and Thorpe, J., "Void Fraction and Current Density Distributions in a Water Electrolysis Cell," *Journal of the Electrochemical Society*, Vol. 116, No. 1, Jan. 1969, pp. 48–54.

[131] Agranat, V., Zhubrin, S., Hinatsu, J., and Stemp, M., "An Integrated Model for Performance Prediction in High Pressure Water Electrolysis Systems," *Proceedings of Fuel Cell Science and Technology 2006*, Sept. 2006.

[132] Minh, N., Chung, B., Doshi, R., Lear, G., Montgomery, K., and Ong, E., "Fabrication and Performance of Zirconia Electrolysis Cells for Carbon Dioxide Reduction for Mars In Situ Resource Utilization Applications," *ISRU III Technical Interchange Meeting*, 1999.

[133] Salerno, L. and Kittel, P., "Cryogenics and the Human Exploration of Mars," *Cryogenics*, Vol. 39, No. 4, April 1999, pp. 381–388.

[134] Vanapalli, S., Lewis, M., Gan, Z., and Radebaugh, R., "120 Hz Pulse Tube Cryocooler for Fast Cooldown to 50 K," *Applied Physics Letters*, Vol. 90, 2007.

[135] Hou, Y., Zhao, H., Chen, C., and Xiong, L., "Developments in Reverse Brayton Cryocooler in China," *Cryogenics*, Vol. 46, 2006, pp. 403–407.

[136] Jensen, H., Nast, T., Glassford, A., Vernon, R., and Ekern, W., "Handbook of External Refrigeration Systems for Long-Term Cryogenic Storage," Tech. Rep. LMSC-A984158, Lockheed Missles and Space Company, Feb. 1971.

[137] Zagarola, M. and McCormick, J., "High-Capactiy Turbo-Brayton Cryocoolers for Space Applications," *Cryogenics*, Vol. 46, 2006, pp. 169–175.

[138] Glaister, D., Donabedian, M., Curran, D., and Davis, T., "An Assessment of the State of Cryocooler Technology for Space Applications," *AIAA Defense and Civl Space Programs Conference and Exhibit*, 1998.

[139] DePasquale, D., Wallace, J., and Charania, A., "Economic Analysis of Lunar Propellant Production: In-Situ Resource Utilization (ISRU) Propellant Services Market," *26th International Space Development Conference (ISDC)*, May 2007.

[140] Hickman, J., Wilhite, A., Stanley, D., and Komar, D., "Optimization of the Mars Ascent Vehicle for Human Space Exploration," *Journal of Spacecraft and Rockets*, Vol. 47, No. 2, March 2010, pp. 361–370.

[141] Wilhite, A., Gholston, S., Farrington, P., and Swain, J., "Evaluating Technology Projections and Weight Prediction Method Uncertainty of Future Launch Vehicles," *Journal of Spacecraft and Rockets*, Vol. 45, No. 3, May 2008, pp. 587–591.

[142] Chai, P. and Wilhite, A., "Quantifying the Effects of Model Uncertainity on Design Mass Margin in Advanced Earth-to-Orbit Launch Vehicles," *AIAA SPACE 2010 Conference and Exposition*, No. AIAA-2010-8631, Aug. 2010.

[143] "Encyclopedia Astronautica: RL-10A-4-2," Website, http://www.astronautix.com/engines/rl10a42.htm.

[144] Polsgrove, T., Thomas, D., Sutherlin, S., Stephes, W., and Rucker, M., "Mars Ascent Vehicle Design for Human Exploration," *AIAA SPACE 2015 Conference and Exposition*, No. AIAA 2015-4416, 2015.

[145] Rocketdyne, P. . W., "SSME: Space Shuttle Main Engine," Online data sheet.

[146] Koelle, D., "The Transcost-Model for Launch Vehicle Cost Estimation and Its Application to Future Systems Analysis," *Acta Astronautica*, Vol. 11, No. 12, 1984.

[147] Arney, D., *Rule-Based Graph Theory to Enable Exploration of the Space System Architecture Design Space*, Ph.D. thesis, Georgia Institute of Technology, Aug. 2012.

[148] Wilhite, A. and Chai, P., "Plan B for U.S. Human Space Exploration Program," *AIAA SPACE 2014 Conference and Exposition*, No. AIAA 2014-4237, 2014.

[149] NASA, "Mission Operations Cost Model," Website. https://web.archive.org/web/20090327071409/http://cost.jsc.nasa.gov/MOCM.html. Accessed 7-6-2015.

[150] Wilhite, A., Pine, D., and Bilardo, V., "Top-Down Manpower Estimating Based on Historical Program Experience," *1st Space Exploration Conference: Continuing the Voyage of Discovery*, No. AIAA-2005-2536, Jan. 2005.

[151] Sanders, G., "Personal Communication," July 2014.

[152] NASA, "Structural Design and Test Factors of Safety for Spaceflight Hardware," Tech. Rep. NASA-STD-5001A, NASA, Washington, DC, Aug. 2008.

[153] AIAA/ANSI, "Recommended Practice for Mass Properites Control for Satellites, Missles, and Launch Vehicles," Tech. Rep. R-020A-1999, AIAA/ANSI, 1999.

[154] Hawkins, K., "Space Vehicle and Associated Subsystem Weight Growth," *47th Annual Confernce of the Society of Allied Weight Engineers Inc.*, No. 1816, May 1988.

[155] de Weck, O., "A Systems Approach to Mass Budget Management," *11th AIAA/ISSMO Multidisciplinary Analysis and Optimization Conference*, No. AIAA 2006-7055, Sept. 2006.